Volume 1

I. Sediment and Flow Modeling

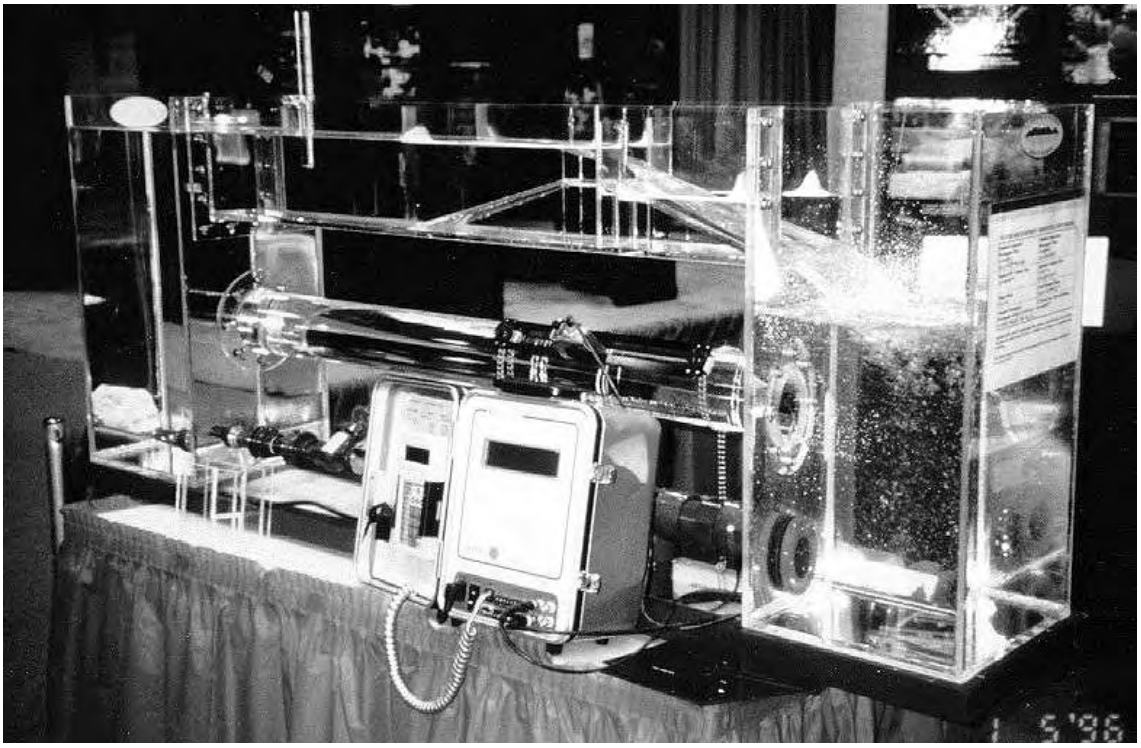

I. Sediment and Flow Modeling

TABLE OF CONTENTS

AnnAGNPS: ESTIMATING SEDIMENT YIELD BY PARTICLE SIZE FOR SHEET & RILL EROSION

By: Ronald L. Bingner, Agricultural Engineer, National Sedimentation Laboratory-Agricultural Research Service-USDA, Oxford, MS and Fred D. Theurer, Agricultural Engineer, National Water & Climate Center-Natural Resources Conservation Service-USDA, Beltsville, MD

ABSTRACT: RUSLE (Revised Universal Soil Loss Equation) is the basis within AnnAGNPS (Annualized AGricultural Non-Point Source Pollution watershed model) for estimating sheet and rill erosion (clay, silt, sand, small and large aggregates) of a watershed's landscape. This sheet and rill erosion is used to predict the sediment yield (clay, silt, and sand) from the watershed landscape by AnnAGNPS, which is a continuous-simulation, agricultural-related, non-point source, pollutant loading watershed model. The fine sediment yield (clay and silt) from sheet and rill erosion of agricultural lands is a major concern for pollutant loadings into water bodies, such as streams and channels. While other sources of sediment (gullies, bed, and bank erosion) are also predicted by AnnAGNPS, RUSLE is used only to estimate the sheet and rill erosion. A simple procedure to estimate the sediment delivery by particle size is necessary to link the sheet and rill erosion to the sediment yield in water bodies. Determining the sediment yield by particle size from each homogenous land area within the watershed (defined as a cell in AnnAGNPS) is critical in assessing the effectiveness of best management practices. The application of RUSLE is used to determine where and when sheet and rill erosion can occur. Algorithms within RUSLE for irregular and segmented slopes are defined in the USDA Agricultural Handbook Number 703, and can be used to determine a raster-weighted LS-factor for each homogenous land area. The delivery ratio procedure in AnnAGNPS is based upon HUSLE (Hydro-geomorphic Universal Soil Loss Equation) and the respective fall velocities of the particle-size classes predicted by RUSLE. The results show that most coarse sediment (sand-size particles) deposit in the fields while most fine sediments (eroded clay and silt size particles that become entrained in the runoff) become wash load and enter the streams and channels.

INTRODUCTION

AnnAGNPS is the pollutant loading (PL) model within a suite of computer models that is designed to analyze the impact of non-point source pollutants from predominately agricultural watersheds on the environment (Cronshey and Theurer, 1998; Theurer et al, 1999). This suite of computer models is called AGNPS 98 and can be located on the Internet at:

"http://www.sedlab.olemiss.edu/AGNPS98.html"

The pollutant loading most frequently of concern to conservationist dealing with agricultural watersheds is fine sediment generally originating from sheet and rill erosion. AnnAGNPS predicts: (1) water; (2) sediment by particle size from sheet and rill, gully, and stream bed and bank; and (3) chemicals from the landscape. Although AnnAGNPS predicts all of these pollutant loadings, this paper will concentrate on the prediction of sheet and rill erosion and subsequent sediment yield. This paper will briefly describe how predictions are made for: (1) sheet and rill erosion (RUSLE); (2) delivery ratio for the sheet and rill erosion to determine sediment yield to receiving reaches of the stream system (HUSLE); and (3) particle-size distribution for the delivered sediment yield to the stream system from sheet and rill erosion. And finally, a comparison of measured sediment data to predicted will be made.

An extremely important point for watershed modeling is that AnnAGNPS predicts the average erosion and subsequent sediment yield from each field or cell in the watershed, which is not the same as calculating the erosion along the most critical flow path and using it for that day's average cell condition. Therefore, each erosion and sediment-related parameter within AnnAGNPS is spatially averaged to account for their nonlinearity.

SHEET AND RILL EROSION

The technology for the Revised Universal Soil Loss Equation (RUSLE, version 1.05) (Renard et al, 1997) is included in AnnAGNPS to predict sheet and rill erosion (Geter and Theurer, 1998). RUSLE is the update to the Universal Soil Loss Equation (USLE) (Wischmeier and Smith, 1978). The RUSLE component within AnnAGNPS will determine some of the necessary RUSLE parameters (R, K, C, and P), but the determination of the topographic or LS factor, which is derived from the slope-length and slope-steepness along a flow profile, is

required. An automated procedure to determine the average LS-factor for each cell in AnnAGNPS using digital elevation maps (DEMs) has been included in AGNPS 98 for use with AnnAGNPS (Bingner and Theurer, *in press*). This is accomplished by using the parameters: generated from a module within AGNPS 98, TOPAGNPS (Garbrecht and Martz, 1993; Garbrecht and Martz, 1995; Bingner et al, 1997); from a user-supplied estimate of when concentrated flow erosion begins and sheet and rill erosion along any given flow path ceases; and from a user-supplied estimate of when deposition begins along any flow path. Individual LS-factors are computed for each raster of the DEM and then averaged for all the rasters within each cell to determine the average LS-factor for the respective cell. The LS-factor procedure recognizes that although sheet and rill erosion may cease along a specific flow path, sheet and rill erosion can still occur beyond the confines of a concentrated flow channel.

Sheet and rill erosion is calculated for each runoff event during a user-defined simulation period and averaged for this same time period. A runoff event can occur from any combination of rainfall, snowmelt, and irrigation. All subsequent sediment is routed throughout the stream system down to the watershed outlet. An account of each individual field contribution to the sediment yield at any user-defined stream location can be determined.

DELIVERY RATIO

Since RUSLE is used only to predict sheet and rill erosion and not field deposition, a delivery ratio of the sediment yield from this erosion to sediment delivery to the stream is needed. The Hydro-geomorphic Universal Soil Loss Equation (HUSLE) is used for this procedure (Theurer and Clarke, 1991).

The procedure was initially developed to predict the total sediment yield at a user-defined point in the stream system using spatially- and time-averaged RUSLE parameters; and to ensure that sheet and rill-related sediment was properly calculated. The form of the equation also lends itself to a non-dimensional ratio where the RUSLE parameters are cancelled and only the hydrograph-related parameters remain.

The sheet and rill component from Theurer and Clarke (1991) is:

$$S_y = 0.22 * Q^{0.68} * q_p^{0.95} * KLSCP \qquad \text{Equation 1}$$

Where: S_y = sediment yield (Mg/ha);

Q = surface runoff volume (mm);

q_p = peak rate of surface runoff (mm/s); and

K,L,S,C,P are RUSLE factors as per AHN 537 or AHN 703.

Note that all three variables (S_y, Q, and q_p) are based on unit area; i.e., divided by their drainage areas as is the proper form for RUSLE.

If a ratio is made of Equation 1 at two different locations in a homogeneous watershed where "2" is downstream of "1" and noting that the unit area runoff volume is identical at all locations within the homogeneous area, the result is:

$$D_r = S_{y2}/S_{y1} = (q_{p2} / q_{p1})^{0.95} \qquad \text{Equation 2}$$

Where: S_{y1} = sediment yield at location "1" (Mg/ha);

S_{y2} = sediment yield at location "2" (Mg/ha);

q_{p1} = peak rate of surface runoff at location "1" (mm/s);

q_{p2} = peak rate of surface runoff at location "2" (mm/s);

D_r = delivery ratio from location "1" to "2"

Since sheet and rill erosion usually occurs within a few tens of feet along their flow paths, resulting in small drainage areas, Equation 2 is computed assuming location "1" is for a zero drainage area, which is the same as a time of concentration of zero, and location "2" is for the time of concentration of the local field or cell. The peak discharge for a time of concentration of zero is the instantaneous peak discharge of the runoff hydrograph and can be easily calculated from TR-55 (SCS, 1986).

PARTICLE-SIZE DISTRIBUTION OF FIELD DEPOSITION

Since RUSLE is used to calculate the amount of sheet and rill erosion and HUSLE is used to determine the delivery ratio for total sediment, the only factor remaining is to determine the particle-size distribution of the deposition in the field. This allows for the particle-size distribution of the sediment yield of the sheet and rill erosion to the receiving reach of the stream system.

The particle-size sediment deposition within the field is assumed to be proportional to the mass fall velocity of the individual particle-size classes. Since the density of both the large and small aggregates are noticeably less than the discrete particles of clay, silt, and sand, a product of the respective densities times its fall velocity is used to represent each particle-size class. This is called the deposition mass rate and has units of mass per length squared per time. The resulting deposition mass rate values for each particle-size class are summed and then normalized with respect to this sum. These normalized values are called deposition rate ratios. They are further normalized with respect to the smallest value, which will normally be clay, and are called the deposition ratio mass rate. From these calculations, the field deposition is determined, but careful consideration is given to exhausting any of the particular particle-size classes; i.e., when any of the particle-size classes are totally deposited, the calculations begin again at that point along the landscape with that particle-size class eliminated from further calculations.

SEDIMENT TRANSPORT

Sediment transport within the stream system is described in detail by Theurer and Cronshey (1998). A modified Einstein equation is used:

$$q_{s2} = q_{sc} + [(q_{s1} - q_{sc}) \bullet \exp(-N_d)] \qquad \text{Equation 3}$$

where: A = Einstein's constant of proportionality, non-dimensional;

L_2 = distance from x1 to x2, m;

N_d = (A·vf·L2)/qw, deposition number, non-dimensional;

q_{sc} = unit-width sediment transport capacity, Mg/s/m;

q_{s1} = upstream unit-width sediment discharge at x1, Mg/s/m;

q_{s2} = downstream unit-width sediment discharge at x2, Mg/s/m;

q_w = unit-width water discharge, m3/s/m; and

v_f = particle fall velocity, m/s.

The current sediment transport capacity model used to determine q_{sc} is the Bagnold equation (Bagnold, 1966).

GOODWIN CREEK WATERSHED

Goodwin Creek Watershed (GCW) is in the Yazoo River Basin near Oxford, Mississippi. GCW is 21.3 km^2 in area with fourteen instream measuring flumes monitored by the USDA-Agricultural Research Service, National Sedimentation Laboratory since 1982 (Blackmarr, 1995). Data collected from each measuring flume include channel flow depth, velocity, and sediment concentration. Climatological data is collected from a central weather station and 32 spatially distributed raingages. Each measuring flume defines an outlet of a subwatershed of various drainage areas. Many of the parameters required by AnnAGNPS have been obtained for GCW, plus selected measuring flumes can be used for model validation purposes.

Figure 1 is a watershed map of Goodwin Creek showing the location of Flannigan's field and the measuring flume at Station No. 12. Flannigan's field is in a steeper part of the watershed at the extreme upper end of Goodwin Creek and was planted in conventionally tilled soybeans during the years from 1982 to 1984 (Bingner et al, 1989). Station No. 12 has a total drainage area of 28.71 ha and is the first GCW measuring flume below Flannigan's field. Other than Flannigan's field, the entire Station No. 12 watershed contains pasture or idle lands, with several gullies forming within those fields. A monitoring flume was also located at the downstream edge of Flannigan's field. This provided a means to compare the sediment leaving a field-sized watershed and the subsequent sediment loading downstream. After harvesting, weeds would be present in the field and continue to grow until

plowing operations in the spring. These weeds were considered in the development of the input parameters and provided cover to the soil during this period.

Rainfall during this period averaged 1624 mm/yr compared to the historical average rainfall of 1400 mm/yr. Measured runoff at Station No. 12 averaged 861 mm/yr and for Flannigan's field averaged 764 mm. The AnnAGNPS predicted runoff from Flannigan's field and from Station No. 12 was adjusted using the SCS curve numbers to correspond to the measured runoff. This was performed to help analyze only the erosion, sediment yield, and sediment loading components of AnnAGNPS. If simulated runoff would be different from measured values this difference would propagate to the erosion determinations and would make the analysis of the erosion results more difficult.

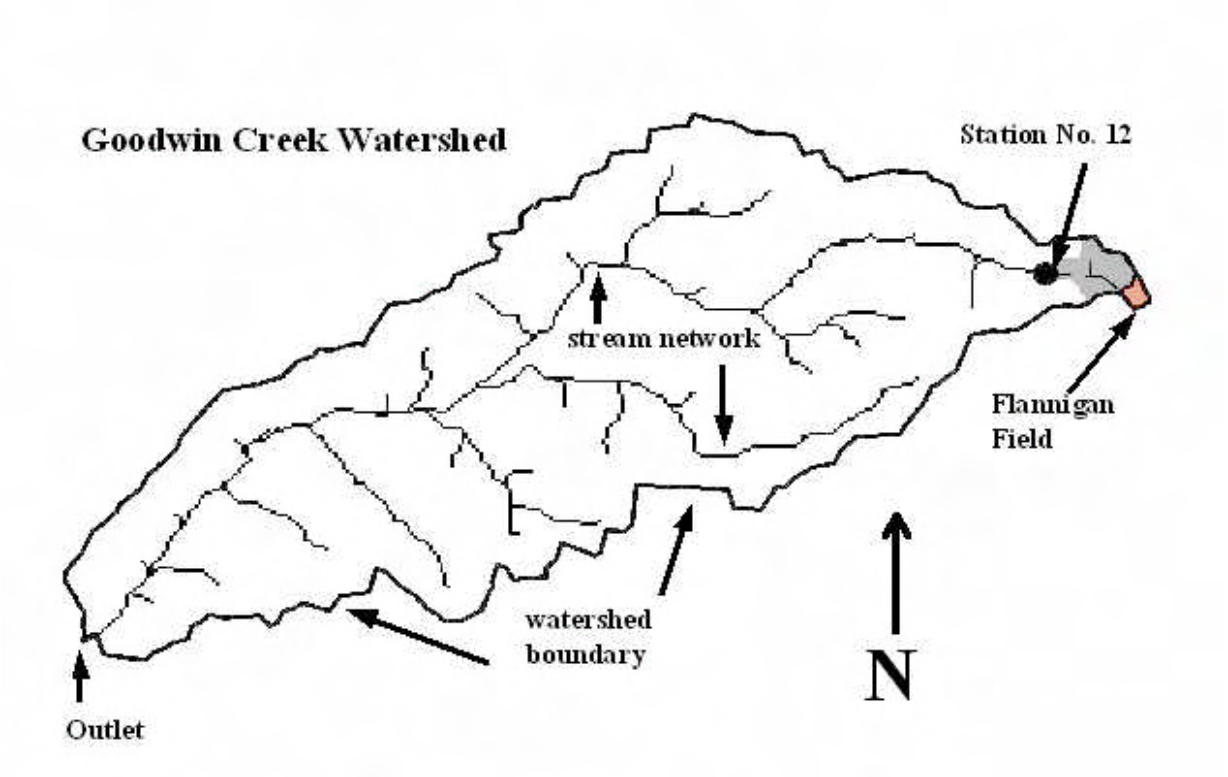

Figure 1: Goodwin Creek Watershed showing location of Flannigan Field and Station No. 12

The erosion and sediment yield by particle-size class predicted values contributed from Flannigan's field as shown in Table 1 from 1982 through 1984. Fines in Table 1 are the sum of clay and silt which usually comprise what sedimentologists consider to be wash load. The units are for the average of the three years divided by the respective drainage areas at the noted locations.

From Table 1, Flannigan field's sheet and rill erosion is determined from the total amount erosion by particle-size class within Flannigan's field divided by the product of its drainage area of 4.32 ha times 3 years.

The results of Flannigan field's sediment yield to the stream are determined from the total amount of sediment yield by particle-size class eroded from within Flannigan's field and delivered directly to its receiving reach of the stream system and divided by the product of its drainage area of 4.32 ha times 3 years.

The results of Flannigan field's sediment yield at Station No. 12 are determined from the total amount of sediment yield by particle-size class eroded from within Flannigan's field, transported to Station No. 12, and divided by the product of its drainage area of 4.32 ha times 3 years.

Finally, the total sediment load at Station No. 12 results are determined from the total amount of sediment yield by particle-size class eroded from within the entire subwatershed above Station No. 12, then transported to Station No. 12, and divided by the product of its drainage area of 28.71 ha times 3 years.

The model predicts five particle-size classes, which are: (1) clay; (2) silt; (3) sand; (4) small aggregate; and (5) large aggregate. AnnAGNPS predicts erosion by these five classes and delivers sediment yield by these same five classes to the receiving reach of the stream system. AnnAGNPS then assumes that the aggregates are mechanically broken down into its constituent discrete particle-sizes immediately upon entering the stream system. For simplicity, the aggregates were mathematically proportioned to their respective discrete particle-sizes, based on the soil in the field, whenever aggregates were present.

Table 1: AnnAGNPS predicted sheet and rill values for years 1982 through 1984.

Average Annual Unit Area Values (Mg/ha/yr)						
	Drainage Area	Particle-Size Class				
		Clay	Silt	Fines	Sand	Total
Flannigan field's sheet and rill erosion	4.32	3.95	19.47	23.42	3.66	27.08
Flannigan field's sediment yield to the stream	4.32	3.93	14.20	18.13	0.00	18.13
Flannigan field's sediment yield at Station No. 12	4.32	3.92	11.74	15.66	0.00	15.66
Total sediment load from sheet & rill at Station #12	28.71	0.60	1.70	2.30	0.00	2.30

For the results in Table 1 for Flannigan's field, only the erosion or sediment yield that originated within the field is shown. The difference between sheet and rill erosion and sediment yield to the stream is due to field deposition. Most aggregates and all of the sand settled in the fields without reaching its receiving reach. The difference between sediment yield to the stream and sediment yield at Station No. 12 is what deposits in the stream bed between the receiving reach and Station No. 12. The total sediment load from sheet and rill sources at Station No. 12 is for the entire drainage area above Station No. 12 and indicates that the major contributor of fine sediment is from Flannigan's field.

Table 2 shows some measured data that corresponds to Table 1.

Table 2: Measured values from all sources for years 1982 through 1984.

Unit Area Values for 1982 – 1984 (Mg/ha/yr)			
	Particle-Size Class		
	Fines	Sand	Total
Flannigan field's sheet and rill erosion	—	—	—
Flannigan field's sediment yield to the stream	17.5	—	—
Flannigan field's sediment yield at Station No. 12	—	—	—
Total sediment load from sheet & rill at Station #12	10.9	—	—

Measured values from Flannigan's field and Station No. 12 represent only the suspended fine material passing through the measuring flumes. The main source of sediment from Flannigan's field was from sheet and rill erosion. The sediment at Station No. 12 represented what was produced from all sources, such as gullies, bed and bank, as well as sheet and rill erosion. Very little sediment was simulated from pasture areas. Although, there were significant gully sources observed in the pasture areas of the watershed of Station No. 12, plus bed and bank erosion within the channels. While total load measurements were taken frequently at several of the measuring flumes of Goodwin Creek, not enough measurements were obtained at Station No. 12 to develop the amount of sand produced from the watershed during this period. Over 20% of the total fine material at Station No. 12 was estimated by AnnAGNPS to be from sheet and rill sources. This corresponds to the conclusion by Grissinger et al. (1991) that 25% of the fine sediment material transported in the channels of Goodwin Creek were from upland sources and the rest were from channel or gully sources.

SUMMARY

AnnAGNPS is a pollutant loading model that can predict sheet and rill erosion's contribution to sediment yield from any field within the watershed at any location within the stream system. RUSLE is the basis for the sheet and rill erosion by particle-size class. HUSLE is used to estimate the total amount of sheet and rill erosion's sediment yield to the receiving reach of the stream. The procedure for determining field deposition described in this paper is used to determine the particle-size class distribution for this sediment yield to the receiving reach of the stream. A modified Einstein equation, modified by using the Bagnold equation to limit the sediment transport capacity, is used for sediment transport within the stream system. AnnAGNPS predicted values shows how well the relative behavior of the sheet and rill erosion responds to decreasing sediment yield as the sediment is transported downstream; i.e., continued deposition of sediment originating from within the fields—coarse sediment largely depositing in the fields and the fine sediment behaving predominately as wash load. This capability of AnnAGNPS provides a powerful tool in assessing the sediment loadings of best management practices within a watershed system. In developing management plans to address total maximum daily loads (TMDLs), states can utilize AnnAGNPS as science-based technology to meet their specific needs.

REFERENCES

Bagnold, R.A. 1966. An approach to the sediment transport problem from general physics. Prof. Paper 422-J. U.S. Geol. Surv., Reston, Va.

Bingner, R. L., C. E. Murphree and C. K. Mutchler. 1989. Comparison of sediment yield models on watersheds in Mississippi. Transactions of the ASAE 32(2): 529-534.

Bingner, R.L., R.W. Darden, F.D. Theurer, and J. Garbrecht. 1997. GIS-Based Generation of AGNPS Watershed Routing and Channel Parameters. ASAE Paper No. 97-2008, St. Joseph, Michigan. 4 pp.

Bingner, R.L. and F.D. Theurer. *In press*. Topographic factors for RUSLE in the continuous-simulation, watershed model for predicting agricultural, non-point source pollutants (AnnAGNPS). Soil Erosion for the 21st Century - An International Symposium, January 3-5, 2001 Honolulu, Hawaii. 4 pp.

Blackmarr, W. A. 1995. Documentation of Hydrologic, Geomorphic, and Sediment Transport Measurements on the Goodwin Creek Experimental Watershed, Northern Mississippi, for the Period 1982-1993 -- Preliminary Release. USDA-ARS-National Sedimentation Laboratory, Oxford, MS, Research Report No. 3, 143 pp.

Cronshey, R.G and F. D. Theurer. 1998. AnnAGNPS—Non-Point Pollutant Loading Model. *In* Proceedings First Federal Interagency Hydrologic Modeling Conference, 19-23 April 1998, Las Vegas, NV, p. 1-9 to 1-16.

Garbrecht, J. and L. W. Martz. 1993. Network and Subwatershed Parameters Extracted from Digital Elevation Models: The Bills Creek Experience. Water Resources Bulletin, American Water Resources Association, 29(6):909-916.

Garbrecht, J. and L.W. Martz. 1995. Advances in Automated Landscape Analysis. *In* Proceedings of the First International Conference on Water Resources Engineering, Eds. W. H. Espey and P. G. Combs, American Society of Engineers, San Antonio, Texas, August 14-18, 1995, Vol. 1, pp. 844-848.

Geter, W.F. and F.D. Theurer. 1998. AnnAGNPS – RUSLE Sheet and Rill Erosion. *In* Proceedings First Federal Interagency Hydrologic Modeling Conference, 19-23 April 1998, Las Vegas, NV, p. 1-17 to 1-24.

Grissinger, E. H., A. J. Bowie and J. B. Murphey. 1991. Goodwin Creek bank instability and sediment yield. *In* Proceedings of the fifth federal interagency sedimentation conference, March 18-21, 1991, pg. 5-51 to 5-60.

Renard, K.G. G.R. Foster, G.A. Weesies, D.K. McCool, and D.C. Yoder, coordinators. 1997. Predicting Soil Erosion by Water: A Guide to Conservation Planning with the Revised Universal Soil Loss Equation (RUSLE). U.S. Department of Agriculture, Agriculture Handbook No. 703, 404 pp.

SCS. 1986. Technical Release 55: Urban hydrology for small watersheds. Soil Conservation Service, USDA.

Theurer, F.D. and C.D.Clarke. 1991. Wash load component for sediment yield modeling. *In* Proceedings of the fifth federal interagency sedimentation conference, March 18-21, 1991, pg. 7-1 to 7-8.

Theurer, F.D., and Cronshey, R.G.,1998. AnnAGNPS-Reach Routing Processes. *In* Proceedings First Federal Interagency Hydrologic Modeling Conference, 19-23 April 1998, Las Vegas, NV.

Theurer, F.D., R.L. Bingner, W. Fontenot, and S.R. Kolian. 1999. Partnerships in Developing and Implementing AGNPS 98: A suite of water quality models for watershed use. *In* Proceedings of the Sixth National Watershed Conference, 16-19 May 1999, Austin, Texas. 10 pg.

Wischmeier, W.H. and D.D. Smith. 1978. Predicting rainfall erosion losses: A guide to conservation planning. U.S. Department of Agriculture, Agriculture Handbook. No. 537.

A SEDIMENT TRANSPORT AND YIELD MODEL FOR ALLUVIAL STREAMS

Leonard J. Lane, Hydrologist, USDA-ARS, Tucson, Arizona

Abstract: We have developed a sediment transport and yield model over the last 20 years. It is based on a hydrograph approximation technique, sediment transport equations for bed-load and suspend load, and the assumption that sediment transport rates are not limited by sediment supply. The model fits observed sediment transport and yield data from a variety of situations when sediment supply in the channels is non-limiting. The calibration and validation studies include data with varying discharge, varying proportions of bed load and suspended sediment, and varying stream channel and bed material characteristics. Validation studies in Arizona and New Mexico suggest the model is appropriate for the situations studied and can be used to predict sediment transport and sediment yield under similar circumstances as existed for the calibration and validation experiments.

INTRODUCTION

Sediment transport equations have been developed for steady, uniform flow conditions, or normal flow. For a comprehensive discussion of assumptions, limitations, and applications of the most commonly used sediment transport equations see Graf (1971). Erosion and sediment yield models usually incorporate normal flow-based sediment transport equations to compute sediment transport capacity for runoff hydrographs. However, runoff hydrographs exhibit unsteady and non-uniform flow, and thus, violate the normal flow assumption.

A method of applying sediment transport equations applicable for normal flow to unsteady and non-uniform flow involves approximating the runoff hydrograph. The approximation method herein uses a double triangle hydrograph. This in turn is approximated by a series of step functions wherein normal flow is assumed for each time interval but rates of flow vary from one time interval to the next (Lane, 1982; Lane et al., 1985; and Lane, 1987). The effects of these hydrograph distortions are unknown because validated sediment transport equations for unsteady and non-uniform flow do not exist.

The purpose of this paper is to describe development, calibration, and validation studies for a sediment transport and yield model based on the above hydrograph approximation technique and the assumption that sediment transport rates are not limited by sediment supply.

THE SEDIMENT TRANSPORT AND YIELD MODEL

Runoff hydrographs characteristic of many small watersheds can be well described by a double triangle approximation (e.g. Diskin and Lane, 1976). The double triangle hydrograph can further be approximated by a series of step functions over the duration of flow. This step function approximation matches the original runoff volume and flow duration exactly and assumes normal flow during each interval representing the hydrograph.

Normal flow is described by the Manning equation,

$$V = 1/n\ s^{1/2}\ R^{2/3} \qquad (1)$$

where:

V = average velocity (L/T),
n = Manning resistance coefficient ($T/L^{1/3}$),
s = slope of energy grade line often equal to the slope of the channel bed, and
R = hydraulic radius as the flow area divided by the wetted perimeter (L).

Einstein (1950) asserted that flow resistance due to the channel banks does not directly contribute to sediment transport on the channel bed. The total cross-sectional area can be divided into an area "pertaining" to the banks and an area "pertaining" to the bed. Relationships then can be developed relating the shear stress on the bed to the hydraulic radius of the bed, the unit weight of water, and the slope of the channel bed. Of the shear stress acting on the bed, a portion acts on cobbles, vegetation, other roughness elements and bedforms and the remainder is available to act upon the sediment particles (grain roughness).

An equation relating a representative grain size to its Manning's n value is of the form

$$n_g = a\,(d_{50})^{1/6} \qquad (2)$$

with d_{50} as the median particle diameter (L). Values of a in Eq. 2 generally range from 0.013 to 0.016 when d_{50} is in mm (see Simons and Senturk, 1992, pp. 281-286). With this information, the shear stress on sediment particles can be related to the hydraulic radius of the bed, the unit weight of water, and the slope of the channel bed.

An arbitrary distinction based on particle size rather than composition of the bed material was made by Lane (1982). The distinction was for particles larger and smaller than 0.062 mm with the larger particles traveling as bed load and the smaller ones traveling as suspended load. Bed material may travel on or near the bed at one flow rate and be suspended in the flow at a higher flow rate. Even so, it is convenient to assume the larger particles travel near the bed (i.e. as bed load). The bed load is modeled with one sediment transport equation. The smaller particles travel in suspension, i.e. suspended load, and are modeled with a second sediment transport equation. As described by Einstein (1950), wash load is not directly computed from open channel flow hydraulics as it originates in upland areas and is controlled by soil erosion processes.

The Duboys-Straub formula (see Graf, 1971) was modified to incorporate grain shear stress and to account for a distribution of particle sizes. The modified equation for bed load sediment transport is

$$g_{sb}(d_i) = \alpha\, f_i\, B_s\,(d_i)\, T_g\, [\, T_g - T_c\,(\, d_i\,)\,] \qquad (3)$$

with:

$g_{sb}(d_i)$= transport capacity per unit width for particles of size d_i (M/TL),
α= a dimensionless weighting factor to ensure that the sum of the individual transport capacities is equal to the transport capacity computed using d_{50},
f_i= fraction of particles in size class i,
d_i = representative diameter of particles in size class i,
$B_s(d_i)$ = a sediment transport coefficient (LT^3/M),
T_g = effective shear stress, bed shear acting on sediment particles (F/L^2), and
$T_c(d_i)$= a critical shear stress for particles in size class i (F/L^2).

Transport of particles smaller than 0.062 mm is computed based on a modification of Bagnold's Equation (Bagnold, 1966). In equation form, the modification is

$$g_{ss} = CAS\, f_{sc}\, T_g\, V^2 \qquad (4)$$

with:

g_{ss} = suspended sediment (<0.062 mm) transport rate per unit width (M/TL),
CAS = suspended sediment transport coefficient (T^3/L^2),
f_{sc} = fraction of particles smaller than 0.062 mm in the bed material,
T_g= effective shear stress (F/L^2), and
V = mean cross-sectional velocity of flow (L/T).

The total sediment yield, G_s, in units of mass flowing past a stream cross-section is then computed as the sum of the sediment < 0.062 mm from Eq. 4 and the summation of bed material transport from Eq. 3 summed over all size fractions, that is

$$G_s = g_{ss} + \sum [g_{sb}(d_i)] \qquad (5)$$

where the summation is over the index i, from i = 1 to i = the number of particle size classes used to characterize the bed sediment material. The resulting model calculates total sediment transport capacity and yield at a point on a stream channel. The model was last modified in 1998, therefore it is called APOINT98 hereafter.

Model Development and Applications: Data collected under near normal flow conditions from the Niobrara River near Cody, NE by Colby and Hembree (1955) were used to calibrate Eqs. 3 and 4 (Lane, 1982). Data from 27

observations on the Niobrara River resulted in a relationship between observed (q_s) and fitted sediment transport rates (g_s) as

$$g_s = 0.90\ q_s^{0.90},\ \text{with } R^2 = 0.97 \qquad (6)$$

Equation 5 and the hydrograph approximation were used with 47 runoff events from 4 small watersheds (less than 10 ha) on the Santa Rita Experimental Range near Tucson, AZ, and from one small watershed (3.7 ha) on the Walnut Gulch Experimental Watershed near Tombstone, AZ (Lane, 1982). The relationship between the observed (Qs) and fitted sediment yields (Gs) was

$$G_s = 0.91\ Q_s^{0.91},\ \text{with } R^2 = 0.78 \qquad (7)$$

In a subsequent study (Lane and Nichols, 1997) the sediment transport equations and the APOINT model were applied to data collected at 3 sites: 1) Muddy Creek, Wyoming, 2) Rio Grande near Bernalillo, New Mexico, and 3) Flumes 1 and 6 at Walnut Gulch, Arizona. Characteristics of the data are presented in Table 1.

Table 1. Summary of database characteristics from Lane and Nichols (1997).

				sediment transport		
Site	sampling dates	# events	discharge (cm/s)	suspended (kg/s)	bed load (kg/s)	sampler
Muddy Creek[1]	4/6 - 8/31/75	35	0.15 - 1.57	--	0.0039 - 0.82	Helly-Smith bedload sampler
Rio Grande[2]	4/25/52 - 5/19/61	21	35 - 286	42 - 870	45 - 840 [4]	US D-49
Walnut Gulch[3]	8/19/63 - 9/12/64	10	0 - 187	0 - 5930	--	US P61 and US DH48

[1] detailed sampling, measurements, and transport rates given by Andrews (1981)
[2] details given by Nordin (1964)
[3] details given by Renard and Laursen (1975)
[4] calculated using modified Einstein method for 2 events (Nordin, 1964)

Lane and Nichols (1997) found that for all 35 bedload measurements at Muddy Creek, 74% of the discrepancy ratios (defined as the ratio of computed to measured sediment transport rates) were within the range 0.5 to 2.0. Andrews (1981) reported that the percentage of discrepancy ratios in the range 0.5 to 2.0 for several sediment transport equations were as follows: Engelund and Hansen (1967) 77% without including samples for ripple bedforms; Yang (1973) 60% for all data; Shen and Hung (1972) 71% for all data; and Ackers and White (1973) 66% for all data. Therefore, for the Muddy Creek data, Lane and Nichols (1997) concluded that the proposed sediment transport procedure produces simulated sediment transport rates comparable in accuracy to several transport equations from the literature.

The sediment transport procedure was also applied to the Rio Grande data and the simulated bed material discharges for material coarser than 0.062 mm were compared to measured values of suspended sediment coarser than 0.062 mm. Discrepancy ratios ranged from 0.56 to 2.18 with only one of 21 values outside of the 0.5 to 2.0 range. From these analyses, Lane and Nichols (1997) again concluded that the proposed sediment transport calculation procedure produces reasonable results.

Runoff, and measured and simulated suspended sediment yield data for 10 unsteady, nonuniform flow events in 1963 and 1964 on the USDA-ARS Walnut Gulch Experimental Watershed were also modeled by Lane and Nichols (1997) using APOINT. The model was applied using values for Manning's n from 0.020 to 0.022. Application of the model resulted in an excellent degree of correspondence (discrepancy ratios varied from 0.56 to 1.11 and simulated sediment yields explained about 99% of the variance in observed sediment yields).

The Need for Additional Validation Studies: An important step in application of physically based models to determine sediment transport rates and yields is to conduct validation studies. These studies are tests of model performance to demonstrate the appropriateness/inappropriateness of a particular model for a specific application (e.g. see Sharika, et al., 2000). Thus, there is a critical need to perform validation studies on APOINT98, the model proposed herein. Additional validation studies are needed at data rich locations such as Walnut Gulch and at other locations where bed load transport is not as large a component of the total sediment load.

EXPERIMENTAL WATERSHEDS USED FOR VALIDATION STUDIES

The Walnut Gulch Experimental Watershed: The 149 sq. km Walnut Gulch Experimental Watershed (or Walnut Gulch) is a rangeland watershed located in southeastern Arizona, at approximately 31 degrees 45 minutes north latitude and 110 degrees west longitude. Elevations range from 1,250 m to about 1,900 m above MSL (Fig. 1). The climate in the Walnut Gulch area is classified as semiarid or steppe. Mean annual precipitation is about 320 mm with about 70% of the annual precipitation occurring from thunderstorms during the summer months. The remainder of the precipitation is usually associated with winter frontal storms with more general rains and less convective activity.

Walnut Gulch is located in the Basin and Range Province of the Southwest and is bounded on the southwest, south, and east by mountain blocks separated by broad alluvium filled basins. The northern 50 to 70% of the 149 sq. km drainage area consists of Quaternary and Tertiary alluvium, derived from the Dragoon Mountains. The remaining southern part of the watershed is composed of more complex geologic structures and composition including limestone, quartzite, and granite.

Soils on Walnut Gulch are mostly well drained, calcareous, gravelly to cobbly loams and are closely associated with the geologic features described above. Shrub vegetation, such as creosote bush, acacia, tarbush, and small mesquite trees, dominates (30 to 40% canopy cover) the lower two thirds of the watershed. The major grass species (10 to 80% canopy cover) on the upper third of the watershed are the grama grasses, bush muhley, and lovegrass, with some invasion of the shrub species and mesquite (Renard et al., 1993). Land use consists primarily of grazing, recreation, mining, and some urbanization. Sediment yield-watershed scale relationships for Walnut Gulch were described by Lane et al., (1997).

The Alamogordo Creek Experimental Watershed: The 174 sq. km Alamogordo Creek Watershed is located in east central New Mexico at approximately 34 degrees 53 minutes north latitude and 104 degrees 7 minutes west longitude (Fig. 1). The watershed is in a relatively flat, recessed basin with a steep escarpment surrounding most of the basin. Elevations range from 1420 m at the outlet to over 1680 m MSL at the upper end of the watershed. Sandstone formations underlie the basin and isolated outcrops in the main stream channels control local grades and gradients. Small areas of the watershed located on the mesa above the escarpment have shallow limestone layers overlying sandstone formations.

The climate at Alamogordo Creek is semiarid with mean annual precipitation of just over 350 mm. Soils are generally heavy in clay: clay to clayloams, to loamy soils, and are less well drained and cobbly than on Walnut Gulch. The central, relatively flat basin areas of Alamogordo Creek are grasslands dominated by grama grasses while juniper trees dominate the steeper escarpment area. Land use is primarily domestic livestock grazing. Additional information on the Alamogordo Creek Watershed is given in Drissel and Osborn (1968) and Renard et al. (1970).

The mean slope of the main stream channel on Alamorgodo Creek is about 0.58% compared with 1.2% at Walnut Gulch. Stream channels on both watersheds are classified as ephemeral. The steeper channels on Walnut Gulch contain coarser material (sands and gravels with up to a few percent silt and clay) in comparison with the finer material (mostly sands with a few percent up to as much as 30% silt and clay) at Alamogordo Creek. Thus, transmission losses (infiltration of streamflow to stream channel beds and banks) are less significant and transported sediment is much finer at Alamogordo Creek than at Walnut Gulch.

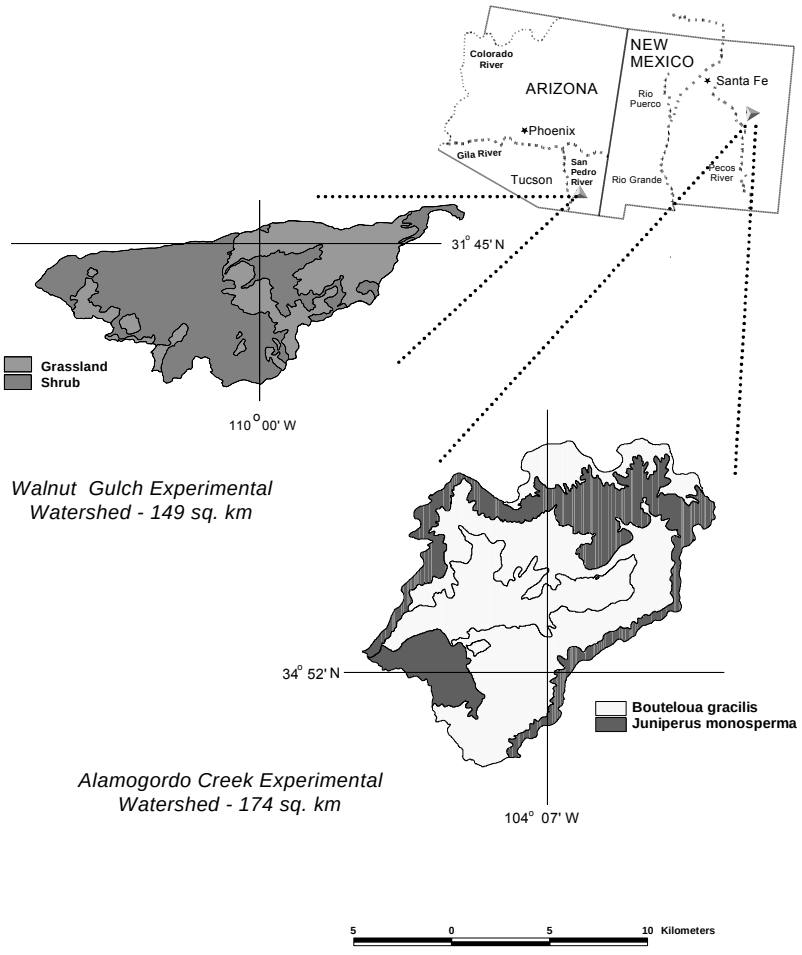

Figure 1. Location map of the Walnut Gulch Experimental Watershed in southeastern Arizona and the Alamogordo Creek Experimental Watershed in eastern New Mexico.

CALIBRATION AND VALIDATION STUDIES

Additional Analyses at Walnut Gulch: Nichols and Lane (2000) applied APOINT98 to data from a small watershed within Walnut Gulch. The APOINT model was calibrated and validated based on data collected during 49 runoff events at Flume 63.103 (Table 2). The flume is located in the main channel that drains the small, 3.68 ha watershed. Calibration was accomplished by varying Manning's n until a maximum R^2 value was obtained and the sum of squared errors was minimized. An optimal value of 0.021 was found for Manning's n.

Table 2. Summary of APOINT calibration and validation at Walnut Gulch Watershed 63.103, 3.68 ha.

Item	Total Sediment Yield (t/ha)			
	Calibration		Validation	
	Observed	Simulated	Observed	Simulated
Number Of Events	24	24	25	25
MEAN	0.404	0.342	0.355	0.355
SD	0.538	0.527	0.652	0.829
Regression Equation	Y= -0.024 + 0.90X		Y = -0.087 + 1.23X	
R^2		0.85		0.98

where Y = simulated sediment yield (t/ha) and X = observed sediment yield (t/ha)

Both the calibration and validation simulations matched the observed means and standard deviations well within the 95% confidence limits. The calibration simulations explained 85% of the variation in observed sediment yield data and the validation simulations explained 98% of the variance.

Analyses at Alamogordo Creek: The APOINT98 model was calibrated to 11 runoff events with measured sediment concentration data. Calibration consisted of varying Manning's n until the value of R^2 was maximized and the sum of squared errors was minimized. A value of n= 0.031 was found to be optimal. The model with n=0.031 was then applied to the 12 validation events, also with measured sediment concentration data, which were not used in the calibration. The results are summarized in Table 3.

Table 3. Summary of APOINT calibration and validation at Alamogordo Creek Watershed, 17,400 ha.

Item	Total Sediment Yield (t/ha)			
	Calibration		Validation	
	Observed	Simulated	Observed	Simulated
Number Of Events	11	11	12	12
MEAN	0.189	0.189	0.081	0.101
SD	0.473	0.457	0.171	0.174
Regression Equation	Y= 0.0065 + 0.97X		Y = 0.022 + 0.97X	
R^2		0.998		0.915

where Y = simulated sediment yield (t/ha) and X = observed sediment yield (t/ha)

Both the calibration and validation simulations matched the observed means and standard deviations well within the 95% confidence limits. The calibration simulations explained over 99% of the variation in observed sediment yield data and the validation simulations explained 92% of the variance.

CONCLUDING REMARKS

The APOINT98 model has evolved over the last 20 years and has been shown to fit observed sediment transport and yield data from a variety of calibration and validation studies, when sediment supply in the channels was non-limiting. The calibration and validation studies included data with varying discharge, varying proportions of bed load and suspended sediment, and varying stream channel and bed material characteristics. Validation studies in Arizona and New Mexico suggest the model is valid for the situations studied and can be used to predict sediment transport and sediment yield under similar circumstances as observed in the calibration and validation experiments. However, it should be noted that sediment yield data are often dominated by total runoff volume. If measured runoff volumes are used to compute sediment yields then the simulated and measured values will agree very well if mean sediment concentration is accurately estimated. This was the case for the validation studies reported herein.

ACKNOWLEDGMENTS

I gratefully acknowledge the USDA-ARS employees who have operated and maintained the Walnut Gulch and Alamogordo Creek Experimental Watersheds over the years, making this research possible. I also acknowledge funding and support provided by the USDA-ARS Southwest Watershed Research Center, Tucson, AZ. Finally, the reviewers of this manuscript helped to improve it significantly.

REFERENCES

Ackers, P. and White, W. R., 1973, Sediment Transport; New approach and analysis. Journal of the Hydraulics Division, ASCE, Vol. 99, (No. HY11), 2041-2060.

Andrews, E. D.,1981, Measurement and Computation of Bed-Material Discharge in a Shallow Sand-Bed Stream, Muddy Creek, Wyoming. Water Resources Research, Vol. 17, (No. 1), 131-141.

Bagnold, R. A.,1966, An Approach to the Sediment Transport Problem from General Physics. U. S. Geological Survey Professional Paper 422-I.

Colby, B. R., and Hembree, C. H., 1955, Computation of Total Sediment Discharge Niobrara River near Cody, Nebraska. U. S. Geological Survey Water Supply Paper No. 1357.

Diskin, M. H., and Lane, L. J., 1976, Application of a Double Triangle Unit Hydrograph to a Small Semiarid Watershed. Hydrology and Water Resources in Arizona and the Southwest, Office of Arid Land Studies, Univ. Of Arizona, Vol. 6, 125-135.

Drissel, J. C. and Osborn, H. B., 1968, Variability in Rainfall Producing Runoff from a Semiarid Rangeland Watershed, Alamogordo Creek, New Mexico. J. of Hydrology, 6, 194-201.

Einstein, H. A., 1950, The Bed-load Function for Sediment Transportation in Open Channel Flow. U. S. Department of Agriculture, Technical Bulletin No. 1026.

Engelund, F. and Hansen, E., 1967, A Monograph on Sediment Transport in Alluvial Streams. In Teknisk Vorlag, Technical University of Denmark, Copenhagen, Denmark. 63 pp.

Graf, W. H., 1971, Hydraulics of Sediment Transport. McGraw-Hill Book Company, New York. 513 pp.

Lane, L. J., 1982, Development of a Procedure to Estimate Runoff and Sediment Transport in Ephemeral Streams. In Recent Developments in the Explanation and Prediction of Erosion and Sediment Yield, IAHS Publ. no. 137, 275-282.

Lane, L. J., Becker, N. M., and Purtymun, W. D., 1985, New Estimating Procedures for Surface Runoff, Sediment Yield, and Contaminant Transport in Los Alamos County, New Mexico. Los Alamos Nat. Lab. Report, LA-10335-MS, 50 pp.

Lane, L. J., 1987, Hydrology Component: Water Routing and Sedimentation. Chapter 5 In: SPUR Simulation of Production and Utilization of Rangelands Documentation and User's Guide. U. S. Department of Agriculture ARS-63, 41-56.

Lane, L. J., Hernandez, M. and Nichols, M., 1997, Processes Controlling Sediment Yield from Watersheds as Functions of Spatial Scale. J. of Environ. Modelling and Software, 12(4), 355-369.

Lane, L. J. and Nichols, M. H., 1997, A Hydrologic Method for Sediment Transport and Yield. In: Management of Landscapes Disturbed by Channel Incision. Eds. S. Y. Wang, E. J. J. Langendoen, and F. D. Shields, Jr., Center for Comp. Hydrosci. And Eng., University of Mississippi, Oxford, MS, May 1997, 365-370.

Nichols, M. H. and Lane, L. J., 2000, An Integrated Systems Approach to Modeling Sediment Yield from Rangelands. Presentation and paper at the ASCE Watershed Management 2000 Conf., In: Science and Engineering Technology for the New Millennium, Colorado State Univ., Ft. Collins, CO, June 20-24, 2000, ISBN 0-7844-0499-2, 8 pp.

Nordin, C. F., 1964, Aspects of Flow Resistance and Sediment Transport Rio Grande near Bernalillo New Mexico. U. S. Geological Survey Water-Supply Paper 1498-H. 40 pp.

Renard, K. G., Drissel, J. C. and Osborn, H. B., 1970. Flood Peaks from Small Southwest Range Watershed. J. Hyd. Div., ASCE, 96(HY3), Proc. Paper 7161, 773-785.

Renard, K. G. and Laursen, E. M., 1975, Dynamic Behavior Model of Ephemeral Stream. Journal of the Hydraulics Division, ASCE, Vol. 101, No. HY5, 511-528.

Renard, K. G., Lane, L. J., Simanton, J. R., Emmerich, W. E., Stone, J. J., Weltz, M. A., Goodrich, D. C., and Yakowitz, D. S., 1993, Agricultural Impacts in an Arid Environment: Walnut Gulch Studies. Hydrol. Sci. and Tech., 9, 145-190.

Sharika, U. S., Ogden, F. L., Downer, C. W., and Sharif, H. O., 2000, On the Calibration and Verification of Two-Dimensional, Distributed, Hortonian, Continuous Watershed Models. Water Res. Research, 36 (6), 1495-1510.

Shen, H. W., and Hung, C. S., 1972, An Engineering Approach to Total Bed-material Load by Regression Analysis. In Sedimentation Symposium Proceedings, ed. H. W. Shen, 14-17.

Simons, D. B. and Senturk, F., 1992, Sediment Transport Technology, Water Resources Publications , Littleton, Co. 897 pp.

Yang, C. T., 1973, Incipient Motion and Sediment Transport. Journal of the Hydraulics Division, ASCE, Vol. 99, (No. HY10), 1679-1704.

Leonard J. Lane
USDA-ARS
Southwest Watershed Research Center,
2000 E. Allen Rd.
Tucson, AZ 85719
Tel. 520-670-6380, Fax 520-670-5550
Email: **ljlane@tucson.ars.ag.gov**

MODES OF SHALLOW AND DISPERSED PARTICULATE TRANSPORT IN SLOPING CHANNELS

By D. Pal, Research Associate, University of Mississippi, University, MS; S. N. Prasad, Professor of Civil Engineering, University of Mississippi, University, MS; M. J. M. Römkens, Soil Physicist / Agricultural Engineer, USDA ARS National Sedimentation Laboratory, Oxford, MS.

Abstract: The evolution of spatially periodic features in sediment beds are routinely observed in natural flow conditions. Especially, sediment transport in steep channels can be highly dynamic in nature. Sediment transport involves crucial parameters such as bed slope, flow depth, flow velocity, particle concentrations, particle size distributions and topographic irregularities. The evolving modes of the sediment phase are not only dependent on the associated unsteady fluid dynamics, but can exhibit organizational structures of its own. Though it is commonly assumed that large-scale vorticities in the carrying fluid are responsible for the generation of such structured flow-fields, the observations in this study demonstrate that intrinsic organization in the particulate phase can also occur under the action of a steady driving force such as gravity. Our study concentrates on the possible similarities and dissimilarities between the origins of structured flow in dispersed solid medium and in the fluid.

INTRODUCTION

The study on the formation of dunes, antidunes, sand-bars and sand-ripples in channel processes began more than 100 years ago. Most of the bed-features in rivers and channels are, in general, periodic in the streamwise flow direction and have their own characteristic scales established over a long period of time. Depending on the magnitude of the flow velocity and its gradients, the spatial scale of the bed features can attain a multitude of wavelengths and velocities. In cases of deep channel flows, where the flow remains subcritical (i.e., $Fr < 1$, where Fr is the Froude number based on the mean velocity of transport and the mean flow depth), the relatively slow process of sediment dynamics close to the bed is often overlooked. Until now, it has been assumed that the erosion and subsequent transport of these particles depend solely on the surface shear stress generated by the velocity profile. The attainment of a critical shear stress at the bed is considered to be the criterion for threshold movement of sediment. The effect of the variations in free surface profiles in channel flows is related to the evolution of bed features through the large-scale vorticity fields in the carrying fluid. In this description, however, no valid argument is presented as to the cause of the natural selection process of establishing specific length and time scales. The application of simplified analytical tools such as linear stability analysis also does not precisely predict the existence of these scales of organized flow.

In shallow channel flows, the effect of a large-scale vorticity field in the fluid medium is always substantially weaker than that in deep channel flows. Overland concentrated flows are often associated with the presence of nonlinear periodic waves in shallow water. These waves are caused by an inequality condition between the surface slope and the surface resistance to the

flow (Dressler, 1949). As the flow energy concentrates in these wave-fronts, the waves transfer energy from the fluid to the sediment on the channel bottom. The authors have previously demonstrated (Pal et al., 2000) the effect of these periodic waves in enhancing the sediment transport rate in shallow channel flows. Thus the issue remains whether the presence of water waves is the only driving mechanism for an organized mode of sediment transport on the channel bed. Our observations of grain waves in dry chute flows (Prasad et al., 2000a, Pal et al. 1999) strongly suggest that the particulate phase itself can exhibit a strong tendency to organize provided certain flow conditions are met. The phenomena of two distinct kinds of self-organization processes at identifiable wavelengths depend on the energy condition of the particles in the two-phase mixture of dispersed solid and the interstitial fluid. In the first mode, referred to as a mid-inertial regime of granular organization, the particles exhibit progressive and periodic density waves that propagate at a smaller velocity than the average particle velocity in most part of the rarefied flow-field (Pal et al. 1999). The waves are characterized by abrupt increases in the volumetric solid fraction of the flowing medium, though the average flow depth does not show a noticeable change in the longitudinal flow direction. In the second mode, referred to as the fully-inertial regime of granular organization, periodic grain waves similar to shallow water waves are observed. The particulate phase not only shows density waves, but there is a substantial variation in the free surface of the dry and dispersed granular flow (Pal et al. 1999). The propagation velocity of such waves is greater than the particle velocity at any point inside the shallow flow.

In view of these observations, it seems more than likely that the sediment dynamics in channel flows must also be governed by the same kind of energetic processes present in dry transport of particles on steep inclines. Though it is understood that the added coherent structures of fluid turbulence in channel flows can dissipate flow energy at a preferred range of the energy spectrum, the flow features in the particulate phase are mostly quite large compared to the scales of turbulent eddies. Since natural sediment contains a wide range of particle sizes and shapes, it is also important to study the organizational dynamics of granular mixtures. The smaller-scale processes such as separation and mixing between constituent sizes can, in fact, play a major role on the character of these organized structures on the channel bed.

EXPERIMENTAL OBSERVATIONS

Observations in Sediment-Laden Channel Flows: In order to illustrate the importance of sediment dynamics in shallow overland flows, a channel flow experiment was conducted. The details of the experimental set-up and the procedures are given in Pal et al. (2000). A channel of 6.75 cm width and 320 cm length was used in this experiment. The channel slope could be varied with the help of a traversing mechanism located underneath the channel. Instead of having a pre-formed sediment-bed on the channel, the sediment was fed from a hopper-feeder arrangement and its subsequent passage was observed downstream. The sediment feed-rate was controlled by a pair of electromagnetic vibrators fitted to the hopper-feeder device. The average particle diameter of coarse sand used in this case was 1 mm. The small channel width and relatively large particle size kept the flow nearly two-dimensional. In order to reduce the fluid inertia relative to the suspended sand particles, the channel slope was kept constant at 1% and the average water flow rate was maintained at 10 liters/min. Though the associated local Froude number still remained in the range of high subcritical (Fr . 0.8) to low supercritical values (Fr . 1.2), the mean

flow velocity was reduced in the range of 0.25 to 0.4 m/sec at this channel slope. The average flow depth was approximately 1 cm. Though the shallow flow was associated with water waves, the corresponding wave height above the average free-surface elevation was less than 0.2 cm.

Figure 1 shows a sequence of channel flow conditions consisting of increasing sediment additions for the aforementioned flow rate. The sediment remains dispersed in the beginning when almost all the added particles are transported in a steady manner. Subsequently, as more sediment is added, the mode of sediment transport becomes unsteady and the sediment particles start forming large clusters that at some stage have length scales comparable to the width of the channel. Depending upon the flow condition, these sediment waves can be moving forward, backward or stay stationary along the length of the channel. The process of this spatial organization of the sediment phase continues until a maximum rate of sediment addition is reached beyond which the flow of water also shows a strong longitudinal variation in its free-surface elevation due to the presence of sediment waves. The resultant longitudinal structures in the sediment phase is, in fact, created by the interaction of the scales of organization in the fluid and the dispersed solid media. The variability in the free-surface elevation can be distinctly identified by the creation of periodic scour holes (high fluid velocity) and sediment deposition regions (low fluid velocity) along the length of the channel (Fig. 1).

In this experiment with comparatively weaker water-wave conditions, the strong interaction between the fluid and the solid phase occurs through an energy sharing mechanism which eventually results in spatial heterogeneity in both phases. It seems that the wave mode of transport is an optimal condition for both the fluid and the suspended sediment. The appearance of spatial structures similar to ripples and dunes can be viewed as a manifestation of variations in the total flow energy instead of treating the sediment phase as only a boundary of deformable shape (Kennedy 1963, Reynolds 1965). The wave-like bedforms, whether moving forward, backward or being stationary, are intrinsically caused by the interaction of limit-cycle energy dissipation processes that exist in both phases. The energy sharing mechanism minimizes the total energy dissipated near the discontinuities of the flowing sediment phase and a quasi-steady transport rate is established. This treatment of the two-phase system is expected to provide an insight into the instantaneous rates of local erosion and sediment transport without depending solely on the critical shear concept.

Granular Organization: The effect of periodic organizations due to large-scale vorticity fields in the fluid medium can be eliminated by providing a steady source of energy to the dispersed granular medium. The spatially uniform supply of energy can be easily derived from the gravitational potential as first shown experimentally by Prasad et al. (2000a). Low-density gravitational flows of grains on an inclined plane go through several distinct phases (Pal et al. 1999) as the material flow rate is gradually increased. Beyond the limit of a thermo-mechanical state of equilibrium that maintains spatial homogeneity in the granular medium, a layer of saltating and spinning particles begins to show periodic organization features in the form of waves. The grain waves are primarily of two-different types: the first shows only density variations (mid-inertial regime) and the second one shows variations both in density and flow depth (fully-inertial regime). In view of the relatively slow processes of granular organization in natural streams, it is likely that an organization process through density variations alone can be strong in such less-energetic flow situations.

Density Waves: In our experiments with dry grain flow, the width and length of the inclined channel were 57 mm and 3.6 meter, respectively. The width of the channel was large compared to the particle diameters which ranged between 106-500 μm. Solid glass spheres (specific gravity = 2.5) were used in this experiment as the particulate medium. The details of this experimental set-up, the control mechanisms for material flow rate (*Q*) and the measurement procedures are described in Prasad et al. (2000a). In order to observe granular organization in the form of slow-moving density waves, the grain flow experiments were conducted for three combinations of grain diameter (d_{av}) and channel slope (*2*) as shown in Table 1. The average particle diameter in each material was based on the arithmetic average of the maximum and minimum grain diameters in a size range. The average sphericity of particles in materials **M1** and **M2** differed by 10% and the choice of channel slope had to be made based on the regularity in particle shape. More irregular particle shapes needed higher channel slopes to exhibit a comparable flow state at similar material flow rates. Figure 2 shows the observed difference between the flow states at a small flow rate (40 gms/min) and at a comparatively larger flow rate (90 gms/min) for **M1** at *2* = 26E. The flow direction is from the top to the bottom of the frames. As particles are fed into the channel, each particle tends to establish a terminal transport velocity appropriate for the given surface condition of the channel and the average solid fraction ($<_v$) of the flowing medium. The average volumetric solid fraction is the fraction of total volume occupied by the solid particles only in the gas-solid mixture. When the material flow rate is maintained below the lower threshold of granular organization (e.g., $<_v < 0.003$), the flow appears practically homogeneous. As the material flow rate is increased beyond this lower threshold, density waves appear with regular wavelengths and detectable wave velocities. Due to the additional frictional resistance offered by the side walls, faster moving particles at the central plane of the channel dissipate more energy with increased inter-particle collisions and form the wavefronts within a shorter time period than the slower moving particles near the side-walls. The relative concentration of particles across a shockfront changes rapidly due to the loss of excess kinetic energy fluctuations (i.e., granular temperature) at the front. The wavefronts are sharper at the rear and diffuse gradually towards the front of each wavelength as particles continue to accelerate in the direction of mean flow.

Figure 3 shows the distribution of average wavelengths (*8*) and wave velocities (*c*) for all three materials tested in our study. The average velocity of the density waves is always smaller than the individual particle velocities at any point in the dispersed flow region within a wavelength. In the domain of organized flow, both wavelength and wave velocity reduced with increasing flow rate. The vertical bars represent the extent of measurement error (i.e., standard deviation over the mean) at each data point. Due to dispersive effects, wave coalescence occurred intermittently and resulted in a wide range of observed wavelengths at the measurement station. The rate of change of average wavelength with material flow rate rapidly decreases as the organization through density variations becomes complete. The variation in flow depth within each wavelength of flowing grains is not substantial in density waves. Though the trend of flow-depth vs. flow-rate (Prasad et al., 2000b) shows a monotonic decrease in flow-depth through increased intensity of condensation in fluctuating kinetic energy, this mechanism is not the primary reason for the appearance of density waves. In fact, the rate of increase in the volumetric solid fraction itself is much larger at the lower threshold of organized grain flow.

Waves in Rapid Flows : Compared to the phenomenon of slow-moving density waves in dispersed granular flows, a fully inertial regime of flow often exhibits periodic waves with variations in both density as well as flow depth. A fully inertial regime of periodic granular flow is created when both the channel slope (*2*) and the material flow rate (*Q*) are increased beyond the mid-inertial flow regime. These kinds of waves have been described in detail by the authors (Prasad et al. 2000a) as a closer analogy to roll waves in shallow water flows. Though there is a smooth variation in the volumetric solid fraction within each wavelength of the flowing gas-solid two-phase medium, the abrupt change in the wave-like structures is most apparent in the flow depth. Therefore, the appearance of shock in the flowing medium is more like that in shallow water waves where wave-heights (i.e., the difference of free-surface depth across a wavefront) can be as large as the mean flow depth itself.

Since our primary interest in this study is to investigate the relevance of wave-modes in sediment transport processes, the mechanics of transport in granular mixtures has been addressed in detail. Natural sediment consists of a large range of particle sizes and shapes. Therefore, the dynamics of a mixture of such constituent entities should be influenced by their relative percentage of total mass in the mixture. A set of experiments with binary granular mixtures was performed in the same experimental set-up of dry granular flows where the relative proportion of the constituents was also varied. Table 2 shows the different mixture constituents and their mass fractions used in the experiments. While proportions 1 and 2 (i.e., **P1** and **P2**) were used for all three mixtures (**MX1**, **MX2** and **MX3**), proportion 3 (i.e., **P3**) could only be used for **MX1**. The average particle diameters of the large and small sizes are represented by d_l and d_s, whereas m_l and m_s stand for the mass fractions of the large and small sizes, respectively. All grain flow experiments for the granular mixtures were conducted at a single channel inclination of *2* = 26E.

When spherical particles of two different sizes are mixed and allowed to flow at small depth under the action of gravity, both sizes experience transverse segregation normal to the direction of mean flow (Savage and Lun, 1988). This partial segregation of two different sizes takes place by virtue of their relative weights and their mean kinetic energy. Though the initial flowing mixture is approximately homogeneous, the smaller particles tend to fill up the void spaces between the larger particles and, therefore, precipitate under the action of gravity. When the mass flow rate of the mixture is small, the inter-particle distance between the larger particles increases between saltations. The smaller particles tend to form a layer next to the boundary and act as a passive damper to saltation impacts. As the large particles saltate in and out of the small particles, they transfer part of their excess kinetic energy to the smaller particles. This process keep the mixture in a state of dynamic equilibrium and prevent total segregation of one size from the other. As the overall flow rate increases, the depth of the wall layer also increases. This build-up effectively consumes a large part of the saltation energy and the flow of mixture enters the wave regime of particle dynamics. Typically, the rarefied regions of the dynamic waves in the fully inertial flow regime are long (– 80% of the wavelength) compared to the dense regions. The demarcation between these two regions is defined by shockfronts. The nature of the waves in terms of wavelength and wave velocity (*c*) depends on the slope of the inclined surface, i.e., the available potential energy per unit mass of the grains, and the average resistive stress in the population of particles. When the waves pass through the medium, it enhances mixing of particles near the shockfront. In the deceleration region of the wavelengths, where the free surface of the granular mass steepens much like shallow water waves, inter-particle distances

reduce quickly. Near the shockfront, the volumetric solid fraction of the particles increase, causing energy dissipation through inter-particle collisions. In a binary mixture of varied mixture proportions, the overall dynamic response of the mixture exhibits the relative importance of inertial and geometric effects on energy transfer and dissipation mechanisms. The longitudinal segregation of particles now takes place solely by virtue of differential acceleration/deceleration of different sizes of particles. As can be viewed in Fig. 4, the large particles tend to float at the top of the mixture and occupy most of the volume near the wavefronts. The rate of change of $<_v$ in the flow of large particles itself becomes more rapid compared to that of the smaller particles near the wavefronts. As shown in Fig. 5, the wave velocities (c) in the fully-inertial regime of flow increases with increased material flow rate of the mixture(Q). The average wave velocity is always larger than the individual particle velocities within each wavelength of flow.

SUMMARY

In view of the above discussions on organized flow of grains in sediment laden channel flows and in dry granular flows, it is evident that flowing particles can exhibit self-organization modes. The typical nature of such organization, manifested as progressive waves, depends on the energetic condition of the dispersed granular mass. When certain threshold conditions are exceeded, the particles choose to flow in a structured way to minimize energy dissipation in the solid-fluid mixture and maximize the rate of overall transport for a given flow condition.

REFERENCES

Dressler, R.F., 1949, Mathematical Solution of the Problem of Roll Waves in Inclined Open Channels. Communications on Pure and Applied Mathematics, New York University 2, 149-194.

Kennedy, J. F., 1963, The Mechanics of Dunes and Antidunes in Erodible-Bed Channels. Journal of Fluid Mechanics 16, 521-544.

Pal, D., Prasad, S. N., Römkens, M. J. M., 1999, Periodic Waves in Shallow Granular Flows. Proceedings of the 3rd ASME/JSME Joint Fluids Engineering Conference, San Fransisco, California, FED-Vol. 248.

Pal, D., Prasad, S. N., Römkens, M.J.M., 2000, Optimal Mode of Sediment Transport by Shallow Flows in Upland Areas. International Journal of Sediment Research 15, 260-267.

Prasad, S.N., Pal, D., Römkens, M.J.M., 2000a, Wave Formation on a Shallow Layer of Flowing Grains," Journal of Fluid Mechanics 413, 89-110.

Prasad, S.N., Pal, D., Römkens, M.J.M., 2000b, Density Waves in a Saltating Layer of Flowing Grains. Journal of Fluid Mechanics, in review.

Reynolds, A. J., 1965, Waves on the Erodible Bed of an Open Channel. Journal of Fluid Mechanics 22, 113-133.

Rose, C. W., Williams, J. R., Sander, G. C., Barry, B. A., 1983, A Mathematical Model of Soil Erosion and Deposition Processes: I. Theory of a Plane Land Element. Journal of the Soil Science Society of America 47, 991-995.

Savage, S.B., Lun, C.K.K., 1988, Particle size segregation in inclined chute flow of dry cohesionless granular solids. Journal of Fluid Mechanics 189, 311-335.

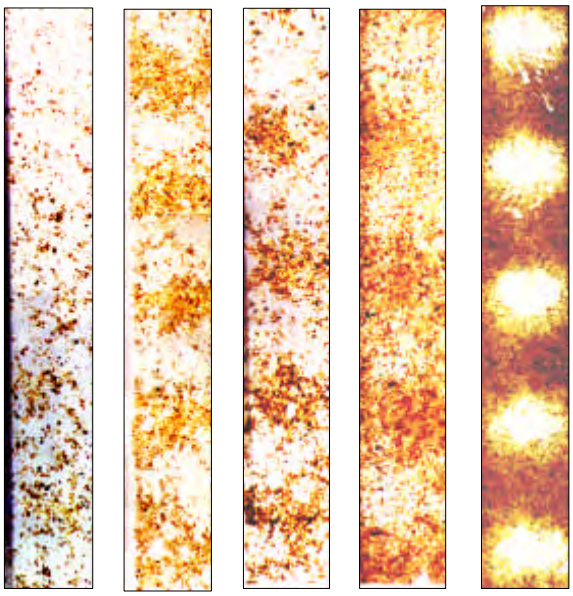

Figure 1. The sequence of photographs from left to right shows granular organization with increasing sediment feed-rate in shallow channel flows. The flow direction is from top to bottom of each frame. The channel slope and the volumetric flow rate were 5% and 10 liters/min, respectively. Experiments were performed with coarse sand (approx. d_{av} = 1.5 mm). As the sediment feed rate is increased for a constant volumetric flow rate of water, the sediment phase organizes with distinguishable wavelength and progresses downstream with a much smaller wave velocity compared to the bulk velocity of transport.

Table 1.

Material Designation	Diameter Range and Sphericity	Average Diameter (d_{av})	Channel Slope (*2*)
M1	200-250 :m 85% spherical	225 :m	26E
M2	200-250 :m 95% spherical	225 :m	23E
M3	300-350 :m 95% spherical	325 :m	20E

(a) (b)

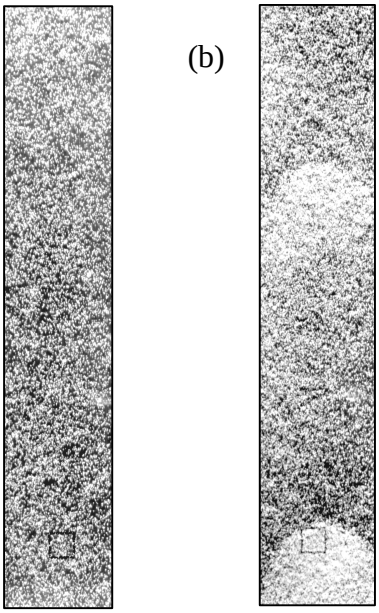

Figure 2. Photographs of a typical homogeneous state of grain flow and subsequent density waves for **M1** at *2* = 26E. The flow direction is from the top to the bottom of each frame.
(a) Homogeneous state at Q = 40 gms/min,
(b) Periodic density fronts at Q = 90 gms/min.

Table 2.

Mixture	Proportion **P1**: m_l = 50%, m_s = 50%	Proportion **P2**: m_l = 25%, m_s = 75%	Proportion **P3**: m_l = 75%, m_s = 25%
MX1: d_l = 213.5 :m d_s = 106.5 :m	T	T	T
MX2: d_l = 500 :m d_s = 213.5 :m	T	T	ς
MX3: d_l = 500 :m d_s = 106.5 :m	T	T	ς

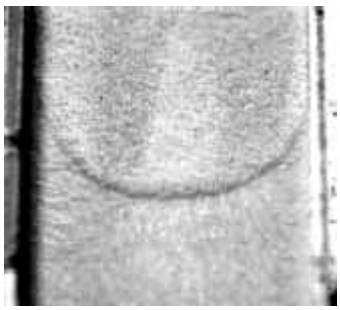

Figure 4. Wave mode of transport in the fully inertial regime of shallow flow of a granular mixture (**MX3**, **P2**) at *2* = 26E. Larger particles accumulate at the wavefront and transfer its energy to the smaller particles to keep the entire mixture in a mobile state.

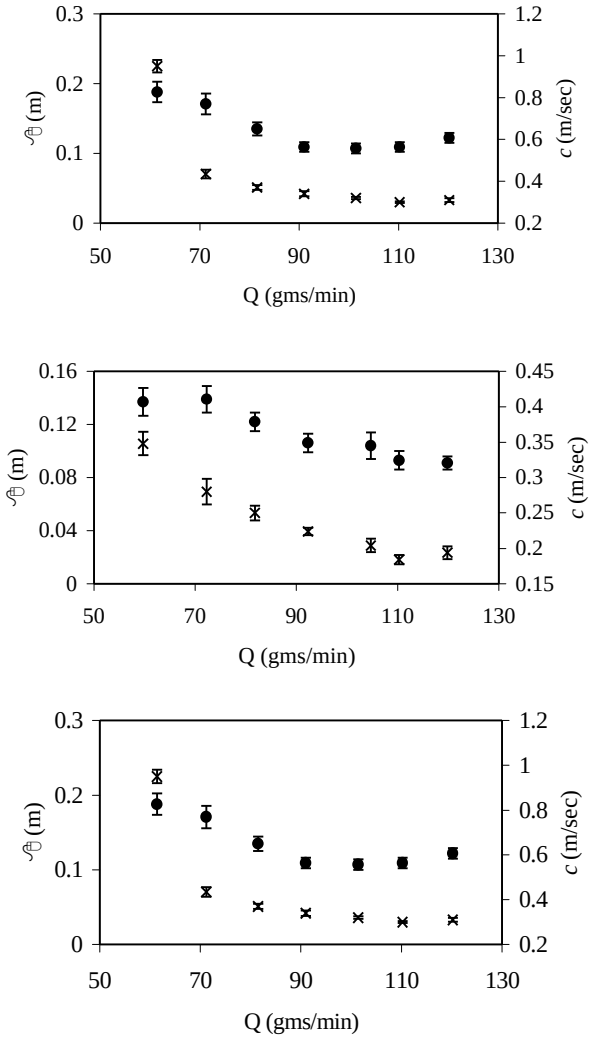

Figure 3. Variation of wavelength (*8*) and wave velocity (*c*) with material flow rate (*Q*) in mid-inertial regime of granular organization. (a) **M1** at *2* = 26E, (b) **M2** at *2* = 23E, and (c) **M3** at *2* = 20E.

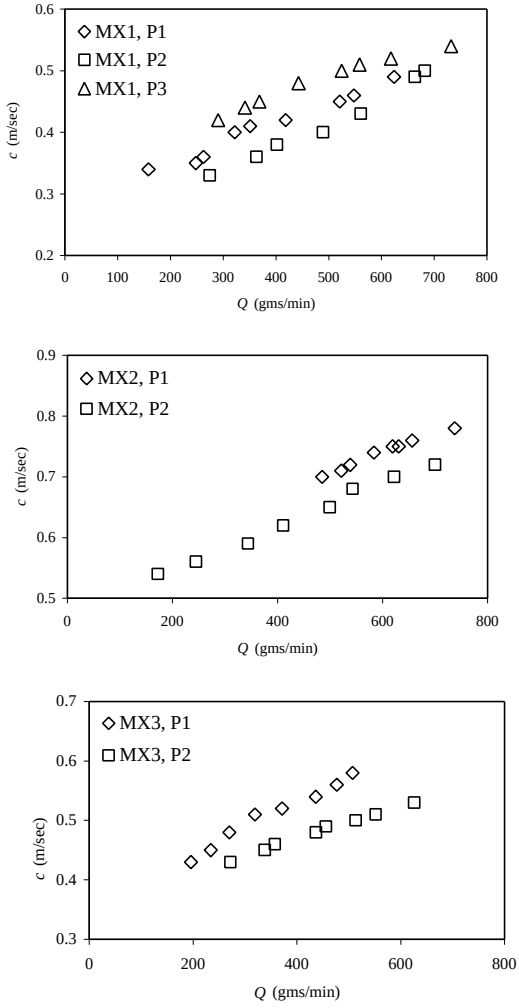

Figure 5. Variation of wave velocity (*c*) with material flow rate (*Q*) in fully-inertial flow regime of granular mixtures. All experiments performed at a channel slope of *2* = 26E. (a) **MX1**, (b) **MX2** and (c) **MX3**.

TECHNIQUES FOR ESTIMATING SEDIMENT YIELD OF UNGAGED TRIBUTARIES ON THE SOUTHERN COLORADO PLATEAU

By R.H. Webb, Research Hydrologist, P.G. Griffiths, Hydrologist, and D.R. Hartley, Hydrologic Technician, U.S. Geological Survey, Tucson, Arizona

Abstract: Numerous regional sediment transport data are used to evaluate three techniques for estimating streamflow sediment yield from ungaged tributaries of the Colorado River in Grand Canyon. These techniques include: (1) a regression equation relating drainage area to sediment yield for all relevant sediment-yield data from northern Arizona, (2) an empirical relation developed by Renard (1972) selected from 8 potentially relevant methods, and (3) a new procedure that combines regional flood-frequency analysis with sediment-rating curves. Results based on techniques (1) and (2) are not significantly different. The third technique requires numerous assumptions, most notably that sediment yield on a decadal average can be described by several floods of recurrence intervals of 2 yr, 5 yr, and 10 yr described by regional flood-frequency relations. Using data collected at gaging stations, we develop a relation between peak discharge and total-event sediment yield derived from hydrographs and sediment-rating curves. This third technique produces sediment yield estimates comparable to those of the regional data regression and Renard (1972) relations and may be a more robust technique for estimating sediment yield when streamflow data are available.

INTRODUCTION

Roughly 768 tributaries of the Colorado River drain the Grand Canyon in northern Arizona (fig. 1). Ranging in size from < 0.1 to 934 km^2, with a mean basin area of 16 km^2 (fig. 2), these ungaged tributaries have ephemeral flow, generating seasonal floods in summer and winter, and cut through bedrock that is predominantly sedimentary. Sediment data from these tributaries are virtually nonexistent, and data from the canyon in general are limited to those collected at gaging stations on the Colorado and its major tributaries (the Paria and Little Colorado Rivers, and Kanab and Havasu Creeks; fig. 1) (Garrett et al. 1993; Rote et al. 1997). However, the southern Colorado Plateau has a wealth of sediment-transport data that can be used to estimate sediment yield from ungaged tributaries. We used three methods to estimate streamflow sediment yield: (1) a regression equation relating drainage area to sediment yield for all relevant sediment-yield data from northern Arizona, (2) an empirical relation developed by Renard (1972), and (3) a new procedure that combines regional flood-frequency analysis with sediment-rating curves. All three methods are compared against regional data to evaluate their appropriateness for estimating sediment yield in Grand Canyon.

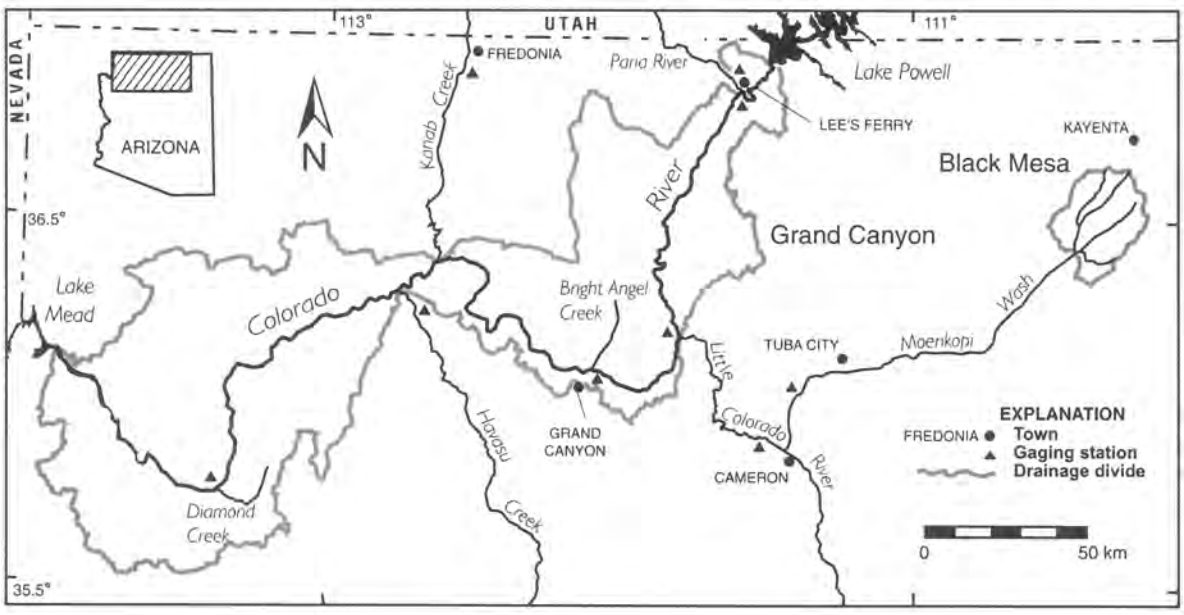

Figure 1. The Colorado River and major tributaries in northern Arizona.

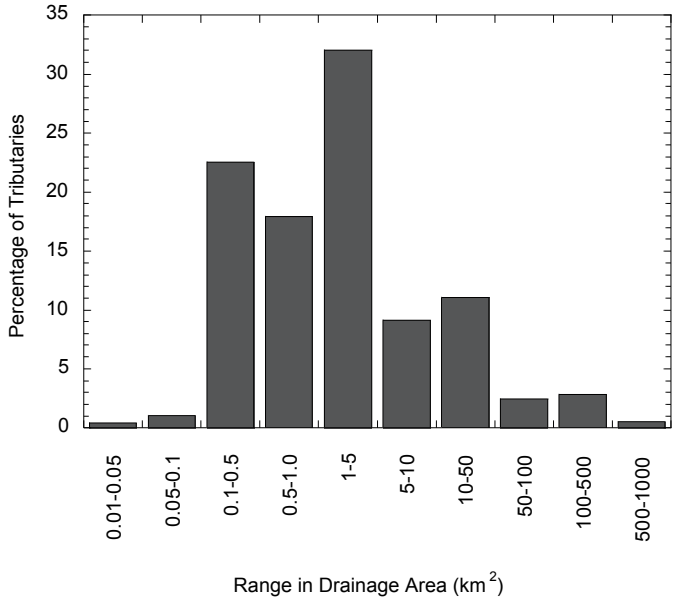

Figure 2. Histogram of drainage areas of ungaged tributaries in Grand Canyon.

ESTIMATING SEDIMENT YIELD

Regional Sediment-Yield Data: Sediment loads at gaging stations on the pre-dam Colorado River, its major tributaries, and small drainages suggest a regional sediment yield of 105-820 Mg km^{-2} yr^{-1} (table 1). These yields assume minimal long-term change in storage (Graf, 1987). On the basis of a range in drainage area most comparable with that of Grand Canyon tributaries, the most appropriate data are sedimentation data from 25 small reservoirs in northeastern Arizona (Fort Defiance region of the Navajo Indian Reservation; Hains et al. 1952). We combined this reservoir sedimentation data with the annual sediment yields from gaging stations in the region, excluding the mainstem Colorado River, and fit a power function to these data (fig. 3) to obtain

$$Q_s = 193 \cdot A^{1.04},\ R^2 = 0.86, \quad (1)$$

where Q_s = sediment yield (Mg/yr), A = drainage area (km^2), and n = 37. The high R^2 value suggests sediment data from the southern Colorado Plateau are readily modeled by a linear relation to drainage-basin area. Consequently, we use this relation interchangeably with the regional data in evaluating the other two estimation techniques.

Empirical Sediment-Yield Relations: We compared several extant empirical relations for estimating streamflow sediment yield (table 2). An implicit assumption in these approaches is that the percent of exposed bedrock in a drainage basin is not a factor in sediment yield. Strand (1975) based his method on reservoir surveys throughout the western United States. Renard (1972) and Renard and Laursen (1975) used both reservoir sediment data and a stochastic runoff model calibrated to southwestern watersheds to calibrate their methods. Dendy and Bolton (1976) related both drainage area and mean annual runoff to sediment yield. Flaxman (1972) developed a more complicated empirical approach that relates sediment yield to mean annual climate (a proxy for vegetation), watershed slope, and soil characteristics. The PSIAC method (Pacific Southwest Inter-Agency Committee, 1968) involves rating a watershed on the basis of nine factors related to erosion (surface geology, soil, climate, runoff, topography, land use, upland erosion, and channel erosion/sediment transport) to produce an estimate of sediment yield. This method can be applied to large areas using pre-calculated PSIAC sediment-yield ratings mapped by the Soil Conservation Service (SCS, 1975; Hedlund and Curtis, 1984). The approaches by Howard and Dolan (1981) and Randle and Pemberton (1987) were developed specifically for Grand Canyon. Howard and Dolan (1981) assumed that ungaged tributaries yielded as much sediment per unit area as the gaged tributaries (table 2). Randle and Pemberton (1987) derived their estimate relating sediment yield to drainage area from reservoir sedimentation surveys of the western United States and adjusted it with data from the Paria and Little Colorado Rivers, and Kanab and Havasu Creeks.

Table 1. Measured sediment loads at selected gaging stations on the Colorado Plateau.

Gaging station name	Years of data (Water years)	Drainage area (km^2)	Sediment load (10^6 Mg/yr)	Sediment yield (Mg $yr^{-1}km^{-2}$)
*Moenkopi Wash #1	1985-1997	29.2	0.0081	277
*Yellow Water Wash #1	1985-1997	52.2	0.030	575
*Coal Mine Wash #1	1985-1997	77.1	0.018	233
*Red Peak Valley Wash	1986-1997	80.9	0.042	519
*Coal Mine Wash #2	1987-1997	94.3	0.0099	105
*Yellow Water Wash #2	1985-1997	100	0.015	150
*Moenkopi Wash #2	1986-1997	131	0.052	396
*Coal Mine Wash #3	1986-1997	293	0.172	587
†Kanab Creek near Fredonia	1968-1973	2,810	0.809	288
†Paria River at Lees Ferry	1949-1976	3,650	3.0	820
†Moenkopi Wash near Tuba City	1977-1979	4,219	0.65	155
†Little Colorado River near Cameron	1957-1970	68,600	9.2	130
†Colorado River at Lee's Ferry	1948-1962	290,000	65	220
†Colorado River near Grand Canyon	1948-1962	366,000	84	230

*Sediment data are unpublished values from Peabody Coal Company.
†Sediment data are annual means for the water years shown from the USGS ADAPS database.

Table 2. Estimates of sediment yield by streamflow from 219 ungaged tributaries of the Colorado River.

Source	Original equation*	Units	Sediment yield† (10^6 Mg/yr)	Sediment yield† (Mg yr^{-1} km^{-2})
§Flaxman (1972)	$\log (Y + 100) = 6.21301 - 2.19113 \log (X_1 + 100) + 0.06034 \log (X_2 + 100) - 0.01644 \log (X_3 + 100) + 0.04250 \log (X_4 + 100)$	ac-ft/mi^2/yr	0.14	42.6
Renard (1972)	$0.001846\ A^{-0.1187}$	ac-ft/ac/yr	0.67	204
Soil Conservation Service (1975)	PSIAC method	ac-ft/mi2/yr	13.5	4,110
Strand (1975)	$1130\ A^{0.77}$	m^3/yr	1.62	494
#Dendy and Bolton (1976)	$1280\ Q^{0.46}\ (1.43 - 0.26 \log A)$	tons/mi^2/yr	0.81	247
**Howard and Dolan (1981)	$780\ A$	Mg/km^2/yr	2.56	780
**Randle and Pemberton (1987)	$1750\ A^{-0.24}$	m^3/km^2/yr	2.4	731
Graf (1987)	$1200\ A^{1.0}$	m^3/yr	3.9	1,190

* A = drainage area km^2 if units are metric; otherwise in area units given.
† Sediment density is estimated as 1,200 kg/m^3.
§ Y = sediment yield in ac-ft/mi^2/yr; X_1 = mean annual precipitation (inches) / mean annual temperature (°F), estimated as 0.19; X_2 = watershed slope, estimated as percent gradient of main channel; X_3 = percent of particles > 1 mm in diameter in the first 2 inches of soil, estimated as 60%; X_4 = soil pH factor, assumed to be 0 (pH of 7).
# Q = annual runoff in inches assumed to be $0.4501\ A^{-0.1449}$ (A in mi^2).
** Derived from daily suspended sediment loads.

We rejected other sediment-yield approaches, such as the Universal Soil Loss Equation (USLE) (Wischmeier and Smith, 1978; Peterson and Swan, 1979) and the CREAMS and WEPP models of the Agricultural Research Service (Knisel, 1980; Gilley et al.1988). The USLE was developed strictly for low-slope agricultural land and is not appropriate for the steep terrain of Grand Canyon. Likewise, the CREAMs and WEPP models were developed for relatively low-slope agricultural and rangeland and require considerable watershed data for proper application.

In order to limit the data collection necessary to evaluate the more complicated relations, we calculated sediment yield for a subset of Grand Canyon tributaries (n = 219) and compared the results. Estimates range through two orders of magnitude, from 43 to 4,110 Mg km^{-2} yr^{-1} (table 2) and most are significantly larger than measurements at gaging stations (table 1). Flaxman's (1972) approach produced the lowest sediment yield (43 Mg km^{-2} yr^{-1}) –

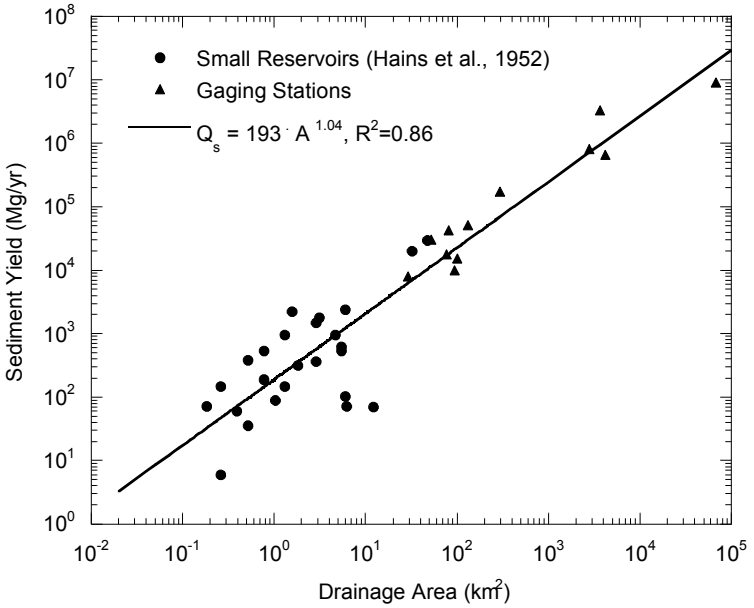

Figure 3. Sediment-yield data from small reservoirs (Hains and others, 1952) and gaging stations on the Colorado Plateau (n = 37).

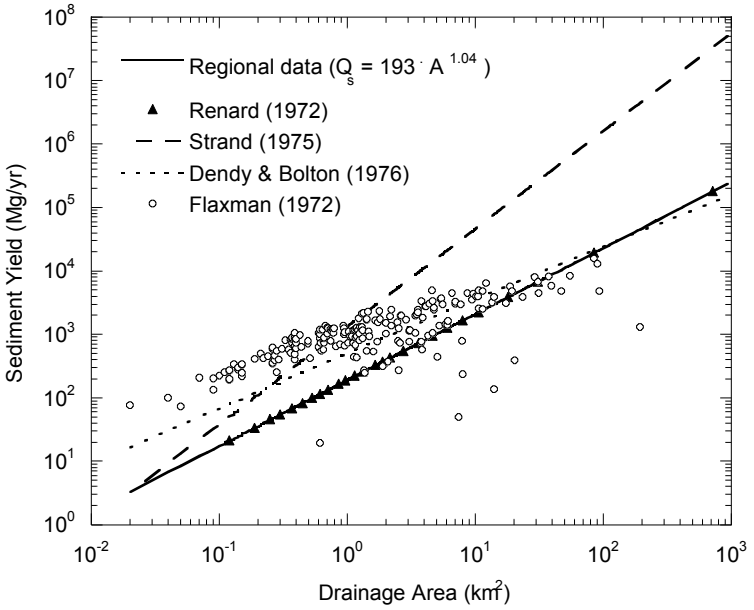

Figure 4. Estimates of streamflow sediment yield from empirical equations and the regional-data regression relation.

underpredicting substantially for larger drainages in comparison to regional data (fig. 4) – while the PSIAC method produced the highest sediment yield (4,110 Mg km^{-2} yr^{-1}). Relations that produced estimates outside the range of regional gage data (Flaxman 1972, the PSIAC method, Howard and Dolan 1981, Randle and Pemberton 1987, and Graf 1987) were eliminated from further consideration.

Sediment yield was calculated for all ungaged Grand Canyon tributaries with each of the three remaining techniques and compared to regional gage data (fig. 4). The Strand (1972) equation consistently overpredicted sediment yield

Table 3. Estimated annual streamflow sediment yield from ungaged tributaries in Grand Canyon, Arizona.

Sediment-yield reach	Drainage area (km^2)	Sediment yield (Mg/yr)		
		Data regression equation*	Renard (1972) equation†	Flood-frequency method*
Lake Powell- Paria River	321	64,800	76,400	45,200
Paria River - Little Colorado River	2,953	610,000	593,000	457,000
L. Colorado R. – Bright Angel Creek	494	97,700	127,000	82,300
Bright Angel – Kanab Creek	1,640	332,000	375,000	240,000
Kanab Creek – Havasu Creek	276	57,000	63,700	40,500
Havasu Creek – Diamond Creek	3,958	821,000	779,000	488,000
Diamond Creek – Lake Mead	3,236	669,000	633,000	397,000
Total	12,878	2,650,000	2,650,000	1,750,000

* Sediment yield is calculated using an equation or method developed during this study.
† Sediment yield is calculated using the Renard (1972) equation converted to metric units with a sediment density of 1.2 Mg/m^3.

relative to regional data, the degree of overprediction increasing significantly with drainage area. The Dendy and Bolton (1976) equation overpredicted sediment yield as well, though to a lesser degree and did better with larger drainages than Strand (1972). However, the relation that best approximates the regional data is the Renard (1972) power function relating sediment yield to drainage area (fig. 4). The Renard (1972) equation, converted to SI units and assuming a sediment density of 1.2 Mg/m^3, is

$$Q_s = 351 \cdot A^{0.88}, \quad (2)$$

where Q_s = streamflow sediment yield (Mg/yr) and A = drainage area (km^2). Sediment yield calculations based on this equation are in close agreement with those from the regional-data regression, always within the same order of magnitude and differing by no more than 30% (Table 3).

The Flood-Frequency, Rating-Curve Technique: We developed a third method for estimating streamflow sediment yield based loosely on the work of Strand (1975) and Strand and Pemberton (1982). This technique uses local flood hydrographs as the link between regional flood-frequency relations and sediment rating curves. This method requires numerous assumptions, one of the most important of which is that the decadal streamflow sediment yield in a tributary can be described by several floods of recurrence intervals described by regional flood-frequency relations. Considering the intermittent-flow regime of these tributaries, which probably have flow less than one percent of the time, this is likely not to be an unreasonable assumption for most of the tributaries

Flood volumes and sediment-rating curves: Hydrographs for floods on Bright Angel Creek (fig. 1) collected between 1924 and 1972 are the only available data concerning the form of streamflow floods in small Grand Canyon tributaries. Although sediment data were collected at Bright Angel Creek between 1991 and 1993, they are of limited extent and possibly seasonally biased (Webb et al. 2000). Instead, we used sediment data collected at 8 gaging stations operated by the Peabody Coal Company on Black Mesa to calculate sediment rating curves (table 4). These gaging stations (table 1) are on Coal Mine Wash (3 gaging stations), Yellow Water Wash (2 gaging stations), Moenkopi Wash (2 gaging stations), and Red Peak Valley Wash (1 gaging station). Although Black Mesa is about 100 kilometers east of Grand Canyon (fig. 1) and is underlain by different geologic formations, the climate at Black Mesa is similar to that of Grand Canyon and the bedrock in both areas is mostly sedimentary. In general, the Cretaceous strata of Black Mesa are notably less competent than the Paleozoic strata of Grand Canyon and include none of the well-indurated carbonates typical of Grand Canyon (e.g., the Redwall Limestone). Consequently, the drainages on Black Mesa likely yield a higher proportion of sediment per unit area than most of the ungaged tributaries of Grand Canyon. Sediment-yield estimates based on these data may overestimate Grand Canyon sediment yield. The drainage areas of the Black Mesa tributaries are also more comparable to those of ungaged Grand Canyon tributaries than those of the larger gaged tributaries (fig. 1 and table 1).

Using hydrographs for 42 flood events in Bright Angel Creek, we applied each of the rating curves from Black Mesa to calculate five estimates of total sediment yield for each event. After separating base flow (0.4 to 1.0 m^3/s) from the runoff to calculate peak discharge for each event, we used linear regression to determine the relation between peak discharge and total sediment yield for each rating curve (table 5). The relation of sediment yield to peak

Table 4. Sediment rating at five gaging stations on Black Mesa, Arizona.

Tributary	Years of data (Water years)	Drainage area (km^2)	Coefficient *a*	Exponent b	R^2	Maximum discharge (m3/s)
Moenkopi Wash #1	1985-1997	29.2	2,540	1.52	0.80	65.1
Yellow Water Wash #1	1985-1997	52.2	9,500	1.16	0.79	42.5
Coal Mine Wash #1	1985-1997	77.1	5,730	1.28	0.84	93.5
Yellow Water Wash #2	1985-1997	80.9	6,410	1.24	0.89	42.4
Coal Mine Wash #2	1985-1997	112.7	4,050	1.28	0.89	24.9

The coefficient and exponent are for the equation $S_y = a \cdot Q^b$, where S_y = sediment yield (Mg/day) and Q = instantaneous discharge (m^3/s). Minimum discharge for the rating curves is 0.1 m^3/s. Ratings are derived from unpublished data, Peabody Coal Company.

Table 5. Linear regression between peak discharge and sediment yield for 42 floods in Bright Angel Creek.

	Sediment rating curve used				
	Yellow Water #1	Yellow Water #2	Coal Mine #1	Coal Mine #2	Moenkopi #1
Coefficient (*a*)	1987	1258	1088	773	404
Exponent (*b*)	1.09	1.17	1.21	1.21	1.45
R^2	0.76	0.77	0.78	0.78	0.82

The coefficient and exponent are for the equation $Q_s = a\ Q_p^b$ where Q_s = sediment yield (Mg/event) and Q_p = instantaneous peak discharge (m^3/s). The Bright Angel Creek gage record runs from 1924 to 1973.

Table 6. Regional regression equations from Roeske (1978) for streamflow flood.

Flood frequency region*	Recurrence interval(yrs)	Flood-frequency relation
1	2	$Q = 19\ A^{0.660}$
	5	$Q = 66.3\ A^{0.600}$
	10	$Q = 127\ A^{0.566}$
4	2	$Q = 1.35\ A^{0.491}\ (E/1{,}000)^{2.25}$
	5	$Q = 0.319\ A^{0.446}\ (E/1{,}000)^{3.60}$
	10	$Q = 0.143\ A^{0.423}\ (E/1{,}000)^{4.31}$

Q = peak discharge (ft^3/s); A = drainage area (mi^2); E = mean basin elevation (ft).
* Region 4 is east of the Colorado River and north of the Little Colorado River; the remainder of Grand Canyon falls within Region 1.

discharge took the form:

$$Q_e = a \cdot Q_p^{\ b}, \tag{3}$$

where Q_e = sediment yield in Mg/event, Q_p = peak flood discharge in m^3/s, and a and b are regression coefficients. The R^2 values ranged from 0.76 to 0.82, indicating a high degree of relation between peak discharge and sediment yield per event (table 5). Of the eight relations, we elected to use that derived from Moenkopi Wash #1 because: 1) it had the highest R^2 (0.82), 2) it had the lowest coefficient and would produce the lowest sediment yield estimate as a counterbalance to potential overestimation of Grand Canyon sediment yield, and 3) the drainage area of Moenkopi Wash #1 (29.2 km^2) is closest to the mean area of ungaged tributaries in Grand Canyon (16 km^2).

Regional flood frequency: We evaluated the regional regression relations for flood frequency given by Thomas et al. (1997) for the southwestern United States, but found significant problems when applying them to the Grand Canyon region (Webb et al. 1997, 2000). Few small drainages in Grand Canyon have gaging records, and therefore these tributaries are poorly represented in the Thomas relations. Additionally, most of the data for these equations come from areas outside northern Arizona. In contrast, the flood-frequency regressions of Roeske (1978), although calculated with shorter gage records and fewer initial basin variables, use Arizona data exclusively and contain the same independent variables of drainage area and mean basin elevation used by Thomas et al (1997). We therefore elected to use the regional-regression equations published by Roeske (1978) for calculating sediment yield in Grand Canyon (table 6).

Calculations of sediment yield: We linked flood-frequency discharge estimates to sediment yield-peak discharge relations using

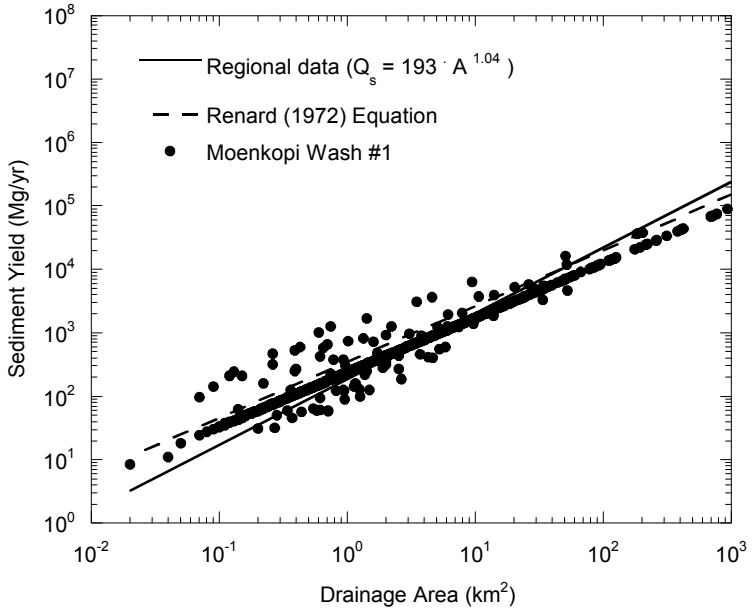

Figure 5. Streamflow sediment-yield estimates for 768 Grand Canyon tributaries calculated using the regional flood-frequency estimates of Roeske (1978) and sediment-rating data from Moenkopi Wash #1 compared to the regional-data regression and Renard (1972) equations.

$$Q_s = [1 \cdot f(Q_{10}) + 2 \cdot f(Q_5) + 5 \cdot f(Q_2)] / 10, \quad (4)$$

where Q_s is sediment yield in Mg/year, Q_t is the peak discharge of the t year flood in m^3/s (from Roeske 1978), and $f(Q_t)$ is the regression relating peak discharge to sediment yield in Mg/event (Q_e calculated for Moenkopi Wash #1). We assumed an expected value for the number of floods to occur in a decade which calls for five 2-yr floods, two 5-yr floods, and one 10-yr flood to deliver most of the sediment to the Colorado River. Regional flood-frequency relations do not produce annual floods, so we have no means of determining the effect of neglecting the smallest events, and we chose not to include the influence of long recurrence-interval floods in the analysis.

Sediment yield calculations based on the flood frequency-rating curve technique are in reasonable agreement with those from the regional-data regression (fig. 5) and with no more scatter than the original regional data (fig. 3). Estimates calculated by reach are lower than those from the regional-data regression and Renard relations (table 3), but still of the same order of magnitude and never vary by more than 40%.

CONCLUSIONS

All three techniques used to estimate sediment yield from small drainage basins in Grand Canyon agreed well with each other and regional data, suggesting they may all be useful in estimating sediment yield elsewhere on the southern Colorado Plateau. In evaluating eight empirical sediment-yield relations, complex multivariate methods, such as that of the PSIAC (1968) and Dendy and Bolton (1976), did not perform as well as simple power functions relating sediment yield to drainage basin area. This suggests that complex relations may not necessarily be more accurate in estimating sediment yield, at least on a regional scale. The new flood-frequency technique was adjusted to fit the data regression relation and is not strictly an independent approach. Nevertheless, close agreement with the other two methods suggests that the technique has strong potential as a new method for estimating streamflow-sediment yield. It may be more robust than the others for estimating sediment yield where local streamflow data are available. Future testing of this technique in settings where sediment yields are known may bear this out. The flood-frequency technique depends on numerous untested assumptions, such as equating decadal sediment yield with the sum of sediment yield from one ten-year, two five-year, and five two-year floods.

REFERENCES

Dendy, F.E., and Bolton, G.C., 1976, Sediment yield-runoff drainage area relationships in the United States. Journal of Soil and Water Conservation 31, 264-266.

Flaxman, E.M., 1972, Predicting sediment yield in Western United States, Journal of the Hydraulics Division, Proceedings of the American Society of Civil Engineers HY 12, 2073-2085.

Garrett, W.B., Van De Vanter, E.K., and Graf, J.B., 1993, Streamflow and sediment-transport data, Colorado River and three tributaries in Grand Canyon, Arizona, 1983 and 1985-86. U.S. Geological Survey Open-file Report 93-174, 624.

Gilley, J.E., Lane, L.J., Laflen, J.M., Nicks, H.D., and Rawls, W.J., 1988, USDA-water erosion prediction project: New generation erosion prediction technology, in Modeling, agricultural, forest, and rangeland hydrology. Symposium proceedings, pub. 07-88.

Graf, W.L., 1987, Late Holocene sediment storage in canyons of the Colorado Plateau. Geological Society of America Bulletin 99, 261-271.

Hains, C.F., Van Sickle, D.M., and Peterson, H.V., 1952, Sedimentation rates in small reservoirs in the Little Colorado River basin. U.S. Geological Survey Water-supply Paper 1100-D, 27.

Hedlund, J.D., and Curtis, N.M., Jr., 1984, A quick and easy approach to estimating erosion on all land in the west, abstract. Proceedings of 39th Annual Meeting of the Soil Conservation Society of America.

Howard, A., and Dolan, R., 1981, Geomorphology of the Colorado River in Grand Canyon. Journal of Geology 89, 269-297.

Knisel, W.G., (editor), 1980, CREAMS. A field-scale model for chemicals, runoff, and erosion from agricultural management systems. U.S. Department of Agriculture, Conservation Research Report No. 26, 640.

Pacific Southwest Inter-Agency Committee, 1968, Report on factors affecting sediment yield in the Pacific Southwest area. Water Management Subcommittee, Sedimentation Task Force, 10.

Peterson, A.E., and Swan, J.B. (editors), 1979, Universal soil loss equation. past, present and future. Soil Science Society of America Special Publication 8, 53.

Randle, T.J., and Pemberton, E.L., 1987, Results and analysis of STARS modeling efforts of the Colorado River in Grand Canyon. Flagstaff, Glen Canyon Environmental Studies Report, 41.

Renard, K.G., 1972, Sediment problems in the arid and semi-arid southwest, in Proceedings, 27th Annual Meeting, Soil Conservation Society of America. Portland, Oregon, 225-232.

Renard, K.G., and Laursen, E.M., 1975, A dynamic behavior model of an ephemeral stream. Journal of the Hydraulics Division, Proceedings of the American Society of Civil Engineers HY 5, 511-528.

Roeske, R.H., 1978, Methods for estimating the magnitude and frequency of floods in Arizona. Phoenix, Arizona Department of Transportation Report for Research Project Arizona HPR-1-15(121), 82.

Rote, J.J., Flynn, M.E., and Bills, D.J., 1997, Hydrologic data, Colorado River and major tributaries, Glen Canyon Dam to Diamond Creek, Arizona, water years 1990-95. U.S. Geological Survey Open-file Report 97-250, 474.

Soil Conservation Service, 1975, Erosion, sediment and related salt problems and treatment opportunities. U.S. Department of Agriculture, 152.

Strand, R.I., 1975, Bureau of Reclamation procedures for predicting sediment yield. U.S. Department of Agriculture Report ARS-S-40, Present and prospective technology for predicting sediment yields and sources, 5-10.

Strand, R.I., and Pemberton, E.L., 1982, Reservoir sedimentation technical guidelines for Bureau of Reclamation. Denver, Colorado, Bureau of Reclamation.

Thomas, B.E., Hjalmarson, H.W., and Waltemeyer, S.D., 1997, Methods of estimating magnitude and frequency of floods in the southwestern United States. U.S. Geological Survey Water-Supply Paper 2433, 195.

Webb, R.H., Griffiths, P.G., Melis, T.S., and Hartley, D.R., 2000, Sediment delivery by ungaged tributaries of the Colorado River in Grand -Canyon, Arizona. U.S. Geological Survey Water-Resources Investigations Report 00-4055, 67.

Webb, R.H., Melis, T.S., Griffiths, P.G., Elliott, J.G., Cerling, T.E., Poreda, R.J, Wise, T.W, and Pizzuto, J.E., 1999b, Lava Falls Rapid in Grand Canyon, effects of late Holocene debris flows on the Colorado River: U.S. Geological Survey Professional Paper 1591, 91.

Wischmeier, W.H., and Smith, D.D, 1978, Predicting rainfall erosion losses - a guide to conservation planning, Agriculture Handbook 537, USDA-SEA.

U.S. Geological Survey, 1675 W. Anklam Rd., Tucson, AZ, 85745; rhwebb@usgs.gov; 520-670-6671 ext 238.

PREDICTION OF COHESIVE SEDIMENT TRANSPORT AND BED DYNAMICS IN ESTUARIES AND COASTAL ZONES WITH INTEGRATED NUMERICAL SIMULATION MODELS

J. Berlamont, Katholieke Universiteit Leuven, Belgium, [Jean.Berlamont@bwk.kuleuven.ac.be]; K. Dyer, University of Plymouth, U.K., [K.Dyer@plymouth.ac.uk]; M. Markofsky, Universität Hannover, Germany, [mark@hydromech.uni-hannover.de]; H. Michallet, Université Joseph Fourrier, Grenoble, France, [michalle@hmg.inpg.fr]; O. Petersen, Danish Hydraulic Institute, Denmark, [Osp@dhi.dk]; W. Roberts & M. Dearnally, H.R. Wallingford, U.K., [mpd@hrwallingford.co.uk]; G. Sills, University of Oxford, U.K., [Gilliane.Sills@eng.ox.ac.uk],; E. Toorman, Katholieke Universiteit Leuven, Belgium, [Erik.Toorman@bwk.kuleuven.ac.be]; D. Violeau, LNHE, Electricité de France, France [damien.violeau@edf.fr]; H. Winterwerp, Delft Hydraulics and T.U. Delft, the Netherlands, [han.winterwerp@wldelft.nl].

Abstract: Within the E.U. fourth framework programme a joint research programme has been carried out between 1997 and 2000 on the «Prediction of cohesive sediment transport and bed dynamics in estuaries and coastal zones with integrated numerical simulation models» (acronymn COSINUS).

The objective of the research programme was to establish well validated physical and mathematical descriptions of the behavior and fate of concentrated near-bed suspensions (CBS or «fluid mud») and their interaction with the water and the sediment bed.

Since there seemed to be a lack of experimental data on the role of flocculation and turbulence in the formation and erosion of mud beds and on the formation of CBS, an experimental programme was set up to obtain these data. It consisted of field measurements in the Tamar estuary (U.K.) on floc formation and laboratory experiments at Delft, Oxford and Grenoble on the formation of mud beds and CBS and the influence of floc structure and turbulence on these processes. The data have been stored in a data base, which is accessible to the public.

Different processes have been studied in detail: turbulence damping in sediment laden flow; turbulence production due to internal waves in concentrated suspensions; flocculation; generation, properties and entrainment of CBS; bed strength development and erosion of mud beds.

The detailed process models have been parameterized to obtain relatively simple formulations which can be implemented into currently used 3D and 2DH engineering system models.
The performance of the improved system models has been tested by application of the models to a schematic estuary for which 2DV solutions with the detailed research models were used as a reference. The models have been applied and tested in three real estuaries (Tamar in U.K., Loire in France and Weser in Germany).

It is felt that great progress has been made in the physically based description of cohesive sediment dynamics with respect a.o. to the formulation of turbulence damping functions; the modelling of the rheology of a CBS, including consolidation; the modelling of flocculation and the modelling of erosion and entrainment of CBS.

Engineering software tools have been improved to enable better predictions of mud dynamics for the benefit of estuarine and coastal managers.

INTRODUCTION

The management of coastal zones and estuaries requires accurate and detailed knowledge to cope with their problems such as wetland protection and restoration, maintenance of navigation channels, dredging and dredged material relocation, effects of construction works on siltation and turbidity levels, pollutant transport, etc. Development and application of this knowledge requires detailed mathematical models, amongst which full three-dimensional codes. This is becoming practically feasible in view of the current developments in soft- and hardware. The physical understanding and mathematical description or "modelling" of the processes however is still lagging behind, especially with respect to the presence of concentrated benthic (near-bed) suspension layers (CBS).

PROJECT METHODOLOGY

The state of the art knowledge of cohesive sediment transport shows that there is still a lack of experimental data on the role of flocculation and turbulence in the formation and erosion of mud beds and on the formation of CBS (concentrated benthic suspensions, or "fluid mud"). Therefore, an experimental programme has been set up to obtain these data. It consisted of field measurements in the Tamar estuary on floc formation and laboratory experiments on formation and erosion of mud beds and CBS, and the influence of floc structure and turbulence on these processes.

The data of the experimental programme, together with other relevant data from literature have been stored in a database, which at the end of the project will be accessible to the public.
Process modules have been developed and implemented into detailed 1D and 2D vertical models which solve the full hydrodynamic, turbulent energy and sediment mass conservation equations. Two different bed models, to be coupled to these hydrodynamic models have been developed as well (1DV point model). The data from the database have been used to calibrate and validate the process modules.

The process modules have been parameterised to obtain relatively simple formulations, which can be implemented into currently used 3D and 2DH engineering system models.

The performance of the improved system models has been tested by application of the models to a schematic estuary, for which a 2DV solution with the detailed research model is used as a reference. Various scenarios have been simulated. The models have also been applied to three real estuaries (Tamar, Loire and Weser). Data to set-up and calibrate the model applications are stored in the database.

From the experience with the large-scale applications feed back has been produced towards the process module development and their parameterisations.

RESULTS

Sediment - turbulence interaction: For the numerical modelling of sediment - turbulence interaction, the most commonly used engineering turbulence models have been used, i.e. the Prandtl mixing length (PML), the k-ε model and also a k-w model.

Suspended sediment particles cause damping of turbulent energy in the flow. Traditionally, this effect is parameterised by the use of semi-empirical damping functions, which are applied to correct the turbulent eddy viscosity (in the PML model) and the sediment mixing coefficient (or eddy diffusivity) for neutral conditions. The k-ε and k-w models include the buoyancy effect explicitly but still needs the damping functions in the bed boundary conditions and the buoyancy term. Data on turbulence damping in stratified flows from the literature have been reanalysed, together with numerical data generated with the k-ε model. Based on these results and on theoretical considerations, new damping functions have been proposed and tested.

High density gradients at the bed result in an apparent reduction of the bottom roughness with consequently higher transport and erosion rates than expected when the model would not account for these buoyancy effects in the bed boundary conditions. A new bottom boundary treatment method has been proposed, which yields the correct bed shear stress.

When a flowing suspension decelerates during a tidal cycle, the combined effect of group settling and buoyancy damping may lead to the formation of a two-layer stratified flow with a distinct density interface, the lutocline. Turbulence can be completely suppressed at this interface. Under certain conditions this interface becomes unstable, resulting in internal waves which generate new turbulence and mixing across the lutocline. It has been proposed to model this turbulence generation in a parameterised form as an additional eddy viscosity.

Flocculation: Because, as far as cohesive suspensions are concerned, laboratory experiments cannot scale the turbulent properties of natural flows adequately, field measurements were obtained of floc characteristics. The measurements were taken in September 1998 in the upper reaches of the Tamar Estuary, and covered the neap and spring tide conditions. In that location the turbidity maximum is well developed and suspension concentrations of the order of g/l are present. The aim of the experiment was to measure floc size and settling velocity and their dependence on salinity, concentration and turbulent shear.

Two stations about 1km apart in the centre of the channel were occupied simultaneously. At both stations frequent profiles of velocity, salinity, temperature, and suspended sediment concentration were obtained, and Owen tube measurements of settling velocity were taken. At the lower station, profiles of floc size were taken with a Lasentec P-100 system (Law et al., 1997), and near bed measurements of floc size, settling velocity, and effective density obtained with the INSSEV instrument (Fennessy et al., 1994). Also turbulence parameters were measured with miniature electromagnetic flowmeters above and below the INSSEV.

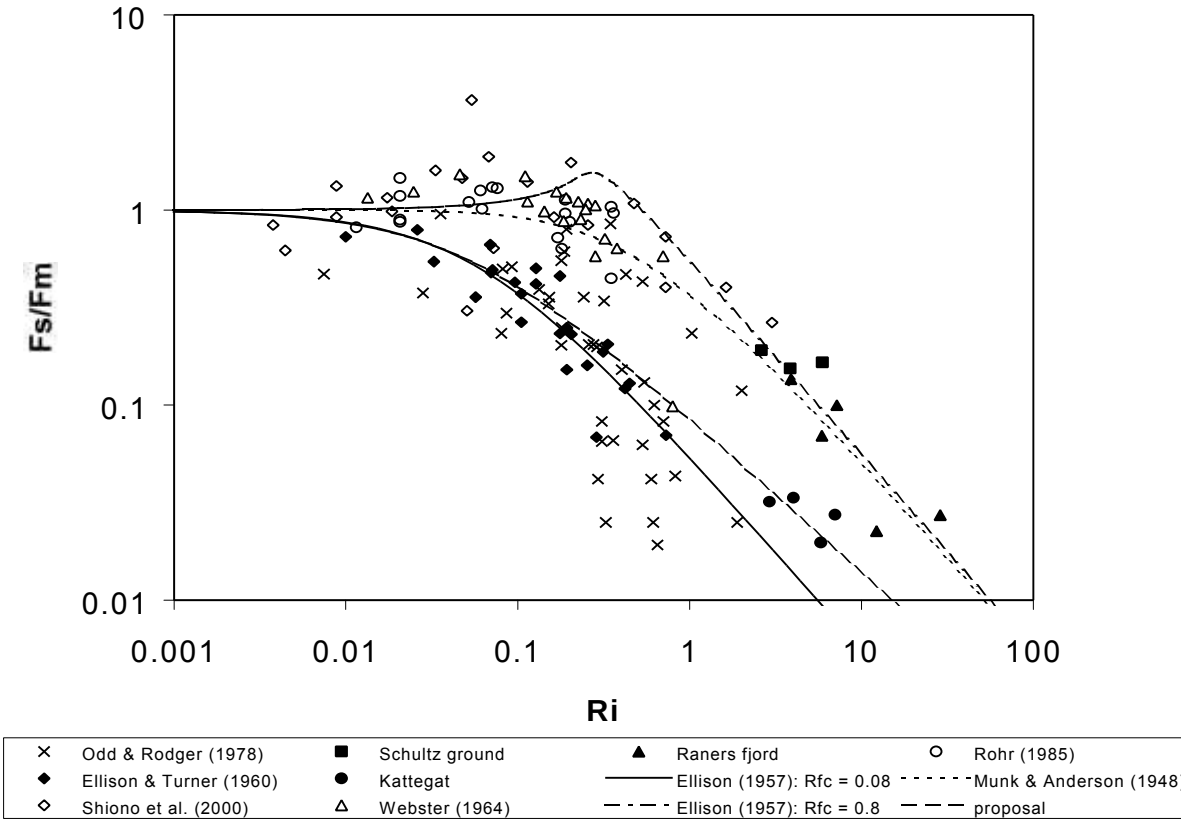

Ratio of the mixing to the momentum damping function (or normalised inverse Schmidt number) as a function of the gradient Richardson number.

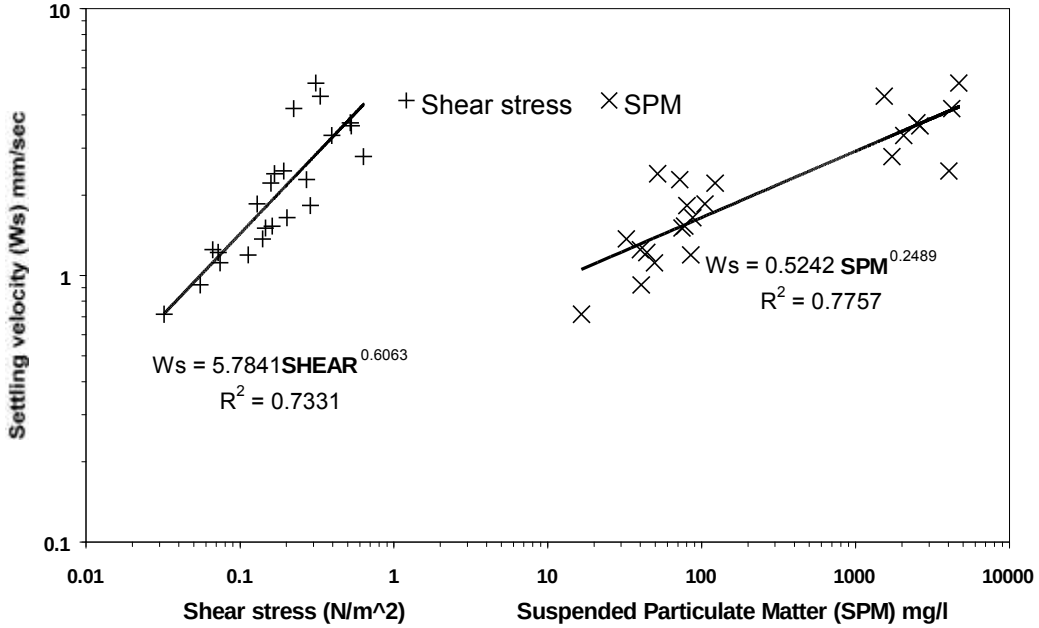

Selected spring and neap tide INSSEV mean macrofloc (> 160 µm) settling velocities plotted against both shear stress and SPM (0.5 m above the seabed).

At the upper station a LISST laser diffraction particle sizer was deployed, and video measurements of floc size and settling velocities were observed within Owen tube samples. Additionally, samples were taken for laboratory analysis of the carbohydrate andcholorophyll - a contents and CHN ratios.

Suspended near bed sediment concentrations ranged from 16 mg/l on a neap tide to 7 g/l on a spring tide. Maximum velocities were 0.5 and 1.5 m/s, respectively. Typical spring tide shear stresses were 0.68 N/m^2 at the level of the INSSEV. The number of flocs per INSSEV sample varied between 14 and 1150. Floc sizes up to 600 microns were observed. Examination of the settling velocity spectra of the flocs has indicated that the settling velocity Ws can be represented in simple linear correlation: $Ws = 5.784\ (Shear)^{0.606}$ and $Ws = 0.524\ (SPM)^{0.249}$, where Ws is in mm/s, shear is in N/m^2 and SPM in mg/l. Also the ratio of macroflocs to microflocs separated at a size of 160 microns was observed to increase with both increasing concentration and shear stress. This suggests that the influence of concentration on aggregation is greater than that of shear on floc break-up. The biochemical results suggest that high carbohydrate levels act as an adhesive assisting the production of the larger faster settling macroflocs formed during low concentrations at neap tides. It also appears that the faster settling macroflocs can selectively scavenge the very small microflocs at a rate faster than that for the medium sized flocs.

A three dimensional flocculation model was derived, accounting for the mutual effects of turbulence-induced aggregation and break-up processes (Winterwerp, 1999). The mud flocs are treated as self-similar fractal entities, which yields a modification of Stokes' formula for the settling velocity, and allows for a description of gelling effects resulting in the formation of fluid mud layers. This flocculation model is solved together with the mass balance for suspended sediment, including the effects of hindered settling, for which an alternative model was derived. The model was applied to simulate the processes in the turbidity maximum in the Ems Estuary and compared to a series of measurements. The simulations showed that the observed rapid decrease in suspended sediment towards slack water can only be obtained if the effects of flocculation and sediment-induced stratification are both taken into account.

CBS dynamics: In 2D models, the modelling of entrainment is important. From flume experiments is has been found that

- due to generation of turbulence in the lower, dense CBS layer, material from the upper, less dense and less turbulent layer is entrained into the lower layer, which thickened accordingly.
- the entrainment velocity appears to be constant in time, which is consistent with theory.
- a freshly deposited CBS behaves as a viscous fluid
- A relationship of the form $E \sim 1/Ri^*$ was found, in which E is the dimensionless entrainment rate and Ri* the overall Richardson number.

From grid tank experiments the formation of CBS layers reaching an equilibrium thickness was observed for different concentration conditions. The time averaged sediment concentration appears to be uniform in the CBS layer for all concentrations. The turbulent kinetic energy decreases with increasing distance from the grid. No decay of turbulent kinetic energy was found for sediment concentrations up to 200 g/l. The flux Richardson number below the lutocline

varies by more than two orders of magnitude when the variation of the settling velocity versus the concentration was taken into account.

Bed dynamics: Extensive settling column experiments have been used to develop and verify numerical models of the consolidation process. The relationship between the properties of the settling flocs, the deposition rates and the properties of the deposited bed (in particular the consolidating density profile and the associated strength development) have been investigated. Using in situ measurements the critical shear stress for erosion has been related to other properties.

A 2DV bed dynamics model based on the generalised Biot theory, extended to deal with extremely large deformations and corresponding density changes, has been developed to study the strength development in cohesive sediment beds during consolidation, fluidisation and liquefaction (e.g. induced by wave action). The model allows the implementation of more realistic constitutive rheological equations (i.e. stress – strain relationships).

With regard to deposition/ erosion the use of a new empirical stress – density relationship has been proposed which accounts for the fact that no strength is developed below the gelling point of the mud. The erosion rate parameter is proposed to be a function of the bed surface density. For deposition the total settling flux is considered, i.e. no critical stress for deposition. In order to distinguish between the settling sediment, which attaches to the bed and the deposited sediment which remains mobile and can readily be entrained, the erosion law has been generalised.

Applied modelling: The goal of the "Applied Modelling" was to provide results using numerical models, including the knowledge resulting from the theoretical aspects of the project. For this purpose, various test cases have been defined, in order to test and validate the new formulations, and to compare the different numerical models. The final goal is to apply the models to the cases of real estuaries, to show their capability to reproduce actual cohesive sediment phenomena.

The first test case is a one-dimensional vertical case, designed to compare the models regarding vertical processes, and particularly the modelling of turbulence damping by suspended sediment. Several sets of conditions for hydrodynamics and sediment have been tested. The computed results show that stratification and saturation effects are very sensitive to the choice of damping functions. It appears, looking at the viscosity and diffusivity profiles, that the influence of the shear velocity at the bottom is an important parameter to make correct sediment transport predictions. However, theoretical work has shown that the shear velocity is not correctly estimated by traditional methods when sediment is involved. Therefore a new formulation has been proposed.

Experimental and theoretical studies of flocculation processes have produced new information, which has been used to develop parameterisations of the sediment settling velocity. Several approaches exist, which have been implemented in the one-dimensional model. Comparisons and sensitivity tests have been carried out. On the other hand, the effects of entrainment of bed materials, resulting from the instability of the lutocline, have also been examined. A parameterisation has been established, which has been tested in the numerical models.

Similarly, the results of detailed studies of bed properties have been used to consider parameterised representations of the bed. There are two main aspects to this: consolidation of bed deposits and erosion. The model developed for consolidation is a variant of the Gibson equation based on a fractal representation of the floc structure (Winterwerp, 1999; Merckelbach, 2000). It has been tested in the one-dimensional model. Resistance of the bed to erosion is a crucial parameter in the modelling of cohesive sediment transport, but less well understood. Based on experimental results and theory new formulations have been proposed and incorporated in the model parameterisation.

Simulations have been carried out with a second test case, a schematic estuary, considered as a two-dimensional vertical model. The results prove the ability of the parameterisation developed to represent correctly the cohesive sediment processes when including advection and realistic estuarine processes, such as unsteady tidal hydrodynamic forcing, river discharges, and stratification due to salinity.

Finally, simulations have been carried out in the cases of three different real estuaries: the Weser, the Tamar, and the Loire estuaries. To validate the model results, these are compared with extensive experimental data from the three estuaries, partly collected during the project. The comparison between the models results and these experimental data show that it is now possible to predict cohesive sediment processes correctly in real estuaries.

CONCLUSIONS

The objective of the research programme was to establish well validated physical and mathematical descriptions of the behaviour and fate of concentrated near-bed suspensions (CBS or «fluid mud») and their interaction with the water and the sediment bed.

An experimental programme has been set up to obtain missing data on floc formation, the formation of mud beds and CBS and the influence of floc structure and turbulence on these processes.

Different processes have been studied in detail: turbulence damping in sediment laden flow; turbulence production due to internal waves in concentrated suspensions; flocculation; generation, properties and entrainment of CBS; bed strength development and erosion of mud beds.

The detailed process models have been parameterised to obtain relatively simple formulations which can be implemented in currently used 3D and 2DH engineering system models. The performance of the improved system models has been tested by application of the models to a schematic estuary for which 2DV solutions with the detailed research models were used as a reference.

The models have been applied and tested in three real estuaries (Tamar in U.K., Loire in France and Weser in Germany). All data have been stored in a database, which is accessible to the public.

It is felt that great progress has been made in the physically based description of cohesive sediment dynamics with respect a.o. to the formulation of turbulence damping functions; the modelling of the rheology of CBS, including consolidation; the modelling of flocculation and the modelling of erosion and entrainment of CBS. Engineering software tools have been improved to enable better predictions of mud dynamics for the benefit of estuarine an coastal managers.
More detailed information can also be found on the COSINUS internet site:
http://sun-hydr-01.bwk.kuleuven.ac.be/COSINUS/cosinus.html

ACKNOWLEDGEMENT

This research has been funded in part by the European Commission, Directorate General XII for Science, Research & Development under grant MAS3 – CT97 – 0082.

REFERENCES

Dearnally, M., Roberts, W., Jones, S., Leurer, K., Lintern, D.G., Merckelbach, L.M., Sills, G.C., Toorman, E.A., Winterwerp, J.C., 2000, Measurements and modelling of the properties of cohesive sediment deposits, 6th International Conference on Nearshore and Estuarine Cohesive Sediment Transport Processes (INTERCOH 2000), Delft.

Dyer, K.R., Christie, M.C., Lintern, D.G., Manning, A.J., Roberts, W., Winterwerp, J.C., Measurements and modelling of flocculation and settling velocity, 6th International Conference on Nearshore and Estuarine Cohesive Sediment Transport Processes (INTERCOH 2000), Delft.

Fennessy, M.J., Dyer, K.R., Huntley, D.A., 1994, INSSEV: an instrument to measure the size and settling velocity of flocs in situ, Marine Geology 177:107-117.

Law, D.J., Bale, A.J., Jones, S.E., 1997, Adaptation of focused beam reflectance measurement to in-situ particle sizing in estuaries and coastal waters, Marine Geology 140:47–59.

Merckelbach, L.M., Consolidation and strength evolution of soft mud layers, PhD-thesis Delft University of Technology, 2000.

Toorman, E.A., Bruens, A.W., Kranenburg, C., Winterwerp, J.C., 2000, Interaction of suspended cohesive sediment and turbulence, 6th International Conference on Nearshore and Estuarine Cohesive Sediment Transport Processes (INTERCOH 2000), Delft.

Violeau, D., Markofsky, M., Petersen, O., Roberts, B., Toorman, E.A., 2000, Numerical simulation of cohesive sediment transport: intercomparison of several numerical models, 6th International Conference on Nearshore and Estuarine Cohesive Sediment Transport Processes (INTERCOH 2000), Delft.

Winterwerp, J. C., 1999, On the dynamics of high-concentrated mud suspensions, PhD thesis,T.U.Delft.

Winterwerp, J.C., Bruens, A.W., Gratiot, N., Kranenburg, C., Mory, M., Toorman, E.A., 2000, Dynamics of Concentrated Benthic Suspension Layers, 6th International Conference on Nearshore and Estuarine Cohesive Sediment Transport Processes (INTERCOH 2000), Delft.

SMALL SCALE PHYSICAL SEDIMENT TRANSPORT MODELING APPROACH USED TO SOLVE A CHRONIC DREDGING PROBLEM ON THE ATCHAFALAYA RIVER AT MORGAN CITY, LOUISIANA

By David C. Gordon, Hydraulic Engineer & Robert D. Davinroy, District Potamologist, Applied River Engineering Center, U.S. Army Corps of Engineers, St. Louis District, St. Louis, Missouri; James W. Austin, Hydraulic Engineer, U.S. Army Corps of Engineers, New Orleans District, New Orleans, Louisiana

U.S. Army Corps of Engineers – St. Louis District
Applied River Engineering Center
Foot of Arsenal Street
St. Louis, Missouri 63118
Phone: 314-263-4230
Fax: 314-263-4166
Email: david.gordon@mvs02.usace.army.mil

Abstract: Severe deposition has been experienced at the harbor facilities adjacent to Morgan City on the Atchafalaya River in Louisiana. Changing flow patterns throughout the years have steadily increased the depositional rate. Repetitive maintenance dredging now occurs at this location approximately twice per year. Nearly one million cubic yards of material was removed from this area in 1999.

The U.S. Army Corps of Engineers New Orleans District must maintain a navigation channel as well as navigable depths on both banks of the river due to the ports, facilities, and boat docks that occupy both banklines in this particular reach of the river. Although the city of Berwick, located on the right descending bank, has sufficient depths to maintain navigation, Morgan City, on the opposite bank, has experienced major deposition that may halt navigation into the port facilities.

This reach also has a severe flow and navigational problem. Three bridge crossings are located within approximately 1/3 mile of each other through this reach. While the two upstream bridges have adequate clearance, the downstream bridge is a lift span railroad bridge with a very narrow navigation span. Until the establishment of a stringent traffic control system by the U.S. Coast Guard, this bridge was listed as the "most hit" in the United States. The direction of flow and the high velocity currents in this area have not been conducive to safe navigation conditions through these bridge spans.

In 1999, the New Orleans District initiated a study to examine a possible structural solution to the dredging problem. The District enlisted the help of the St. Louis District's Applied River Engineering Center to model this reach using micro modeling technology. Micro modeling is extremely small-scale, physical hydraulic sediment transport modeling of a river or stream. The modeling technique was used to evaluate the current sediment and flow response trends through this problem area. The model was then used to determine the design and placement of several underwater weir configurations that would lessen the impact of the sediment and flow problems experienced at the site.

INTRODUCTION

Background: "The Atchafalaya River is the largest of all distributaries of the Mississippi River. The Corps of Engineers is responsible for maintaining a 12-foot deep by 125-foot wide Atchafalaya navigation channel that extends from the Mississippi River via the Old River Lock downstream to the Gulf Intracoastal Waterway System (GIW) at Morgan City. Navigation is thereby shortened by almost 172 miles for vessels sailing between the Mississippi above the Old River Lock and the GIW in Southern Louisiana, saving time, money, and energy, and lessening traffic congestion at the port of New Orleans. The Lower Atchafalaya River is the natural outlet for the Atchafalaya River Basin, draining flows past Morgan City and Berwick into the Atchafalaya Bay and Gulf of Mexico." (U.S. Army Corps of Engineers) This study encompassed the Berwick Bay reach, which is located on the Atchafalaya River between Morgan City and Berwick, Louisiana. This section of waterway is comprised of a complex network of GIW branches that converge through this reach to produce a very congested area.

Sedimentation Problem: This particular stretch of river has been one of the most troublesome reaches on the Atchafalaya River in terms of dredging cost, frequency, and volume. The New Orleans District must maintain 12-foot navigation depths along the banklines of both cities to ensure adequate depths for the ports, facilities, and boat docks that are located in this area. Although Berwick has sufficient depth to maintain navigation, Morgan City is faced with a large depositional area that may accumulate enough sediment to halt navigation into the port facilities. Throughout the years, the planform of the river upstream of Berwick Bay has gradually changed. These changes have altered the flow patterns within the Bay, which has caused a steady increase in the rate of deposition at the Morgan City harbor. The New Orleans District currently dredges at this location approximately twice per year. Nearly one million cubic yards of material was removed from this site in 1999. Figure 1 is an aerial map showing the existing planform of the river.

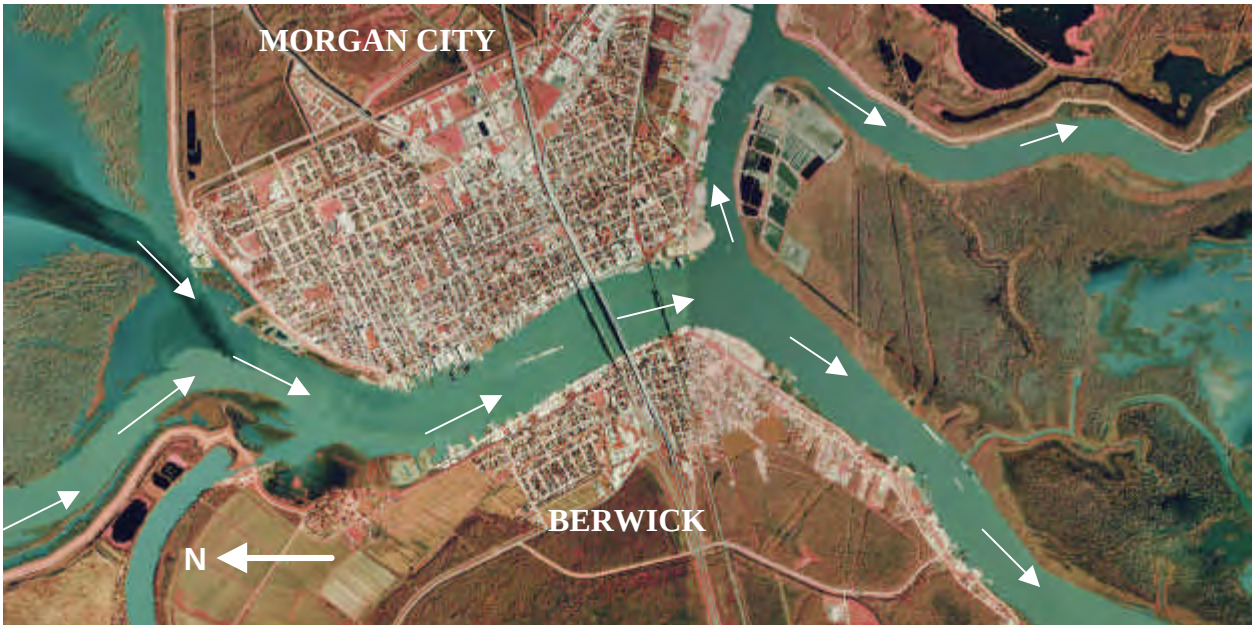

Figure 1: Aerial Photograph of the Atchafalaya River at Morgan City and Berwick, Louisiana.

Navigation Problem: Another concern in this reach of river is safety. Within Berwick Bay, three bridge crossings are located within a 1/3-mile stretch of river. Both the old and new U.S. Highway 90 bridges are located near Mile 121.0 while the Southern Pacific Railroad Bridge is located at Mile 121.3. The two highway bridges contain adequate navigation span widths of 580 feet and 520 feet. The Southern Pacific Railroad Bridge contains a lift-span with an extremely narrow navigation width of approximately 320 feet. Until the establishment of a stringent traffic control system by the U.S. Coast Guard in 1974, this bridge was listed as the "most hit" in the United States. Historically, the flow and direction of currents in this area have not been conducive to safely navigating through these bridge spans. While the navigation spans of the bridge crossings are located in the center of the channel, the thalweg and the main concentration of flow are located along the right descending bankline on the Berwick side of the river. Therefore, downbound vessels navigating through the bridge spans have experienced the tendency to be directed by the river currents toward the right descending bank. The misalignment of currents with the navigation spans has forced tow pilots to make careful adjustments to their vessels while approaching the bridges from well upstream. A slightly misguided tow could easily collide with the many bridge piers located within the channel.

The following report was posted on the U.S. Coast Guard web site. "The Berwick Bay Vessel Traffic Service (VTS) was established by the US. Coast Guard in 1974 under the authority of the Ports and Waterways Safety Act of 1972 to improve maritime safety in Berwick Bay. This is one of the most hazardous waterways in the United States due to strong currents and a series of bridges that must be negotiated by inland tows traveling between Houston, Baton Rouge and New Orleans. In 1987, VTS Berwick Bay became part of the newly formed Marine Safety Office in Morgan City, Louisiana. This busy intersection, coupled with the narrow bridge navigation spans requires the VTS to maintain one-way traffic flow through the bridges. During seasonal high water periods, the VTS enforces towing regulations that require inland tows transiting the bridges to have a minimum amount of horsepower based on the length of tow. The direct control nature of the VTS's operations, and the high water towing regulations it enforces, makes VTS Berwick Bay unique among Coast Guard Vessel Traffic Services. These measures have successfully reduced the accident rate for inland tows transiting Berwick Bay from approximately four accidents per 1000 tow transits in 1990 to 0.38 accidents per 1000 tow transits in 1998. This amazing success resulted in the VTS being awarded a Vice-Presidential Hammer Award in 1996." (U.S. Coast Guard)

MICRO MODELING

Berwick Bay Micro Model: The model used for this study was constructed according to the high-resolution aerial photograph of the study reach shown in Figure 1. Figure 2 is a photograph of the Berwick Bay hydraulic micro model used in this study. The scales of the model were 1 inch = 600 feet, or 1:7200 horizontal, and 1 inch = 100 feet, or 1:1200 vertical, for a 6 to 1 distortion ratio. This distortion supplied the necessary forces required for the simulation of sediment transport conditions similar to those of the prototype (Davinroy). The bed material used was granular plastic urea, Type II, with a specific gravity of 1.4.

In all model tests, an effective discharge or hydrograph was simulated in the Atchafalaya River channel. This hydrograph served as the average design energy response of the river. Because of

the constant variation experienced in the prototype, this hydrograph was used to theoretically analyze the ultimate expected sediment response. Each hydrograph simulated a discharge range between extreme low flow to high "within-channel" flow. Flow rates in the model ranged between 0.85 to 1.35 gallons per minute. The most important factors during the micro modeling process are an equilibrium condition of sediment transport and the simulation of high and low energy conditions. High flow in the model simulated a peak energy condition representative of the river's bed forming flow and sediment transport potential at bankfull stage. The time increment or duration of each hydrograph cycle (peak to peak) was two minutes.

Figure 2: Morgan City Micro Model

The calibration/verification of the micro model involved the adjustment of water discharge, sediment volume, hydrograph time scale, model slope, and entrance conditions of the model. These parameters were refined until the measured bed response of the model was similar to that of the prototype. Data available from the prototype used for the calibration process included several hydrographic surveys, Acoustic Doppler Current Profiler (ADCP) velocity data, aerial photographs, and on-site field reconnaissance. Model calibration was achieved once a favorable comparison of the prototype surveys was made to several surveys of the model. The resultant bathymetry of this bed response served as the base test of the micro model. Figures 3 and 4 show the prototype survey used for model calibration and the resultant bed configuration of the micro model base test. The depositional area is shown in both surveys along the left descending bankline. The base test was developed from the simulation of successive repeatable design hydrographs until bed stability was reached and a similar bed response was achieved as compared with prototype surveys. This survey then served as the comparison bathymetry for all design alternative tests.

In addition to the bathymetry recorded from the model, flow visualization information was also collected. Photographic time exposure was used to examine the general surface current patterns of the base test and of each design alternative test. Flow visualization photographs were taken at both low flow and high flow to better understand the flow patterns associated with each design alternative.

Figure 5 shows the flow visualization photo of the base test, which served as the comparison flow patterns for all design alternative tests. The trends of the model were very similar to the prototype velocity vectors established from the ADCP data. The model demonstrated that most of the flow was concentrated along the right descending bank and to the right of the navigation spans which are located in the center of the channel.

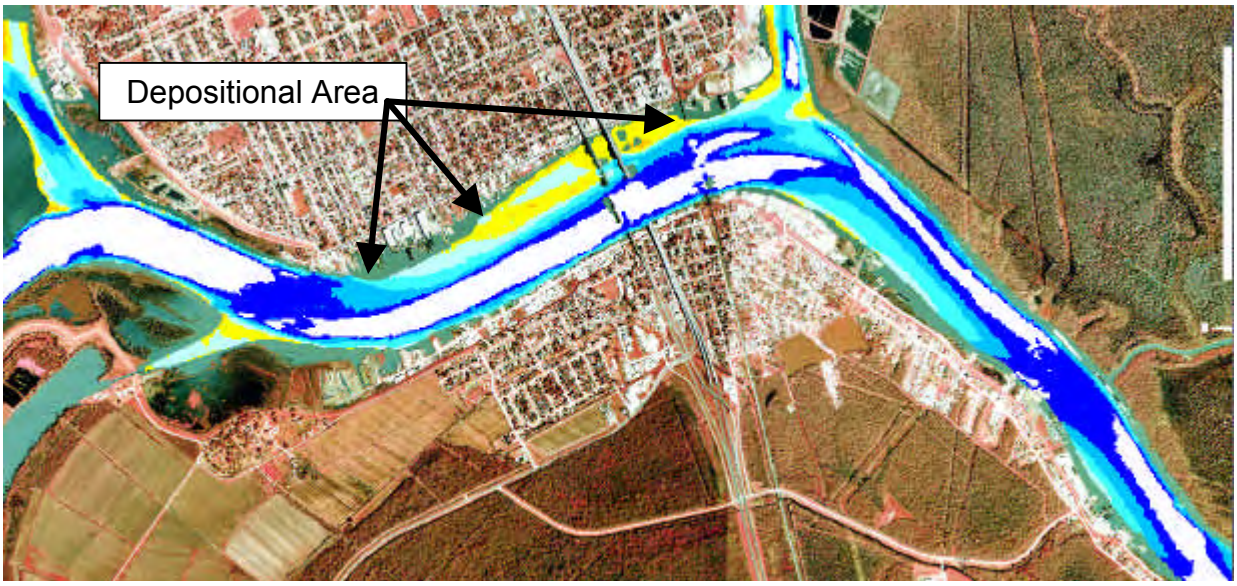

Figure 3: Bathymetry from the Atchafalaya River used to Calibrate the Micro Model.

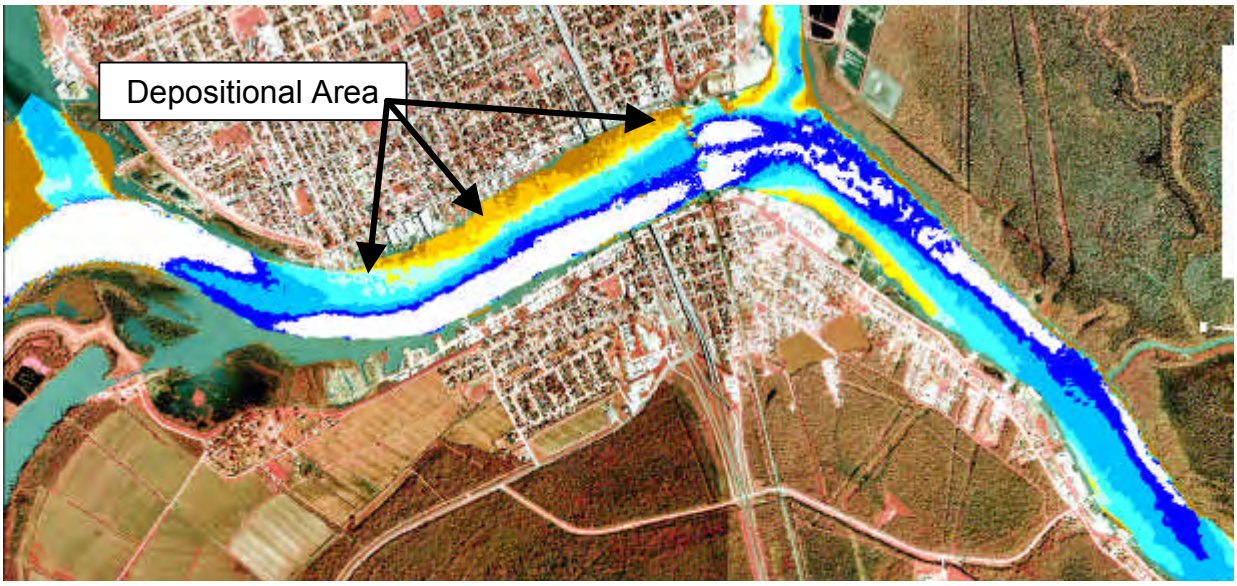

Figure 4: Bathymetry from the Micro Model Base Test.

Eleven design alternative plans were model tested to examine methods of changing the sediment response to improve sediment distribution, flow conditions and navigation through the Berwick Bay reach. The impacts induced by each alternative design were assessed by examining both the flow and sediment response of the model. The effectiveness of each design was evaluated by comparing the resultant bed configuration and flow patterns to those of the base test condition.

The only river training structures model tested to solve the problems in the Morgan City/Berwick Bay reach was of the underwater variety. It was required by the study that any design solution could not restrict vessel movement between both banklines of the river. Therefore, traditional dike structures were not considered feasible. All the weir designs studied in the micro model were tested at depths suitable for the passage of barge traffic at all river stages.

RESULTS

The micro model indicated that the most effective design to solve the problems consisted of 10 bendway weirs located within a one-mile reach of river and at a depth of –20 feet below the low water stage. The resultant flow patterns and bathymetry developed by this design in the model are shown in Figures 6 and 7. The results demonstrated that the design proved very effective at removing a substantial portion of the depositional area along the left descending bankline. The design also completely shifted the thalweg towards the center of the channel at the upstream portion of the reach. The weir field effectively created a smooth transition of the thalweg from the bend towards the middle of the channel and into the straight reach upstream of the bridges.

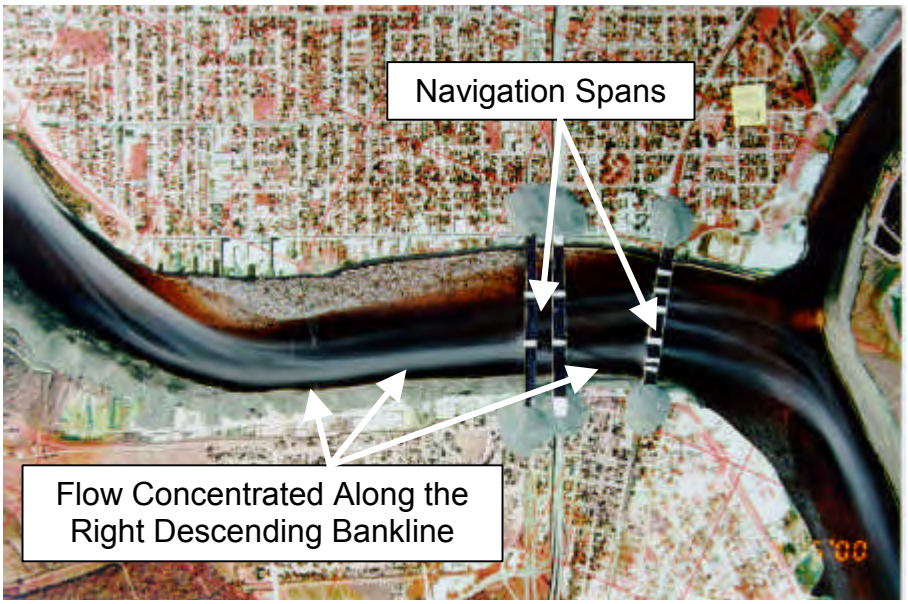

Figure 5: Micro Model Base Test Flow Visualization

Figure 6: Flow Patterns Developed by Bendway Weirs in the Alternative Design

The flow visualization photos demonstrated a significant redistribution of flow across the channel width. The design indicated that the flow patterns were more evenly distributed across the entire channel width and were no longer concentrated along the right descending bankline. This change in flow patterns may decrease the dangerous currents that effect downbound tows navigating through the bridge openings

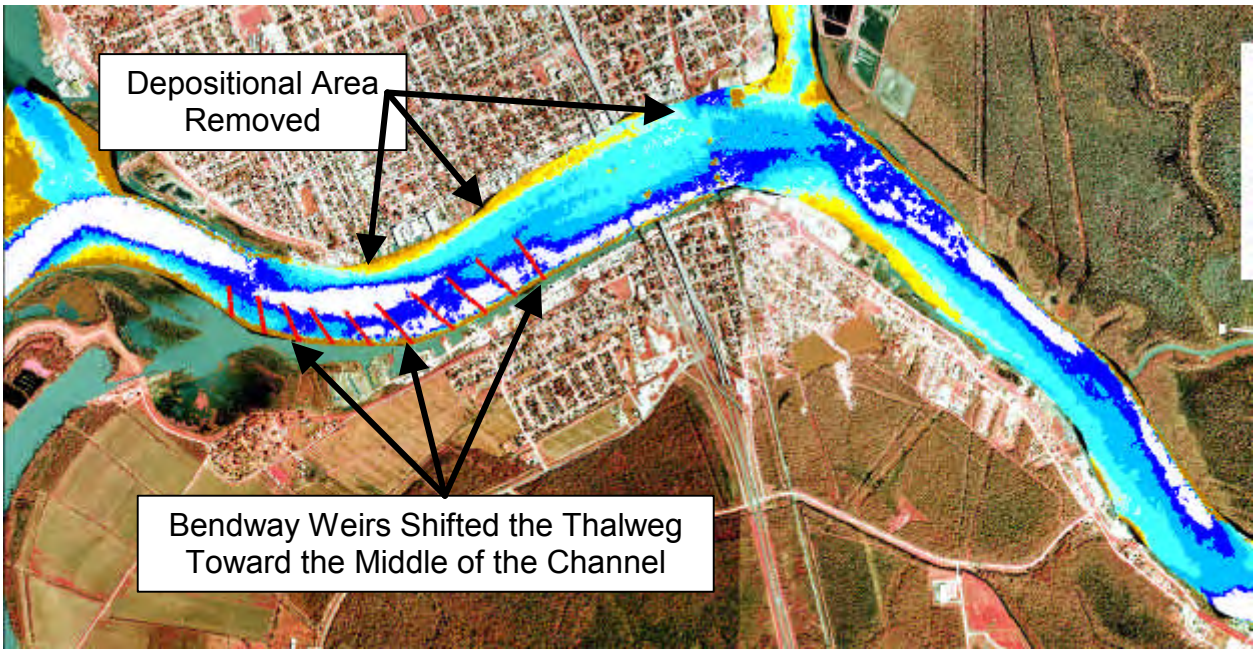

Figure 7: Bathymetry Developed by Bendway Weirs in the Alternative Design

The historically precarious nature of this reach of river has caused river engineers to use extreme caution when significantly changing the flow patterns in this dangerous and busy reach of river. Therefore, the results of the micro model will be used in a three-dimensional numerical flow model at the University of Iowa to further evaluate the flow conditions induced by the bendway weir design. The results from this model will then be applied to a computer navigation simulator at the Corps of Engineer's Coastal and Hydraulics Laboratory in Vicksburg, Mississippi to study the effects of these flow conditions on a typical tow navigating this reach of river. Construction of the design may begin only after these models are completed and approvals are obtained from the towing industry and the U.S. Coast Guard.

REFERENCES

Davinroy, Robert D., 1994, Physical Sediment Modeling of the Mississippi River on a Micro Scale, University of Missouri-Rolla Thesis.

Gordon, David C., Davinroy, Robert D., 2000, Sedimentation and Navigation Study of the Lower Atchafalaya River at Morgan City & Berwick, Louisiana, River Miles 188.5 to 124.0, Hydraulic Micro Model Investigation.

Leopold, Luna B., 1995, A View of the River.

U.S. Army Corps of Engineers, 1999, Atchafalaya River Navigation Charts.

U.S. Coast Guard, 2000, U.S. Coast Guard Web Site: http://www.uscg.mil/d8/uscgd8.htm.

NUMERICAL MODELING OF DYNAMIC RIVER ADJUSTMENT

Blair Greimann, (1), Chih Ted Yang (2), and Drew Baird (3)

(1) Hydraulic Engineer, United States Bureau of Reclamation, Denver Federal Center, Bldg. 67, P.O. Box 25007 (D-8540), Denver, CO 80225-0007, PH (303) 445-2563, FAX (303) 445-6351, email: bgreimann@do.usbr.gov
(2) Manager, Sedimentation and River Hydraulics, United States Bureau of Reclamation, Denver Federal Center, Bldg. 67, P.O. Box 25007 (D-8540), Denver, CO 80225-0007, PH (303) 445-2554, FAX (303) 445-2550, email: tyang@do.usbr.gov
(3) United States Bureau of Reclamation, 505 Marquette Ave NW, Suite 1313, Albuquerque, NM, 87102, PH 505-248-5335, FAX 505-248-5356, email: dbaird@uc.usbr.gov

Abstract: The principle of minimum energy dissipation rate is used in static and dynamic models to predict channel geometry in the Rio Grande. The static model is simple to apply and gave reasonable predictions of channel width. It did not predict channel slope or depth well, however. A dynamic model was also applied to the same reach. The bed profile and total channel deposition were simulated with reasonable accuracy. However, the principle of minimum energy dissipation rate has not yet been incorporated into the simulation. Further work is directed towards this goal and to evaluating the sensitivity of the model to the required inputs.

INTRODUCTION

Changes in flow and sediment supply can cause changes in the depth, width, slope and roughness of a river. This paper focuses on using the theory of minimum energy dissipation rate to develop models to predict channel geometry. Models using minimum energy dissipation rate to predict channel geometry can be divided into two main groups: static models and dynamic models. Static models calculate the channel geometry assuming that the variables being considered are practically constant over a specified length and time. Dynamic models calculate the rate of channel geometry change in response to changing boundary conditions, such as changes in flow or sediment supply.

Examples of static models can be found in Yang et al. (1981), who employed a derivative of minimum energy dissipation rate theory, the minimum unit stream power concept, to derive coefficients relating depth and width to flow rate. Deng and Zhang (1994) used the principle of maximum entropy and the concept of unit stream power to derive equations for the channel depth and width. It should be noted that using the second law of thermodynamics, maximizing the entropy corresponds to minimizing the energy dissipation rate.

An example of a dynamic model using minimum energy dissipation rate theory is GSTARS2.0 (Generalized Stream Tube Alluvial River Simulation Model, Version 2.0, Yang et al. 1998). In this model, the channel roughness is assumed constant and the width and depth are free to change so that the energy dissipation rate is minimized.

In this paper, we first describe the general procedure to predict the width, depth and slope of a river given the flow rate, sediment concentration, channel roughness and bed particle size. We then apply this to the case of the Upper Soccorro reach of the Rio Grande. Next, we describe the

general principles used in GSTARS2.0 to predict the dynamic changes in channel geometry and apply it to the same reach. As this is an ongoing project, only preliminary results are available from dynamic modeling.

GOVERNING EQUATIONS OF CHANNEL MORPHOLOGY USING MINIMUM UNIT STREAM POWER

In uniform channels, the common variables associated with channel geometry are:

$$C, Q, W, V, D, S, d_p, n$$

where C is the sediment concentration (defined here as $C = Q_s/Q$, where Q_s is the sediment flow rate), Q is the water flow rate, W is the channel width, V is the channel velocity, D is the channel depth, S is the energy slope, d_p is the representative particle diameter, and n is the channel roughness. The equations available are:

Continuity:

$$Q = VWD \qquad \text{Eq. 1}$$

Stream Hydraulics:

(R_h is the hydraulic radius)

$$V = \frac{C_m}{n} R_h^{\frac{2}{3}} S^{\frac{1}{2}} \qquad \text{Eq. 2}$$

Sediment transport:

(a_1 and a_2 are functions of S, D and d_p, w_f is the fall velocity, V_c is the critical velocity of sediment motion)

$$\log C = a_1(S, D, d_p) + a_2(S, D, d_p) \log\left(\frac{(V - V_c)S}{w_f}\right) \qquad \text{Eq. 3}$$

We still need another equation to solve the problem and it can be obtained by using the concept of minimum energy dissipation rate and the result of Yang (1973) to give:

Minimum Unit Stream Power:

$$VS \rightarrow \min \qquad \text{Eq. 4}$$

To solve this problem, the fixed quantities and free variables need to be determined. For specific reaches of stream Q, C, and d_p can be considered as fixed quantities specified as input. It will be assumed that the variables W, D, S, V and n are free to adjust so that the Eq. 4 is minimized and the constraints given in Eqs. 1 to 3 are satisfied. Therefore, in general, these five variables are dependent variables. The sediment transport relation is given in the form of Yang's (1973) equation, but other equations could be substituted in this analysis as well. However, Yang's (1973) equation is consistent with the assumption that the unit stream power is the dominant variable in determining sediment transport and channel morphology.

A program was written to systematically vary n and solve for the resulting W, D, S, and V that gave the minimum VS subject to the constraints given in Eqs. 1 to 3. For a given n, the minimization was performed by first systematically varying W over the range of physically reasonable widths. For each W, the D, S and V that satisfy Eqs. 1 to 3 were found and then the W

that gave the minimum *VS* was chosen as the solution. In the next section, this program is applied to the Upper Soccorro reach of the Rio Grande.

APPLICATION TO THE CHANNEL MORPHOLOGY OF THE RIO GRANDE

During the period from 1972 to 1992, the Upper Soccorro reach of the Rio Grande has experienced channel narrowing and deepening (see Figure 1). It is suspected that the decrease in the average sediment concentration starting in 1973 (see Figure 2) was the major cause of this narrowing. The decrease in sediment concentration was largely due to the closing of Cochiti Dam in 1972.

In Figure 1, one can see that the narrowing has not yet extended into the lower reaches. However, it is possible that the general narrowing due to the reduced sediment supply is gradually propagating downstream and will eventually impact the lower reaches. Therefore, it would be useful to first see if we can simulate the historical channel narrowing seen in the Upper Soccorro and then predict what will happen in the future in this reach and others.

Table 1. Location of reaches in term of river mile (RM).

Reach	**Approximate RM**
Upper Socorro	116.1 to 97.8
Lower Socorro	97.8 to 87.3
Upper Bosque	87.3 to 77.1
Lower Bosque	77.1 to 69.3
Ft. Craig	69.3 to 60.8

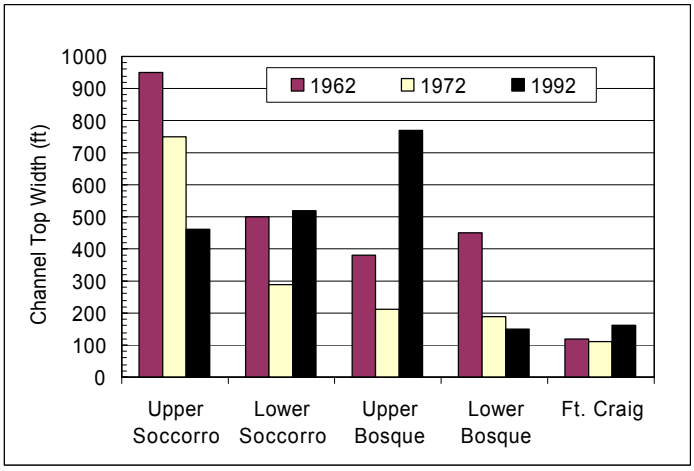

Figure 1. Channel top width for a flow of 5000 cfs from 1962 to 1992.

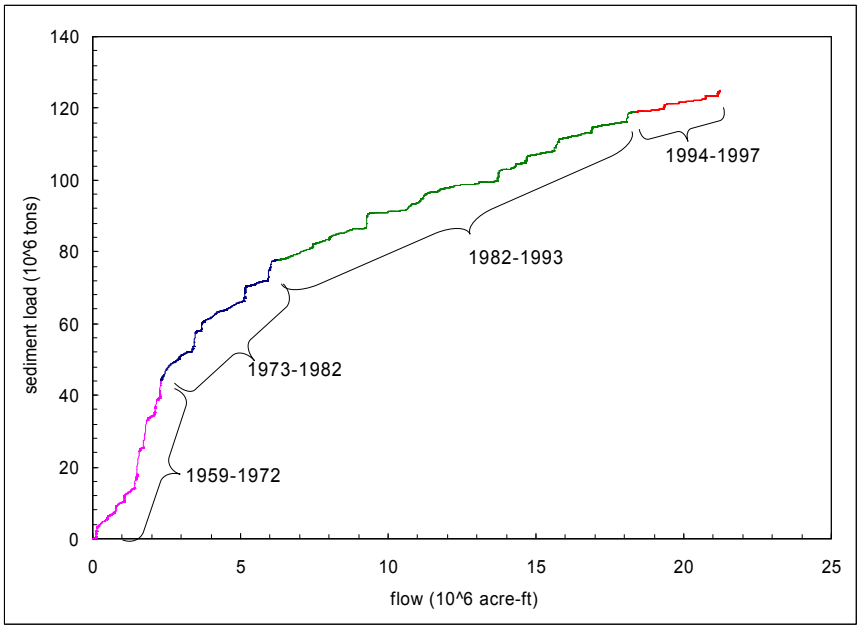

Figure 2. Double mass curve showing the decrease in average sediment concentration starting in 1973 and continuing until the present.

The program to solve Eqs. 1 to 4 was used to simulate the channel narrowing to the Upper Soccorro reach from 1972 to 1992. To use this program it is necessary to determine the representative flow rate (Q), the representative diameter (d_p), the concentration (C) corresponding to the dominant flow rate, and the expected range of channel roughness (n). Determining these variables is not trivial and is the most important part of the solution. Based on analyses of channel response to flow, the channel forming flow was determined to be the average of the peak flows from the previous 5 years. The representative diameter (d_{50}) was chosen as the diameter that 50% of the material is finer than. The concentration is calculated by first fitting a curve to the measured sediment loads for the size class that includes the representative diameter. Then that load is converted into a concentration and is divided by the fraction of that size class in the bed. The total sediment concentration of all the size classes should not be used because that often includes a significant amount of wash load, or sediment load that simply passes through the system and does not significantly affect channel formation. The period of record used to compute the sediment concentration was the prior 10 years. The roughness coefficients found in Table 2 are estimates from previous water surface profile simulations in that reach.

Table 2. Measured channel properties for upper Socorro.

year	Width (ft)	Depth (ft)	Slope (-)	Flow (cfs)	d_{50} (mm)	Roughness n	Concentration (mg/l)
1972	715	2.75	0.00089	4200	0.20	0.020	3100
1992	435	3.45	0.00086	4100	0.25	0.020	1300

The simulated channel width, depth and slope are given in Table 3. It was assumed that the n = 0.020 for all the simulations. The channel roughness can in reality change in response to

sediment load. However, the channel width proved rather insensitive to the choice of n and therefore assuming it is constant does not significantly affect the results for channel width. For example, in the 1972 simulation, the channel width varied between 862 and 767 ft for n varying from 0.01 to 0.04.

The widths were well predicted, but the slope and depth were generally not well predicted. The over prediction in slope could be due to the fact that the channel is assumed to be rectangular. In reality, the channel has a deep portion that conveys most of the sediment and water. This configuration is more efficient in transporting sediment than a rectangular section because the sediment flow rate per width is proportional to the water discharge per width raised to a power greater than one. Non-uniform flow in the transverse direction is more efficient in transporting sediment than uniform flow in the transverse direction. As a result, a slope greater than the actual slope is required in the simulation to provide the transport seen in the natural channel.

Table 3. Variables computed using procedure outlined in Eqs. 1-4. Other variables were assumed from Table 2.

year	Width (ft)	Depth (ft)	Slope (-)
1972	810	1.4	0.0018
1992	420	2.4	0.0010

INCORPORATION OF MINIMIZATION INTO SEDIMENT ROUTING MODELS

Reclamation has developed models that have incorporated minimization principles into a hydraulic and sediment routing model (e.g. GSTARS2.0). In a hydraulic and sediment routing model, the following variables are introduced:

$$Q_{si}, Q, W_i, V_i, D_i, Z_i, d_{p_i}, n_i, L_i \;;\; i = 1, N \;;\; N = \text{number of reaches}$$

where Z_i is the channel bottom elevation, and L_i is the distance between cross sections.
The equations available to compute channel morphology and sediment transport are listed below in simplified form:

Continuity:

$$Q_i = V_i W_i D_i \qquad \text{Eq. 5}$$

Stream Hydraulics:

$$\frac{V_i^2}{2g} + Z_i + D_i = \frac{V_{i-1}^2}{2g} + Z_{i-1} + D_{i-1} + \overline{S_{i,i-1}} L_i \;;\; \text{for } j = N \text{ to } I \qquad \text{Eq. 6}$$

Sediment Transport:

$$Q_{si} = f\left(Q_i, W_i, D_i, V_i, d_{pi}\right) \qquad \text{Eq. 7}$$

Bed elevation change:
(A_b is the cross sectional area of the bed above some datum)

$$\Delta A_{bi} = \frac{\left(Q_{si-1} - Q_{si}\right)\Delta t}{L_i} \qquad \text{Eq. 8}$$

Minimum Energy Dissipation Rate Principle:

$$\sum_{i=1}^{N} \gamma Q_i S_{fi} L_i \rightarrow \min \qquad \text{Eq. 9}$$

In GSTARS2.0, the flow rate (Q_i), the roughness (n_i) and the distance between cross sections (L_i) is fixed as well as the sediment flow rate at the upstream cross section (Q_{s1}). At each time step, the channel width (W_i) and/or bottom elevation (Z_i) is adjusted so that the summation in Eq. 9 is minimized. The depth (D_i), velocity (V_i), particle diameter (d_{pi}), and sediment flow rate (Q_{si}, i = 2, N) are also free to adjust but are not explicitly incorporated into the minimization process.

APPLICATION TO THE CHANNEL MORPHOLOGY OF THE RIO GRANDE

The GSTARS2.0 model was used to simulate the sediment transport and channel morphology from 1972 to 1992 of the upper portion of the Upper Soccorro reach of the Rio Grande. At the time of the writing of this paper, the model has only been run without incorporating the minimization principle. The input to the model includes the flow rates (Q), sediment loads (Q_s), channel roughness (n), the initial channel geometry (Z, D), and the initial bed material (d_p). In addition, several computational parameters are required, such as the active layer thickness, angle of repose, sediment transport formula, and number of stream tubes used.

Flow rates were taken from the average daily flows published in the US Geological Survey stream gage record (USGS gage Rio Grande Floodway At San Acacia, Station number 08354900). Several suspended sediment load measurements were taken from 1967 to 1993. The suspended sediment load was converted into the total load using the modified Einstein approach. The resulting total loads were analyzed to determine the average fraction of each size class as a function of flow rate. Previous simulations in downstream reaches used a modified Laursen formula (Madden, 1993) and this transport formula was used here as well.

The model was first calibrated so that the overall channel deposition and erosion were simulated correctly without employing the minimization concept. In this mode, the model behaves similarly to more convention sediment transport models (e.g. HEC-6, US Army Corp of Engineers, 1993). The main calibration parameters were the Manning roughness coefficients and active layer thickness. The calibrated roughness coefficient was 0.02 and the active layer thickness was 50 times the diameter of the largest particle, which translates to an active layer thickness of approximately 7 cm in most of the reach. In GSTARS2.0, there is the ability to use multiple stream tubes to route the sediment. In the initial simulations, however, only one stream tube was used in the main channel.

The comparison between the simulated and actual bed profile in 1992 is found in Figure 3. There is very good agreement for locations downstream of RM 113. Upstream of RM 113, the elevations are too low. Part of discrepancy is because the most upstream cross section has been artificially armored with large rock, as it is located immediately downstream of San Acacia. The model does not presently take this into account. The comparison between the simulated and measured channel erosion is found in Figure 4. Both the total and main channel measured deposition is shown in Figure 4. The model was calibrated to reproduce the total deposition. The agreement between simulated and measured deposition is accurate upstream of RM 107. Downstream of RM 107 the erosion is over predicted. The interaction between the floodplain

and main channel is not accurately represented and this could cause some of the discrepancy. A hint that this is the case is that fact that the magnitude of deposition follows that of the total cross section, but the trend follows that of the main channel.

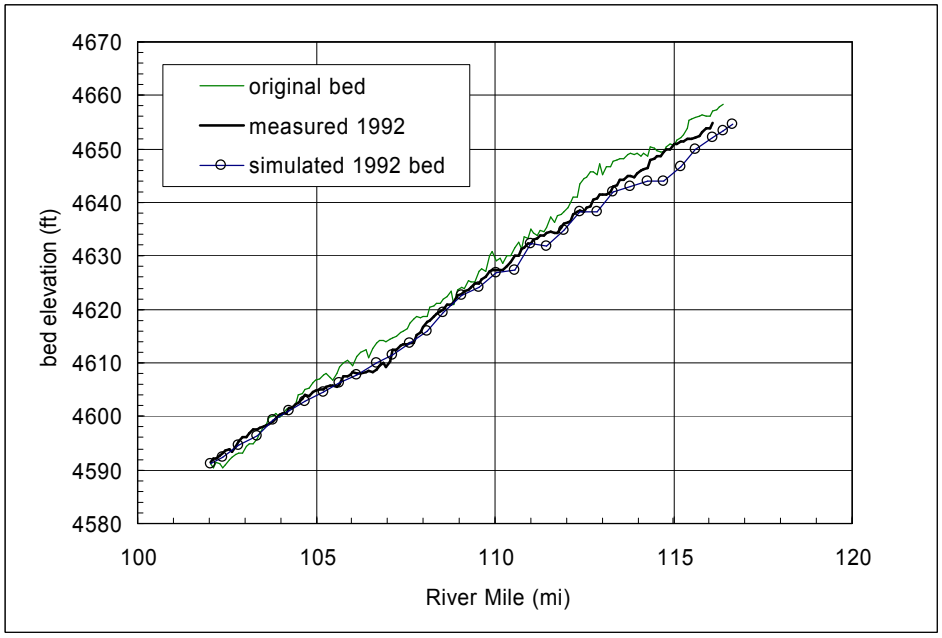

Figure 3. Minimum bed elevation profile in modeled reach.

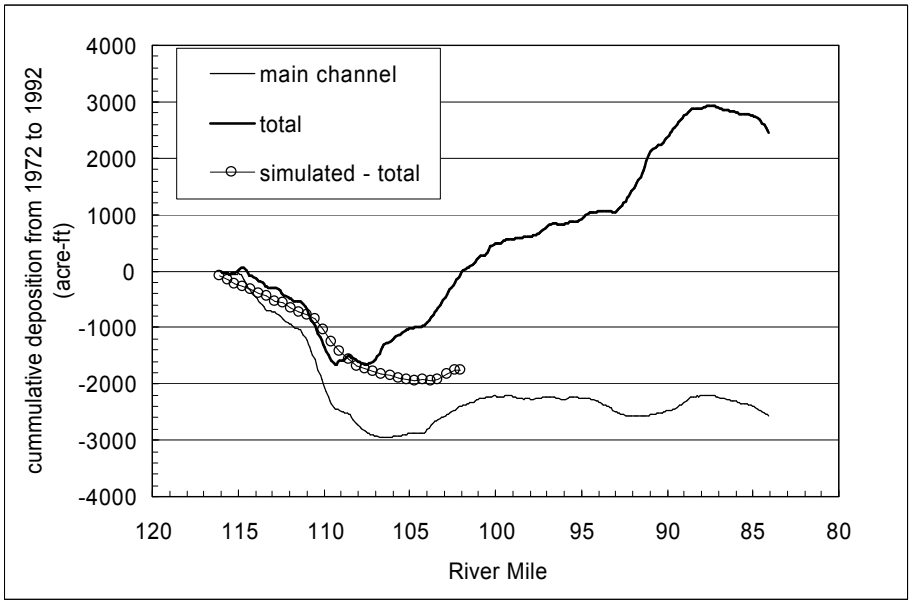

Figure 4. Measured and simulated cumulative deposition in the Rio Grande from 1972 to1992.

SUMMARY AND FUTURE WORK

Using hydraulic principles along with the principle of minimum energy dissipation rate or its simplified form of minimum unit stream power, a program was developed to predict the static width, depth and slope of channel given the flow rate, sediment supply, channel roughness and

bed material. This program was used to predict the channel width, depth and slope of the Rio Grande in 1972 and 1992.

A sediment routing model (GSTARS2.0) that predicts the dynamic adjustment of the width, depth, and slope in response to specific input was used to simulate the same reach for the same time period. The agreement between the simulated bed profile and overall channel deposition with measurements is reasonable. Further work is necessary to incorporate the minimization of energy dissipation rate into the simulation and predict changes in river width. Future work will also aim to more accurately represent interactions between the main channel and floodplain.

REFERENCES

Deng, Z., and Zhang, K., 1994, "Morphological Equations Based on the Principle of Maximum Entropy," Internation Journal of Sediment Reserach, Vol. 9., No. 1, pp. 31-46.

Madden, E.B., "Modified Laursen Method for Estimating Bed-Material Sediment Load", US Army Corps of Engineers, Waterways Experiment Station, Contract Report HL-93-3, Oct 1993.

U.S. Army Corps of Engineers – Hydrologic Engineering Center, August 1993, HEC-6 Scour and deposition in rivers and reservoirs, User's Manual, Version 4.1.

Yang, C.T., Song, C.C., Woldenberg, M.T., 1981, "Hydraulic Geometry and Minimum Rate of Energy Dissipation," Water Resources Research, Vol. 17, pp. 877-896.

Yang, C.T., 1973, "Incipient Motion and Sediment Transport," J. Hydr. Div, ASCE, Vol. 99, No. 10.

Yang, C.T., Treviño, M.A., and Simões, F.J.M., 1998, User's Manual for GSTARS2.0, Bureau of Reclamation, Denver, CO.

MODELING OF SEDIMENTATION PROCESSES IN CHANNEL NETWORKS

By Dalmo A. Vieira, Research Associate; Weiming Wu, Research Scientist; Sam S. Y. Wang, Director, National Center for Computational Hydroscience and Engineering, The University of Mississippi, University, MS.

Abstract

The CCHE1D modeling system is designed to simulate long-term sedimentation processes in channel networks. The model simulates bed aggradation and degradation, bed material composition (hydraulic sorting and armoring), bank erosion, and the resulting channel morphologic changes under unsteady flow conditions. CCHE1D uses a watershed-based approach, in which the watershed is segmented according to its natural drainage network. The channel model can be easily used in conjunction with existing watershed processes models to produce more accurate and reliable estimations of sediment loads and morphological changes in channel networks. CCHE1D has a GIS-based graphical interface that provides support for automated spatial analysis, digital mapping, and visualization of modeling results.

INTRODUCTION

CCHE1D is a software system that simulates flow and sedimentation processes in channel networks. CCHE1D considers a channel network as an integral part of the watershed, and was especially designed to provide straightforward integration with watershed processes (rainfall-runoff and field erosion) models. The CCHE1D channel network model computes unsteady flows using either the Dynamic or Diffusion Wave approaches. The model is able to account for the influence of in-stream hydraulic structures such as low and high drop structures, culverts, measuring flumes, and bridge crossings on flow and sediment yield.

CCHE1D calculates non-equilibrium, non-uniform sediment transport and the resulting channel bed changes and bed material sorting. The model also simulates channel-widening processes through bank erosion and stability analysis algorithms. It offers four sediment transport capacity formulas and a variety of methods for the computation of parameters such as bed material porosity, mixing layer thickness, movable bed roughness coefficient, and the adaptation length for non-equilibrium transport, which allows the model to be applicable to a wider range of real-life problems.

CCHE1D utilizes Geographical Information Systems (GIS) technology to provide support for automated spatial analysis, digital mapping, and visualization. The definition of the channel network and its corresponding subcatchments can be automatically obtained from a Digital Elevation Model (DEM) through the landscape analysis model TOPAZ. The system includes a data management module that generates maps and graphics and performs the necessary data conversions and transfers. CCHE1D also manages the generation of a computational mesh based on the extracted channel network, and provides a graphical user interface for the control of all phases of simulation, and pre- and post-processing operations.

CCHE1D can be used as a tool for the evaluation of the effectiveness of erosion control and channel remediation measures on sediment yield, and to study the influence of land use changes

and agricultural management practices on sedimentation. The CCHE1D model has been validated using a series of laboratory experiments of aggradation and degradation processes, and it has been applied successfully in the prediction of sediment yield and channel morphologic changes of the Goodwin Creek watershed, in Northern Mississippi.

CHANNEL PROCESSES MODELING

CCHE1D performs continuous simulations of unsteady flow, sediment transport, and the resulting morphological changes. The model accounts for dynamic effects due to flow unsteadiness, which allows for a more realistic computation of erosion and sedimentation processes. In many watersheds, important morphological changes are usually caused by large storm events that occur only a couple of times during the calendar year and are usually associated with flooding. Flow parameters are in rapid and continuous change. When evaluating the transport of sediment and the consequent changes in the channel bed and banks, it is important to account for these dynamic effects. In many instances, the computation of sediment transport under the assumption of steady flow can lead to important inaccuracies because the flow conditions vary substantially, not only because of the passing of the flood wave itself, but also as result of changes in the river bed due to erosion or deposition. Accounting for the effects of floodplains in the computation of flow hydraulics is also important for the more accurate determination of water flow rates and stages.

CCHE1D contains special procedures for the computation of flow across hydraulic structures like culverts, low and high-drop structures, bridges and measuring flumes. Usually in-stream structures determine the local flow hydraulics, therefore affecting the erosion and sedimentation processes in their neighborhood. Some of these structures are built as erosion control devices; therefore it is important that the model simulates their effect on sediment transport with reasonable accuracy.

CCHE1D computes the transport of non-uniform sediment using the non-equilibrium approach. The model computes variations of the bed material gradation by dividing the bed into several layers, simulating hydraulic sorting and armoring processes. These processes are common in natural river systems, and their correct representation is necessary especially for long-term predictions of channel evolution.

The model provides several well-known equations for the determination of transport capacity, and a series of options for the computation of auxiliary parameters such as bed material porosity, mixing layer thickness, non-equilibrium adaptation length, wash load size range, movable bed roughness coefficient, etc. This allows the modeler to choose which formulation suits best the case under study.

CCHE1D computes sediment transport, bed changes, and bed material gradation using an advanced coupling procedure (Wu et al., 2000). The main advantage of the coupled approach is enhanced numerical stability. However, the sediment computations are decoupled from the flow calculations.

Bank erosion and channel widening can significantly affect the sediment balance of a channel system. These processes must be modeled for the prediction of sediment yield and channel morphological evolution. Bed degradation and lateral erosion at bank toes may cause river banks to become unstable. CCHE1D simulates toe erosion using an empirical relationship (Arulanandan et al., 1980). A bank stability algorithm computes a safety factor defined as the

ratio of the resistance and driving forces for the bank failure. Once the stability criterion is exceeded, a mass failure event occurs. The failed bank materials deposit first on the bed near the bank toe (or are saved to a virtual tank), and then are eroded away by bank toe erosion.

CCHE1D SOFTWARE

The CCHE1D flow and sediment transport model is a part of a software system that supports the user and makes it easier to be applied in the solution of real-life problems. The model is incorporated into a graphical interface program that provides a series of support utilities, including Geographical Information Systems (GIS) functionality. CCHE1D uses the ArcView GIS program to implement many of its features. The interface integrates several programs, providing the user with a set of dynamic menus and buttons that controls all operations. CCHE1D provides graphical feedback by displaying most of the spatial data sets in the form of maps. Point-and-click tools help the user supply information such as channel cross-section data (geometry, bed and bank properties).

CCHE1D promotes integration with watershed models for the determination of the upland contribution of water and sediment. Results from rainfall-runoff and soil erosion simulations performed by watershed models such as AGNPS-98 (AGricultural Non-Point Source Pollutant Model 98, Bosch et al., 1998) or SWAT (Soil and Water Assessment Tool, Arnold et al., 1993) can be used to determine the boundary conditions (water and sediment flow rates) for the channel network simulation.

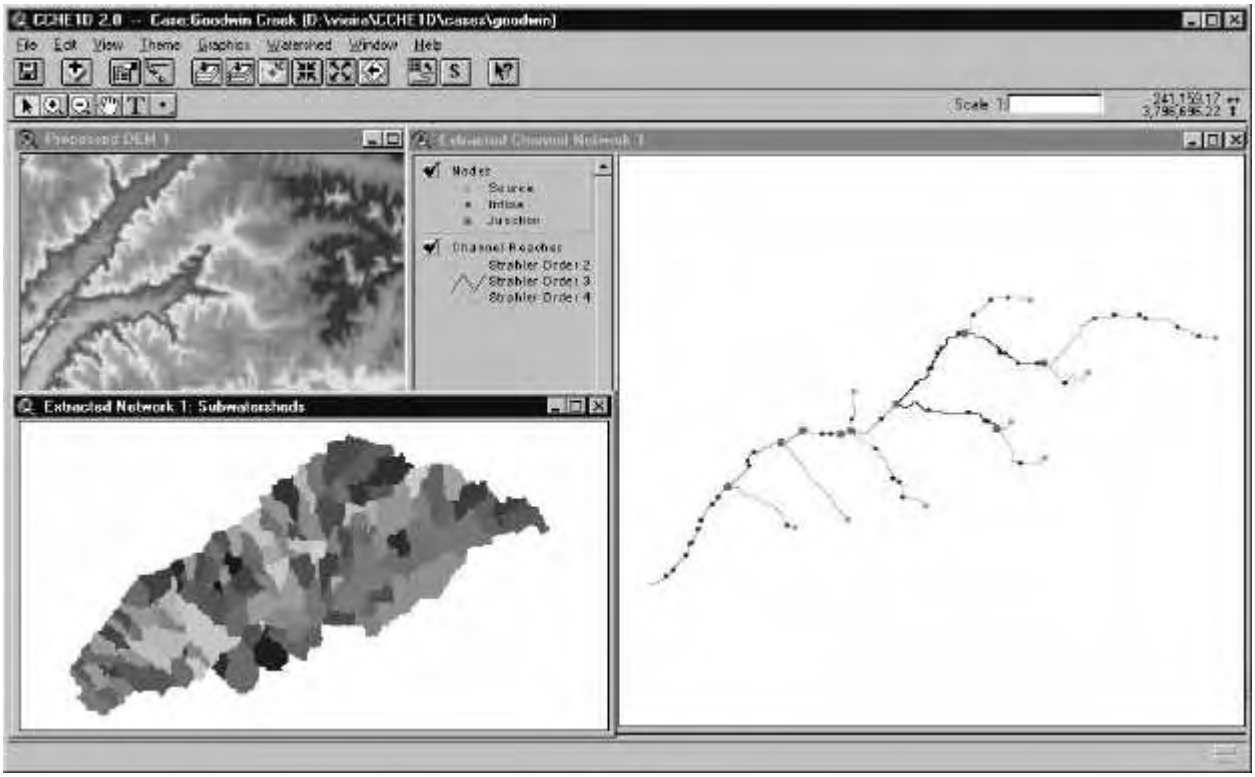

Figure 1 – CCHE1D graphical interface, showing channel network and corresponding subcatchments for the Goodwin Creek Experimental Watershed, Mississippi

CCHE1D also integrates landscape analysis tools that allow the automatic creation of a channel network based solely on digital elevation data. The landscape model TOPAZ (Garbrecht and Martz, 1995) is fully integrated to the CCHE1D's graphical interface. TOPAZ also generates a digital map of subcatchments that correspond to the channels of the network. Watershed models can use this subcatchment map in the computation of upland runoff and soil loss.

The system maintains a relational database in which all data are stored. The database is automatically updated in response to user interaction or to data generated or modified by the modeling programs. The database provides an efficient data storage mechanism, which is complemented by an array of routines that perform data format conversions, consistency checks, and data transfer among the programs of the system.

CCHE1D version 2.0 presents a series of improvements such as more advanced sediment transport modeling (Wu et al, 2000). The implementation of the full St. Venant equations enhances the accuracy of the model in situations where dynamic effects cannot be neglected, and permits the model to be applied to a wider range of flow conditions. The graphical user interface has also been updated, including new tools that allow easier specification of input data. The model now allows users to provide boundary conditions such as water discharges and sediment loads in a more flexible manner. The model also offers the user greater control of the sediment transport simulation, for which a variety of options, parameters and computational methods can be chosen. The new version also includes interactive tools for management of the simulation runs and for tailoring the output of modeling results.

CCHE1D 2.0 has been released for public use in the form of a Beta-testing version. The package is available from the National Center for Computational Hydroscience and Engineering – NCCHE.

MODEL APPLICATIONS

CCHE1D has been tested and validated for a series of laboratory experiments (Wu and Vieira, 2000). These test cases were used to evaluate the performance of the model when calculating sediment yield, predicting channel bed changes, and simulating scouring and deposition processes.

Channel bed degradation (uniform sediment) The channel degradation experiments of Newton (1951) were reproduced by CCHE1D. A straight flume 9.14m long, 0.3048m wide and 0.61m deep with a sand bed with a mean size of 0.690mm was used in the tests. The bed degradation experiment run number three has been calculated with CCHE1D model. Flow discharge was maintained constant at the rate of 0.00566m3/s. The sand bed was initially set with a slope of 0.0061. The measured Manning's roughness coefficient for the flume bed was used in the simulation. Figure 2 shows the evolution of the bed profiles with time.

Channel bed degradation (non-uniform sediment) The performance of CCHE1D calculating bed scouring of non-uniform sediment was tested for the experiments of Ashida and Michue (1971). These tests were devised for the study of clear water erosion and the associated armoring of the bed that may occur downstream of dams. CCHE1D was able to predict the progression of scour as well as the changes in the bed material composition as illustrated in Figure 3.

Bed Aggradation (non-uniform sediment) CCHE1D was used to simulate the development and progression of the aggradation wedge through a laboratory flume as observed in tests performed at the St. Anthony Falls Hydraulic Laboratory (SAFHL; Seal et al., 1995). The sediment fed at the flume entrance was a weakly bimodal mixture of grain sizes in the range 0.125 mm to 64 mm. Figure 4 shows the bed profiles at different times, as well as the water surface profile at the end of the experiment. CCHE1D was able to predict well both the deposition heights and the advance of the deposition front.

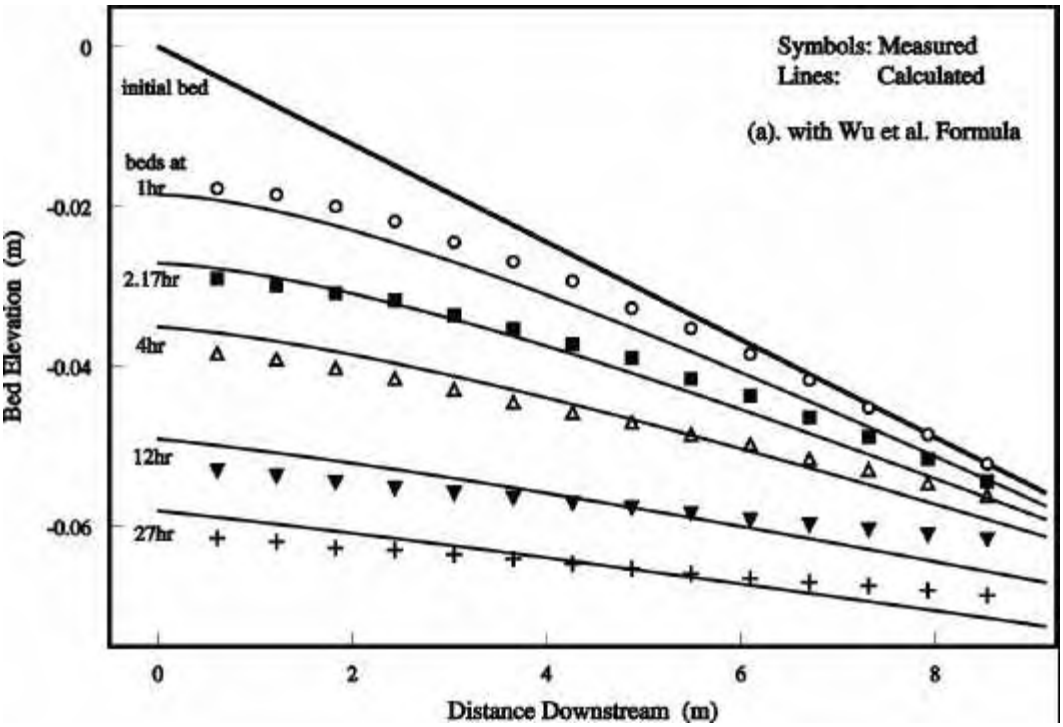

Figure 2 – Channel bed profiles at different times, for degradation test run no. 3 of Newton (1951).

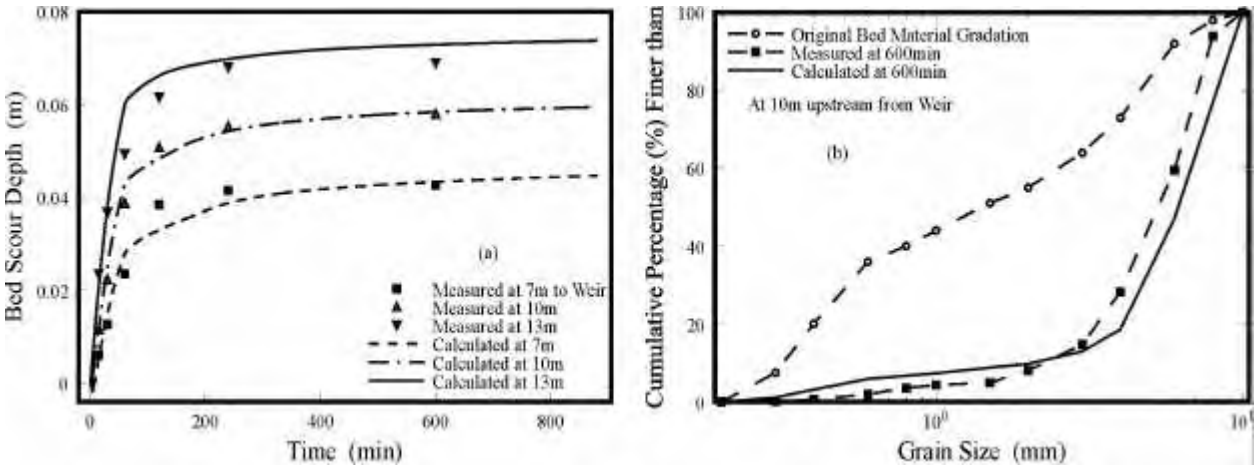

Figure 3 – Bed degradation and change of bed material composition at the mixing (surface) layer for Ashida and Michue's (1971) experimental run no. 6.

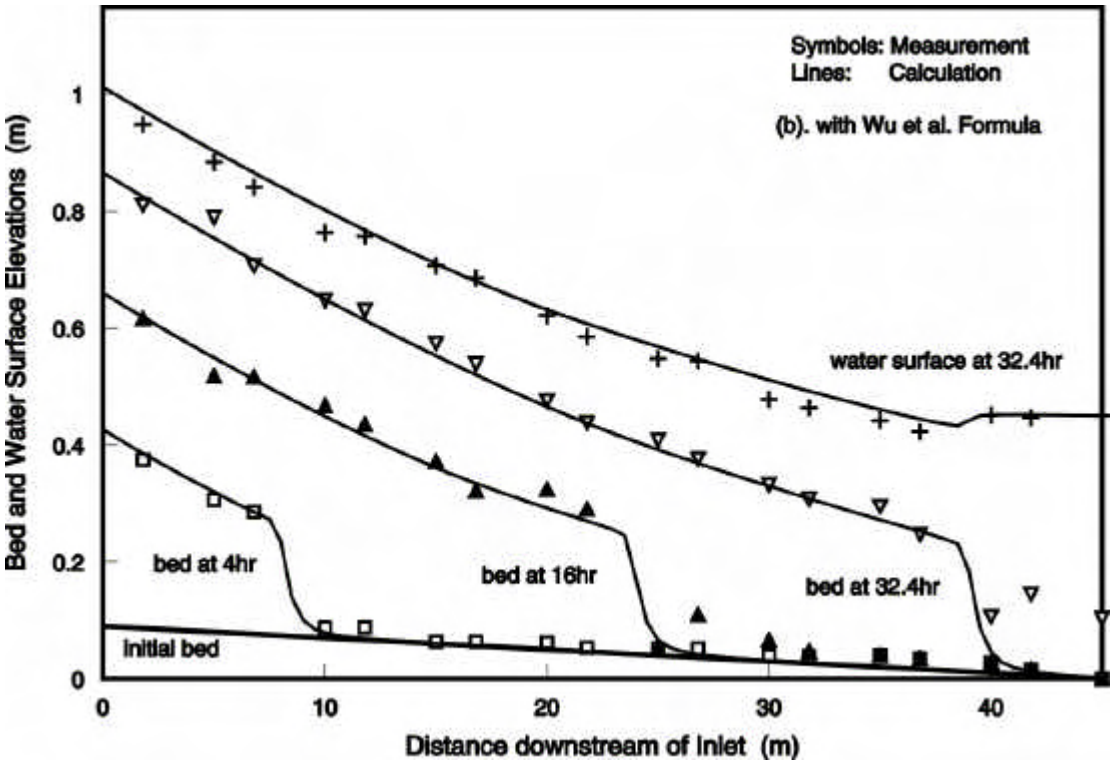

Figure 4 – Bed and water surface profiles in SAFHL's aggradation experiment no 1 (Seal et. al., 1995)

The above tests show that CCHE1D is able to simulate with good accuracy the basic processes of scouring and deposition. The capability of including hydraulic sorting and armoring phenomena can lead to better predictions of transport of non-uniform sediments, usually found in natural streams.

Application to the Goodwin Creek Watershed CCHE1D was used to simulate sediment yield and channel morphological changes in the Goodwin Creek watershed, in North Mississippi. This watershed is instrumented with 14 measuring flumes that control channel degradation and monitor runoff and sediment yield. The watershed model SWAT was used to compute runoff and sediment yield from the fields (Bingner et al., 1996). The simulation was performed with nine sediment size classes ranging from silt to gravel, using the non-equilibrium approach and including bank toe erosion and mass failures. Figure 5 shows the total annual sediment yield at the watershed outlet, computed with the channel network generated by TOPAZ shown in Figure 1.

CONCLUSIONS

CCHE1D can be a valuable predictive tool for the evaluation of flow and sedimentation processes in primarily agricultural watersheds. Its watershed-based approach facilitates the integration of channel modeling to the modeling of rainfall-runoff and upland field processes. The integration of tools such as the automatic extraction of the channel network and delineation of subcatchments facilitates the application of the model to real-life problems. The interactive graphical interface with GIS features and database management capabilities diminishes the effort required for the preparation of input data.

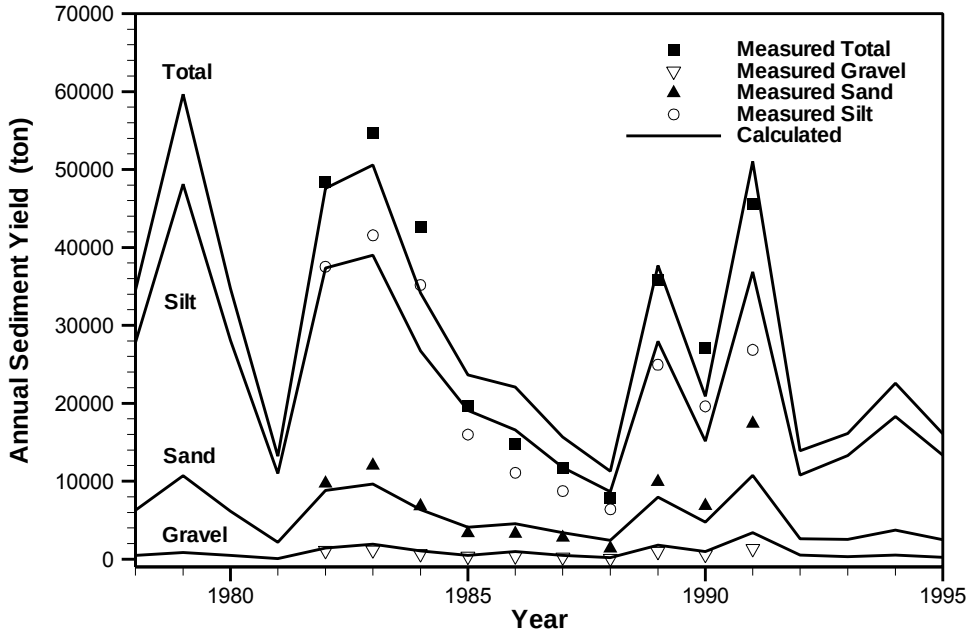

Figure 5 – Extracted channel network and total annual sediment yields (silt, sand, gravel, and total) between 1978 and 1995.

CCHE1D's flow model is capable of simulating the dynamic effects of natural flood hydrographs. The procedures for computation of flow through hydraulic structures ensure their influence is properly represented. Its advanced sediment transport model is capable of high quality predictions that include the effects of flow unsteadiness, non-equilibrium transport, non-uniformity of bed sediment, and sorting and armoring phenomena. The bank erosion and bank stability modules account for extra source of sediment due to channel widening.

CCHE1D is applicable to the simulation of system responses to hydrological processes, agricultural management practices, and man-made modifications to the channels or upland areas, such as the inclusion of erosion control structures, water diversions, etc. It can be used as a tool in the evaluation of the long-term channel-watershed system response to remedial measures for the control of erosion and sedimentation. The model is suitable for the determination of local erosion and deposition patterns, as well as for the determination of sediment yield.

CCHE1D is being further developed to improve the quality of flow and sediment transport simulations. Planned features include a better description of channel and floodplain properties (geometry and roughness), new types of in-stream structures, such as weirs and dams, and the continuous enhancement of the graphical interface, visualization tools, and data input and output facilities.

The framework of the CCHE1D software facilitates the inclusion of new capabilities. Current research includes the integration of transport and fate of pollutants in channel networks, which will eventually be used in studies of the overall water quality of streams and watershed-scale analysis of point and non-point source pollution. CCHE1D could become a valuable tool for the determination of Total Mean Daily Loads (TMDLs) for sediment and other pollutants, under the dynamic conditions of natural streams.

REFERENCES

Arnold, J.G., Allen, P.M. and Bernhardt, G., 1993, A comprehensive surface-groundwater flow model, J. of Hydrology, 142, pp. 47-69.

Arulanandan, K., Gillogley, E. and Tully, R., 1980, Development of a quantitative method to predict critical shear stress and rate of erosion of naturally undisturbed cohesive soils, Rep. GL-80-5, US Army Engineers Waterway Experiment Station, Vicksburg, Mississippi.

Ashida, K. and Michiue, M., 1971, An investigation of river bed degradation downstream of a dam, Proc. 14th Congress of the IAHR.

Bingner, R. L., 1996, Runoff simulated from Goodwin Creek Watershed using SWAT, Trans. of the ASAE, 39(1): 85-90.

Bosch, D., Theurer, F., Bingner, R., Felton, G. and Chaubey, I., 1998, Evaluation of the AnnAGNPS Water Quality Model, ASAE Paper No. 98-2195, St. Joseph, Michigan.

Garbrecht, J. and Martz, L. W., 1995, An automated digital landscape analysis tool for topographic evaluation, drainage identification, watershed segmentation and subcatchment parameterization, Report No. NAWQL 95-1, National Agricultural Water Quality Laboratory, USDA, Agricultural Research Service, Durant, Oklahoma.

Newton, C.T., 1951, An experimental investigation of bed degradation in an open channel, Trans., Boston Society of Civil Engineers, pp. 28-60.

Seal, R., Parker, G., Paola, C. and Mullenbach, B., 1995, Laboratory experiments on downstream fining of gravel, narrow channel runs 1 through 3: supplemental methods and data, External Memorandum M-239, St. Anthony Falls Hydraulic Lab., University of Minnesota.

Wu, W., Vieira, D. A., 2000, One-dimensional Channel Network Model CCHE1D 2.0 – Technical Manual, Technical Report No. CCHE-TR-2000-1, National Center for Computational Hydroscience and Engineering, The University of Mississippi, University, Mississippi

Wu, W., Vieira, D. A., and Wang S. S. Y., 2000, New capabilities of the CCHE1D Channel Network Model, ASCE's 2000 Joint Conference on Water Resources Engineering and Water Resources Planning and Management, Minneapolis, MN (on CD-ROM).

Contact Information:

National Center for Computational Hydroscience and Engineering

http://www.ncche.olemiss.edu
Dalmo A. Vieira

hyvieira@ncche.olemiss.edu

Phone: +1 (662) 915-5763

THREE-DIMENSIONAL SIMULATION OF SEDIMENT TRANSPORT IN SCOURING PROCESS

By Y. Jia, Research Associate Professor, National Center for Computational Hydroscienc and Engineering; Sam, S.Y. Wang, F.A.P. Barnard Distinguished Professor, Director, NCCHE.

Abstract: Local scouring is often associated with highly three-dimensional, turbulent flows exited by hydraulic structures or impinging jet flows. In these situations, the mechanism of sediment entrainment and transport is different from those observed in uniform flows because the vertical and fluctuating motion of the flow are so strong that they have to be considered as part of the mechanism dominating sediments' motion. In this paper, the simulation results of scouring processes using a three-dimensional model, CCHE3D, are reported. The hydrodynamic part of the model has been verified by using analytical method, physical experimental data and field data. The mechanism of additional effects of turbulent flow on the sediment transport in the scouring hole has been added to the sediment transport modules. Realistic results are obtained from the simulations.

INTRODUCTION

Sediment transport modeling deals with the hydrodynamics and the interaction between the motions of sediment and the flow, the transport processes are complicated especially with complex flow morphology. Simulating the transport processes requires sophisticated hydrodynamic and sediment transport models. Many physical experiments have been conducted, most of them are only interested in the main flow property, sediment property, shape of the structure and the maximum scour depth (Kandasamy and Melville, 1997), detailed flow structure and sediment transport mechanism are less reported quantitatively (Melville and Raudkivi, 1977, Graf and Yulistiyanto, 1999, Ahmed and Rajaratnam, 1998). The relationships between the flow structure, property and the sediment transport processes have rarely been attempted. Because numerical simulation needs such information, researches in the area of local scour simulation are difficult and the associated publications are relatively less than those of hydrodynamics. One has to assume the sediment transport function developed for uniform flow is still valid in the scour hole in order to study the scouring process numerically (Olsen and Melaaen, 1993). Studies trying to use generalized sediment transport formulation introducing turbulence fluctuation properties are introduced and more realistic results are obtained.

VERIFICATION OF CCHE3D MODEL

CCHE3D is a finite element based numerical simulation model for three-dimensional, free surface turbulent flows developed at the National Center for Computational Hydroscience and Engineering, the University of Mississippi. This model solves the full unsteady, three-dimensional Reynolds equations, free surface kinematic equation and dynamic pressure. The turbulence closure schemes included are the parabolic, mixing length eddy viscosity models, k-ε models as well as the non-linear k-ε model for reproducing anisotropic turbulence. Many publications using analytical approach (Torro and Wang, 1993), physical experimental data (Jia and Wang, 1993, 1996, 1999, 2000) and field data (Jia, et al. 2000) have demonstrated that this model is free from errors of mathematical derivation, numerical discretization, computer

programming, etc. Due to the page limit of the paper, only very closely related verification cases are shown. Figure 1 shows the simulated results of the flow in the scour hole around a bridge pier. The computed horse shoe vortex is in good agreement with the data. The velocity magnitude of the vortex in the scour hole is about $0.5U_0$ in the experiment and so does in the simulation. Figure 2 shows the simulated shear stress near the bed surface due to a turbulent impinging jet. The maximum shear stresses of a series of simulation are compared with the data of the impinging jet, the agreement of these data for different flow conditions indicates that the numerical model is consistent with the physical model.

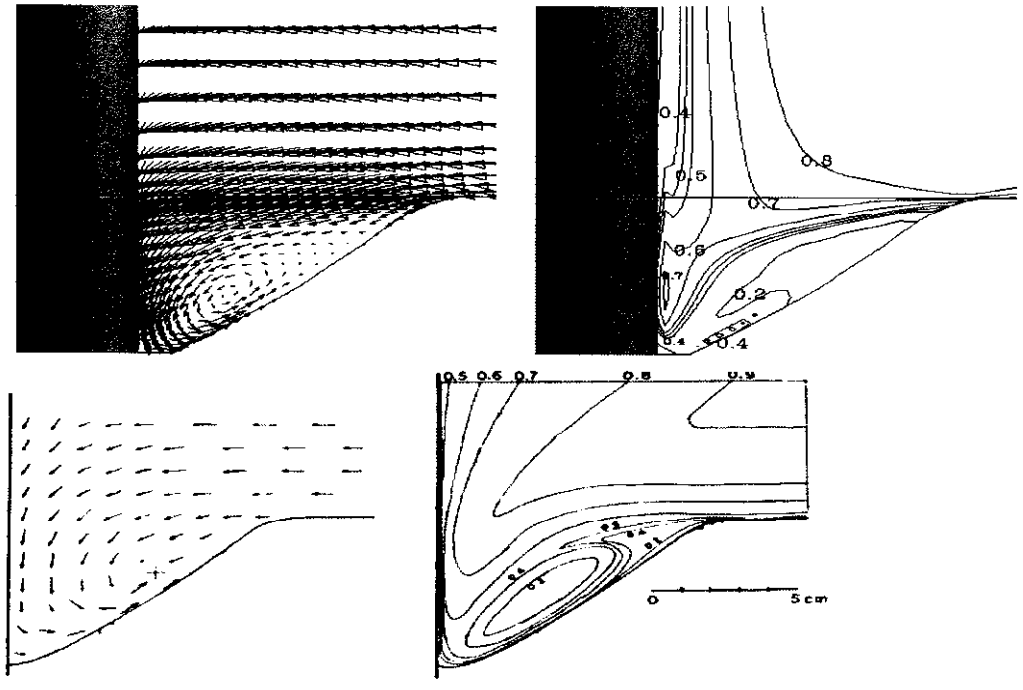

Figure 1. Comparisons of simulated flow field in a scour hole with the measurements.

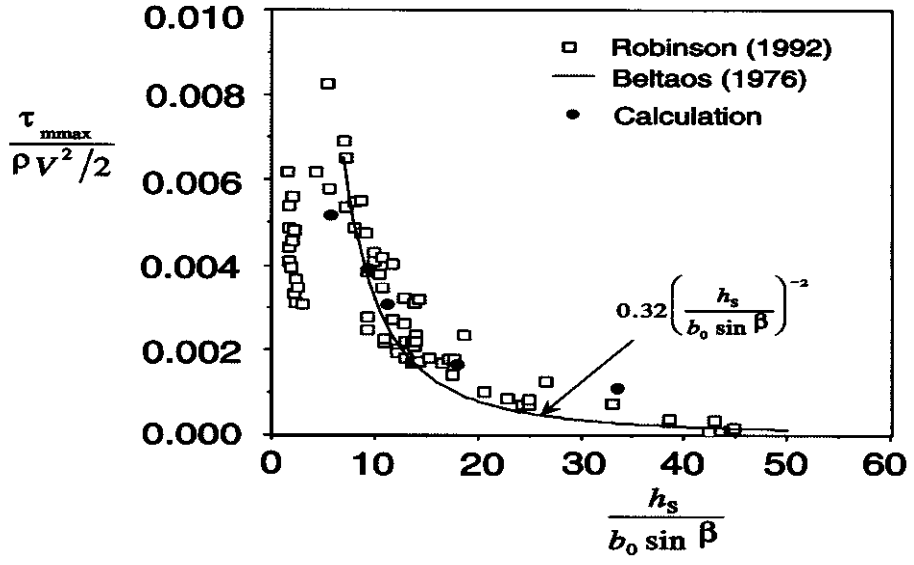

Figure 2. Comparison of simulated and measured shear stress on the bed surface induced by an oblique impinging jet.

SIMULATION OF LOCAL SCOURING AND HEADCUT PROPAGATION

As the simulation software develop, more and more people have realized the importance of physically based modeling techniques. The sediment transport model has to reflect the dominant physical processes in the scour hole, the model can then predict the scour hole development realistically. The early development in this direction for the local scouring around a spur dike was made by Zaghloul and McCorquodale (1973) who introduced an empirical function to account for the effects of vortices and turbulence intensity on the effective shear stress. This function could not predict true effect of vorticity and turbulence intensity because it was formulated for a two-dimensional model.

Recognized that sediment transport in the scour zone could be influenced by three-dimensional flow structures in addition to the shear stress on the bed surface, Jia and Wang (1996) proposed an effective shear stress which is a combination of shear stresses due to different effects:

$$\tau = \tau_s + \tau_v + \tau_t \tag{1}$$

where τ_s is the friction shear stress computed with the wall function, $\tau_v = \rho u_{v\bullet}^2$ was selected to represent the effect of vortex and $u_{v\bullet}$ is the shear velocity due to vortex:

$$u_{v\bullet} = k_v D(\frac{\omega}{\omega_{\max}})\omega_{app} \tag{2}$$

where ω is vorticity, the subscript "*max*" and "*app*" denote the value of ω near the obstruction and of the approach flow, respectively. van Rjin's sediment transport function (1993) was used to calculate scouring, its mobility function $T = (\tau - \tau_{cr})/\tau_{cr}$ was computed using Eq. 1. It was

found the effect of τ_v is more significant than that of τ_t. The sediment continuity equation was utilized to calculate the scouring process.

Dou *et al* (1998) proposed a function of sediment transport capacity, T_c, to account for the three-dimensional flow properties mentioned above:

$$T_c = f_0\sigma_0 + f_1\sigma_1 + f_2\sigma_2 + f_3\sigma_3 \tag{3}$$

where f_0, f_1, f_2 and f_4 are coefficients and

$$\sigma_0 = \frac{U_{av}^3}{gh\varpi}, \quad \sigma_1 = \frac{|w| - |w|_{app}}{U_{av}}, \quad \sigma_2 = \frac{(\omega - \omega_{app})D}{U_*}, \quad \sigma_3 = \frac{i - i_{app}}{\omega} \tag{4}$$

represent the effects of main flow in the channel, downflow, vorticity, and turbulence intensity, respectively. It is seen the transport capacity is affected by the 3D-flow field only near the obstruction where downflow, vorticity and turbulence intensity are substantially higher than those of the approach flow. A stochastic turbulence model, capable of predicting anisotropy of turbulence, developed by Dou (1987) was adopted to the CCHE3D flow model to improve the turbulence closure scheme. Non-equilibrium sediment transport equation is used to calculate bed change: bed form change is proportional to the difference of T_c and critical capacity of the flow. Good results were obtained for cases of local scouring around the cylindrical pier, square pier and trapezoidal shaped bridge abutment.

Recently, the CCHE3D model has been applied to simulate the local scouring induced by a plunging jet (Jia et al, 2000). To account for the sediment entrainment caused by pressure fluctuations of the turbulent flow, data of many physical experiments have been used. The sediment pick up rate in the jet impingement condition is formulated as a function of both shear stress and the lift force due to pressure fluctuation as shown in Figure 3.

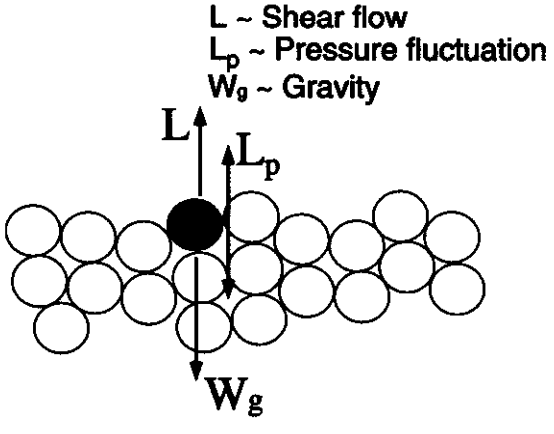

Figure 3. Sketch of sediment pick up mechanism in scouring hole

This formulation has been applied successfully to predict realistic shape of scour hole and its development process caused by the impinging jet. The correct prediction is attributed to the modeling of pick up mechanism due to pressure fluctuation. For example, the shear stress near the stagnation point is small due to small velocity, but it is where the maximum scour hole depth

occurs; the large lift force due to pressure fluctuation would enable the model to entrain the sediment and move them to downstream. Figure 4 shows the simulated results of the scouring hole development, the data from Stein and Julien (1993) have been used.

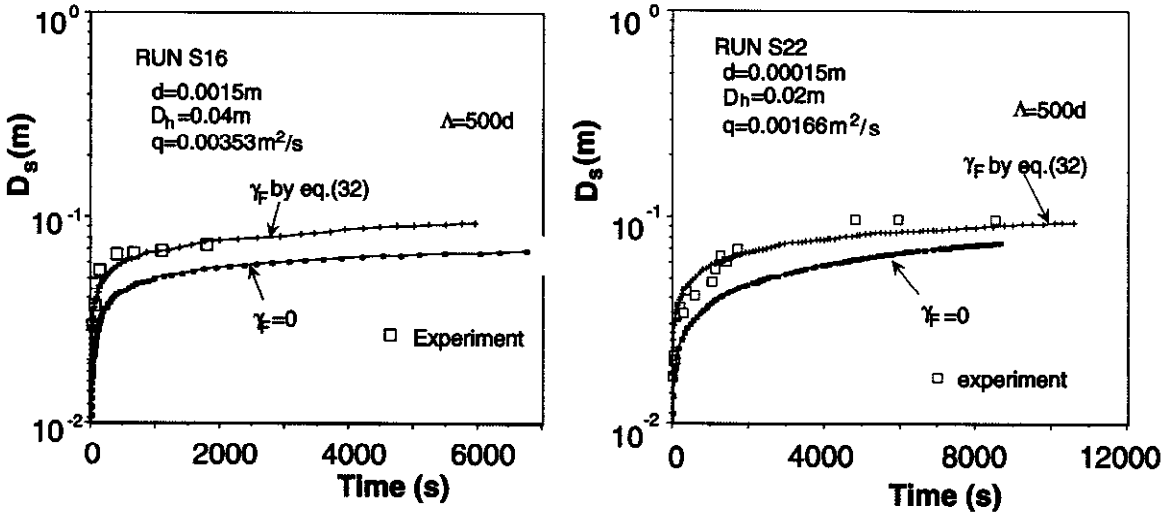

Figure 4. Comparisons of the simulated and measured scour hole development due to a plunging jet with two flow conditions.

This model is then applied to simulate the headcut propagation processes, because the basic sediment transport process in the scour hole with or without headcut propagation is similar. The only difference is that the headcut migration will induce additional sediment influx to the scouring hole due to the collapse of the headcut surface and therefore affect the shape and depth of the hole. Figure 5. shows the simulated process of headcut migration. The figure indicates that at the beginning, the process is to deepening the scour hole, and the migration would start after the depth has reached to a certain value. This is in agreement with the observation of physical experiments Bennett (1997).

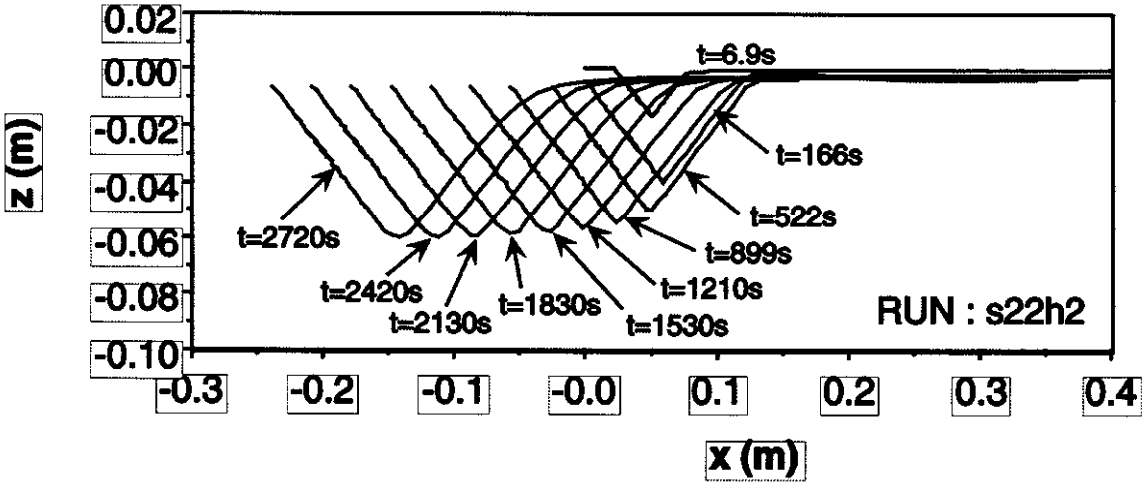

Figure 5. Simulated headcut migration. Lift force due to pressure fluctuation is considered.

CONCLUSIONS

Local scouring is often associated with highly three-dimensional, turbulent flows caused by hydraulic structures or impinging jet flows. The sediment erosion and transport mechanisms are different from those observed in uniform flows because the vertical and fluctuating motion of the flow become very important. The simulation results of scouring processes using a three-dimensional model, CCHE3D, are reported. The mechanism of additional effects of turbulent flow on the sediment transport in the scouring hole has been added to the sediment transport modules and realistic results are obtained. It is evident that physical mechanisms have to be correctly reflected in the sediment entrainment functions for local scouring simulations.

ACKNOWLEDGEMENT

This work is a result of research supported in part by the USDA Agriculture Research Service under Specific Research Agreement No. 58-6408-7-035 (monitored by the USDA-ARS National Sedimentation Laboratory) and the University of Mississippi.

REFERENCES

Ahmend, F., and Rajaratnam, N., 1998, "Flow around bridge piers", Journal of Hydraulic Engineering, Vol. 124, No. 3, pp. 288-300.

Bennett, S. J., Alonso, C. V., Prasad, S. N. and Romkens, M.J.M. (1997). "Dynamics of head-cuts in upland concentrated flows", *Proceedings of the Conference on Management of Landscapes Disturbed by Channel Incision*, Oxford, Mississippi, pp.510-515.

Dou, X, Jia, Y., Wang, S.S.Y., and J. Sterling Jones, 1998 "An alternative methodology to study local scour at bridge piers", Proceedings of the first federal interagency hydrologic modeling conference, pp. 3.1-8.

Graf, W.H., and Yulistiyanto, B., 1998, "Experiments on flow around a cylinder; the velocity and vorticity fields", Journal of Hydraulic Research, Vol. 36, No. 4, pp. 637-653.

Jia, Y., "Computational Model Verification Test Case using Flume Data," presented at ASEC Water Forum, Baltimore, MD, August, 1992, and Published in the Hydraulic Engineering, pp. 436-441, ASCE, 1992.

Jia, Y., and Wang, S.S.Y., 1993 "3D Numerical Simulation of Flow Near a Spur Dike". Advances in HydroScience and Engineering, Vol. I Part B, pp 2150-2156. University of Mississippi, June, 1993.

Jia,Y., and Wang, S.S.Y. 1996, "A Modeling Approach to Predict Local Scour Around Spur Dike Like Structures," Proceedings of the 6th FISC, Vol. 1, pp. 90-97, Las Vegas, NV,

March 1996.

Jia, Y., Kitamura, M, and Wang, S.S.Y. 1999 "Numerical experiments on head-cut of a two layered stratigraphic bed" Submitted to the ASCE, Journal of Hydraulic Engineering for consideration of publication.

Jia, Y., Kitamura, T., and Wang, S.S.Y. 2000, "A model for simulating scour process in a plunging pool of loose bed-material", ASCE, Journal of Hydraulic Engineering, accepted.

Jia, Y., Scott, S., and Wang, S.S.Y., 2000, "Numerical model verification and simulation of free surface flow in Mississippi River", ASCE, 2001 Congress, Orlando, Florida.

Kandasamy, J.K., and Melville, B.W., 1997, "Maximum local scour depth at bridge piers and abutments", Journal of Hydraulic Research, Vol. 36, No. 2, pp. 183-198.

Melville, B.M., and Raudkivi, A., 1977,"Flow characteristics in local scour at bridge piers", Journal of Hydraulic Research, Vol. 15, No. 4, pp 373-380.

Olsen, N.R.B., and Melaaen, M.C., 1993 "Three dimensional calculation of scour around cylinders", Journal of Hydraulic Engineering, Vol. 119, No. 9, ASCE, pp. 1048-1053.

Stein, O. R. and Julien, P. Y. (1993). "Criterion delineating the mode of headcut migration, Journal of Hydraulic Engineering, ASCE, Vol.119, No.1, pp.37-49.

APPLICATION OF CCHE2D MODEL TO FLOW SIMULATION IN LOCK AND DAM

By Abdul A. Khan, Research Assistant Professor, National Center for Computational Hydroscience and Engineering, University of Mississippi; Sam S.-Y. Wang, F.A.P. Barnard Professor and Director, National Center for Computational Hydroscience and Engineering, University of Mississippi.

Abstract: The CCHE2D model, developed at the National Center for Computational Hydroscience and Engineering, University of Mississippi, was applied to investigate the flow downstream of the Lock and Dam No. 2 situated in the Red River, Louisiana. The aim of the study was to accurately predict and identify the flow patterns that were impeding the navigability of the barges approaching the lock and dam structure. The depth-averaged $\kappa-\varepsilon$ turbulence closure scheme was used to accurately predict main flow and the re-circulation zones occurring downstream of the dam. The re-circulation in the approach path of the barges was clearly identified. The results agree qualitatively with the field observations.

INTRODUCTION

In this study the navigational problems in the channel downstream of the Lock and Dam No. 2, located in the Red River, Louisiana, is investigated computationally using the CCHE2D model. The bed topography and the extent of the simulation domain are shown in Fig. 1.

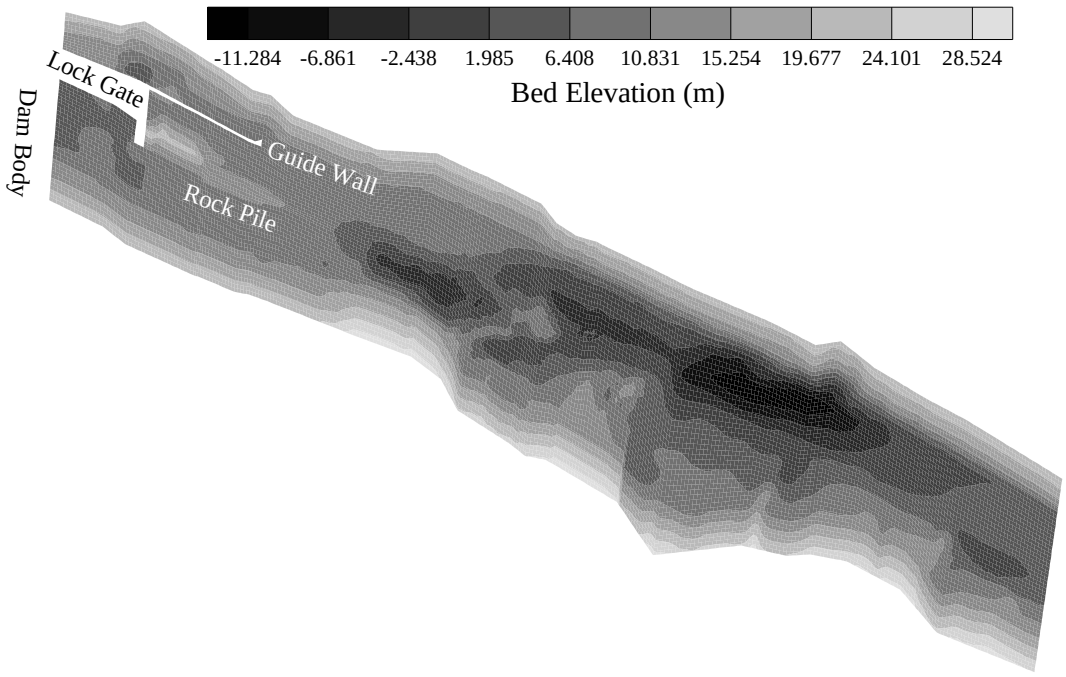

Fig. 1 Bed topography of the downstream channel

The major features of the bed topography are rock pile, guide wall, and submerged dikes situated at the right bank of the channel. The rock pile divided the channel into two, the left tributary acts as an approach channel to the lock, while the flow from the dam moves down the right channel. The upstream half of the rock pile is always exposed, while the lower half has a crest elevation

of 15.24 meters (50 feet) and is submerged for the water surface elevation considered in this study. A guide wall is located to the left of the rock pile and defines the other boundary of the approach channel. The bed topography also shows submerged dikes at the right bank of the channel that play an important role in diverting the flow towards the left bank of the channel (based on the preliminary simulation results). Two scour holes, one immediately downstream of the rock pile and the other further downstream and near the left bank, can clearly be identified in the figure above and show the path of the main flow.

The minimum water surface level in the channel downstream is about 12.2 meters (40 feet). The topographic survey was conducted during low flow conditions (about 40 feet downstream water surface elevation) and was confined within the waterline. However, according to field engineers, a water surface level upward of 15.24 meters (50 feet) downstream of the dam caused the most serious navigation problems. The downstream water surface elevation selected for this study was about 16.77 meters (55 feet). In order to simulate the flow for the water surface level described above the survey data was extrapolated at a slope of 1:4 (vertical to horizontal ratio) up to 21.34 meters (70 feet) elevation. The above extrapolation of the topographic data was based on the field observation. A Manning's coefficient of 0.03, based on the bed material size, was used in this study.

The simulation was performed using the CCHE2D model developed at the National Center for Computational Hydroscience and Engineering, University of Mississippi. The CCHE2D is a two-dimensional, depth-averaged, unsteady, turbulent flow and sediment transport model. The details of the model are provided in the following section.

CCHE2D MODEL

Governing Equations: The two-dimensional, depth-averaged mass and momentum conservation equations used in the CCHE2D model are

$$\frac{\partial h}{\partial t}+\frac{\partial hu}{\partial x}+\frac{\partial hv}{\partial y}=0 \qquad (1)$$

$$\frac{\partial u}{\partial t}+u\frac{\partial u}{\partial x}+v\frac{\partial u}{\partial y}+g\frac{\partial \eta}{\partial x}=\frac{1}{\rho h}\frac{\partial h\tau_{xx}}{\partial x}+\frac{1}{\rho h}\frac{\partial h\tau_{xy}}{\partial x}-\frac{\tau_{bx}}{\rho h}+f_{cor}v \qquad (2)$$

$$\frac{\partial v}{\partial t}+u\frac{\partial v}{\partial x}+v\frac{\partial v}{\partial y}+g\frac{\partial \eta}{\partial y}=\frac{1}{\rho h}\frac{\partial h\tau_{yx}}{\partial x}+\frac{1}{\rho h}\frac{\partial h\tau_{yy}}{\partial x}-\frac{\tau_{by}}{\rho h}+f_{cor}u \qquad (3)$$

where h is the depth of flow, u and v are longitudinal and transverse velocity components, x and y are spatial coordinates in longitudinal and transverse directions, t represents time, g is gravitational acceleration, η is the water surface elevation, ρ is the density of water, τ_{xx} and τ_{yy} are normal turbulent stresses in the longitudinal and transverse directions, τ_{xy} and τ_{yx} are

shear stresses, τ_{bx} and τ_{by} are bed shear stresses in the longitudinal and transverse directions, and f_{cor} is a Coriolis parameter.

The turbulent normal and shear stresses are approximated according to Boussinesq's assumption as follows

$$\tau_{xx} = 2\rho\nu_t \frac{\partial u}{\partial x} \quad \text{.....(4)}$$

$$\tau_{xy} = \tau_{yx} = \rho\nu_t \left(\frac{\partial u}{\partial y} + \frac{\partial v}{\partial x} \right) \quad \text{.....(5)}$$

$$\tau_{yy} = 2\rho\nu_t \frac{\partial v}{\partial y} \quad \text{.....(6)}$$

where ν_t is turbulent eddy viscosity.

Eddy Viscosity Models: Three methods for calculating depth-averaged eddy viscosity are available in the CCHE2D model. First, by assuming a parabolic distribution of turbulent viscosity (see Fischer et al. (1988)), the resulting depth-averaged eddy viscosity is given below

$$\nu_t = 0.17\kappa u_* h \quad \text{.....(7)}$$

where κ is the von Karman's constant and u_* the shear velocity. The depth-averaged mixing length formulation as given by Rodi (1984), is modified and defined as

$$\nu_t = \ell^2 \sqrt{2\left(\frac{\partial u}{\partial x}\right)^2 + \left(\frac{\partial u}{\partial y} + \frac{\partial v}{\partial x}\right)^2 + 2\left(\frac{\partial v}{\partial y}\right) + \left(\frac{\alpha u_*}{\kappa h}\right)^2} \quad \text{.....(8)}$$

$$\ell = 0.267\kappa h \quad \text{.....(9)}$$

where ℓ is the depth-averaged mixing length and α is the coefficient that recovers equation (7) for uniform flow conditions (i.e., no velocity gradients). A standard depth-averaged $\kappa - \varepsilon$ turbulent closure scheme as illustrated by Rodi (1984) is implemented as a third option.

Numerical Scheme: The CCHE2D model employs the efficient element, fully implicit, numerical scheme to solve the momentum equations. The scheme requires a quadrilateral mesh system. A working element is formed around each node. The working element consists of a central node (the node at which the variables are calculated) and eight surrounding nodes. Quadratic interpolation functions are used to approximate the variables and its derivatives. For details of the scheme the readers are referred to Wang and Hu (1992). The continuity equation is solved for water surface elevation by drawing a control volume around the central node of each element and applying the integral form of the continuity equation described as

$$\frac{\partial \eta}{\partial t} + \frac{1}{A_e} \int_{\Gamma} h \vec{V} . \vec{n} d\Gamma = 0 \quad \text{.....(10)}$$

where V is the velocity vector, n is the unit normal to the surface, A_e is the area of control volume, and Γ represents the surface around the control volume. For further details the readers can refer to Jia and Wang (1999).

Boundary Conditions: Three types of boundary conditions are identified in the CCHE2D model: solid wall boundary; inlet boundary; and outlet boundary. At the wall boundary, the normal component of the velocity is set to zero. The user can set the tangential component of the velocity to zero (no slip condition), or to total slip at the wall. The model also allows for the application of log-law at the solid boundary. The log-law approach allows a partial slip at the wall to accurately predict the shear stress at the wall. For the application of log-law or no slip boundary condition, the mesh near the wall should be relatively fine to accurately predict the boundary layer profile. For most natural river applications, a total slip condition suffices.

At the inlet boundary specific discharge or total discharge can be applied. At the outlet boundary stage or open boundary conditions (also known as kinematic wave condition) can be prescribed. The second boundary condition at the outlet is useful when the stage at the outlet cannot be ascertained.

SIMULATED RESULTS

The mesh was generated for the domain shown in Fig. 1. The mesh consisted of 6 x 6 meters quadrilateral elements with 55 nodes across and 309 nodes along the flow. The boundary conditions of 16.9 meters (55.4 feet) water surface elevation at the downstream end and a discharge of 2265.4 cms (about 80,000 cfs) at the upstream end of the channel were prescribed. The stage and discharge values were selected from the rating curve provided. As described above, water surface level upward of 15.24 meters (50 feet) presented the worse conditions for the navigability that is why a downstream level of 16.9 meters (55.4 feet) is considered in this study. The preliminary results obtained using the depth-averaged parabolic eddy viscosity showed that a re-circulation zone, near the left bank of the channel, might play an important role in the navigability of the channel. To accurately predict both the magnitude and extent of the re-circulation zone, depth-averaged $\kappa - \varepsilon$ model was adopted for final simulation.

The computed results of water surface level and velocity magnitude in the form of color filled contours are shown in Figs. 2 and 3 respectively. The velocity magnitude plot shows that the main flow is contained in the right part of the channel by the rock pile, while the left part of the channel carries no flow. Downstream of the rock pile a shear layer develops at the boundary between the high velocity jet in the right side of the channel and quiescent flow in the left part of the channel. In addition the submerged dikes move the flow jet towards the left bank of the channel. The combined effect of the two phenomena discussed above is a re-circulation zone that develops downstream of the rock pile near the left bank and extends all the way up to the guide wall in the upstream direction. The re-circulation zone is depicted in Figs. 4 and 5 in the form of the particle path and velocity vectors.

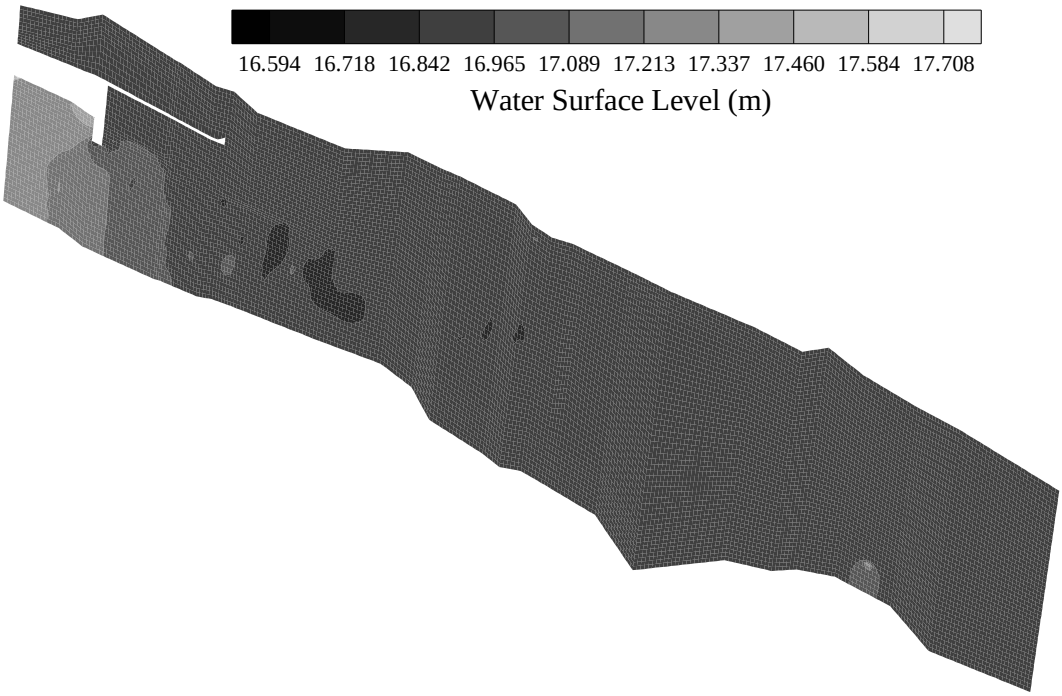

Fig. 2 Water surface level

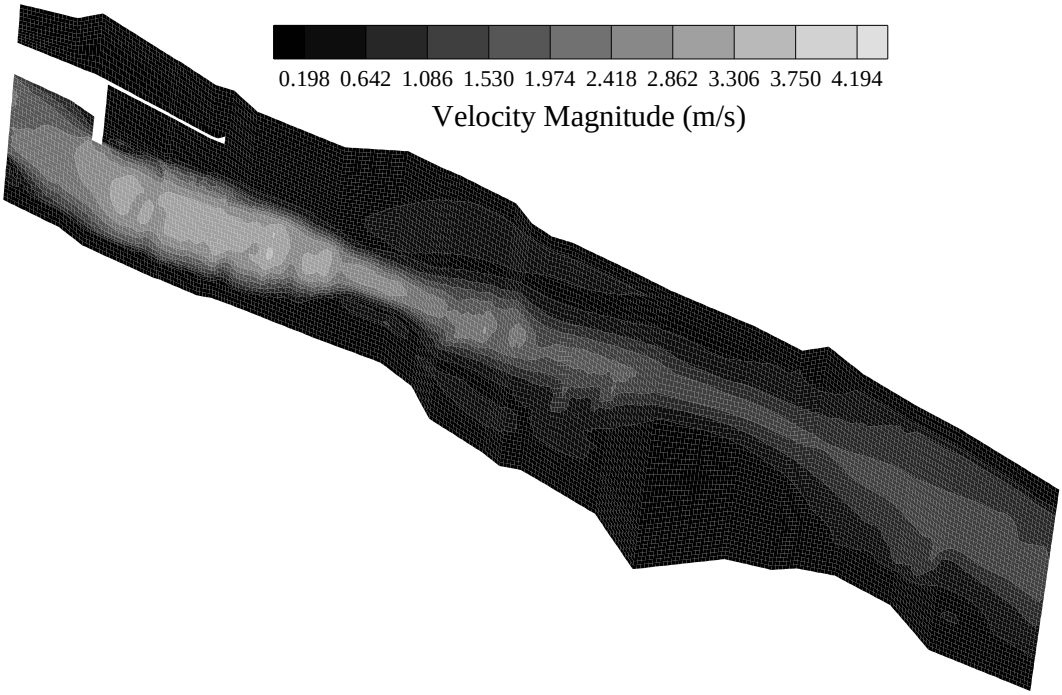

Fig. 3 Velocity magnitude

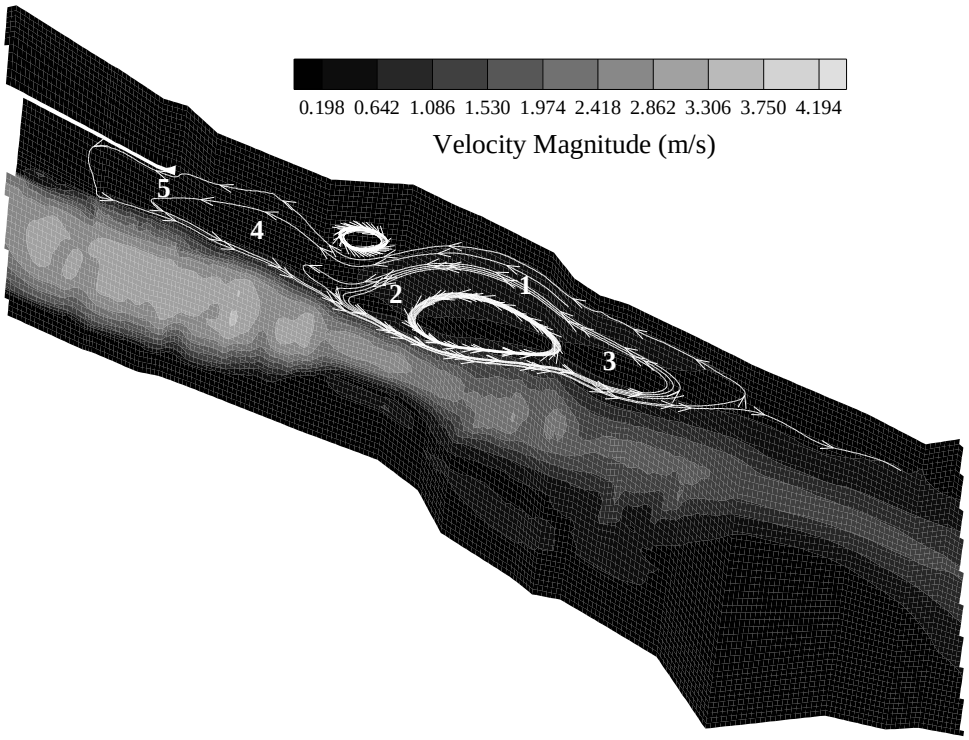

Fig. 4 Particle path

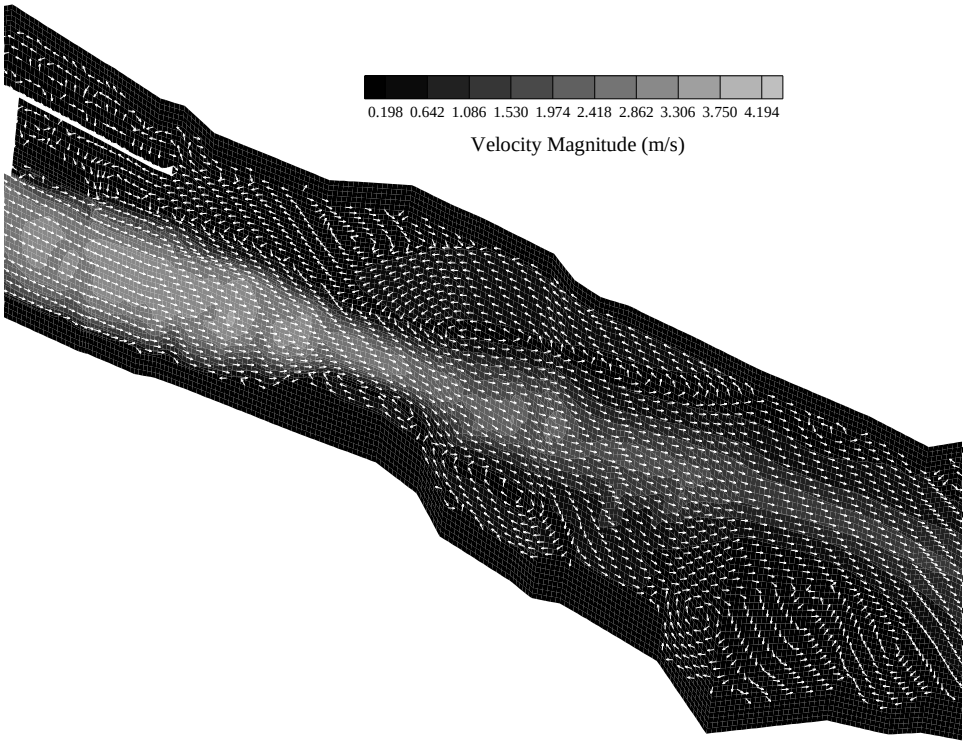

Fig. 5 Velocity vectors

The computed velocity magnitude at the points 1, 2, 3, 4, and 5 marked in Fig. 4 are 0.56 m/s, 0.32 m/s, 0.08 m/s, 0.06 m/s, and 0.05 m/s respectively. These points are located in the re-circulation zone and provide a measure of the re-circulation strength of the flow near the left bank of the channel and agree well with qualitative field observations. The barge moving towards the approach channel along the left bank of the channel would suddenly experience a sharp velocity gradient that may cause navigation problems especially at the junction of forward and re-circulation flow zones.

SUMMARY OF RESULTS

In this study the flow downstream of the Lock and Dam No. 2, situated in the Red River, Louisiana, was investigated computationally using the CCHE2D model. The barges moving upstream near the left bank of the channel are known to face steering problems under certain flow condition. The aim of the study was to identify flow features that might cause navigation problems. To accurately predict the flow features, especially the magnitude and extent of the re-circulation zone, a depth-averaged $\kappa - \varepsilon$ turbulence closure scheme was used to simulate the flow. The computed results showed that the main velocity jet in the right part of the channel developed a shear layer at the boundary of the main flow and quiescent flow at the left side of the channel. This shear layer together with the deflection of the jet towards the left bank by the submerged dikes caused a re-circulation zone near the left bank of the channel. The strength and extent of the re-circulation agreed satisfactorily with the qualitative observations in the field. The re-circulation might be the main flow feature impeding the navigability of the barges in the channel.

REFERENCES

Wang, S. S.-Y., Hu, K. K., 1992, Improved methodology for Formulating Finite-Element Hydrodynamic Models. Finite Elements in Fluids, Hemisphere Publication Corporation, Washington, Vol. 8, 457-478.

Rodi, W., 1984, Turbulence Models and Their Application in Hydraulics - A State-of-the-Art-Review. IAHR.

Fischer, H. B., List, E. J., Koh, R. C. Y., Imberger, J., Brooks, N. H., 1988, Mixing in Inland and Coastal Waters. Academic Press Inc., Orlando.

Jia, Y., Wang, S. S.-Y., 1999, Numerical Model for Channel Flow and Morphological Change Studies. Journal of Hydraulic Engineering, ASCE, 125(9), 924-933.

APPLICATION OF AERIAL INFRARED VIDEOGRAPHY AND A 2-DIMENSIONAL FLOW MODEL TO INVESTIGATE SANDHILL CRANE ROOSTING HABITAT ALONG THE PLATTE RIVER, NEBRASKA

P.J. Kinzel, J.M. Nelson and R.S. Parker, USGS WRD, Lakewood, CO

Box 25046 Denver Federal Center, MS 413, Lakewood, CO 80225, USA

Abstract: Observations suggest that the roosting patterns of sandhill cranes are influenced by the streamflow patterns over and around sandbars. We utilized a 2-dimensional flow model to compute local depths and velocities at both a high and a low discharge during an artificial flow fluctuation through a study reach. The magnitude and distribution of hydraulic variables computed by the model at the two discharges were compared with aerial infrared thermal imagery of roosting sandhill cranes taken during these discharges. Distributions of roosting cranes were spatially correlated with flow depth, with cranes occupying a relatively narrow range of flow depths for each discharge. Notably, the ranges of depths utilized by the cranes changed slightly with discharge, with cranes showing greater tolerance for shallower areas during low flows and for deeper areas during high flows. The crane distributions also show spatial correlation with velocity fields; however, the separation of depth and velocity effects requires further analysis due to the correlation between these two variables.

INTRODUCTION

The narrowing of the Platte River channel in central Nebraska during the past 130 years represents one of the most dramatic transformations of any alluvial river in the Western United States. Concern that this change in morphology of the river has decreased available habitat for migratory birds has focused interest on the reach of the Platte River between Lexington and Chapman, Nebraska. This "Big Bend" reach intersects the North American Flyway and, therefore, the migratory path of many species of waterfowl including sandhill cranes and whooping cranes. Over half a million sandhill cranes use the central Platte River as a staging area on their annual northward migration in early spring. Cranes spend most of their diurnal hours feeding in cornfields and wet meadows adjacent to the river while spending most of their nocturnal hours roosting in the river.

Concern for endangered species, including the pallid sturgeon, piping plover, least tern, and whooping crane, led to a cooperative agreement between the states of Colorado, Nebraska, and Wyoming and the U.S. Department of the Interior to improve critical habitat for these species in the Platte River Basin. This agreement resulted in a program that is involved in the acquisition and restoration of land for habitat. The program also manages an environmental water account, which can be used to augment streamflow to benefit habitat. As the program moves toward adaptive management of the river corridor, interdisciplinary research is being conducted by the U.S. Geological Survey (USGS) to explore the linkages that exist between hydrologic, biologic, and geomorphic processes in the Platte River. The selection of roost sites by sandhill cranes is influenced by a number of variables including channel width, water depth, distance to human disturbances, and distance to wet meadows (Norling et al., 1990; Sidle et al., 1993). The experiment reported here is one step in determining specific linkages between river flow and roosting habitat available for sandhill cranes.

STUDY SITE

The National Audubon Society's Lillian Annette Rowe Sanctuary is located within the Big Bend reach of the Platte River (figure 1). The property includes 4.65 km^2 of riverine and grassland habitat and is intensively managed to preserve a relatively wide unobstructed river channel for roosting cranes. One aspect of this management is the mechanical removal of vegetation from sandbars in the river and along riparian areas. The channel is approximately 250 to 350 meters wide throughout this reach. Because of the high density of cranes from late February to early April each year, the sanctuary attracts visitors from around the world.

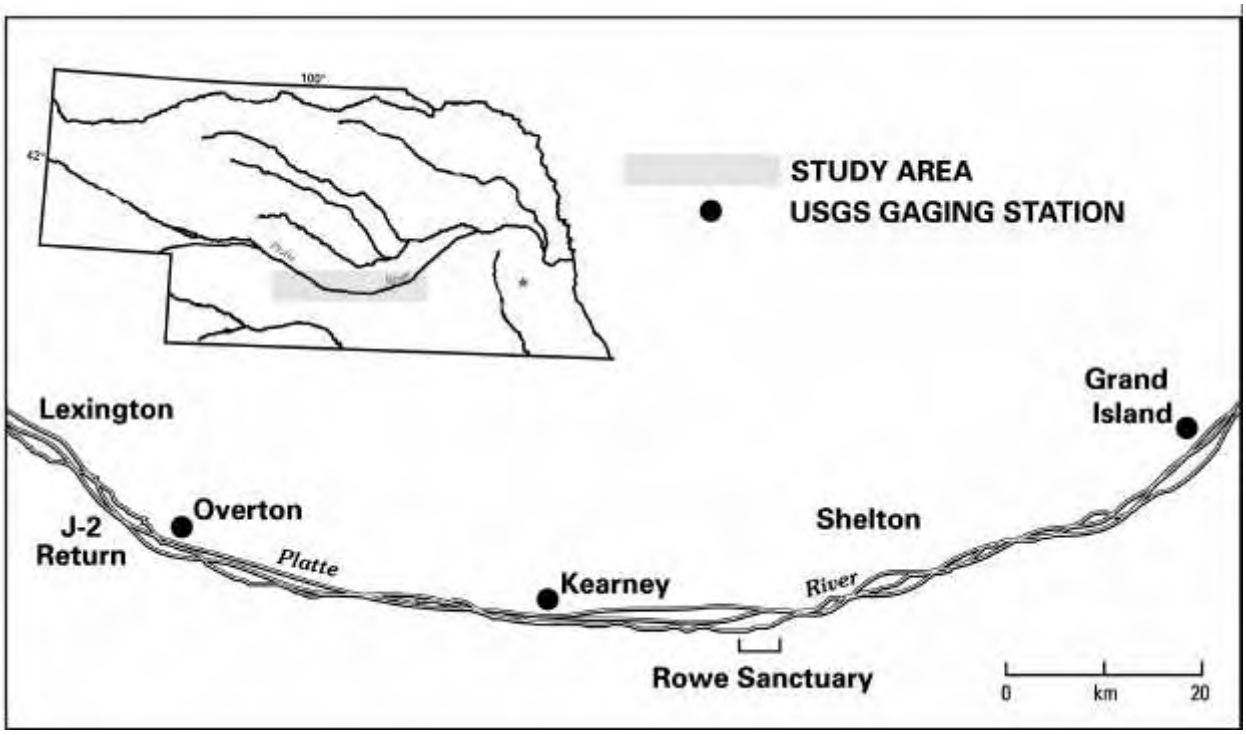

Figure 1. Map of the Central Platte River, Nebraska

METHODS

Infrared Video: During the Spring migration season, sandhill cranes return to roost in the Platte River approximately one hour after sunset and begin to leave their roost sites about one hour before sunrise. In the past, aerial photography taken during early morning hours has been used to obtain images of sandhill cranes roosting in the Platte River (Latka and Yahnke, 1986; Norling et al., 1990). However, one drawback of this technique is the uncertainty about the number of cranes that may have departed their roosts prior to an early morning photograph. Two previous workers have demonstrated that there is sufficient thermal contrast between sandhill cranes and the water that they roost in to obtain images using an infrared sensor. Pucherelli (1985) used a classified military thermal infrared sensor to image sandhill cranes in the Platte River. Sidle et al.

(1993) persuaded the Nebraska Air National Guard to image sandhill cranes in the Platte River as part of a training mission. The USGS employed a private commercial service in March 2000 to image sandhill cranes using an infrared detector with output to a digital video recorder.

During the week of March 24 to March 31, 2000, five flights of approximately four hours in duration were flown between the hours of 10 pm to 2 am to image sandhill cranes roosting in the Platte River. Flights extended east to Grand Island and west to Lexington (figure 1). Resolution of individual birds with the video system proved difficult at altitudes greater than 600 meters above ground level (agl). Lower altitudes, while capable of resolving individuals, did not permit sufficient field of view to capture the entire width of river channel.

In an effort to satisfy both the need to image crane roost locations across the width of the river channel and to obtain information on the density of individual birds, we elected to fly at three separate altitudes. These altitudes are categorized as high (about 1000 meters agl), midlevel (about 600 meters agl), and low (about 300 meters agl). This strategy provided sufficient overlap at all levels of resolution and spatial extents. The reach from the Shelton Bridge to the Kearney Bridge, which includes the Rowe Sanctuary reach, was flown every night at all three altitudes. Other portions of the river were flown more sporadically at the high altitude to delineate the size and location of roost sites.

In addition to the nighttime flights, on the afternoon of March 27 a 35mm camera was used to take aerial photographs of the reach of the Platte River between the Shelton bridge and the Kearney bridge. On the afternoons of March 28 and March 30, aerial digital videography was taken along the length of the Platte River between Grand Island and Overton (figure1). The daytime photographs and video images proved useful to delineate the size and location of sandbars in the river.

Hydraulic Modeling: To examine the influence of river stage upon the hydraulics over and around sandbars in the Platte River, we employed a depth-averaged two-dimensional flow model to calculate depth and velocity throughout a 1 km reach at the Rowe Sanctuary. A detailed series of cross-sections, longitudinal profiles and detailed bank and island topographic points were mapped using a survey-grade global positioning system (GPS). The hydraulic model grid was created by interpolation of these surveyed points along a curvilinear coordinate system defined by the channel centerline. Two boundary conditions were employed in the flow computation. A downstream water surface elevation was obtained from a recording pressure transducer at the downstream end of the study reach, and a discharge was obtained from a previously computed fixed proportion of the upstream discharge recorded at a USGS gage (06770200 Platte River at Kearney, Nebraska). The 2-dimensional hydraulic model computes water surface elevation, two components of velocity, and two components of boundary shear stress at each grid cell, as shown in figure 2a and 2b. The model output can be exported in the Cartesian coordinate system of the surveyed data, as can any georeferenced imagery, in this case a UTM projection with a NAD 83 datum.

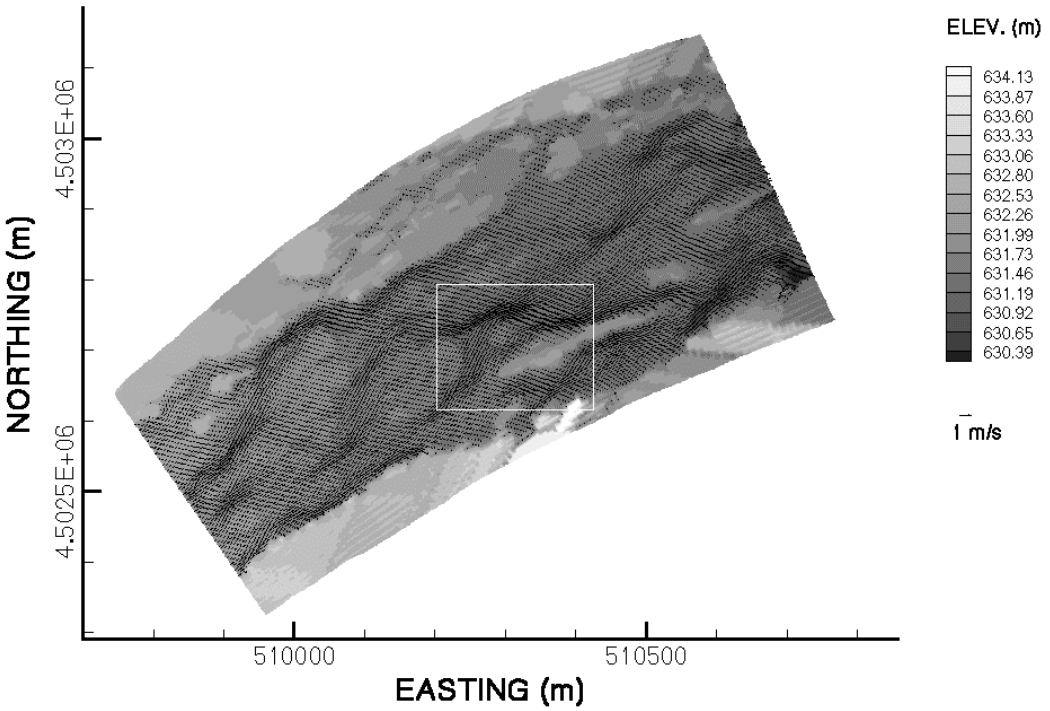

Figure 2a. Topographic grid and velocity vectors along Rowe Sanctuary reach, Q = 57 cms.

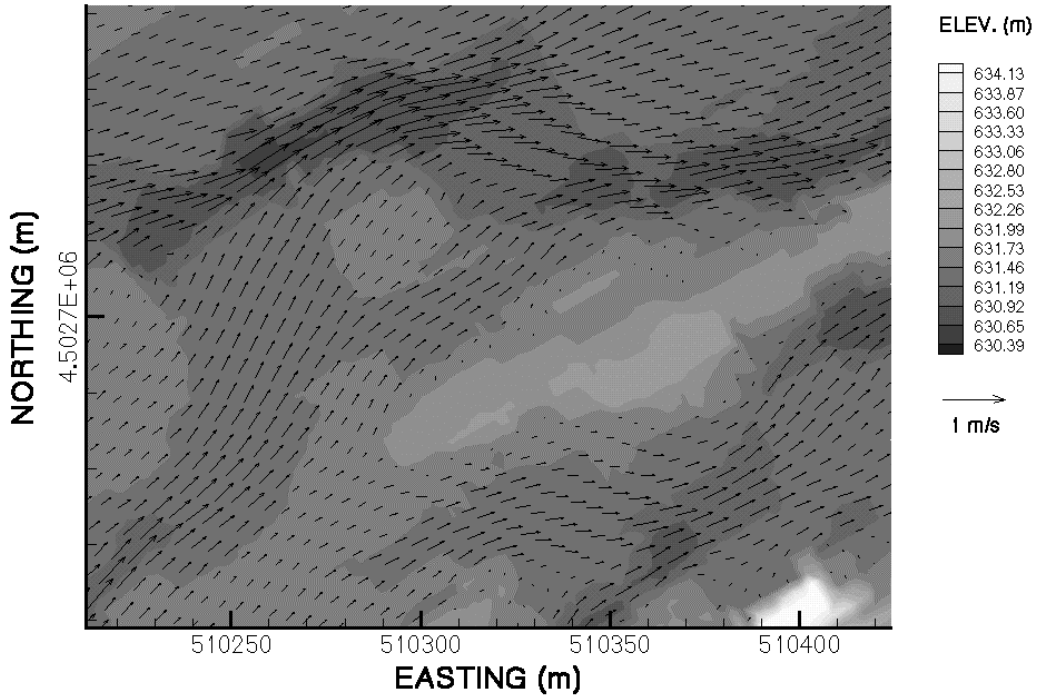

Figure 2b. Magnification of inset in Figure 2a. showing modeled velocity field, Q = 57 cms.

Image Processing: Approximately nine hours of digital videotape was acquired during the week of the experiment. Individual digital video frames were captured to image files on a desktop PC using a commercial software package for digital video editing. The individual images were then imported into a commercial geographic information system (GIS) and registered to a 1998 1: 24,000 scale color infrared (CIR) digital orthophoto that was used as a basemap. Scanned daytime color 35mm photographs and daytime digital video images taken of the study reach were also registered to the basemap to show the location of submerged and exposed sandbars and vegetated islands. It was possible to mosaic individual infrared video frames together to create a series of properly scaled and rotated images of crane roost locations along the study reach. The GIS software was then used to digitize polygons outlining the location of roosting areas.

RESEARCH FLOW

On the morning of March 29 and continuing through the night of March 30, water that would ordinarily contribute to the flow in the Platte River by passing through the Johnson Hydroplant or J2 power return was diverted. This was to permit routine maintenance on the J2 return by Central Nebraska Public Power and Irrigation. This diversion caused a drop in flow in the Platte River from approximately 85 cubic meters per second (cms) to approximately 28 cms at the Kearney gage, as shown in figure 3, resulting in an 0.18 m decline in water surface elevation at the lower end of the Rowe Sanctuary study reach. Sandbars that would have been inundated at higher flow were exposed at the lower flow and portions of the reach that consisted of deeper high-velocity sections became shallower and had decreased velocity.

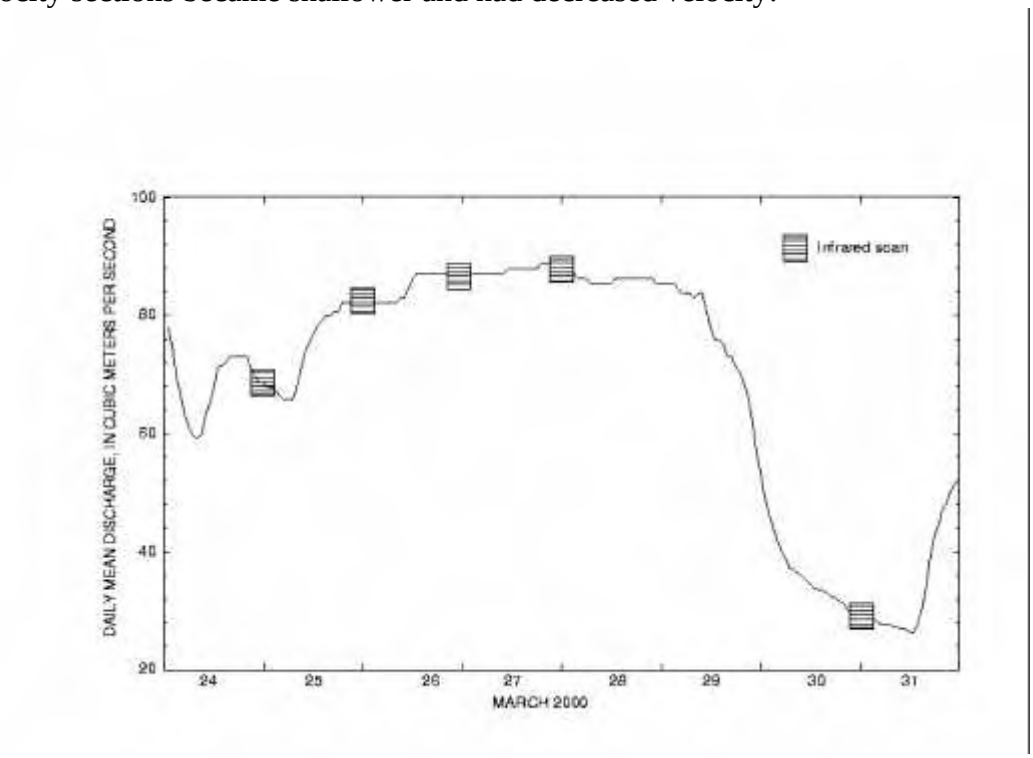

Figure 3. Provisional streamflow during the experiment at USGS gaging station number 06770200 Platte River at Kearney, Nebraska.

RESULTS

The GIS software was used to overlay and compare the depth and resultant velocity vector grids from the model runs, areas of roosting cranes obtained from the infrared video, and daylight images of sandbars. The roost site areas utilized on the nights of March 24, 26,27, and 30 are shown in figure 4. These areas are somewhat correlated with flow. Higher discharges on the March 26 and 27 showed slightly less total roost area through the study reach than the lower discharges of March 24 and March 30. The overall distribution and separation of the roosting areas on the nights of March 24, 26, and 27 are similar, whereas on the low flow night, March 30, the roosts are more connected.

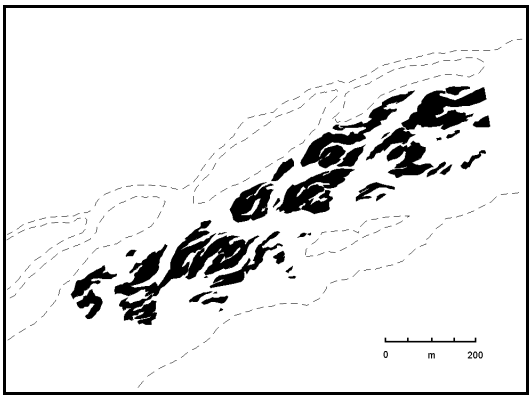

Night of 3/24/00 ~ 46 cms (60,610 m^2)

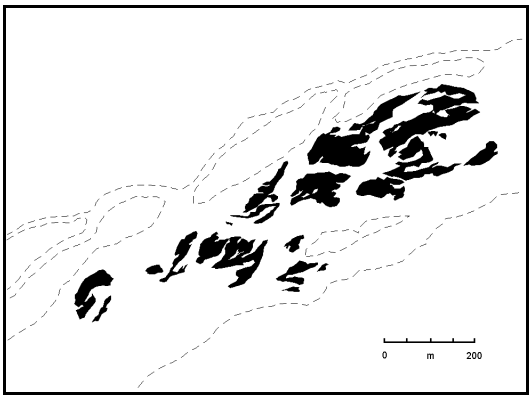

Night of 3/26/00 ~ 57 cms (54,460 m^2)

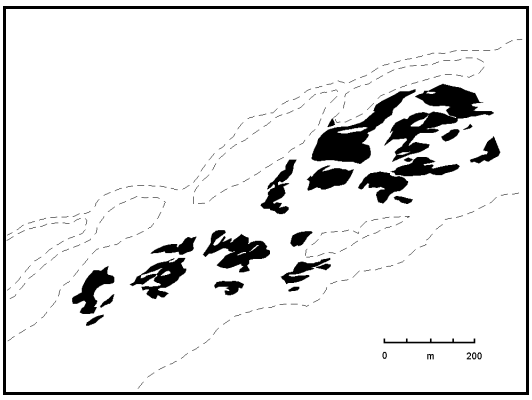

Night of 3/27/00 ~ 57 cms (54,398 m^2)

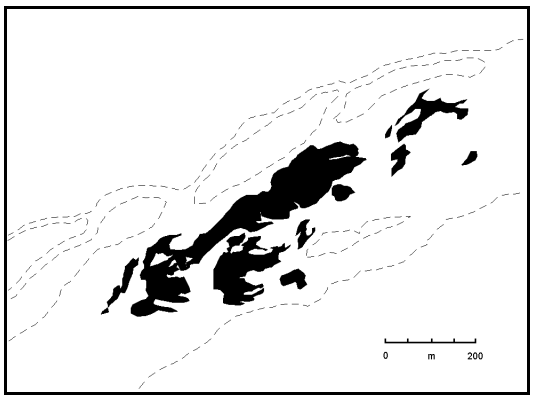

Night of 3/30/00 ~ 19 cms (60,591 m^2)

Figure 4. Roost distribution and area at Rowe Sanctuary reach for various flows.

The spatial distributions of roosting cranes are correlated with depth and velocity, as evidenced by the avoidance of deep high-velocity areas at high flow and increased use of the same areas at lower flow. Histograms of depth and velocity classes were created to show the distribution of these variables within the roost sites at both high and low discharges (figures 5a and 5b). The histograms delineate the range of these variables tolerated by the cranes at the two flows.

Although some sandbars in the reach contained tolerable depth and velocities, no cranes utilized them. The sandhill crane is a social bird and roosting behavior offers protection against predation. Therefore, when an individual crane approaches the river to select a roost site, the decision of where to roost may be governed by the presence of other roosting cranes (Paul Tebbel, Rowe Sanctuary, personal communication). Cranes were observed to continue to fly into occupied roosts while other unoccupied seemingly acceptable roosting sites were available for use.

The purpose of this experiment was to develop a technique to integrate biological and physical data to investigate the roosting preferences of sandhill cranes along a study reach of the Platte River. Currently, the velocity and depth tolerances derived from the histograms at Rowe Sanctuary are being applied to other surveyed reaches of the Platte River to assess available roosting habitat for modeled flow conditions. In the future, with more detailed topographic resolution along longer reaches, sediment-transport algorithms will be incorporated with the flow model to predict the geomorphic response of sandbars to controlled releases from upstream dams. The tools and techniques used in this paper can be extended to model and validate the effectiveness of using these releases to build in-channel sandbars along reaches of the Platte River, with the intention of increasing available roosting habitat for cranes.

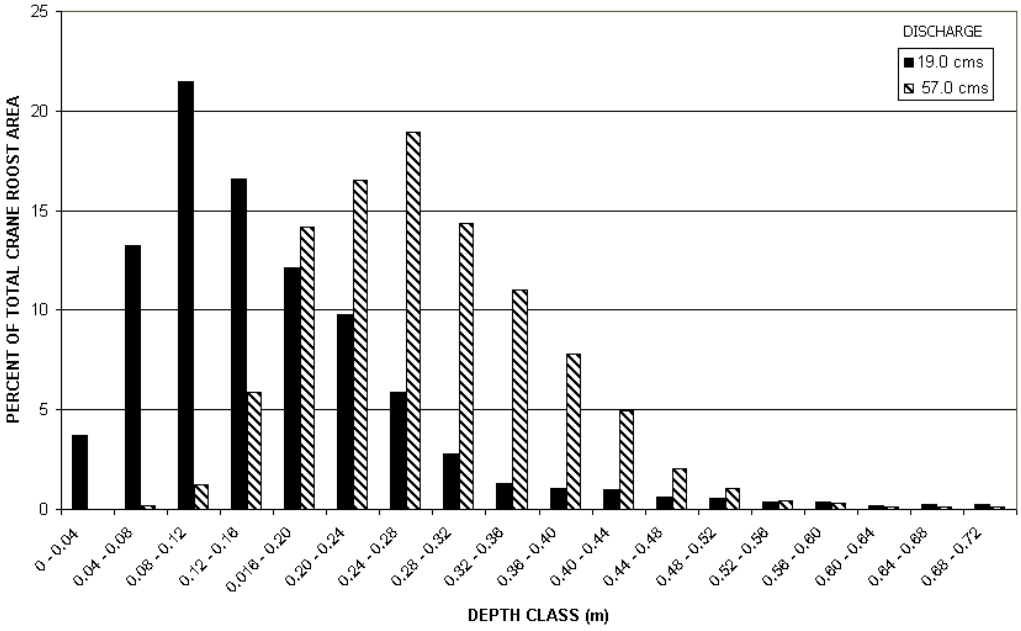

Figure 5a. Depth class distribution for roost sites in Rowe Sanctuary study reach.

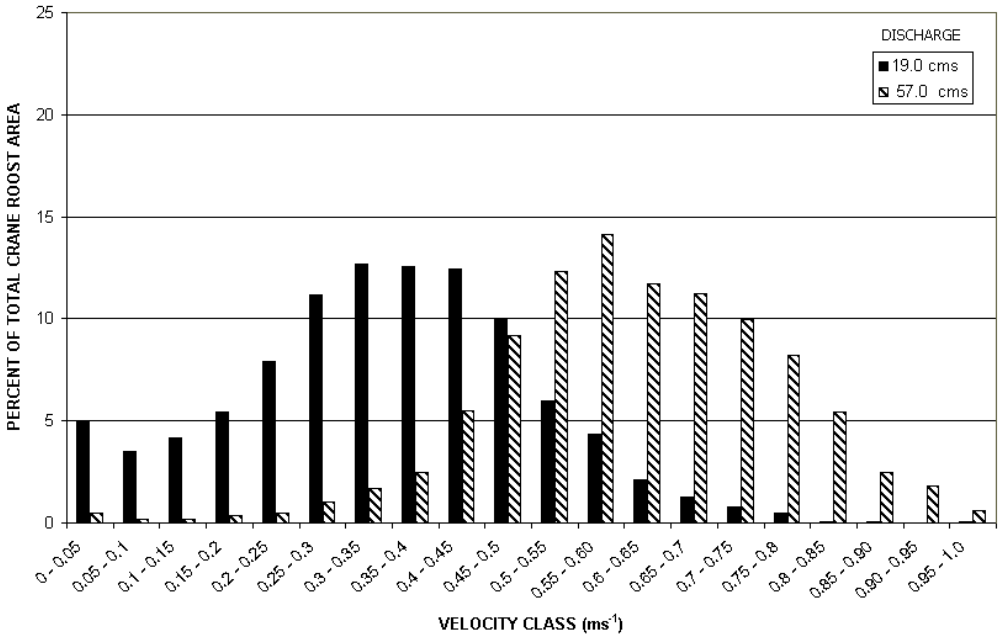

Figure 5b. Velocity class distribution for roost sites in Rowe Sanctuary study reach.

REFERENCES

Latka, D.C., and Yahnke, J.W.,1986, Simulating the roosting habitat of sandhill cranes and validating suitability-of-use indices. in J. Verner, M.L. Morrison & C.J. Ralph (eds), Wildl. 2000: Modeling Habitat Relationships of Terr. Vertebrates, Univ. Wis,19-22.

Norling, B.S. , Anderson, S.H. and Hubert, W.A.,1990, The influence of water depth, unobstructed area, and disturbance features on the selection of roost sites by sandhill cranes along the Platte River, Nebraska, project Rep., U.S. Fish and Wildlife Service, Laramie, WY.

Pucherelli, M.J.,1985, Determining sandhill crane (Grus canadensis) roosting sites using aerial thermography and geographical information systems. unpubl. rep., U.S. Bureau of Reclamation, Denver, CO.

Sidle, J.G., Nagel, H.G., Clark, R., Gilbert, C., Stuart, D., Willburn, K. and Orr, M., 1993, Aerial infrared thermal imaging of sandhill cranes on the Platte River, Nebraska. Remote Sens. Environ. 43, 333-341.

THREE-DIMENSIONAL MODELING OF FLOW THROUGH SPARSE VEGETATION

By Francisco J.M. Simões, Hydraulic Engineer, U.S. Bureau of Reclamation, Sedimentation and River Hydraulics Group, P.O. Box 25007 (D-8540), Denver, CO 80225

Abstract: This paper presents a three-dimensional model for simulating the effects of rigid vegetation on the flow passing through it. The effects of vegetation are modeled separately from bed roughness and turbulence. The method has been implemented in a free-surface three-dimensional numerical model. In this paper, it is applied to simulate the flow in a straight compound channel whose flood plains are covered by sparse rigid vegetation. Two algebraic eddy viscosity models are employed for the turbulence closure. Comparisons with experiments are shown and conclusions are drawn regarding the applicability of the models.

INTRODUCTION

Flow through vegetated canals, wetlands, and vegetated flood plains, are of great concern to hydraulic engineers and environmentalists. In recent times of increased ecological awareness, it became apparent that the processes occurring in those areas are of fundamental importance for the equilibrium of ecosystems. Understanding the physical processes governing the transport in such systems is, therefore, of great importance, especially in regions where contaminants endanger the quality of the waters.

Traditionally, the modeling of the effects due to vegetation has been done by adding friction terms to the governing equations. This practice, which is largely based on field calibrations of empirical constants such as the roughness coefficient, has been largely used in one-dimensional models and, to much smaller extent, in two-dimensional models. There have been successful attempts at higher order modeling of turbulent flows through vegetation, mostly by the use of the k-ε turbulence model (e.g., Shimizu and Tsujimoto, 1994). However, Simões and Wang (1996) have shown that simpler algebraic eddy viscosity models can have accuracies comparable to some of the higher order closures. In this paper we further investigate how simple eddy viscosity models fare in this type of environmental flows.

This paper applies a numerical model to flow through vegetation. The time-dependent, free-surface model uses a collocated finite-element method to solve the Navier-Stokes equations. Turbulence closure is achieved using two algebraic eddy viscosity models. The model is applied to a straight compound channel with vegetated flood plains. This case constitutes a good test of the governing equations and their implementation, because of the two effects contributing to momentum transfer between main channel and flood plains: the effects due to the transverse gradient in bed elevation, and to the presence of drag due to vegetation over the flood plains. Combined, these two effects contribute to strong velocity gradients near the main channel/flood plain interface, with significant impacts on the flow field and its turbulence characteristics. Detailed comparisons between measurements and computations are presented in the paper.

GOVERNING EQUATIONS

The vegetation layer constitutes an obstacle to the flow. If the vegetation is rigid and can be approximated by cylinders, then the drag force exerted by a section of that cylinder with approximately constant diameter is given by

$$F_D = \frac{1}{2}\rho A C_D U_0^2 \tag{1}$$

where A = sectional area; ρ = fluid density; U_0 = flow velocity, and C_D = drag coefficient. C_D is a function of the Reynolds number $R_e = U_0 D/\nu$, where D = the diameter of the cylinder and ν = kinematic viscosity. It can be easily found from existing tabulated values (e.g., Rouse 1946). For a given vegetation density, N, expressed in terms of rods per unit volume of water, the total drag force per unit volume is given by

$$F = \frac{1}{2} N \rho A C_D U_0^2 \tag{2}$$

The governing flow equations are the usual continuity and Navier-Stokes equations, expressing conservation of mass and momentum for the fluid phase. For an incompressible turbulent flow, these equations can be written as

$$\frac{\partial u_i}{\partial x_i} = 0 \tag{3}$$

$$\frac{\partial u_i}{\partial t} + u_j \frac{\partial u_i}{\partial x_j} = \frac{F_i}{\rho} + g_i - \frac{1}{\rho}\frac{\partial p}{\partial x_i} + \frac{\partial}{\partial x_j}\left(-\overline{u_i' u_j'}\right) \tag{4}$$

where t = time; u_i = velocity in the x_i direction (i = 1,2,3); p = pressure; g_i = component of the gravitational force (per unit volume) in the ith direction; F_i = external force per unit volume, and all quantities are time averaged in the Reynolds sense. In the above equations, Einstein's summation convention is used. The term $-\overline{u_i' u_j'}$ represents the turbulent stresses which, in the present paper, are modeled using Boussinesq's eddy viscosity concept, i.e., via a turbulent eddy viscosity, ν_t:

$$-\overline{u_i' u_j'} = \nu_t \left(\frac{\partial u_i}{\partial x_j} + \frac{\partial u_j}{\partial x_i} \right) - \frac{2}{3}\delta_{ij} \tag{5}$$

where δ_{ij} = Kronecker delta. Finally, the force per unit volume is given by

$$F_i = \frac{1}{2} N_D A \rho C_D u_i \left\| \vec{u} \right\| \tag{6}$$

where $\left\| \vec{u} \right\|$ = magnitude of the velocity vector. Note that in eq. (6) the components u_i are the components normal to the vegetation elements and $\vec{u}$ is the vector that represents the component of the total velocity vector normal to the vegetation elements. In other words, if the vegetation elements are aligned along the z direction, only $u_1 = u$ and $u_2 = v$ will enter in the drag computations, and $\left\| \vec{u} \right\| = \sqrt{u^2 + v^2}$.

NUMERICAL MODEL

The above equations were implemented in a three-dimensional numerical model, in which further simplifying assumptions were made. If the pressure is hydrostatic and there are no significant vertical accelerations:

$$\frac{\partial p}{\partial z} = -\rho g \tag{7}$$

where the gravitational force has a component only along the z axis. This allows the replacement of the z-momentum equation by eq. (7). The pressure terms in the x- and y-momentum equations can be replaced by the gradient of the free surface elevation (neutrally stratified flow):

$$\frac{1}{\rho}\frac{\partial p}{\partial x} = g\frac{\partial \eta}{\partial x}, \quad \frac{1}{\rho}\frac{\partial p}{\partial y} = g\frac{\partial \eta}{\partial y} \tag{8}$$

where η = free surface elevation. η is computed by using the depth-integrated continuity equation:

$$\frac{\partial h}{\partial t} + \frac{\partial (hU)}{\partial x} + \frac{\partial (hV)}{\partial y} = 0 \tag{9}$$

where h = water depth and U and V are the depth-averaged velocities (computed by integrating along the vertical the u and v components of the velocity obtained by solving the three-dimensional x- and y-momentum equations).

In the numerical model, the governing equations are discretized using a finite-element collocated method — for more details see Simões (1995). This allows for a discretization of the computational domain in a boundary-conforming, non-uniform mesh setting. For the calculations presented in the next sections, a second-order Runge-Kutta scheme was used to march in time. Typical boundary conditions used are the logarithmic law of the wall at solid boundaries, discharge at the inlet boundaries, and Orlanski's (1976) non-reflective condition at the outlet:

$$\frac{\partial \eta}{\partial t} + c_\phi \frac{\partial \eta}{\partial \hat{n}} = 0 \tag{10}$$

where $\hat{n}$ = direction normal to the outlet boundary and c_ϕ = phase speed of the wave $\left(= \sqrt{gh}\right)$.

NUMERICAL SIMULATIONS

To validate the model, the Wallingford (1992) experimental data sets were used. The experiments were carried out in a laboratory flume 50 m long with a compound cross section and symmetrical flood plains. The channel geometry

and dimensions are shown in Figure 1. The channel bed and walls were made of cement mortar, providing a very smooth finish of the solid boundaries. The flood plain vegetation was represented by vertical cylindrical rods extending through the full depth of the water. They were placed in a triangular pattern with a density of 12 rods per m^2. Three different discharges were chosen for the simulations, designated as runs 070601, 070701, and 070801 to use the same nomenclature as in the original Wallingford's report. The main hydraulic characteristics of these flows are shown in Table 1.

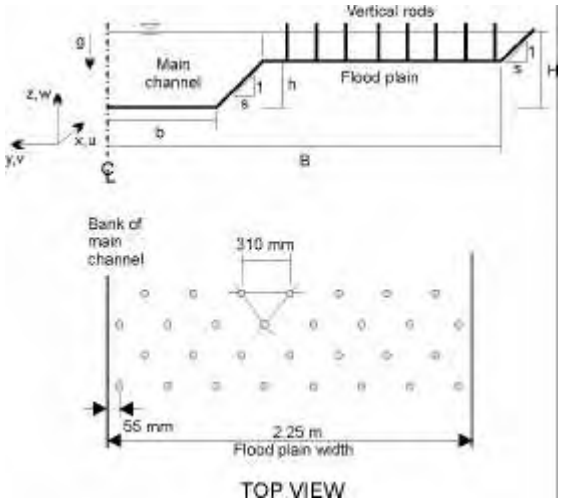

Figure 1. Top: compound channel cross-sectional configuration and notation. The centerline is placed at the middle of the main channel, at $y = 0$. $B = 3.150$ m, $b = 0.75$ m, bed slope $S_0 = 1.027\times10^{-3}$, $s = 1$, $h = 150$ mm. Bottom: pattern of the rod placement over the flood plains. The triangle formed by the rods is equilateral.

Table 1. Hydraulic characteristics of the flows simulated.

Quantity	Run 070601	Run 070701	Run 070801
Water depth, H (mm)	218.8	249.8	302.5
Discharge, Q (m^3/s)	0.343	0.424	0.543
Manning's roughness, n ($s/m^{1/3}$)	0.0141	0.0174	0.0321
Water surface slope, S_w (–)	1.05×10^{-3}	1.03×10^{-3}	1.05×10^{-3}
Froude number, F_r (–)	0.326	0.414	0.326
Reynolds number, R_e (–)	3.15×10^{5}	2.57×10^{5}	3.15×10^{5}

For turbulence closure, two eddy viscosity models were used: a parabolic eddy viscosity distribution, given by

$$\nu_t = \kappa U^* z\left(1-\frac{z}{h}\right) \tag{11}$$

and a mixing length formulation

$$\nu_t = l_m^2\left[\frac{\partial u_i}{\partial x_j}\left(\frac{\partial u_i}{\partial x_j}+\frac{\partial u_j}{\partial x_i}\right)\right]^{1/2} \tag{12}$$

where the mixing length l_m is given by

$$l_m = \kappa h\sqrt{1-\frac{z}{h}}\left[\frac{h}{z}+\pi\Pi\sin\left(\frac{\pi z}{h}\right)\right]^{1/2} \tag{13}$$

In the equations above, κ = von Kármán's constant (= 0.41); U^* = shear velocity; z = vertical direction starting at bed of channel; h = water depth; Π = Coles parameter (≈ 0.2 for high Reynolds numbers).

The simulations were carried out in a nonuniform, boundary-conforming mesh system having 8 nodes in the vertical and 21 nodes along the transverse directions. A uniform mesh spacing with $\Delta x = 0.25$ m was used in the longitudinal direction, yielding a total of 33,768 computational nodes. The results showed to have converged for this mesh system, when the time-dependent code was allowed to run until the steady state solution was reached.

SIMULATION RESULTS

The results of the simulations are shown in Figure 2 for the bed shear stress distributions, and in Figures 3 and 4 for the flow field. The simulated flow depths and velocities show an overall close agreement with the experiments for the two flows with the higher discharges (runs 070701 and 070801). As the discharge decreases, the predicted flow distribution tends to be less accurate, particularly at the main channel/flood plane interface near the water surface. For the shallowest flow (run 070601), the mixing length model was able to produce clearly better results than the parabolic eddy viscosity model, especially over the vegetated region of the flood plain. In particular, the parabolic eddy viscosity model shows a much stronger tendency to overpredict the flow velocity near the free surface.

Overall, the predicted values of the local shear stress are in close agreement with the corresponding experimental values over the flood plains, but not so at the interface between the main channel and flood plain. Here, there is a clear advantage of the mixing length model over the parabolic eddy viscosity model. At the center of the main channel, the parabolic eddy viscosity model has a tendency to underpredict the bed shear stress, while the mixing length model tends to overpredict it at higher depths. At the interface region, however, predicted values of the bed shear stress are always smaller than the corresponding measured values. The maximum discrepancies using the parabolic eddy viscosity model range from 25% of the experimental data for run 070601, to nearly 50% for flow for runs 070701 and 070801. The mixing length model has a better behavior in that region, but also falls short of the ideal conditions, especially for flow 070601 (see Figure 2).

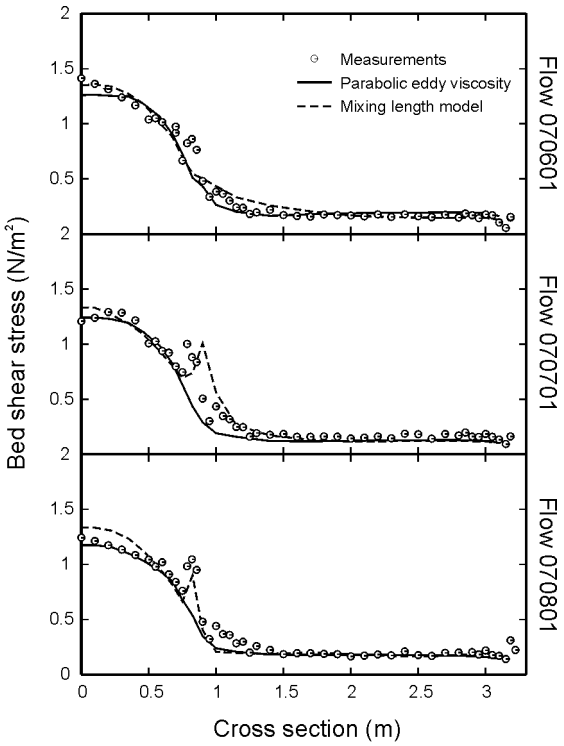

Figure 2. Bed shear stress distribution. The centerline of the channel is located at coordinate 0.

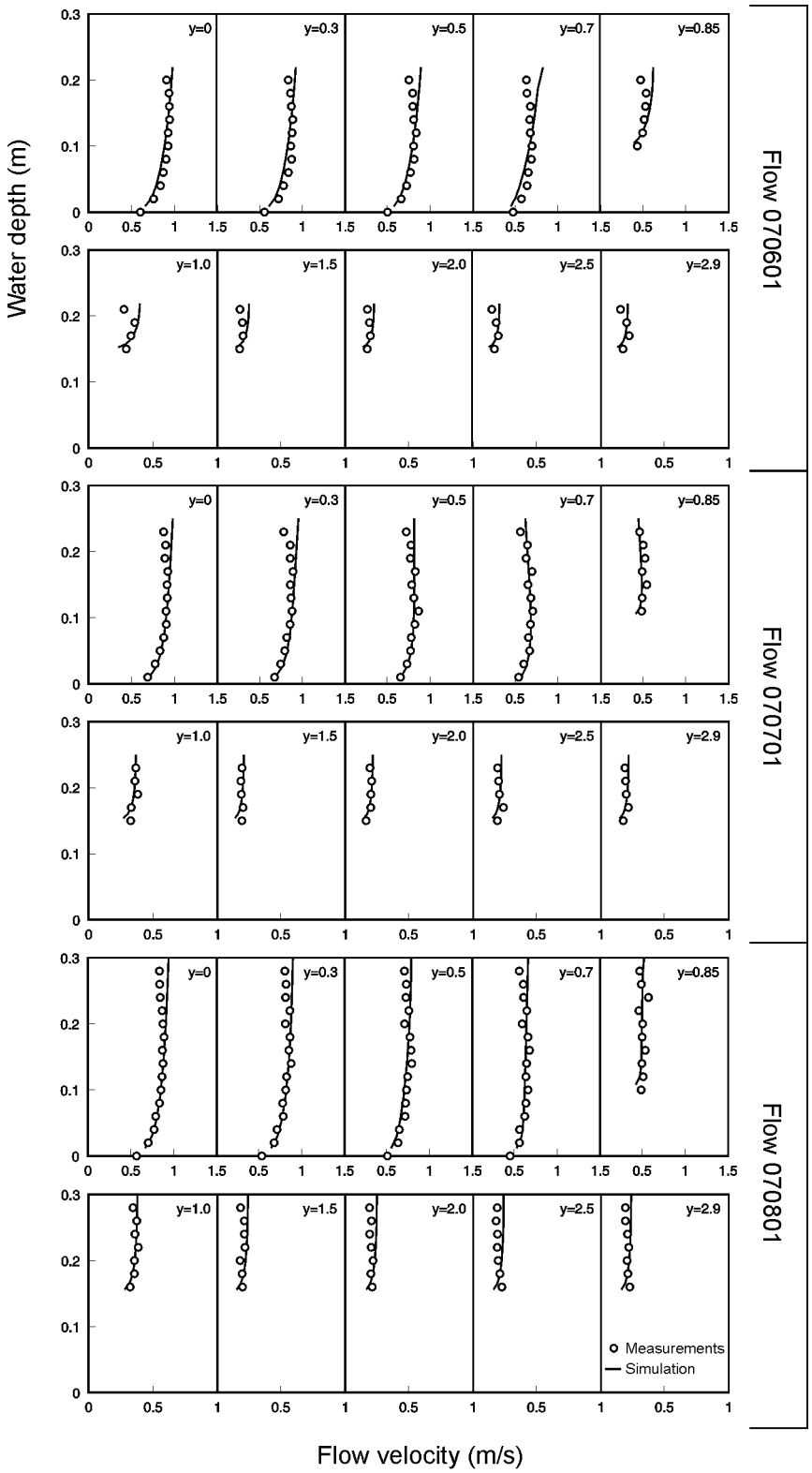

Figure 3. Flow field distribution using the parabolic eddy viscosity model, eq. (11). The coordinate *y* is measured from the centerline of the channel, in meters.

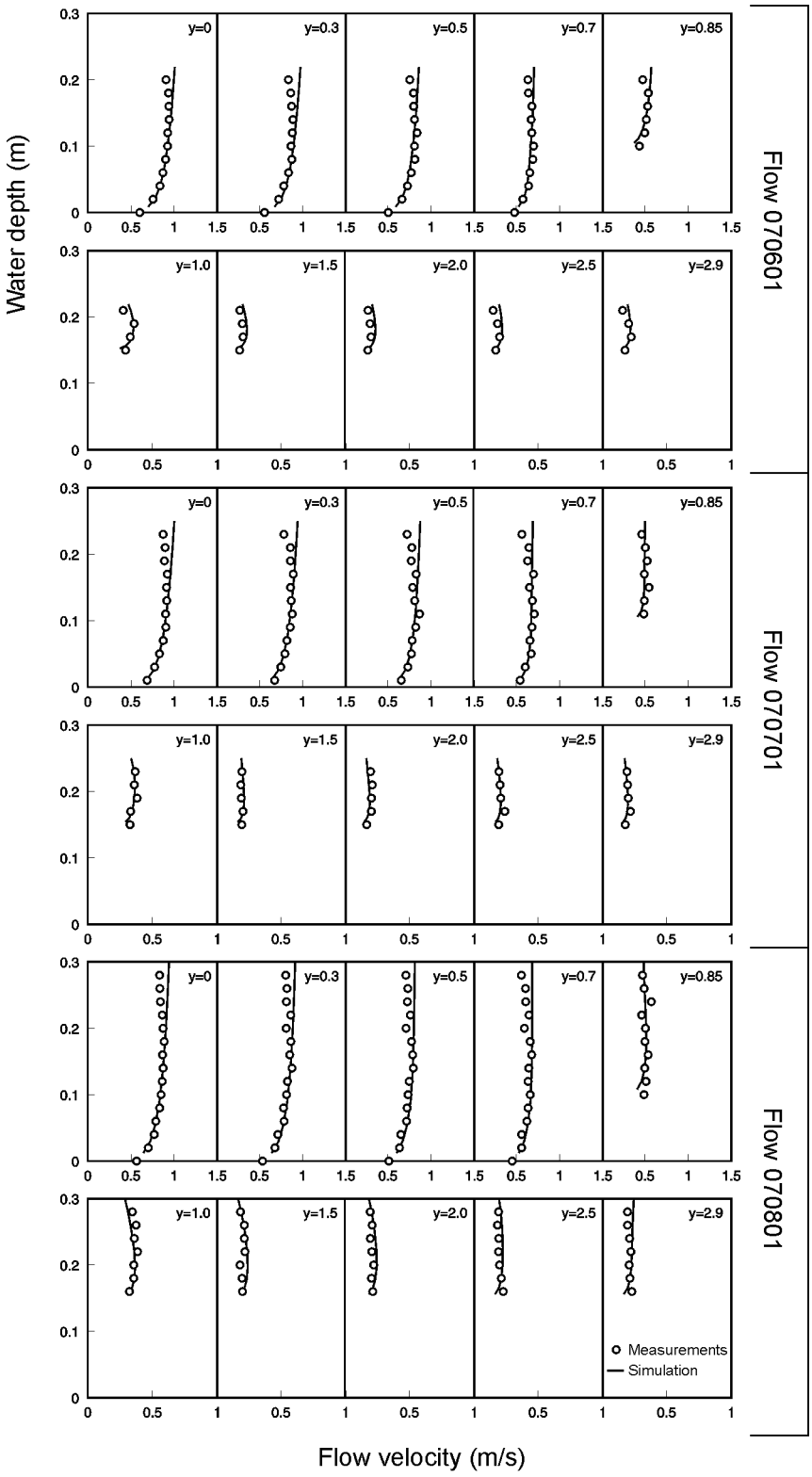

Figure 4. Flow field distribution using the mixing length model, eqs. (12) and (13). The coordinate *y* is measured from the centerline of the channel, in meters.

The distribution of the total flow discharge between main channel and flood plain is shown in Figure 5. The mixing length model also shows better agreement with the measurements, consistent with what was observed above. The accuracy of both models is very good, indicating that both models are able to capture well the mean bulk flow quantities.

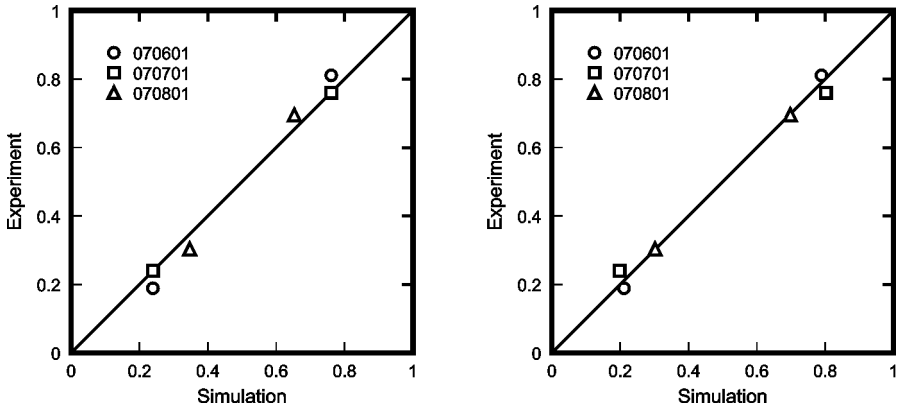

Figure 5. Model results and comparison with the experiments for the distribution of the total flow discharge (in m^3/s) between main channel and flood plain. Left: parabolic eddy viscosity model; right: mixing length model.

One of the reasons for the observed discrepancies between simulation and experiments may be due to an oversimplified model to simulate the effects of the vertical rods. For example, the model uses the local value of the depth-averaged velocity in each computational cell to compute a single value of C_D for the entire flow depth, while in practice the lower velocities near the bed (i.e., lower R_e) do predict higher values of C_D in that region. However, the fact that the most accurate results were obtained over the flood plains, where the rods are located, indicates that there is a more important source of error. This may be in the turbulence model used. First, there is experimental evidence (Shiono and Knight, 1991) that the distribution of the turbulent shear stresses is not linear at the main channel/flood plain interface. Therefore, in that region the parabolic eddy viscosity distribution is not a good approximation. Furthermore, algebraic eddy viscosity models based on the Boussinesq approximation are unable to predict turbulence-generated secondary flows in straight, uniform channel flows, which may account for the differences observed near the main channel/flood plain interface and at the center of the main channel.

CONCLUDING REMARKS

A numerical model was presented to carry out the three-dimensional modeling of the flow over flood plains with rigid vegetation. The model was validated against experimental data collected in a laboratory flume, in which vegetation was simulated by sparsely distributed vertical rigid cylinders. Two different turbulence models were used, both based on Boussinesq's eddy viscosity concept. The simulations show an overall close agreement with the experiments, but some discrepancies were observed at the main channel/flood plain interface. These discrepancies are attributed to the turbulence model rather than to the vegetation model and the results obtained suggest that the model presented here can be used to predict the flow around sparse rigid vegetation.

The model presented was developed for sparse vegetation. This means that the fundamental nature of turbulence is not significantly affected by the presence of the rigid cylinders. If that is not the case, significant changes may preclude the use of simpler models such as the ones used here. Even the k-ε model needs significant modifications to deal with denser vegetation, and no known published results exist as how to successfully accomplish such a modification.

If the vegetation is dense, the values of the drag coefficient will be affected by the presence of the wake of nearby upstream cylinders. This interference, which was nonexistent in the Wallingford's experiments, will cause a reduction in the bulk drag coefficient, and C_D will decrease with increasing vegetation density. Drag coefficient reduction models can be derived from experimental data, as shown in Figure 6. In Figure 6, the non-dimensional rod

density, R_D, is expressed in terms of sectional area (area presented to the flow by the rods) per unit of bed area and per unit of channel depth, normalized with the rod diameter. For the experiments presented in this paper, the Reynolds number was in the range of 1,000 – 5,000, yielding a reasonable constant value of $C_D = 0.99 \pm 0.03$ for a single rod in free flow. Using this fact and the data collected by Nepf (1998), the effects of dense vegetation on C_D can be found from

$$C_D = \frac{1}{1.01 + 20.6 R_D^{1.45}} \tag{14}$$

Eq. (14) was found by fitting the data of Figure 6, and is valid for Reynolds numbers in the range of about 1,000 to 5,000. Note that $\lim_{R_D \to 0} C_D = 0.99$.

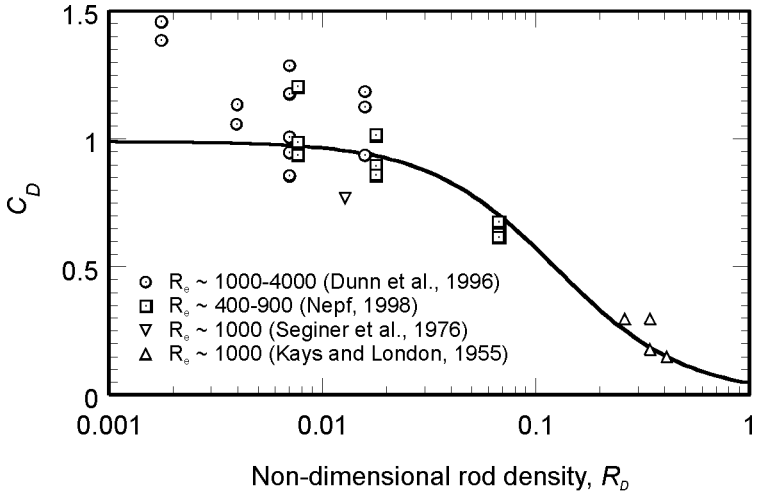

Figure 6. Drag coefficient reduction model for a single vertical cylinder due to nearby cylinders, in horizontal flow. The line represents eq. (14).

REFERENCES

Dunn, C., Lopez, F., and Garcia, M. (1996). "Mean flow and turbulence in a laboratory channel with simulated vegetation," *Hydr. Eng. Ser.* **51**, University of Illinois, Urbana, IL.

Kays, W., and London, A. (1955). *Compact Heat Exchangers*. National Press, Palo Alto, CA.

Nepf, H. (1998). "Drag, turbulence, and diffusion in flow through emergent vegetation," submitted to *Water Resources Research*.

Orlanky, I. (1976). "A simple boundary condition for unbounded hyperbolic flows," *J. Comput. Phys.* **21**, 251-269.

Rouse, H. (1946). *Elementary Mechanics of Fluids*. Dover Publications Inc.

Seginer, I., Mulhearn, P., Bradley, E., and Finnigan, J. (1976). "Turbulent flow in a model plant canopy," *Boundary-Layer Meteo*. **10**, 423-453.

Shimizu, Y., and Tsujimoto, T. (1994). "Numerical analysis of turbulent open-channel flow over a vegetation layer using a k-ε turbulence model," *J. of Hydrosc. and Hydr. Eng.*, JSCE, **2**, 57-67.

Shiono, K., and Knight, D. (1991). "Turbulent open-channel flows with variable depth across the channel," *J. Fluid Mech.* **222**, 617-646.

Simões, F.J.M. (1995). Modeling Turbulent Flow and Mixing in Compound Channels. Ph.D. Thesis, The University of Mississippi.

Simões, F.J.M., and Wang, S.S.-Y. (1997). "Numerical prediction of three-dimensional mixing in a compound open channel," *J. of Hydr. Res*. **35**(5), 619-642.

Wallingford (1992). "SERC Flood Channel Facility Experimental Data — Phase A," Vol.7, Report SR314, HR Wallingford, Ltd.

SEDIMENT IMPACTS OF PROPOSED MODIFICATIONS TO THE RIO GRANDE AND LOW FLOW CONVEYANCE CHANNEL BELOW SAN MARCIAL

Christi Young, Hydraulic Engineer, Bureau of Reclamation Denver, CO;
Cassie Klumpp, Hydraulic Engineer, Bureau of Reclamation Denver, CO; and
Drew Baird, Senior Hydraulic Engineer, Bureau of Reclamation Albuquerque, NM

Abstract: The Bureau of Reclamation has proposed modifications to Rio Grande floodway and Low Flow Conveyance (LFC) Channel system. The project area is the Rio Grande valley between San Marcial, New Mexico, and the Narrows of Elephant Butte Reservoir, New Mexico. The modifications would directly impact about a 23-mile long portion of valley in this reach. The valley width varies from about 2/3 of a mile up to 2 miles. The LFC Channel was constructed in the 1950's to increase water delivery to Elephant Butte Reservoir. A levee constructed to protect the LFC Channel restricts the Rio Grande from portions of its historic floodplain. Channel aggradation and deposition of sediments in the narrow strip of floodplain east of the levee has caused the river to become perched at an elevation higher than the valley floor. With the riverbed so high, there is a frequent threat of overtopping or breaching during high river flows. Reclamation has continued to raise and reinforce the levee in the San Marcial Reach, but the practicality of continued levee raising is in doubt.

Historically, the deposition of sediment above Elephant Butte Reservoir has been a severe and chronic problem. The current rate of sediment inflow into Elephant Butte Reservoir is about 4000 mg/l—a heavy load for a river to carry. Sediment affects channel capacity, drainage and irrigation, reservoir storage capacity, water delivery to the reservoir, cultural resources, and biological systems. Management of the Rio Grande's heavy sediment load is fundamental to successfully managing the river and controlling the effects of sediment on adjacent lands. Two proposed realignment options and a discontinue maintenance option are compared to the option of continued current maintenance.

Sediment impacts have been analyzed from San Acacia Diversion Dam to the Narrows for this study (see figure 1). The benefits of providing the river with a significantly wider active floodplain through realignment of the river downstream of San Marcial could extend as far upstream as Cochiti Dam. Projected aggradation, width, and hydraulic property trends will be discussed for the four options presented.

INTRODUCTION

The Rio Grande between San Antonio and the Narrows of Elephant Butte Reservoir (a distance of ~ 45 miles) has been naturally aggrading for thousands of years. This natural phenomenon has been influenced in recent history by man's activities; i.e., irrigation, construction of Elephant Butte Dam, introduction of exotic vegetation, construction of the Low Flow Conveyance (LFC) Channel and its levee, and river channelization. The historical response of the Rio Grande to changes in hydrology and man's actions have been documented via aerial and land based surveys and gauge records of streamflow and sediment transport rates.

Higher than recent average flows in the Rio Grande in the 1980's filled Elephant Butte Reservoir, high flows in the 1990's maintained pool level at near full conditions. The combination of high flows with the full reservoir pool has increased sediment deposition in the reach just upstream of the reservoir. Aggradation from the reservoir backwater effects has extended upstream of San Marcial and has caused the need for increased maintenance activities to insure efficient delivery of water to the reservoir and to maintain flood control protection in the valley. The San Marcial railroad bridge crosses the Rio Grande near San Marcial. The hydraulic capacity of the railroad bridge has diminished over time as a result of riverbed aggradation. Consequently, to the extent possible, peak flow releases from Cochiti Dam are regulated to avoid inundating the bridge. The main focus of this study was to determine how the river would respond to various sediment management options. Sediment transport modeling was used in conjunction with geomorphic interpretation and projection of historic trends to compare the options. The operation of Middle Rio Grande facilities was not a focus of this study but impacts of the projected hydraulic capacity at San Marcial railroad bridge were incorporated into the analysis.

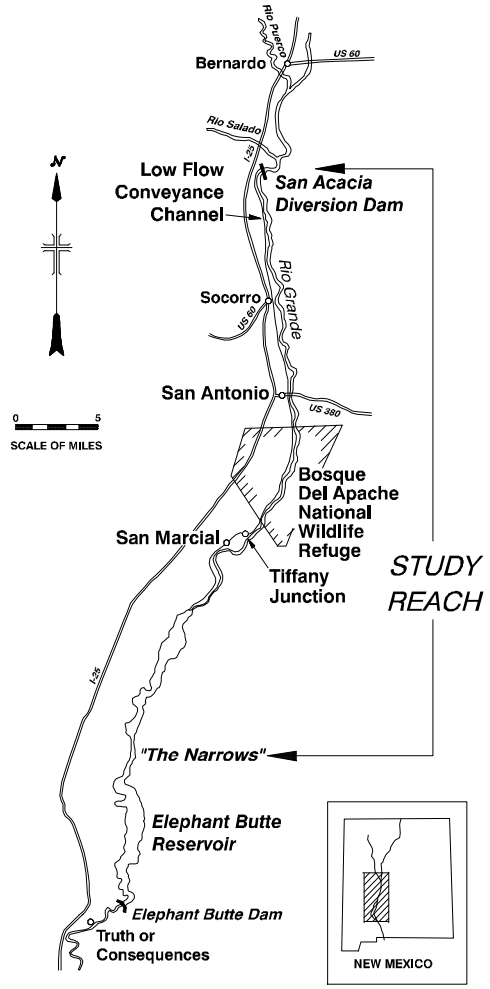

Figure 1. Location Map

DESCRIPTIONS OF SEDIMENT MANAGEMENT OPTIONS

Continued Current Maintenance: The river is currently held to the eastern portion of the historical floodplain by a levee maintained to protect the Low Flow Conveyance (LFC) Channel from San Acacia Diversion Dam to near the full pool of Elephant Butte Reservoir. The present maintenance program for this active portion of the floodway and the LFC Channel includes (Reclamation, 2000):

- maintenance and reinforcement of existing levees as needed to overcome riverbed aggradation and increasing hydrostatic pressures,
- excavation of channels within the reservoir delta to initiate floodway headcutting and reduce the aggradation rate near San Marcial,
- instigation of channel avulsions by vegetative clearing and pilot cut excavation in preferred channel locations,
- construction and maintenance of riverside berms in areas subject to plug formation,
- excavation of pilot channels through sediment plugs,
- maintenance of the LFC Channel integrity via vegetation management and slope repairs,
- installation and maintenance of culverts and low water crossings in the riverside berms and levee to promote overbank flooding in areas isolated from the river, and
- removal of salt cedar adjacent to the river channel to promote channel widening and native species regeneration.

To date, the present maintenance program has successfully maintained the river and LFC Channel system. The few

breaches that have occurred have been repaired. The ability to effectively and economically maintain the system in the future is in question.

Discontinue Maintenance: In this option, it was simply assumed that all maintenance activities would be discontinued for the floodway, LFC Channel, and any of the levees or berms along the channels. It is anticipated that without maintenance of the channel or the levees that multiple breaches in the levee and movement of the river to the lower, western floodplain downstream of the breaches would be inevitable. A viable channel to the reservoir would likely be lost.

River Realignment: Consideration was also given to a staged, gradual relocation of the river to the western floodplain within the boundaries of Reclamation land downstream from San Marcial. Two means to accomplish the river relocation were studied, one was to start the relocation at San Marcial and progress downstream, the Top Down option, and the other was to begin relocating the river just upstream of the full reservoir pool and progress upstream, the Bottom Up option. Both cases include proposed measures to prevent an uncontrolled headcut from progressing upstream in the existing channel. Extensive headcutting could isolate the overbanks from the river channel and drop the elevation of the groundwater table too quickly for habitat in the river corridor to survive.

Relocation of at least 8 miles of the LFC Channel to the western edge of the floodplain downstream of San Marcial would by necessity proceed the river relocation. With the Bottom Up option the LFC Channel construction could be phased. Construction costs for the LFC Channel and levee relocation represent a significant portion of the costs associated with the realignment options. A transition period to complete the relocation of some 20 miles of river would be needed to accommodate the construction of the necessary structural elements and to adapt proposed methods to best manage the sediment and create habitat in the new channel and floodplain. Present maintenance program activities would also be applied in the realignment options.

Top Down Option: All diversions from the existing channel for this construction option would be routed through a gated drop structure constructed near San Marcial. The diversion structure would be designed with a maximum capacity of 2000 ft^3/s. A series of sediment ponds would be created downstream of this structure by constructing dikes across the western floodplain. Sediment-laden flows would be diverted into the upstream-most pond, clear water would be decanted through culverts into the relocated LFC Channel. Once the pond was sufficiently filled with sediment, the dike would be strategically breached to route flow into the next pond. This process would continue until each of the successive ponds has been filled. A series of 7 ponds was assumed for this analysis. The diversion structure would be removed prior to routing the full river flow to the western alignment. It was anticipated that mechanical intervention might be necessary to distribute sediments throughout the ponds and establish a new channel in the deposits.

Bottom Up Option: In this option a series of breaches would be constructed in the existing levee. Each breach would include a simple drop structure, utilizing materials such as sheet piling and large riprap to control head cutting upstream and scour downstream. The drop structures would have the capacity to divert the majority of the river flow to the western floodplain. The deposition pattern downstream of each breach was assumed similar in shape to the elongated conical delta deposits observed at the river-reservoir interface. Assumptions regarding the extent and composition of the deposits were based on modeling results and physical constraints such as the elevation differential between the existing channel and the western floodplain and the distance between the existing levee and proposed levee for the realigned LFC Channel. A breach location would be abandoned once sediment begins to redeposit in the existing channel upstream of the site and the next upstream drop structure would then be opened.

Drop structures were proposed at 5 locations, the exact location and elevation of each would be sequentially set to effectively distribute the sediment and maximize channel capacity without impacting overbank inundation frequencies or groundwater levels. Throughout the transition period, maintenance flows would be provided to the existing channel downstream of the active breach site. It was assumed that mechanical intervention might be required to direct the realigned channel away from the levee of the relocated LFC Channel.

ANALYSIS METHODS

Hydrologic Analysis: Stochastic hydrologies were developed based on 98 years of recorded flow at the San Marcial gage (Lane, 1995 and 1997; Sailer, 1998). Of the 20 hydrology traces generated, 3 were selected through a ranking process and modeled for each sediment management option—traces representing average, below average, and above average hydrologic conditions. Although, each of these generated hydrologies is one possible future within the realm of all possible future scenarios, results showed that impacts varied with the magnitude of the cumulative flow volume but that the relative differences between the options remained consistent. Therefore, this paper focuses on results obtained from an average hydrology.

The three hydrographs were modified based on operational constraints to develop specific hydrographs for the drainage and conveyance operations. No diversions would be made to the LFC Channel at San Acacia Diversion Dam for drainage operations. The LFC Channel would simply salvage drainage flows from adjacent lands. For conveyance operations, the LFC Channel would be used to more efficiently transport water to Elephant Butte Reservoir. Diversions up to 2000 ft^3/s would be made to the LFC Channel with the constraints to maintain a minimum flow in the river channel and cease diversions during two weeks of spring peak flows. Responses to any future variations in LFC Channel operations should be bracketed by the responses predicted for these two operations. Hydrologic input data for the sediment model consisted of inflows for the river and LFC Channel segments and the associated reservoir elevations.

Sediment Transport Analysis: A version of the HEC-6T computer model, Sedimentation in Stream Networks (Thomas, 1996), specifically adapted to the Rio Grande study, was used in the analysis of water and sediment transport through the portion of the study reach between San Antonio and the Narrows—the Bosque, Fort Craig, and Reservoir Reaches. The reaches delineated best reflect geomorphic, habitat, and maintenance considerations. The Bosque Reach was defined as the upper-most reach extending about 18 miles between the Highway 380 bridge near San Antonio and San Marcial. The river channel in the upstream half of this reach is generally wider and more braided than the downstream portion. The downstream portion of this reach is subject to greater aggradation rates and higher frequency of sediment plug formation, and consequently more maintenance efforts. The Fort Craig Reach is about 8 miles in length and extends from San Marcial to near the full pool of Elephant Butte Reservoir (Rangeline (RL) 24). It is in this reach that the majority of the river realignment would be accomplished. The Reservoir Reach extends from RL 24 to the Narrows (RL 59), some 18 miles. The portion of riverine versus reservoir cross sections in the Reservoir Reach varies with the reservoir elevation. Current delta channel maintenance activities and the proposed river relocation extend into the upper portion of this reach.

The LFC Channel was generally modeled as a 33 mile tributary joining the river at RL 32. The sediment supply for the drainage flows was assumed to be small; therefore, modeling sediment transport in the LFC Channel for the drainage scenarios was not necessary. The LFC Channel was modeled for conveyance operations. The 2000 ft^3/s capacity LFC Channel matched the existing design with a 32-foot bottom width, 2:1 side slopes, a 0.0005 channel slope and a roughness coefficient of 0.020. The capacity was maintained during the simulation by annual dredging. The model was initially calibrated using available historic cross section, hydrology, sediment, and hydraulic data sets. Then base data sets for geometric, sediment, and hydrologic properties were generated for the predictive models incorporating specific details for each maintenance option. The sediment input for the floodway included using a Manning's n roughness coefficient of 0.017 for the main channel and 0.10 for the overbanks; unit weights 41, 50, and 93 lb/ft^3 for clay, silt, and sand, respectively; and a sediment rating curve of $Q_s = 0.92 * Q^{1.411}$ at San Antonio. The Laursen and Madden sediment transport equation (Madden, 1993) was used. Additional sediment properties were determined from laboratory testing and from field observations (Vermeyen, 1995).

An analysis period of 20 years was used in this study. The simulations were continuous but were run as a sequence of individual years. At the end of each year, as needed, modifications were made to the files such as adding or removing conveyance limits at sections impacted by the reservoir fluctuations and dredge commands for inundated portions of the LFC Channel. In the current maintenance and realignment options, channel maintenance impacts were periodically applied to geometry data using criteria based on the rate of predicted aggradation, the reservoir contents, and the projected hydraulic capacity at the San Marcial railroad bridge. For example, reservoir delta channel maintenance excavations are typically about 2 miles in length, 5 feet deep, 200 feet wide at the base with 5H:1V side slopes. It was assumed that the LFC Channel levee would be maintained at an elevation that would prevent overtopping by a 10,000 ft^3/s flow.

For the Top Down realignment option, the length of the transition period (an estimated 6 to 11 years) and the composition of the sediment pond deposits were projected using Reclamation's SETSIZE settling basin program (Randle, 1984) and spreadsheet analysis in combination. HEC-6T was used to model the delta development of one breach scenario for the Bottom Up realignment option. Conclusions drawn from that modeling effort were applied to the other breach locations. A volumetric spreadsheet analysis was also used to determine that 4 to 9 years would be required to complete the series of breaches depending upon the hydrology. A rating curve developed from San Marcial gage data, $Q_s = 0.783 * Q^{1.411}$ was used in the transition period analysis of both realignment options.

The 20-year modeling analysis of each realignment option included the transition period for the river relocation. HEC-6T modeling on the entire reach was performed for the period remaining in the 20-year simulation after the transition period. The cross-section geometries for the Fort Craig Reach were modified substantially to reflect the river realignment based on results from the transition analyses and assumptions regarding the configuration of the sediment deposition. The channel established matched the configuration of the delta maintenance channels described above. Geometries for the Bosque and Reservoir Reaches were based on model results for the same period of time using the existing channel simulations.

Width Change Projection Analysis: To augment the one-dimensional sediment transport modeling results, a regression analysis was conducted on historical flow and width data (Makar and Strand, 2000). The active channel width was defined as the width of the sand bed channel that the river had cleared of most vegetation. The reach average active channel width was regressed on the average of the previous 5 years peak mean daily discharge, the assumed channel forming flow, to obtain the best fit to the power relationship $w = a*Q^b$. Relationships were defined for sub-reaches delineated by slope and width trends. Historical data reveal differences between the subreaches in average width, variability of widths, and the amount the change in width over time. For example, the upper portion of the Bosque Reach has been the most responsive to changes in hydrology, whereas the lower portion of that reach has remained narrow since it was channelized and relocated in the 1950's. The Fort Craig Reach has always been the narrowest, with the least amount of variability in width.

Throughout the simulations the amount of flow that could be passed under the San Marcial railroad bridge was monitored. These flows or bridge capacities were assumed to correlate with the anticipated peak flows that would be routed through the modeled reach. Two projections of percent width change were developed for each subreach based on bridge capacity projections and the derived empirical relationships. Projected reach averaged widths were compared to the 1992 calculated widths to estimate the percent change caused by an option in each subreach. The projected width changes were applied to cross-section data obtained from the sediment transport simulations. One projection was the average width change calculated over the 20-year simulation period. Another projection was based on maintaining peak flows equal to the year 20 estimated bridge capacity for the five years following the simulation period, the year 20 bridge capacity was simply input as the channel forming flow in the regression equations. This projection was used to show the potential for width change beyond the simulation period.

For the 20-year average width change projections, it was assumed that the Rio Grande would be operationally managed to meet bridge capacity limits at San Marcial, therefore in the width projection analysis, the spring peak flows in the generated hydrology were limited to the projected bridge capacities. In many cases, the annual peaks in the generated hydrologies were much less than the bridge capacities and therefore not limited. Summer thunderstorm peaks were not limited because there is no flow regulation facility between the Rio Puerco, the major contributor to thunderstorm events, and the modeled reach. Annual width values projected based on these peak flows were averaged over the simulation period to obtain the reported width change projection.

Hydraulic Property Analysis: Historical hydraulic properties from 1962, 1972, and 1992 were calculated using HEC-RAS (USACE, 1999) from observed data to evaluate trends from San Acacia Diversion Dam to the Narrows. The reach from San Acacia to San Antonio, the Socorro Reach, was not modeled in the sediment transport analysis but was included in the hydraulic property analysis because this reach has historically not been an aggrading reach. Channel roughness values were increased from the 0.017 used in the downstream reaches to 0.020 for the lower portion and 0.024 for the upper portion of this reach to reflect the coarser nature of the bed.

Future hydraulic properties were projected by applying the projected width changes to cross-section data resulting

from the sediment transport analysis and the importing the revised cross-section data into HEC-RAS. Hydraulic properties were calculated for a variety of flows, 200- (average summer base flow), 500- (average winter base flow), 3000-, 5000-, and 10,000-ft^3/s flows. Reach averaged hydraulic properties such as channel width, depth, velocity, and width-depth ratio and overbank depth, width, and inundated area were used in associated studies to evaluate the impacts of the various maintenance options on wildlife and their habitats.

SEDIMENT IMPACT PROJECTIONS

The sediment impacts were evaluated through comparison of the projected depositional patterns, maintenance requirements, and projected width changes and resulting hydraulic properties associated with each option. The depositional volume in the Bosque Reach was used as an indicator of sediment transport capacity. Depositional volumes for the Fort Craig and Reservoir Reaches were somewhat misleading because of intentional filling prescribed for the realignment options prior to relocation of the river. Bottom profiles were also compared, the riverbed elevation and the hydraulic capacity at the San Marcial railroad bridge were used as a specific indicators. Maintenance impacts included quantity differences in activities such as excavating channels in the delta, dredging the LFC Channel, and raising the levee. Some of the results are presented as ranges representing the differences between conveyance and drainage operations.

Sediment Deposition: The results showed that the deposition volumes in the Bosque Reach for the Continue Current Maintenance option of 10,700 to 11,800 acre-feet, were nearly double those projected for the Bottom Up option, 5,800 to 6,200 acre-feet. The Discontinue Maintenance value was 9,200 acre-feet while the Top Down option values varied between 8,500 and 8,800 acre-feet. Comparison of these values indicates the highest sediment transport capacity was associated with the Bottom Up realignment option. The results show that Rio Grande will continue to aggrade in the study area, maintenance and operation practices can reduce the rate or change the location of the deposition but will not reverse the trend.

The channel invert elevations at the San Marcial railroad bridge site demonstrate the impact the various alternatives have on the average bed rise. Values for the realignment options (4468.9 to 4471.9 feet) were lower than current maintenance (4473.3 to 4474.8 feet) and discontinue maintenance (4473.0 feet) projected values. Average bed rise of the Bosque Reach tended to be less for the realignment options as a result of the headcutting associated with river relocation. Lower riverbed elevations, especially when accompanied by channel widening, correspond to increased flow capacity for the existing railroad bridge configuration and levee heights.

Required Maintenance: The frequency of channel excavations in the delta was based primarily on the reservoir contents. For a specific hydrology scenario, delta channel excavations were modeled at about the same points in time for each option. In most cases, the channel was excavated in an adjacent alignment in the delta at the previously described depth, width, and length. It was an exception when cross sections in the delta still had sufficient capacity when the reservoir content constraint was met. Therefore, the excavation quantities determined were similar and all were in excess of 1.1 million cubic yards.

Variations in dredge volumes between options are mainly affected by the number of years diversions were made into the LFC Channel. It was assumed that only relatively clear drainage or decanted water would be conveyed in the channel during the transition period for both realignment options. Dredge volumes for the current maintenance option (5.1 million cubic yards) were greater because diversions were made to the LFC Channel throughout the 20-year simulation whenever river flows were sufficient. Realignment dredge volumes varied between 4.0 and 4.4 million cubic yards. The location of the LFC Channel connection point at Rangeline 32 caused the impacts associated with reservoir inundation to somewhat overshadow the differences between the options.

The average required increase in levee height also did not show significant differences between the options. The increase in elevation of the levee in the Fort Craig Reach would be lower in the realigned options (1.3 to 1.6 feet) than the current maintenance option (2.3 feet). The levees will continue to require additional height over time, if maintained. With a wider floodplain in which to distribute sediments in the realigned Fort Craig Reach, the rate of increase in levee height should be less.

Hydraulic Capacity at the San Marcial Railroad Bridge: The hydraulic capacity at the railroad bridge would increase for either of the realignment options as a result of the limited headcutting initiated by routing flows to the lower western floodplain during the transition period. With the location of the gated drop structure just downstream of the railroad bridge the Top Down option should experience greater initial capacities than the Bottom Up option. The bridge capacity would probably level off once the first few sediment ponds nearest to the bridge were filled. Bridge capacities for the Bottom Up transition period would incrementally increase as the active breach location moves upstream closer to the railroad bridge site. The Bottom Up simulation projected the highest bridge capacity (> 10,000 ft^3/s) and, following that, the lowest rate of capacity loss. These capacity increases were mainly a result of the steeper channel slope projected downstream from the railroad bridge. Channel degradation projected for the uncontrolled levee breach modeled in the Discontinue Maintenance option also resulted in a temporary increase in bridge capacity. The wider western floodplain would provide opportunities for channel avulsions, natural or man-induced, to spread out the sediment deposition. Model results showed that higher bridge capacities could be sustained longer for the realignment options because of the wider floodplain. The 20-year average bridge capacities are shown in Table 1 to reflect some of the variation in capacity over the simulation period. Eventually, unless the there are large changes to the water sediment relationship, the capacity at the bridge would decrease over time for all of the options. Still, many of the realignment scenarios were projected to have bridge capacities greater than the initial 4200 ft^3/s capacity at the end of the 20-year simulations (see Table 1).

Table 1. Projected hydraulic capacities (ft^3/s) at San Marcial Railroad Bridge and percent width change

Option		Continue Current Maintenance		Discontinue Maintenance	Top Down Realignment		Bottom Up Realignment	
Operation		Convey.	Drainage	Drainage	Convey.	Drainage	Convey.	Drainage
Hydraulic capacity at San Marcial railroad bridge	20 yr. ave.	2500	3300	3700	5300	4200	7400	7300
	At yr. 20	1400	2400	2700	6000	4000	9400	7200
Projected percent width change for the Fort Craig Reach	20 yr. ave.	-30	-30	-20	-10	-20	10	25
	At yr. 20	-40	-35	-35	70	-5	230	125

Projected Percent Width Change: Trend differences in these averages reflect the relative impact of each option on active channel width. The projected percent width change values shown in Table 1 for the Fort Craig Reach are representative of the relative trends observed for the other reaches. Interpretation of the results must include the realization that the 20-year average percent width change results were calculated by averaging annual projected width values. The annual width calculations were based on actual and generated flows that may or may not have been high enough to be limited by the bridge capacity data. The actual hydrology data available for the 5 years preceding the simulation period were used in width calculations for years 1 through 4 of the simulation. The value used in the regression equation is the bridge capacity limited spring peak flow or the unlimited summer peak flow (discussed previously), not the bridge capacity. The Rio Grande hydrology is such that there are many years that the magnitude of the peak flows is too low to impact channel width. This was not the case with the year 20 projections that are based on the assumption of 5 years of peak flows equal to the bridge capacity at year 20.

Many sources of error were present in deriving these percent changes; even so, the trends noted are useful. Basically, the greater the bridge capacity or allowable peak flow, the wider the channel would be. The Bottom Up option is projected to result in channel widening. All of the other options are projected to result in channel narrowing for the 20-year average width projection. The widening projected for the Bottom Up option is based on the higher bridge capacities that are a result of establishing the relocated channel in the western-most, lowest point in the floodplain. A wider channel was projected for the Discontinue Maintenance option than the Continue Current Maintenance option because of the temporary increase in bridge capacity resulting from the simulated levee breach.

Hydraulic Property Trends: Hydraulic property trends were obtained to assist in the evaluation of sediment management impacts on critical habitat for native and endangered species in an associated study. Changes in most of the properties evaluated were related to the width changes. Examples of some general trends are presented. For each of the modeled flows, channel hydraulic depth and velocity increase as the width reduces. In realigning the

river to the western floodplain in the Fort Craig Reach, not only is the available overbank area significantly greater, the channel planned for the realignment alternatives in many cases is much wider than the existing channel. Therefore, an increase in the flow required for overbank inundation was noted. For the upstream reaches, generally the total top width and total flow area for the 3,000 ft^3/s flow decrease as width decreases because the majority of the flow was still contained within the main channel. For all of the riverine reaches, nearly any width reduction increased overbank flow width and inundation area values for the 5,000 ft^3/s flows.

CONCLUSIONS

There were pressing needs to evaluate sediment management options for the Rio Grande between San Acacia Diversion Dam and the Narrows of Elephant Butte Reservoir. Sedimentation rates are affecting channel capacity, drainage and irrigation, reservoir storage capacity, water delivery to the reservoir, cultural resources, and biological systems. With the limitations of the current maintenance program, maintenance costs and the potential for perched portions of the river to overtop or breach the LFC Channel levee increase with time. Consequences of discontinuing maintenance include uncontrolled levee breaches, obliteration of portions of the LFC Channel eliminating the ability to convey even drainage flows, and loss of a viable channel to the reservoir. Proposed realignment options have high initial construction costs but provide an opportunity to restore a broader floodplain reducing the rate of average bed rise and increasing habitat diversity. Management of the Rio Grande's heavy sediment load is fundamental to successfully managing the river and controlling the effects of sediment on adjacent lands.

REFERENCES

Bureau of Reclamation, 2000, Rio Grande and Low Flow Conveyance Channel Modifications-Draft Environmental Impact Statement, Albuquerque Area Office, Albuquerque, New Mexico

Lane, W.L., 1995, Elephant Butte Reservoir-Middle Rio Grande Project-Analysis of Water Surface Elevations, Bureau of Reclamation, Denver, CO

Lane, W.L., 1997, Headwaters of Elephant Butte Reservoir Sediment Transport Modeling and Analysis of River Management Alternatives-Rio Grande Stochastic Hydrology Modeling Portion-San Acacia to Elephant Butte Reservoir, W.L. Lane Consulting Hydrology and Water Resource Engineering, Golden, CO

Madden, E.B., 1993, Modified Laursen Method for Estimating Bed-Material Sediment Load, Contract Report HL-93-3, U.S. Army Corps of Engineers, Waterways Experiment Station, Vicksburg, MS

Makar, P.W. and Strand, R.I., 2000, Geomorphic Responses of the Middle Rio Grande: San Acacia to the Narrows of Elephant Butte Reservoir, Bureau of Reclamation, Technical Service Center, Denver, CO

Randle, T.J., 1984, User's Guide to Computer Modeling of Settling Basins, Bureau of Reclamation, Denver, CO

Sailer, M.R., 1998, Addendum to: Headwaters of Elephant Butte Reservoir Sediment Transport Modeling and Analysis of River Management Alternatives-Rio Grande Stochastic Hydrology Modeling Portion-San Acacia to Elephant Butte Reservoir, Bureau of Reclamation, Denver, CO

Thomas, W.A., 1996, Sedimentation in Stream Networks User Manual, Mobile Boundary Hydraulics, Vicksburg, MS

US Army Corps of Engineers, 1999, HEC-RAS River Analysis System Version 2.2.1, Hydrologic Engineering Center, Davis, CA

Vermeyen, T., 1995, Erosional and Depositional Characteristics of Cohesive Sediments found in Elephant Butte Reservoir, New Mexico, Report R-95-15, Bureau of Reclamation, Denver, CO

EVENT BASED SEDIMENT TRANSPORT SIMULATION OF A RIVER REACH UPSTREAM OF A TEMPORARY DREDGE CHANNEL, ELEPHANT BUTTE DAM, NEW MEXICO

By Robert S. Padilla, Hydraulic Engineer, River Analysis Team, Albuquerque Area Office, U.S. Bureau of Reclamation and Dr. Richard Heggen, Department of Civil Engineering, University of New Mexico, Albuquerque, New Mexico

Abstract: An investigation was undertaken to apply and calibrate an event based sediment transport numerical model to predict the upstream channel response to a downstream increase in slope for the duration of a spring runoff hydrograph. HEC-6T (Thomas, 1996), a one-dimensional sediment transport model simulated the river channel bed response upstream of a temporary dredge channel. Key inputs and options included the pre- and post-event channel and delta cross sectional data, cross sectioning of the temporary dredge channel, the Yang (1973) sediment transport equation, a 91 day spring runoff hydrograph measured at the San Marcial gage, and an inflow bed-material rating function developed for the gage. The model was calibrated for the observed subreach volume changes in the river channel upstream of the temporary dredge channel for the spring runoff event. The calibration simulation accuracy had a root mean square error of 32,775 cubic yards, translating to a 0.71ft. over-prediction of degradation for the entire reach upstream of the dredge channel. Sensitivity analysis with the model's sediment inflow rating function increased by 20 percent reduced over-prediction to 0.19 ft. The simulated bed profile accurately represented the general trend of measured degradation. Comparison of the simulated and measured subreach volume change was reasonable. Both the individual cross section and entire cumulative volume changes were indicative of what was observed.

INTRODUCTION

The Elephant Butte Reservoir and delta are located on the Rio Grande approximately 45 miles downstream of Socorro, New Mexico and 30 miles upstream of Elephant Butte Dam. During 1995 and 1996, a severe drought in this region resulted in a 300,000 acre-feet decrease in Elephant Butte storage. The reservoir pool receded approximately 2 miles further into the reservoir. In the winter and early spring of 1997, the U.S. Bureau of Reclamation excavated a temporary dredge channel through approximately 1 mile of exposed delta to connect the river channel to the reservoir pool (figure 1). Immediately following the excavation activity, a 91 day spring runoff event flowed through the temporary dredge channel and into the reservoir pool. Channel bed degradation upstream of the dredge channel for a length of approximately 3 miles was observed as a result of the spring runoff flows and the temporary dredge channel.

A sediment transport numerical model was applied to simulate the upstream sand bed channel's 1997 spring runoff response. Channel geometry, sediment properties and parameters, and hydrology were incorporated into the model based on field measurements, previous research and investigative analysis for the study area. Once a calibration was achieved, sensitivity analyses were performed on the model. Model sensitivities to time-step duration, other sediment transport functions, channel bed roughness, the sediment inflow rating function, and the channel's bed material size distribution were evaluated.

APPROACH

Model Synthesis: The one dimensional sediment transport model HEC-6T (Thomas, 1996) was used to perform the simulation. The primary input component was the cross sectional data defining the channel geometry of the study reach (figure 1), as-built cross sectioning of the temporary dredge channel, and reservoir cross sections. Cross-sections EB-17 thru EB-26 represented the three-mile study reach upstream of the temporary dredge channel. The hydrologic data for the model consisted of the historical mean daily flows, the monthly water temperature of the Rio Grande Floodway at San Marcial (USGS Gage 08358400), and the daily reservoir pool storage (USGS Gage 08360500) translated to pool elevations for the spring runoff of 1997. Key sediment inputs involved river bed material gradations obtained at river cross sections, the Yang (1973) unit stream power equation, and an inflow bed material rating function developed by Slater and Baird (1991) based on the Modified Einstein Procedure developed by Colby and Hembree (1955). A Manning's "n" value of 0.017 was utilized as the roughness coefficient for the main river channel and a value of 0.10 for the vegetated overbank areas.

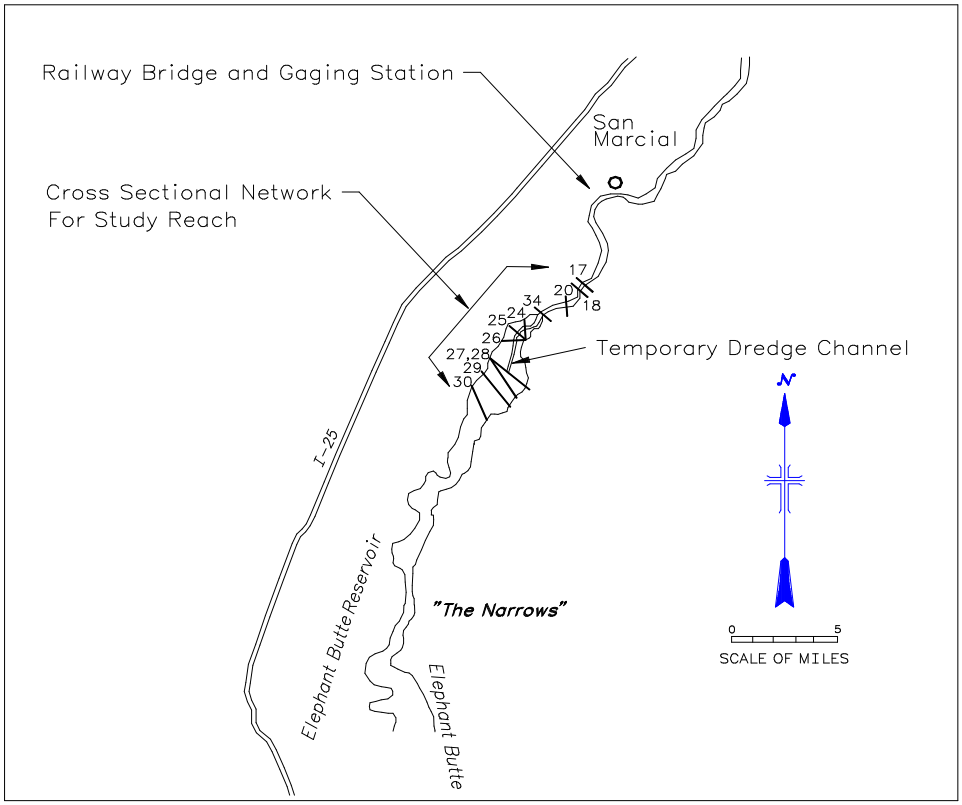

Figure 1 - Cross sectional Network for Study Reach

Model Calibration:. The model was calibrated to best match the observed channel bed response upstream of the temporary dredge channel. The channel bed response was assessed in terms of the subreach volume changes. A subjective calibration procedure allowed for the adjustment of the input variables to determine output values which most closely agreed with the observed subreach volume changes. To measure the model's calibration accuracy a standard error analysis of the simulated and measured subreach volume changes was utilized. A minimum Root Mean Square (RMS) error (Snedcor and Cochran, 1980) between the simulated and measured subreach volume changes in the test reach determined the simulation's calibration. A secondary indicator utilized for model calibration was the discrepancy ratio, the ratio of the computed reach volume to the measured reach volume.

Through numerous iterations of individual input variable adjustment, model simulation, and comparison of output results, a minimum RMS error of 32,775 cubic was realized (Table 1). Comparison of the simulated and measured subreach volume change was reasonable (figure 2). This RMS error translated to an approximate over estimate of 0.71 feet of degradation for the entire reach. The primary adjustments for the model's calibration were to the daily time step duration.

Table 1 - Calibration Error Evaluation with Minimum Root Mean Square Error (32,775 cubic yards)

Cross Section	Measured Change in Volume at Mobile Bed Section (cy)**	Simulated Change in Volume at Mobile Bed Section (cy)**	Difference Between Measured and Computed Values (cy)	Subreach Length (feet)	Error per Linear Foot (cy/ft)	Ratio of Subreach Length to Overall Test Reach Length	Weighted Error
EB - 17	-6826	-12551	5725	2900	1.97	0.09	0.19
EB - 18	26495	15831	10664	6800	1.57	0.22	0.35
EB - 20	-7739	-72219	64480	6540	9.86	0.21	2.10
EB - 34	-5211	-33047	27836	5260	5.29	0.17	0.91
EB - 24	-87580	-86654	-926	4340	-0.21	0.14	-0.03
EB - 25	-30414	-66580	36166	3120	11.59	0.10	1.18
EB - 26	-26045	-18460	-7585	1720	-4.41	0.06	-0.25
Total	-137320	-273680		30680			4.44

Subreach Weighted Error For Entire Reach 4.44 Cubic Yards Per Linear Foot of Channel

Estimated Error for Bed Elevation for Entire Reach Per Foot of Channel 0.71 Feet per Linear Foot of Channel

* Assuming Average Channel Width of 170 feet for Entire Reach

** Negative Sign Denotes Channel Degradation

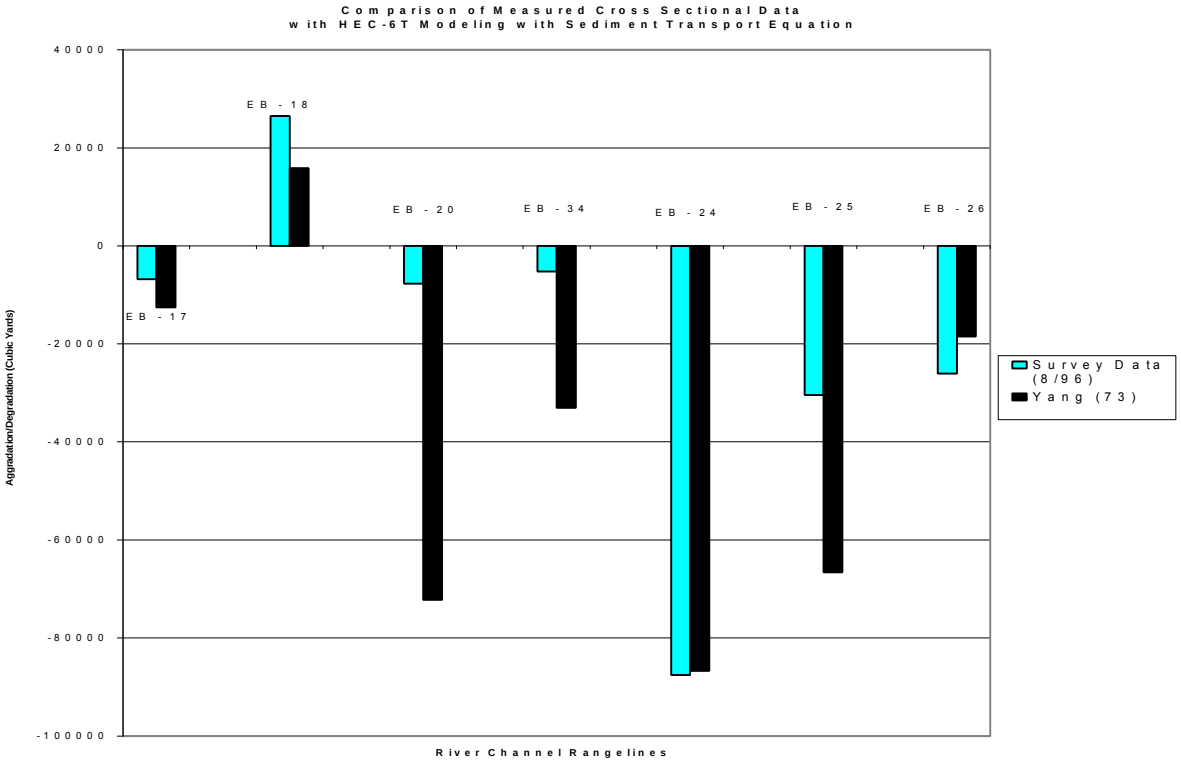

Figure 2 - Comparison of Volume Changes of Test Reach with Calibrated Simulation

Sensitivity Analysis: A sensitivity analysis was conducted for the following input parameters: 1) time-step duration, 2) sediment transport function, 3) sediment inflow rating function, 4) Manning's "n" for main channel, 5) reservoir sediment bed gradation.

Based on the sensitivity tests (Table 2), the approach of a smaller time step duration gives the best results. Also, based on the sensitivity testing, the author recommends the Yang (1973) equation for this case study. The Yang (1973) equation is applicable for predicting sediment transport under a varying range of conditions. Sensitivity analysis of the sediment inflow rating function, indicted that an increase of 20 percent, yielded a significant increase in the model's accuracy (Table 3). This RMS error translated to a 0.19-foot overall over estimate of reach degradation.

Sensitivity tests also found the model to be highly sensitive to the Manning's "n" roughness coefficient. A range of 0.017 to 0.020 would be the most appropriate for this case study reach. Sensitivity tests performed on the bed material size distribution were inconclusive.

CONCLUSIONS

A comprehensive evaluation and analysis of the sediment transport numerical model developed for this case study demonstrated that the model is applicable and useful for predicting channel bed response during a spring runoff event in a sand bed channel environment. The predictive estimates of channel bed degradation volumes compared well with the measured observations given the range of error associated with sediment transport prediction.

A 20 percent increase in the bed-material sediment inflow rating function increased the model's accuracy significantly. Further investigation is recommended to determine the influence of the sediment inflow rating function on the model's accuracy for the case study.

The procedure and model applied can be useful in the assessment of the upstream channel response to an increase in downstream energy slope. The increase in the energy slope may be as a result of a temporary dredge channel, a re-channelization project, or natural channel avulsion. It has been demonstrated that the model is usef in its assessment of the hydraulic and sediment transport physical processes occurring during an event. This model and procedure developed for the case study is efficient and can be incorporated into future prediction of channel bed response. The model removes the drudgery of performing numerous computations and allows refined focus on the mechanics of the fluvial sediment transport processes.

Table 2 - Sensitivity of Root Mean Square Errors and Discrepancy Ratios.
1) Daily Time Step Duration
2) Sediment Transport Functions
3) Sediment Inflow Rating Function
4) Manning's "n"
5) Reservoir Sediment Bed Material Gradation

Simulation	Root Mean Square Error of Measured and Computed Volumes for Test Reach	Discrepancy Ratio of Cumulative Measured and Computed Volumes for Test Reach*
Calibrated Simulation	32775	1.99
1) Daily Time Step Duration Sensitivity		
-Time Step Duration = 1.0 days	63486	0.34
-Time Step Duration = 0.5 days	32625	1.79
-Time Step Duration = 0.25 days	32898	1.80
2) Sediment Transport Function Sensitivity		
- Toffaleti (1969) Function	41076	0.30
- Laursen's (1958) Function	44892	1.33
3) Inflow Sediment Rating Curve Sensitivity		
- Increase of Inflow Rating Function by 25 Percent	29161	1.44
- Decrease of Inflow Rating Function by 25 Percent	47344	0.89
- Increase of Inflow Rating Function by 20 Percent	28742	1.27
4) Manning's "n" Value Sensitivity		
- Manning's "n" = 0.015 for Main Channel Bed	36281	2.17
- Manning's "n" = 0.020 for Main Channel Bed	35638	1.30
- Manning's "n" = 0.024 for Main Channel Bed	61347	-0.18
- Manning's "n" = 0.034 for Main Channel Bed	74757	-0.70
5) Reservoir Sediment Bed Material Gradation Sensitivity		
- Reach Comprised of Coarse Sands	35981	0.94
- Reach Comprised of Medium Sands	40237	2.38
- Reach Comprised of Fine Sands	42242	2.47
- Reach Comprised of Very Fine Sands	34493	0.57

* Negative sign denotes reach degradation

Table 3 - Simulation Error Evaluation with 20% Increase in Sediment Inflow Rating Function

Cross Section	Measured Change in Volume at Mobile Bed Section** (cy)	Simulated Change in Volume at Mobile Bed Section** (cy)	Difference Between Measured and Computed Values (cy)	Subreach Length (feet)	Error per Linear Foot (cy/ft)	Ratio of Subreach Length to Overall Test Reach Length	Weighted Error
EB - 17	-6826	-2886	-3940	2900	-1.36	0.09	-0.13
EB - 18	26495	37066	-10571	6800	-1.55	0.22	-0.34
EB - 20	-7739	-57232	49493	6540	7.57	0.21	1.61
EB - 34	-5211	-17273	12062	5260	2.29	0.17	0.39
EB - 24	-87580	-54647	-32933	4340	-7.59	0.14	-1.07
EB - 25	-30414	-63018	32604	3120	10.45	0.10	1.06
EB - 26	-26045	-16743	-9302	1720	-5.41	0.06	-0.30
Total				30680			1.22

Subreach Weighted ErrorFor Entire Reach 1.22 Cubic Yards Per Linear Foot of Channel

*Estimated Error for Bed Elevation for Entire Reach Per Foot of Channel 0.19 Feet per Linear Foot of Channel

* Assuming Average Channel Width of 170 feet

** Negative Sign Denotes Channel Degradation

REFERENCES

Colby, B.R. and Hembree, C.H., 1955. “Computation of Total Sediment Discharge, Niobrara River near Cody, Nebraska”, U.S. Department of Interior, Geological Survey Water Supply Paper No. 1357.

Snedcor, G.W. and Cochran, W.G., 1980, Statistical Methods, 7th Edition, Iowa State University Press.

Slater, R., and Baird, D.C., 1991. “ San Marcial Gauge Sediment Transport Analysis 1978-1989", United States Department of the Interior, Bureau of Reclamation, Albuquerque Projects Office, Albuquerque, New Mexico.

Thomas, W.A., 1996. Sedimentation in Stream Networks, HEC-6T User’s Manual, Mobile Boundary Hydraulics, Vicksburg, Mississippi.

Yang, C.T., 1973. “Incipient Motion and Sediment Transport”, Journal of the Hydraulics Division, ASCE, vol. 99, No. HY10, Proceeding Paper 10067, pp. 1679-1704.

Yang, C.T., 1996. “Sediment Transport Theory and Practice”, McGraw Hill Companies, Inc., New York, NY.

SEDIMENTATION ANALYSIS – PANOLA-QUITMAN FLOODWAY, MISSISSIPPI

By M. Trawle, ASCI Corporation, Mclean, VA; B. Arthur, Hydraulics Branch, US Army Engineer District, Vicksburg, MS; L. Banks, Hydraulics Branch, US Army Engineer District, Vicksburg, MS

Abstract: A one-dimensional sedimentation model of the Panola-Quitman Floodway (PQ), located in northwest Mississippi, has been developed to study the effect of the Upper Yazoo Project (UYP) on changes in sedimentation along the PQ and, consequently, changes in sediment delivery to the Tallahatchie River. The UYP is a flood control project consisting of channel enlargement on 179 miles of the Yazoo-Tallahatchie-Coldwater River system, which will lower flood stages about 3 to 5 feet at the mouth of the PQ. The PQ delivers water released from Sardis and Enid lakes and numerous unstable hill tributaries below the lakes to the Tallahatchie River. The model is also being used to evaluate the impact of proposed sediment control features located in the lower portion of the PQ.

The HEC-6T model was used to calculate sedimentation along the PQ as well as downstream sediment delivery to the Tallahatchie River. The modeled reach extends downstream from the confluence of the Yocona River with the PQ to the mouth of the PQ where it enters the Tallahatchie River, a distance of about 13 miles. The model includes a secondary channel loop that carries east overbank flow from the upper portion of the modeled reach of the PQ channel and returns it to the lower PQ channel.

Data required for model development and verification included channel and overbank cross sections, bed sediments, inflowing sediment concentrations, daily upstream discharges, and daily downstream stages. The period of record used for model verification was from 1962 to 1997. Sedimentation verification focused on comparing the computed and observed channel thalweg profile change over the period from 1962 to 1997.

The verified model was then applied to assess the impact of the UYP on the PQ sediment delivery to the Tallahatchie River. The hydrologic record was modified to reflect the lowered stages on the Tallahatchie River resulting from the UYP in place. The model was used to assist in the design of proposed sediment control features at the lower end of the PQ.

INTRODUCTION

Panola-Quitman Floodway History: During the 1920s local interests (PQ Drainage District) constructed a diversion channel about 25 miles in length to bypass the lower Little Tallahatchie River, where the stream bed was largely blocked by trees, debris, sand, and silt. The work performed by the Drainage District also included development of spoil banks along the channel which formed a floodway about one-half mile wide.

The PQ functioned satisfactorily until about 1935. At that time, the channel started filling with sand and silt at several locations. During the next few years, the channel was cleaned out several times at various points in an attempt to keep it open. However, large flood flows from the Little Tallahatchie and Yocona Rivers caused numerous crevasses in the locally constructed levee

system. The Sardis Dam on the Little Tallahatchie was completed in 1941, and the Enid dam on the Yocona River was completed in 1951.

The existing PQ levee on the west side was completed in the late 1960s. A smaller, locally maintained levee is in place along the east bank of the floodway channel from about mile 12 to about mile 5, protecting agricultural land adjacent to the floodway (USAED, Vicksburg 1965). Since originally constructed, the PQ channel has been remarkably stable in planform, with little bank erosion.

Hydrology: The PQ carries runoff from the Little Tallahatchie and Yocona Rivers. The floodway flows in a southern direction and enters the Tallahatchie River (Figure 1). The drainage area of Panola-Quitman Floodway is 2,600 square miles. Sardis Dam controls the flow from 1,545 square miles of the drainage area and Enid Dam controls the flow from 560 square miles.

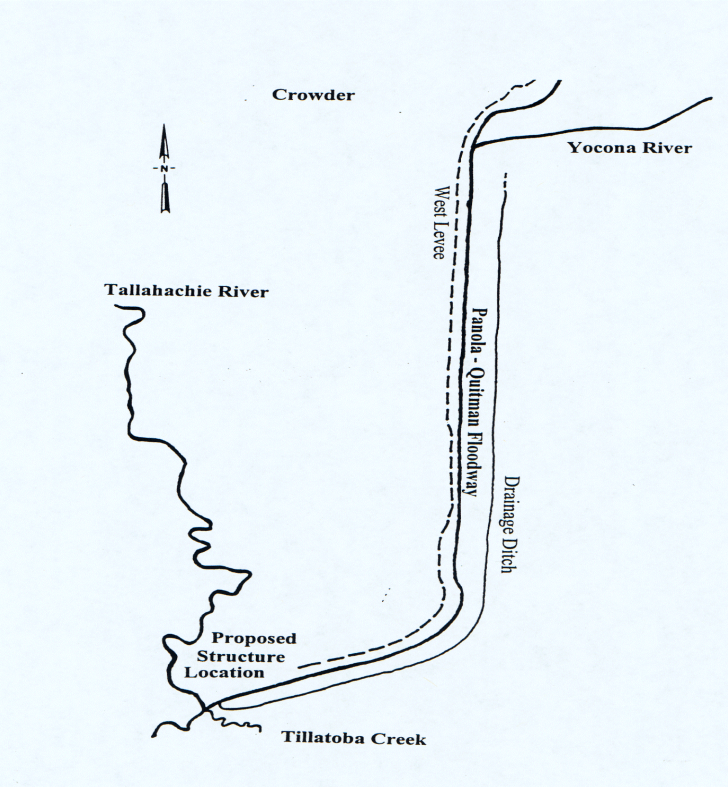

Figure 1. Location Map

Study Objective: Implementation of the UYP, which includes the Tallahatchie River, will result in lower water-surface levels at the mouth of the PQ. Lowered water-surface levels at the mouth of the PQ will have an effect on sedimentation within the lower portion of the floodway. The HEC-6T sedimentation model was used to calculate sedimentation along the lower 12 miles of the floodway as well as downstream sediment delivery to the Tallahatchie River. The modeled reach extended from just downstream of the confluence of the Yocona River to the mouth of the Floodway where it enters the Tallahatchie River. The hydrologic period of record for model simulations was from 1962 through 1996, a period of 35 years. The model was used

to assist in the design of proposed sediment control features at the lower end of the PQ with the UYP in place.

THE MODEL

Description: The HEC-6T version of the HEC-6 computer program was used to develop the numerical model for this study. The computer program was initially developed by Mr. William Thomas at the US Army Engineer District, Little Rock. Further development at the US Army Engineer Hydrologic Engineering Center (HEC) by Mr. Thomas produced the widely used HEC-6 generalized computer program for calculating scour and deposition in rivers and reservoirs (HEC, 1977). During the 1980s and early 1990s, modifications and enhancements were made to the basic program by Mr. Thomas at the US Army Engineer Waterways Experiment Station. More recently, further improvements have been made and new features added by Mr. Thomas at Mobile Boundary Hydraulics (Mobile Boundary Hydraulics, 1999) resulting in HEC-6T.

Model Geometry: The numerical model extends from just upstream of the confluence with the Tallahatchie River (Mile 0.04) to just downstream of the confluence of the floodway and the Yocona River (Mile 12.51). The model geometry used for the study was based on a survey conducted during September, 1997. The distance between survey cross-sections averaged about one mile. In addition to the surveyed cross-sections, the model included infill cross-sections that were simply repeats from the downstream adjacent surveyed cross-sections, thus reducing the cross-section spacing to about one-half mile.

The model includes a secondary channel loop that carries west overbank flow from the upper portion of the modeled reach of the floodway channel and returns it to the lower floodway channel. The model consists of four segments (Figure 2). A typical model cross section developed from the 1997 survey and located about 7 miles above the mouth is shown in Figure 3.

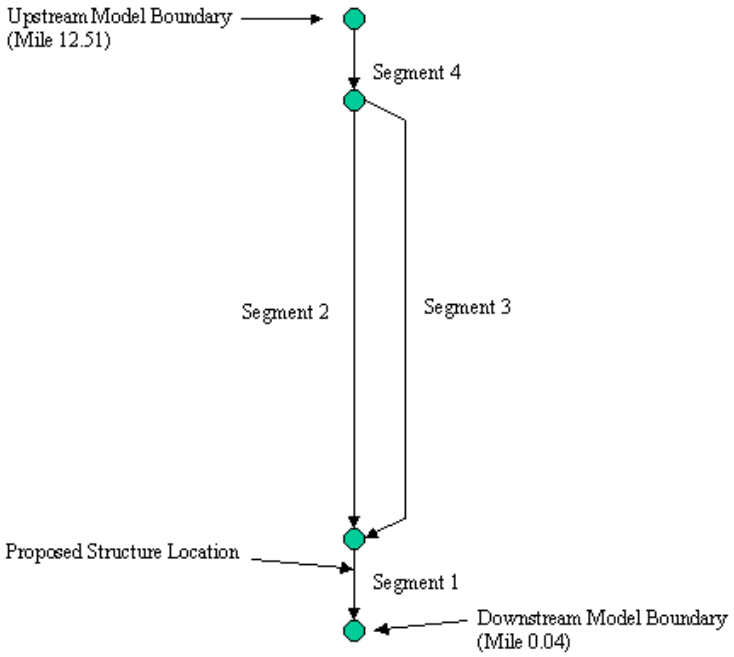

Figure 2. Schematic of model layout showing segments

Upstream Discharge Hydrograph: Discharge hydrographs are simulated in the model by a series of steady-state events. A hydrograph simulated by a series of steady-state events is called a histograph. The histograph used in the calibration study was based on combining historical data from two sources. The first source was a discharge range on the Little Tallahatchie River just above the PQ, which included discharges from the Sardis dam as well as tributaries drainage from below the dam. The second source was the Yocona River discharge, which was represented by the Enid dam discharge. These two discharges were combined to create the daily discharge applied to the model. The period of record used was from 1962 through 1996.

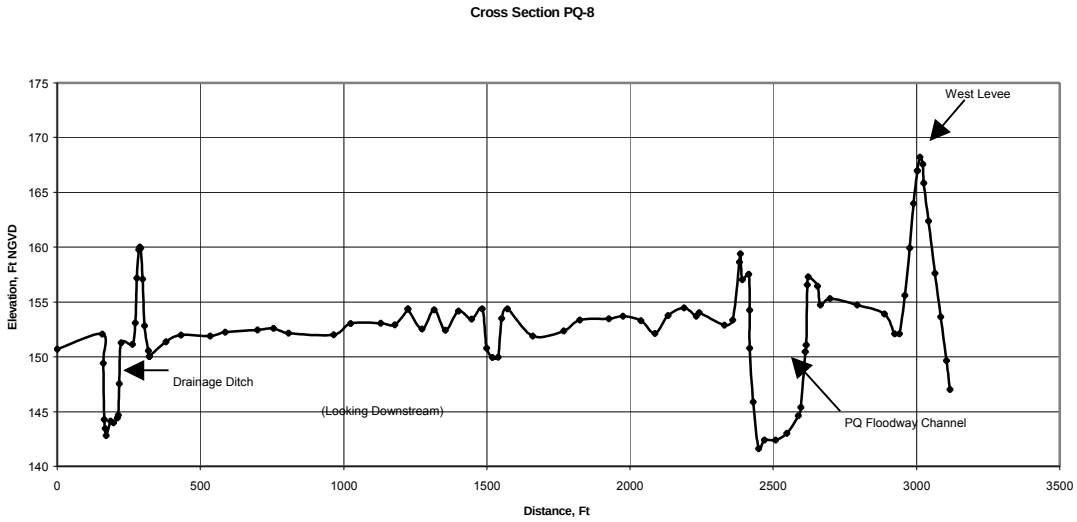

Figure 3. Cross section PQ-8, located about 7 miles above the mouth of the PQ

Downstream Water-Surface Elevation: Since there is no gage located at the mouth of the PQ, a downstream water-surface elevation for the existing condition had to be interpolated using nearby gages. With the UYP in place, water surface elevations at the Mouth of the PQ were lowered by 3 to 5 feet.

Bed Material: The bed material gradation for the numerical model was based on samples taken in October and December 1999. The bed gradation plot for a bed sample collected about 6 miles above the mouth of the PQ is shown in Figure 4.

Channel Roughness: Hydraulic roughness is influenced by grain size, bed form, water depth, bank roughness, changes in channel shape, and changes in flow direction or concentration due to bends and confluences. In the one-dimensional numerical model these effects are accounted for by the Manning's roughness coefficient. Based on model calibration for this study, the PQ channel was assigned a manning's n value of .035 and the secondary channel was assigned a value of .038. The overbank areas had n values ranging from 0.10 to 0.15.

Sediment Inflow: Inflowing sediment data for the PQ are extremely limited. These limited data are inadequate for developing sediment rating curves. During sediment calibration, suspended sediment rating curves by sand grain size were developed by trial and error. Without sufficient measured data to develop rating curves, this approach was required. The primary sediment sources to the PQ are the numerous unstable hill tributaries below the Sardis and Enid lakes.

Transport Function: Based on the transport function selection guidance provided from the Hydraulic Design Package for Channels (USAE-ERDC, 1999) and model testing, the Toffaleti transport function was selected for use in this study (Toffaleti, 1966).

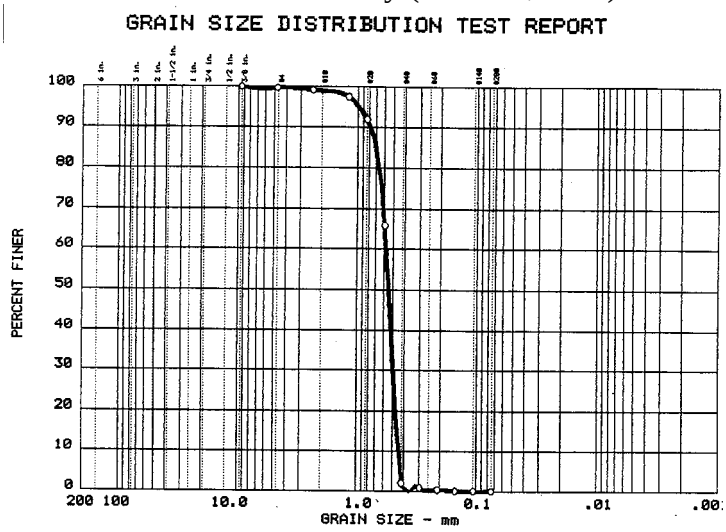

Figure 4. Bed material gradation curve at mile 6.14

MODEL CALIBRATION

Aggradation Calibration: Available channel geometry data consisted of the 1962 thalweg profile (USAED, Vicksburg 1965) and the 1997 hydrographic survey. The model was constructed using the 1997 hydrographic survey. By adjusting the channel depths in the model to match the 1962 thalweg profile as the initial bed condition, and by using the hydrologic record available from 1962 to 1997, channel sedimentation (aggradation) over that period was simulated. The overall comparison between model and prototype is shown in Figure 5.

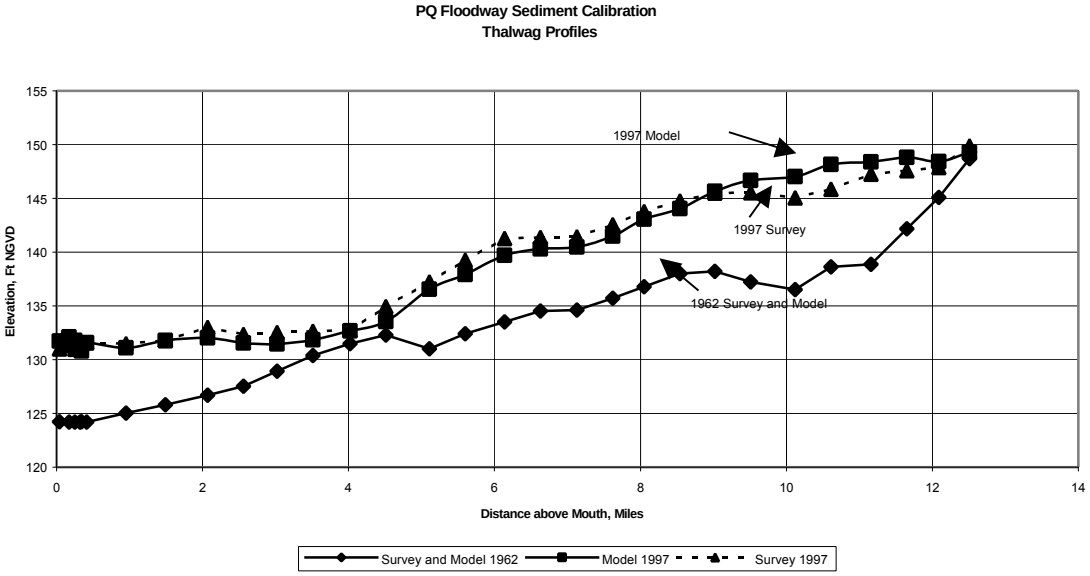

Figure 5. Comparison of model and prototype thalweg profiles

SEDIMENTATION RESULTS

Future without UYP: Thalwag profiles for the Future-without-UYP condition after 35-year simulation is shown in Figures 6. As can be seen, over the 35-year period, the bed is stable except the upper reach, which indicates 2 to 4 feet of aggradation.

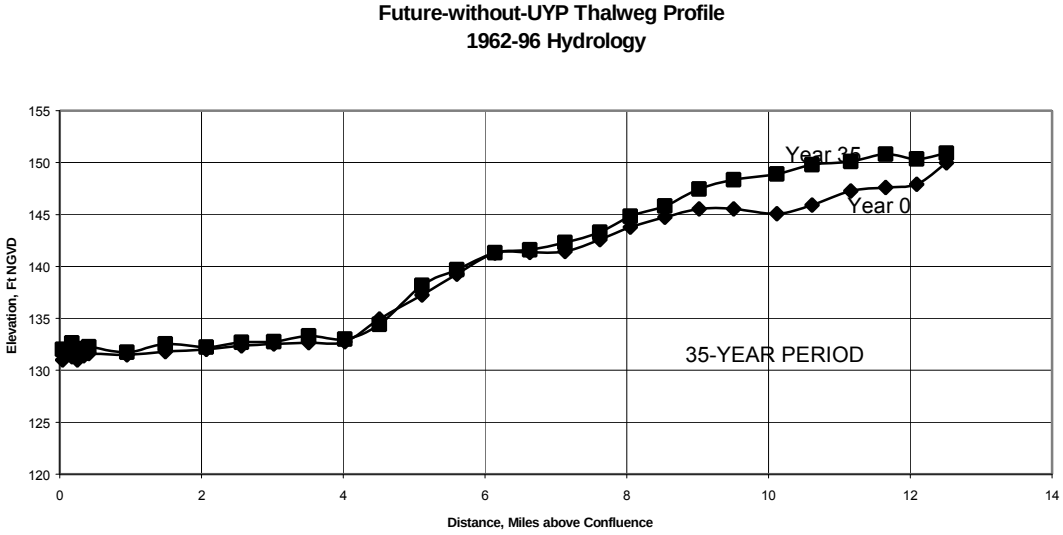

Figure 6. Future-without-UYP thalweg profile after 35-year simulation

Future with UYP Only: The **t**halweg profile for the Future-with-UYP-Only condition after 35 years is shown in Figure 7. As shown, the channel was degraded from the mouth to about mile 9, with maximum degradation of about 5 feet occurring at the lower end.

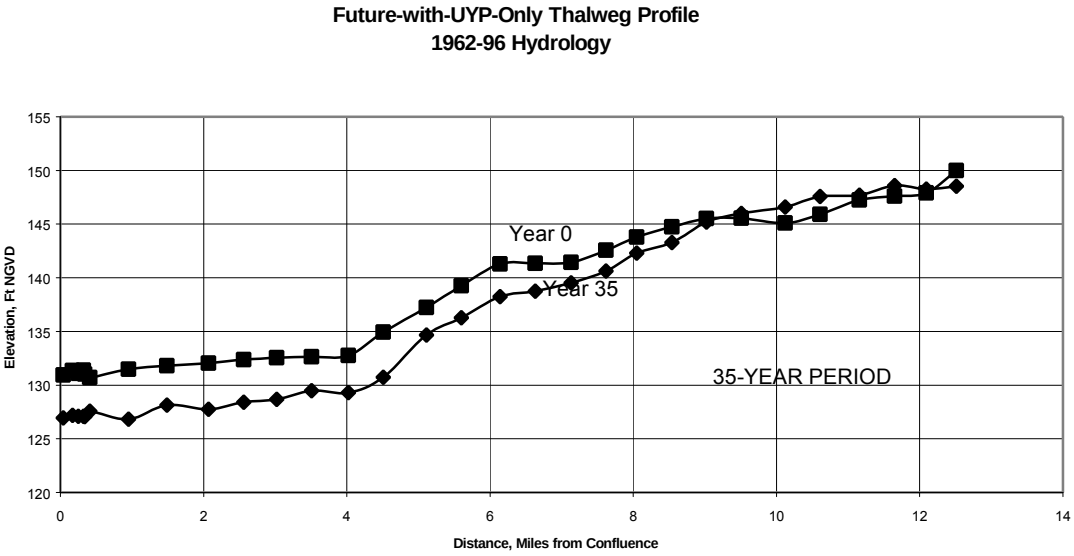

Figure 7. Future-with-UYP-Only thalweg profile after 35-year simulation

Future-with-UYP-and-PQ-Sediment Control: The **t**halweg profile for the Future-with-UYP-and-PQ-Sediment-Condrol condition after 35 years is shown in Figure 8. As can be seen, the bed aggraded about 3 feet downstream of the structure, degraded slightly from the structure to about mile 7, and aggraded 2 to 3 feet from about mile 7 to mile 12.

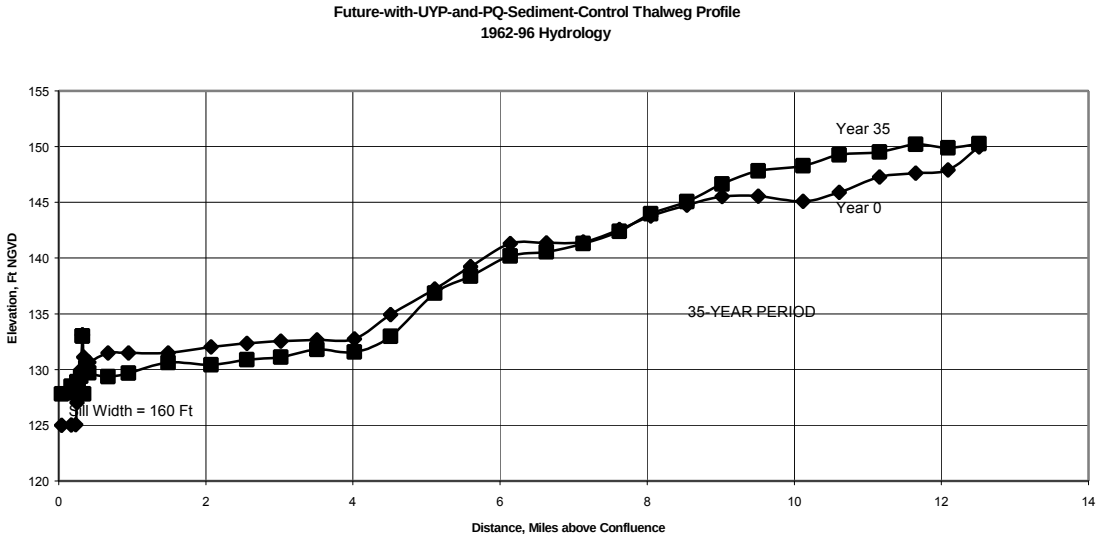

Figure 8. Future-with-UYP-and-PQ-Sediment-Control thalweg profile after 35-year simulation

Sediment Storage and Delivery: The model consisted of four segments, as previously shown in Figure 2. Segment 4 represents the most upstream reach and Segment 1 is the downstream reach of the model. Accumulated sediment storage, as well as accumulated sediment inflow and outflow, in each segment after 35 years for each scenario are tabulated as follow:

	Accumulated Sediment Inflow Million Cu Yds	Accumulated Sediment Outflow Million Cu Yds	Accumulated Sediment Storage Million Cu Yds
Segment 1 (Downstream)			
Without UYP	21.8	21.7	0.1
With UYP Only	24.4	24.4	0.0
With UYP and PQ Sediment Control	22.8	22.8	0.0
Segment 2			
Without UYP	22.8	21.7	1.1
With UYP Only	23.6	24.3	-0.7
With UYP and PQ Sediment Control	22.8	22.7	0.1
Segment 3			
Without UYP	0.8	0.0	0.8
With UYP Only	1.0	0.1	0.9
With UYP and PQ Sediment Control	0.5	0.0	0.5

	Accumulated Sediment Inflow Million Cu Yds	Accumulated Sediment Outflow Million Cu Yds	Accumulated Sediment Storage Million Cu Yds
Segment 4 (Upstream)			
Without UYP	25.0	23.6	1.4
With UYP Only	25.0	24.1	0.9
With UYP and PQ Sediment Control	25.0	23.8	1.2

SUMMARY

Conclusions: Under the Future-without-UYP condition, over the 35-year period, the channel bed is stable for the lower 7 miles, slightly aggradational from mile 7 to 9 (+1 ft), and aggradational from mile 9 to 12 (+2 to +4 ft).

The Future-with-UYP-Only condition results in significant channel degradation over the lower 9 miles of the floodway, with a maximum of -5ft over the lower 4 miles of the floodway. Such channel degradation will most likely cause future bank instability and failure. Above mile 9, the channel is slightly aggradational (+1 ft) over the 35-yr period.

The Future-with-UYP-and-PQ-Sediment-Control will result in a slightly degraded channel bed (-1 ft) upstream of the structure over the lower 7 miles of the floodway channel. This slight degradation above the structure is the result of an increased water slope with UYP in place. At higher discharges, the structure is submerged, allowing the steeper water slope to transport more sediment. From mile 7 to 9, the channel is stable. From mile 9 and above, the channel is aggradational (+2 to +4 ft).

Sediment delivery to the Tallahatchie River for the Future-without-UYP condition totaled about 21.7 million cubic yards over the 35-yr period. For the Future-with-UYP-Only condition, sediment delivery increased to about 24.4 million cubic yards. For the Future-with-UYP-and-PQ-Sediment-Control condition, sediment delivery totaled about 22.8 million cubic yards.

REFERENCES

Hydrologic Engineering Center, 1977, User's Manual—HEC-6 Scour and Deposition in Rivers and Reservoirs.

Mobile Boundary Hydraulics, 1999, Sedimentation in Stream Networks (HEC-6T), User's Manual.

Toffaleti, F. B., 1966, "A Procedure for Computation of Total River Sand Discharge and Detailed Distribution, Bed to Surface", Committee on Channel Stabilization, US Army Corps of Engineers, Washington DC.

US Army Engineer District, Vicksburg, 1965, "General Design Memorandum, Panola-Quitman Floodway Levees, Design Memorandum No. 1".

USAE-ERDC, 1999, "Hydraulic Design Package for Channels (SAM)", Draft Report.

SAND TRANSPORT AND BED EVOLUTION MODELING APPLICATIONS IN THE COLORADO RIVER, GRAND CANYON

Stephen M. Wiele, Hydrologist, and Margaret A. Franseen, Geologist,
US Geological Survey, Denver, CO

INTRODUCTION

The closure of Glen Canyon Dam in 1963 shut off the mainstem sand supply and altered the natural flows in the Colorado River through the Grand Canyon. The effect of these alterations to the natural river has been the subject of ongoing research, including studies of the changes in sand supplies and sedimentary processes, with an emphasis on the erosion and restoration of sand bars. One component of these studies has been the development and application of unsteady flow models (Wiele and Smith, 1996; Wiele and Griffin, 1997), 1-dimensional sand transport models (Randle and Pemberton, 1987; Bennett, 1993), and multi-dimensional models of flow, sand transport, local erosion and deposition (Wiele and others, 1996; Wiele, 1997; Wiele and others, 1999; Wiele and Franseen, 1999). This paper is a brief overview of the multi-dimensional model and outlines modeling applications to date.

BACKGROUND

Prior to the closure of Glen Canyon Dam (Fig. 1), approximately 57 million metric tons of sediment, 40% sand, was delivered to the Grand Canyon in the mainstem annually (Topping and others, 2000a). Two main tributaries continue to supply sand. The Paria River, located about 24 km downstream from the dam, delivers about 3 million metric tons of sediment annually, 50% sand (Topping and others, 2000a), and the Little Colorado River, located about 120 km below the dam, supplies about 8.6 million metric tones of sediment annually, 30 to 40% sand (Topping and others, 2000a). Ungaged tributaries deliver about 0.70 million metric tons of sediment, 75% sand, between the dam and the Little Colorado River confluence (Webb and others, 2000). Peak discharges, which typically exceeded 2800 m^3/s during spring flows prior to the dam, currently rarely exceed the 900 m^3/s maximum that can used for power generation at the dam.

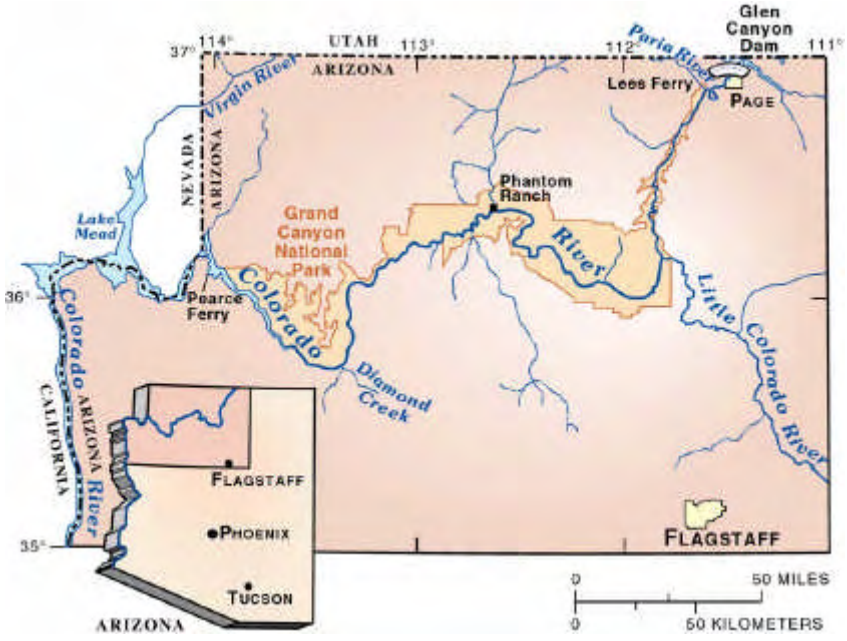

Figure 1. Map of the Colorado River below Glen Canyon Dam.

Maintenance and restoration of sand deposits has focused on distributing the sediment supplied by tributaries to near-shore sites by releasing high discharges in excess of power-plant capacity (Bureau of Reclamation, 1994). Optimum use of tributary-supplied sediment would require high flows to coincide with or shortly follow tributary activity (BOR, 1994). Timing releases with Little Colorado River flows was recommended by Lucchita and Leopold (1999). Careful analysis of suspended sediment measurements and the implications for sand transport processes by Topping and others (2000b) led to their recommendation that high releases instead be triggered by Paria River flows. They concluded that this would produce maximum deposition in the critical Marble Canyon reach, which is upstream from the confluence with the Little Colorado River and has a relatively small sand supply.

A controlled release from the dam in 1996 of 1270 m^3/s for 6 days, although not closely following major tributary activity, rejuvenated many of the near-bank sand bars, especially below the confluence with the Little Colorado River (see Schmidt, 1999, for a summary of monitoring and research results). This release demonstrated that judicious high releases from Glen Canyon Dam can be effective in mitigating some of the deleterious effects of the dam on the downstream river corridor. The model described below is designed to provide a predictive capability of the effects of sand supply and dam operation on sand deposits.

OVERVIEW OF THE MODEL

The multi-dimensional model is an extension of a model initially developed to study bank erosion and bar formation and stability in gravel-bed rivers (Wiele, 1992). For Grand Canyon applications, suspended-sand transport was added. The flow field is calculated with the vertically averaged momentum and continuity equations for open channel flow. A 3-dimensional advection-diffusion equation that governs the suspended sand field is solved using a parabolic eddy viscosity related to the local shear velocity to quantify the turbulent mixing. A sand concentration near the bed (Smith and McLean, 1977; Wiberg and Rubin, 1985) is used for the lower boundary condition. The sand fall velocity is calculated using the method of Dietrich (1982). The vertical variation in velocity is estimated using a logarithmic velocity profile consistent with the parabolic eddy viscosity. The product of the velocity and suspended sand concentration is integrated vertically to calculate the local suspended sand discharge. The sand transported as bedload is calculated using a bedload function (Meyer-Peter and Mueller, 1948) including the effect of local bed slope on transport rates (Nelson and Smith, 1989). In areas with sufficient sand thickness, local roughness and skin friction are calculated using the method of Bennett (1995) that relates bedform dimensions to flow conditions and sand size. In areas with little or no sand, local channel roughness is calculated as a function of the spatial variability in the bathymetric measurements that form the basis for the gridded channel topography. Local change in bed elevation is then calculated for a small time step with a sediment continuity equation. More detailed descriptions of the model can be found in Wiele and others (1996, 1999).

The bathymetry used to generate the gridded topography in the model was measured by the U.S. Geological Survey (USGS) and the Grand Canyon Monitoring and Research Center. Sand flux into the reaches was taken from measurements (Konieczki and others, 1997) or rating curves for specific events (G.G. Fisk, USGS, personal communication, 1994), or from a model that predicts sand flux as a function of discharge for specified sand supplies (Topping, 1997).

MODEL APPLICATIONS

The model has been used to examine processes during a tributary flood, compare the effects of natural and dam-generated high flows on sand deposits, predict the effects of variations in water discharge and sand supply on deposition rates and magnitude, and examine the effect of channel shape on locations of deposition and scour and changes in deposit volume. Applications to other disciplines include predictions of sand bar response in reaches containing archeological artifacts (Wiele and Franseen, 1999) in which preservation has been linked to the size and persistence of sand bar deposits (Hereford and others, 1993; Thompson and Potochnik, 2000). The flow component has been used to examine the effect of discharge on endangered fish habitat.

A comparison of natural and artificial events and the effect of sand concentration on sand deposition was examined by Wiele and others (1999) by comparing the results of a flood on the Little Colorado River (LCR) in 1993 and the 1996 controlled release from Glen Canyon Dam. The LCR flood transported about 4 million metric tons of sand into the main channel and increased the mainstem water discharge to a peak of about 950 m^3/s. Massive sand deposits

were observed after the LCR flood receded, especially in the 20 km below the confluence. The USGS measured 3 to 5 channel cross sections in 4 reaches ranging from 1/4 to about 1 km in length before and after the LCR flows. The reaches are typically bounded upstream and downstream by riffles or rapids that are formed by debris flows that partially constrict the channel. Recirculation zones form in the lee of the debris fans and can act as effective sand traps. Sand input into the mainstem estimated from gage records (G.G. Fisk, USGS, personal communication, 1993) was used to set the upstream sand boundary-condition for the reaches.

In the reach known colloquially as the Salt reach (Fig. 2a), about 129 km below the dam, model predictions agree well with the measured cross sections (Wiele and others, 1996). Both the model and the measured cross sections show deposition in the main channel, filling a deep hole scoured into the bedrock downstream from the reach inlet, as well as extensive deposition within the recirculation zone during the LCR flood (Fig. 2b). This result contrasts sharply with the deposition pattern during the 1996 controlled release (Fig. 2c) during which sand concentrations were much lower than during the LCR flood and the water discharge was higher. During the 1996 controlled release, which had a discharge of 1270 m^3/s, the main channel was scoured. Deposition in the recirculation zone was focused at the reattachment point. Sand was carried in suspension into the recirculation zone and initially deposited rapidly. Once the initial accommodation space (defined by Hazel and others, 1999, as the underwater volume of potential deposition sites) was filled, the model shows that further deposition could proceed only at the rate at which sand was redistributed within the recirculation zone as bedload. Model predictions are compared to bathymetric measurements during the 1996 controlled release (Andrews and others, 1999). The model accurately predicts the general deposition and scour patterns recorded by the bathymetric measurements (Wiele and others, 1999). A disparity exists, however, downstream from the main channel scour zone where deposition was documented by the bathymetric measurements in a high-stress zone. This discrepancy is likely a result of the transport and deposition of coarser material than is represented in the model.

In reaches in which deposition is dominated by recirculation zones, model predictions of sand deposition as a function of water discharge and sand supply follow a consistent pattern. A reach designated the Palisades reach (Fig. 3) by Hereford and others (1991, 1993), at 134 km below the dam, was modeled with 2 discharges, 1270 and 2800 m^3/s, and with 3 different sand supplies (Topping, 1997). The sand conditions represent sand supplies during historically high measurements (high); during the 1996 controlled release, which is representative of the post-dam conditions (intermediate); and a relatively depleted state resulting from prolonged high discharges approaching 2800 m^3/s after the closure of the dam (low). At the highest flows modeled, 2800 m^3/s, with the lowest sand supply, modeled deposit volume exceeds the volume deposited predicted at lower discharges even with the highest sand supply (Fig. 4) . This result demonstrates the importance of the magnitude of the accommodation space in determining deposit volume and the effect of the hydraulic isolation from the main channel on the accumulation of sand in the recirculation zones.

Recirculation zones have tended to be the focus of sediment research due to the effectiveness with which they retain sand. While reaches dominated by recirculation zone show a consistent pattern, other reaches can show considerable variability in response to discharge and sand supply. The reach designated the Above Lava-Chuar (ALC) reach (Fig. 5a), about 133 km below the dam, contains a relatively constrained recirculation zone, but also has a gradual expansion with a sand deposit just downstream from the reach inlet. At 1270 m^3/s and the intermediate sand supply, this bar is partially eroded (Fig. 5b), but at 2800 m^3/s with the intermediate sand supply, the bar is scoured out (Fig. 5c). This modeling result is consistent with the conclusions of Melis (1997) that the slope of the channel side at constrictions plays an important role in determining whether scour or deposition occur in the lee of the constrictions. Increased scour at the higher discharge for a given sand supply is opposite to the response in recirculation zones. Overall, the response of sand deposits in reaches such as the ALC reach is likely to be far outweighed by deposition in recirculation zones, but the response is of particular interest in some reaches, such as those containing archeological artifacts.

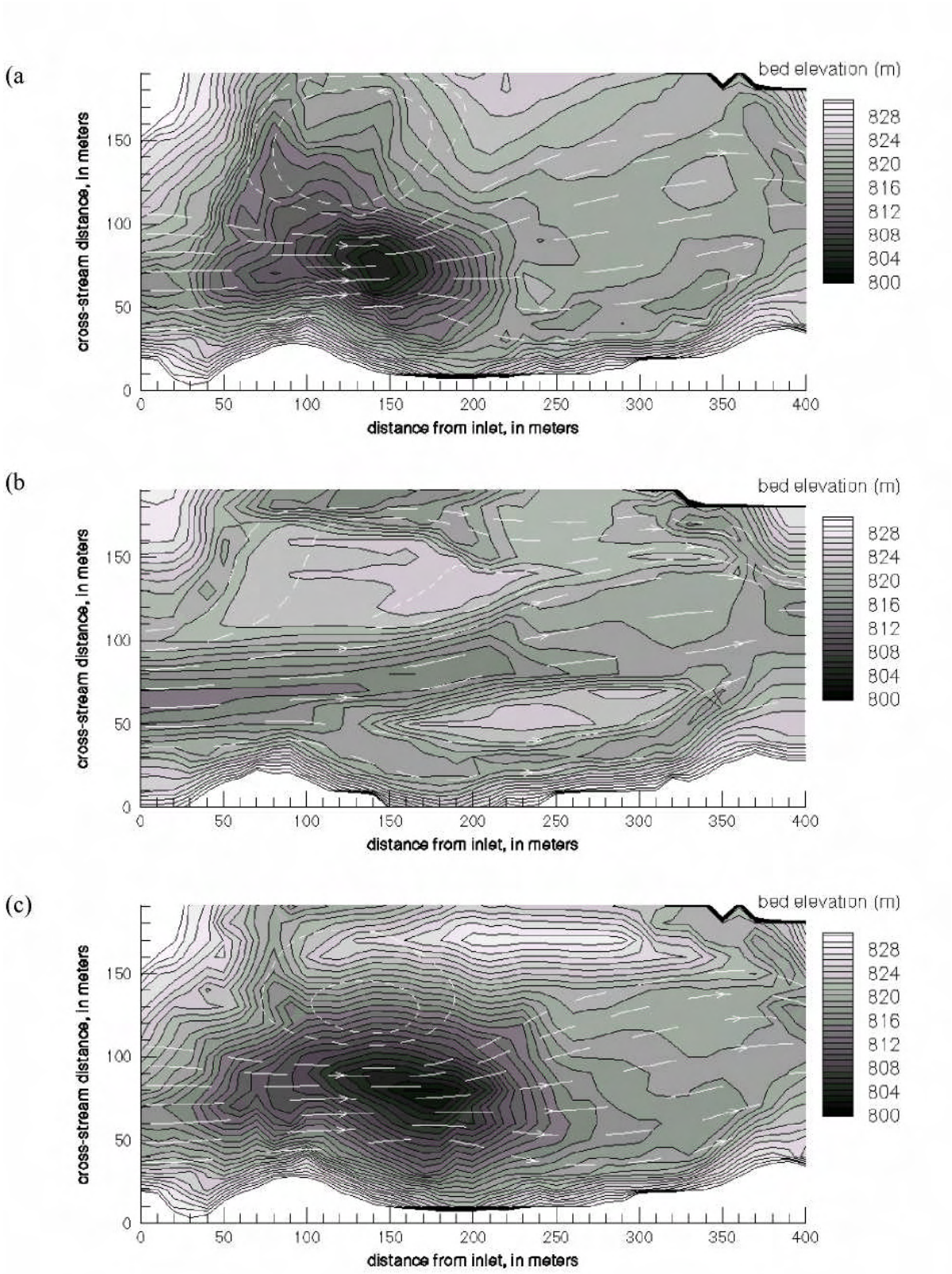

Figure 2. Contour map of the Salt reach showing (a) the initial bathymetry prior to the 1993 LCR flood, (b) the calculated bathymetry during the LCR flood after 72 hours, and (c) the calculated bathymetry during the 1996 controlled release after 72 hours. Flow is from left to right. Contour interval is 1m. The dashed lines are calculated stream lines. Each dash shows the distance traveled in 30 seconds.

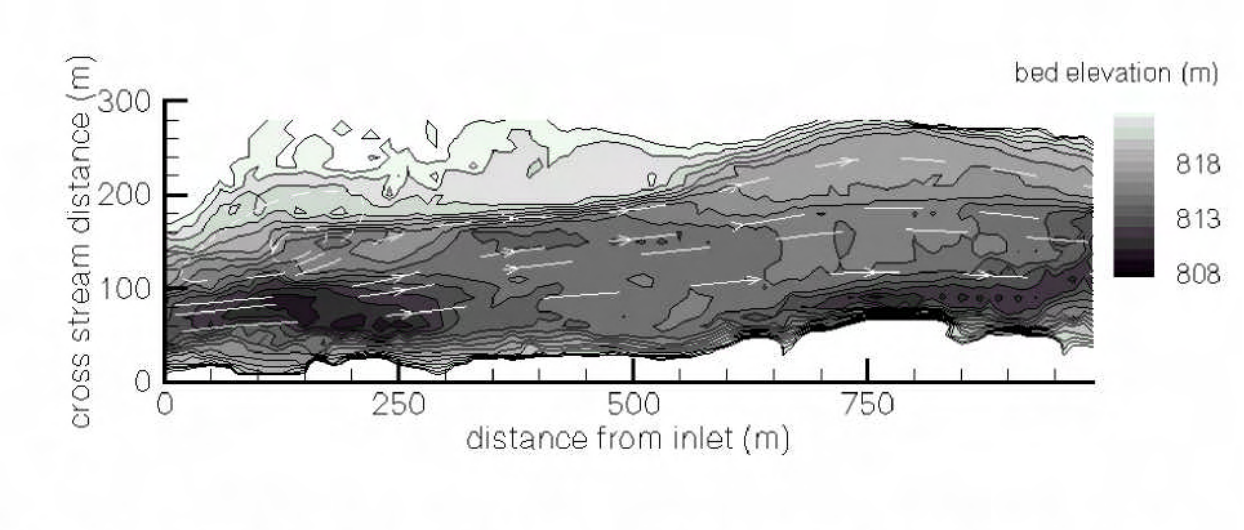

Figure 3. Contour map of the Palisades reach showing the initial bathymetry. Flow is from left to right. Contour interval is 1 m. The dashed lines are calculated stream lines. Each dash shows the distance traveled in 30 seconds.

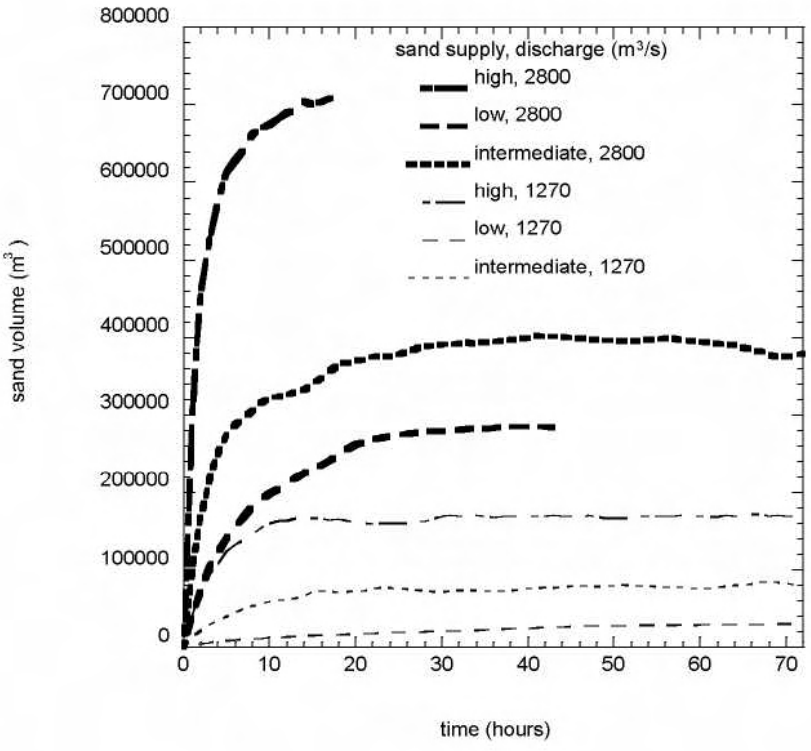

Figure 4. Graph showing modeled sand deposition volumes in the Palisades reach for two discharges and three sand supplies.

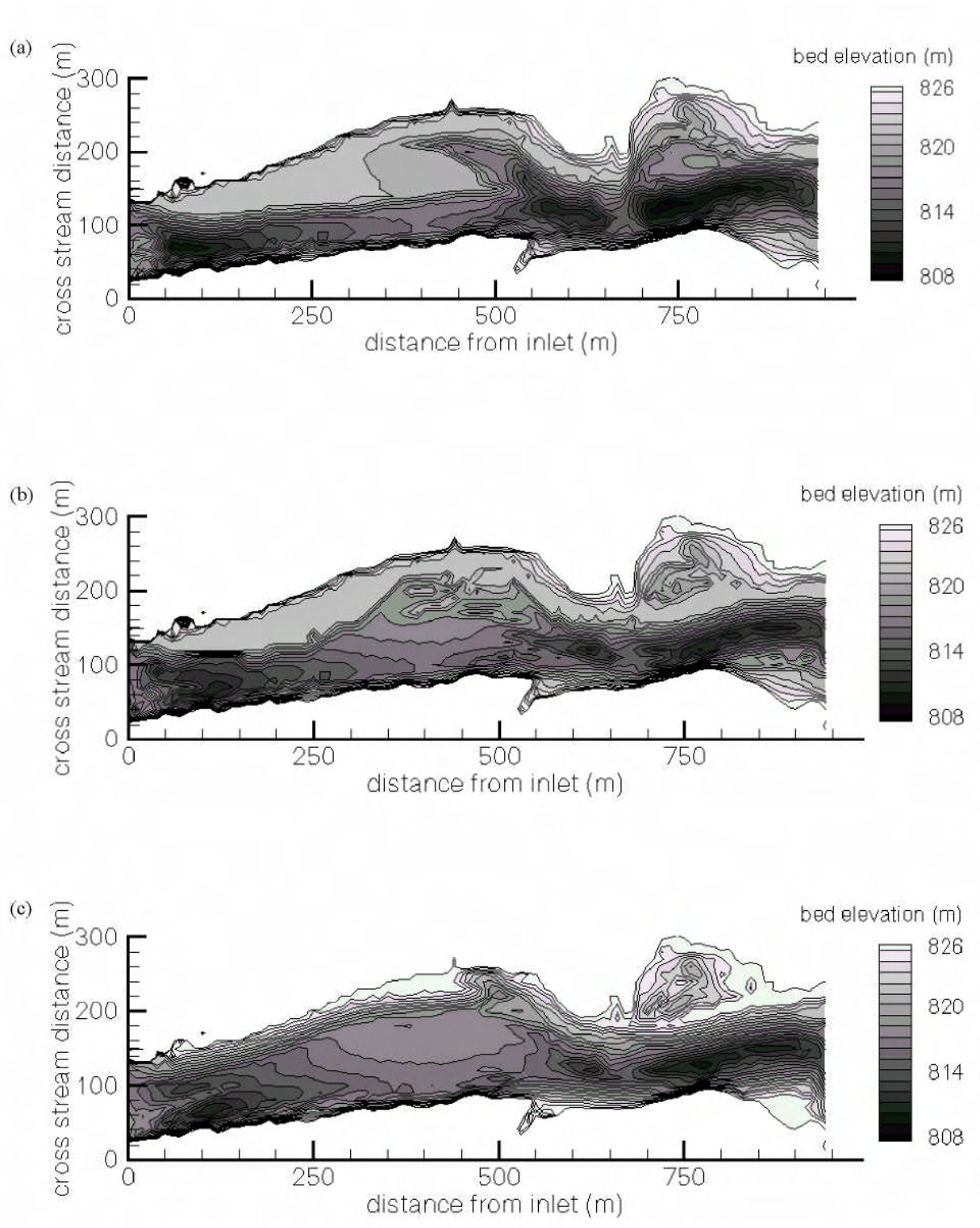

Figure 5. Contour map of the above Lava-Chuar reach showing (a) the initial bathymetry, (b) the calculated bathymetry at 1270 m^3/s with intermediate sand supply after 72 hours, and (c) the calculated bathymetry at 2800 m^3/s with the intermediate sand supply after 22 hours. Flow is from left to right. Contour interval is 1 m.

REFERENCES

Andrews, E.D., Johnston, C.E., Schmidt, J.C. and Gonzales, M., 1999, Topographic evolution of sand bars, in Webb, R.H., Schmidt, J.C., Marzolf, G.R., and Valdez, R.A. (eds.), The Controlled Flood in Grand Canyon: Washington, D.C., American Geophysical Union, Geophysical Monograph 110.

Bennett, J.P., 1993, Sediment transport simulations for two reaches of the Colorado River, Grand Canyon, Arizona, Water Resources Investigations Report 93-4034, U.S. Geological Survey.

Bennett, J. P., 1995, Algorithm for resistance to flow and transport in sand-bed channels, J. Hydr. Engrg., ASCE, 121(8), 578-590.

Bureau of Reclamation, 1994, Operation of Glen Canyon Dam: Colorado River Storage Project, Arizona, Final Environmental Impact Statement, December, 337 p.

Dietrich, W.E., 1982, Settling velocity of natural particles, Water Resources Research, vol.18, no.6, pp.1615-1626.

Hazel, J.E., Kaplinski, M., Parnell, R.A., Manone, M.F., and Dale, A.R., 1999, Topographic and bathymetric changes at thirty-three long-term study sites, in Webb, R.H., Schmidt, J.C., Marzolf, G.R., and Valdez, R.A. (eds.), The Controlled Flood in Grand Canyon: Washington, D.C., American Geophysical Union, Geophysical Monograph 110.

Hereford, R., Fairley, H.C., Thompson, K.S., and Balsom, J.R., 1993, Surficial geology, geomorphology, and erosion of archeological sites along the Colorado River, eastern Grand Canyon, Grand Canyon National Park, Arizona, U.S. Geological Survey Open-File Report 93-517, 46 p.

Konieczki, S.D., Graf, J.B., and Carpenter, M.C., 1997, Stage, streamflow, and sediment transport data collected to determine the effects of a controlled flood in March and April 1996 on the Colorado River between Glen Canyon Dam and Diamond Creek, Arizona: U.S. Geological Survey Open-File Report 97-224.

Lucchitta, I. and Leopold, L.B., 1999, Floods and sandbars in the Grand Canyon, GSA Today, v. 9, n. 4, 1-7.

Melis, T.S., 1997, Geomorphology of debris flows and alluvial fans in Grand Canyon National Park and their influence on the Colorado River below Glen Canyon Dam, Arizona, Ph.D. dissertation, University of Arizona, Tucson.

Meyer-Peter, E. and Mueller, R., 1948, Formulas for bed-load transport, Intern. Assoc. Hydr. Res., Second Meeting, Stockholm.

Nelson, J.M. and Smith, J.D., 1989, Evolution and stability of erodible channel beds, In: Ikeda, S. and Parker, G. (eds.), River Meandering.

Randle, T.J., and Pemberton, E.L., 1987, Results and analysis of STARS modeling efforts of the Colorado River in Grand Canyon: Glen Canyon Environmental Studies Report, 41 p. plus 95 figures and 26 tables.

Schmidt, J.C., 1999, Summary and synthesis of geomorphic studies conducted during the 1996 controlled flood in Grand Canyon, in Webb, R.H., Schmidt, J.C., Marzolf, G.R., and Valdez, R.A. (eds.), The Controlled Flood in Grand Canyon: Washington, D.C., American Geophysical Union, Geophysical Monograph 110.

Smith, J.D. and McLean, S.R., 1977, Spatially averaged flow over a wavy surface, J. Geophys. Res., 84(12), pp. 1735-1746.

Thompson, K. and Potochnik, A., 2000, Development of a geomorphic model to predict erosion of pre-dam Colorado River terraces containing archaeological resources, prepared for Grand Canyon Monitoring and Research Center, Flagstaff, Arizona.

Topping, D., 1997, Flow, sediment transport, and channel geomorphic adjustment in the Grand Canyon, Arizona gage reach of the Colorado River during the Grand Canyon flood experiment: Abstracts and executive summaries, Symposium on the 1996 Glen Canyon Dam Beach/Habitat-Building Flow, Flagstaff, Arizona.

Topping, D.J., Rubin, D.M., Vierra, Jr., L.E., 2000a, Colorado river sediment transport, 1, Natural sediment supply limitation and the influence of Glen Canyon Dam, Water Resources Research, v. 36, n. 2, 515-542.

Topping D. J., Rubin, D.M., Nelson, J.M., Kinzel III, P.J., and Corson, I.C., 2000b, Colorado river sediment transport, 2, Systematic bed-elevation and grain-size effects of sand supply limitation, Water Resources research, v. 36, n. 2, 543-570.

Webb, R.H., Griffiths, P.G., Melis, T.S., and Hartley, D.R., 2000, Sediment delivery by ungaged tributaries of the Colorado River in Grand Canyon: U.S. Geological Survey Water-Resources Investigations Report 00-4055, 67p.

Wiberg, P.L. and Rubin, D.M., 1985, Bed roughness produced by saltating sediment, J. Geophys. Res., 94, C4, 5011-5016.

Wiele, S.M., and Smith, J.D., 1996, A reach-averaged model of diurnal discharge wave propagation down the Colorado River through the Grand Canyon: Water Resources Research, v. 32, p. 1375-1386.

Wiele, S.M., 1992, A computational investigation of bank erosion and mid-channel bar formation in gravel-bed rivers. Unpublished Ph.D. dissertation, University of Minnesota, Minneapolis.

Wiele, S.M., Graf, J.B., and Smith, J.D., 1996, Sand deposition in the Colorado River in the Grand Canyon from flooding of the Little Colorado River: Water Resources Research, v. 32, p. 3579-3596.

Wiele, S. M., and Griffin, E.R., 1997, Modifications to a one-dimensional model of unsteady flow in the Colorado River through the Grand Canyon, Arizona, U.S. Geological Survey Water-Resources Investigation Report 97-4046.

Wiele, S.M., 1997, Modeling of flood-deposited sand distributions for a reach of the Colorado River below the Little Colorado River, Grand Canyon, Arizona, U.S. Geological Survey Water-Resources Investigation Report 97-4168.

Wiele, S.M., Andrews, E.D., and Griffin, E.R., 1999, The effect of sand concentration on depositional rate, magnitude, and location, in Webb, R.H., Schmidt, J.C., Marzolf, G.R., and Valdez, R.A. (eds.), The Controlled Flood in Grand Canyon: Washington, D.C., American Geophysical Union, Geophysical Monograph 110.

Wiele, S.M., and Franseen, M.A., 1999, Modeling of mainstem flow and sediment dynamics at selected cultural resource locations, interim report to the Grand Canyon Monitoring and Research Center.

EVALUATING SELECTED SCOUR EQUATIONS FOR BRIDGE PIERS IN COARSE STREAMBEDS IN NEW YORK

By L. J. Welch Jr., Graduate Assistant, U.S. Geological Survey, Troy, New York; G.K. Butch, Hydrologist, U.S. Geological Survey, Troy, New York

Abstract: The U.S. Geological Survey analyzed cross-section data from 29 bridge sites in New York and developed a best-fit, linear-regression equation to estimate the depth of scour that would result at a bridge pier from a single peak flow in coarse streambeds. The equation is based on 61 field measurements that are associated with specific peak discharges and includes a stream-force factor and a bed-material grain-size factor. The equation and three other equations – the Federal Highway Administration (FHWA) equation, the Mueller-modified FHWA equation, and the Froehlich equation were applied to 116 field measurements made during 1943-96 for comparison. The difference between estimated scour and measured scour ranged from -0.8 meters to 0.5 meters for the best-fit equation, from 0.9 meters to 6.0 meters for the FHWA equation, from 0.1 meters to 2.9 meters for the Mueller-modified FHWA equation, and from -0.2 meters to 2.3 meters for the Froehlich equation.

INTRODUCTION

Many equations have been developed to estimate scour depth at bridge piers. Because most equations were developed for sand-bed channels, they overestimate scour depth in New York streams, which typically are armored with gravel, cobbles, and (or) boulders. Failure of these equations to account for this armor layer produces results that rarely agree with field measurements.

In 1988, the U.S. Geological Survey (USGS), in cooperation with the New York State Department of Transportation, analyzed 116 cross-section measurements made during 1943-96 at 29 selected bridge sites in New York (Butch 1993a). The criteria for site selection and methods of data collection are described in Butch (1991). Streambed cross sections were measured before, during, or after high flows. The depth of a scour hole was defined as the difference between the ambient streambed elevation and the minimum elevation in the scour hole. Ambient streambed elevations were calculated from the 116 cross-section measurements through a simple computer program to eliminate bias (Butch 1996). Hydraulic values for factors such as water depth and flow velocity were calculated from a step-backwater model calibrated to water-surface elevations and discharges measured by the USGS (Butch 1993b).

A best-fit, linear-regression equation was developed to estimate the depth of scour that would result at a bridge pier from a single peak flow in coarse streambeds. The equation and three other equations -- the Federal Highway Administration (FHWA) equation (Richardson and Davis 1995), the Mueller-modified FHWA equation (Mueller 1996), and the Froehlich regression equation (Froehlich 1988) were applied to 116 field measurements made during 1943-96 for comparison. This report describes the methods that were used to develop the New York scour equation and compares scour depths estimated from the New York equation with scour depths obtained by the other three equations.

DATABASE

The New York database (referred to herein as the "total New York database") consists of 116 (55 historical and 61 discrete) scour measurements made during 1943-96 at 29 bridge sites across the State. Statistics for the total New York database, the historical data set, and the discrete data set are given in Table 1; accuracy of scour-depth measurements is about 0.1 m. The 55 historical scour measurements (Table 1) were derived from cross-section data collected during 1943-89; the measured scour depths are assumed to be the result of the maximum peak flow from bridge construction. The 61 discrete scour measurements (Table 1) represent data collected during 1972-96; the measured scour depths are associated with a specific peak discharge. This association is considered valid because the time between cross-section measurements was generally less than 1 year, and most field observations and measurements in the project confirmed that scour holes had not become back filled (Butch 1994).

All bridge piers represented in the database are aligned with the direction of flow. Scour depths that were affected by ice or debris were omitted from the analysis. Many measurements in the total New York database represent the deepening of previous scour holes, but neither the effects of previous scour holes nor the length of time during which a discharge exceeded a given hydraulic condition (such as mean velocity or water depth) were analyzed, although the length of time may affect the scour process (Butch and Lumia 1994).

The total New York database includes 27 zero-scour measurements. Only the highest discharge was included for bridge piers at which multiple high flows resulted in zero scour. Inclusion of zero-scour measurements in the database decreased a bias of the equation to estimate scour for every flow. Zero-scour measurements correspond to peak flows in which hydraulic conditions did not produce scour, even though some peak flows had recurrence intervals exceeding 100 years. Additional field data are needed to define the onset of the scour process.

Table 1. Statistics on eight variables that affect scour at bridge piers in New York. [D_{xx}, grain diameter that exceeds *xx* percent of armor layer].

Variable	Min.	Max.	Std. dev.	Mean	Median
A. Total database (116 measurements, 29 bridges, 1943-96)					
Flow velocity at pier (m/s)	0.2	4.6	0.9	2.6	2.7
Water depth at pier (m)	1.4	9.7	1.8	4.1	3.8
Discharge (m^3/s)	59	6,600	1,380	1,290	816
Pier width (m)	0.9	3.0	0.5	1.6	1.5
D_{50} armor layer (mm)	22	68	10	37	34
D_{84} armor layer (mm)	38	134	21	75	72
Scour depth (m)	0.0	1.9	0.4	0.3	0.2
Stream force ($kg \cdot m/s^2$)	46	154,000	32,300	35,000	26,400
B. Historical data (55 measurements, 23 bridges, 1943-89, scour depth assumed to be a result of maximum flow from bridge construction)					
Flow velocity at pier (m/s)	0.2	4.6	1.0	2.5	2.4
Water depth at pier (m)	1.4	7.7	1.3	3.6	3.7
Discharge (m^3/s)	114	6,600	982	1,080	818
Pier width (m)	0.9	3.0	0.5	1.6	1.5
D_{50} armor layer (mm)	22	68	11	39	38
D_{84} armor layer (mm)	38	134	22	80	76
Scour depth (m)	0.0	1.0	0.3	0.4	0.3
Stream force ($kg \cdot m/s^2$)	51	154,000	29,700	29,000	19,400
C. Discrete data (61 measurements, 20 bridges, 1972-96, scour depth associated with a specific peak discharge)					
Flow velocity at pier (m/s)	0.2	4.2	0.8	2.7	2.7
Water depth at pier (m)	1.4	9.7	2.0	4.6	4.4
Discharge (m^3/s)	59	5,350	1,640	1,480	637
Pier width (m)	0.9	3.0	0.6	1.6	1.7
D_{50} armor layer (mm)	27	57	8.0	35	33
D_{84} armor layer (mm)	53	127	19	71	66
Scour depth (m)	0.0	1.9	0.4	0.3	0.2
Stream force ($kg \cdot m/s^2$)	46	147,000	33,700	40,400	31,700

Scour Equations: Scour is the result of work—the movement of bed material from one location to another. The force for this work is provided by flowing water that is redirected and accelerated as it flows around a pier. The equation developed in this study relates the magnitude of stream force directly upstream of a pier to the scour depth. Stream force is calculated from the water depth and flow velocity directly upstream from a pier and a flowwidth of 1 meter:

$$Sf = r y_1 w V_0^2, \quad (1)$$

where Sf = stream force ($kg \cdot m/s^2$);
r = density of water (assumed 1,000 kg/m^3);
y_1 = water depth directly upstream from pier (m);
w = flow width (1 m); and
V_0 = approach flow velocity directly upstream from pier (m/s).

The equation expresses estimated scour as a function of the ratio of stream force near the pier to grain size:

$$scour = f\left(\frac{Sf}{D_{84}}\right), \tag{2}$$

where Sf = stream force ($kg \cdot m/s^2$); and
D_{84} = grain size exceeding that of 84 percent of the armor layer (mm).

Including D_{84} as part of the stream-force regression term provided a better correlation with local scour than D_{50}, D_{90}, or D_{95} grain sizes and was also less sensitive to sampling error than D_{90} or D_{95}. The D_{84} grain size represented the armor layer at the surface of the streambed. The armor layer is assumed to be present throughout the reach over which the bridge was constructed and the grain-size distribution is assumed to represent the gradation of the armor layer.

Pier width and pier shape did not correlate well with scour depth within the limited range of bridge geometry of this study (Butch 1993b) and therefore were not included in the regression analysis. About 90 percent of the total-database values are derived from piers ranging from 0.9 to 2.1 m in width; 71 percent of the total database represents round-nosed piers, 26 percent represents sharp-nosed piers, and 3 percent represents square-nosed piers. Using a pier-width factor to calculate stream force rather than the 1-m flow width gave no significant improvement in scour estimates.

Regression Analysis: The initial linear regression analysis used all data collected during 1943-95 (97 measurements). The equation for the best-fit line, herein called the 1995a equation, was:

$$scour\ (m) = 0.09 + \left[6.01 \times 10^{-4} \times \frac{Sf}{D_{84}}\right]. \tag{3}$$

The 1995a equation was then used to calculate scour corresponding to 19 scour measurements made in 1996. The mean error (estimated value minus measured value) was 0.3 m. One explanation for the positive mean error (overestimation) could be the greater percentage of zero-scour values in the 1996 data set — 53 percent (10 of the 19 measurements) were zero, compared to 18 percent (17 of the 97 values) for 1943-95. The mean error decreased to 0.1 m when the estimates were compared with the measurements made at the nine cross sections where scour was greater than zero. The reason for the large number of zero-scour measurements in 1996 is unknown; the recurrence intervals of the peak flows ranged from 2 years to greater than 100 years.

An alternative explanation for the positive mean error between the 1995a equation estimates and the 1996 measured scour values could be that the assumption that historical scour depths (Table 1) resulted from a single peak flow may be incorrect. The effect of the historical scour data was evaluated through a second regression equation, herein called the 1995b equation (eq. 4), which was developed only from discrete scour-data collected during 1943-95 (42 values).

$$scour\ (m) = -0.03 + \left[6.44 \times 10^{-4} \times \frac{Sf}{D_{84}}\right]. \tag{4}$$

Applying the 1995b equation to the 1996 data resulted in a mean error of 0.2 m for all 19 measurements and 0.0 m for scour measurements greater than zero. These improved results indicate that the historical scour data, which could be affected by multiple high flows, ice, or debris, affected the accuracy of the equation estimates for 1996.

The final linear regression equation, herein called the New York equation (eq. 5), is based on 61 discrete scour measurements (1972-96) that include 18 zero-scour values (Table 1). Applying this equation to the 1943-96 data gave a standard error of 0.3 m and an R^2 of 0.66.

The New York equation is:

$$scour\ (m) = -0.07 + \left[6.21 \times 10^{-4} \times \frac{Sf}{D_{84}} \right] . \quad (5)$$

The regression line for the New York equation is shown in figure 1. Regression residuals were well distributed, although they indicate a tendency to overestimate measured scour at, or near, zero. The user needs to consider the standard error of equation 5 (0.3 m) when evaluating scour estimates because the −0.07 intercept can result in slightly negative scour values (aggradation). The intercept is not set equal to zero because several regression statistics (such as R^2 and t-ratio) lose their usual meaning when the intercept term is removed from the equation (Helsel and Hirsch 1992).

A sensitivity analysis of the New York scour equation indicated that the variable to which the equation is most sensitive is flow velocity (the squared term in the stream-force factor). The percent change in estimated scour when one variable is varied (water depth, D_{84}, or flow velocity) while the others are held constant at their median values is plotted in figure 2. The equation also is sensitive to grain size (D_{84}) at values less than −20 percent of the median (about the minimum D_{84} in the discrete database). The sensitivity to water depth was nearly linear— a 50-percent change in water depth resulted in about a 70-percent change in estimated scour depth.

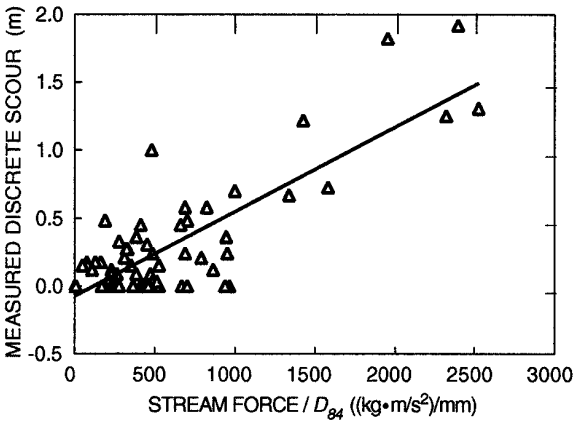

Figure 1. Measured discrete scour as a function of stream force / D_{84} for New York regression equation.

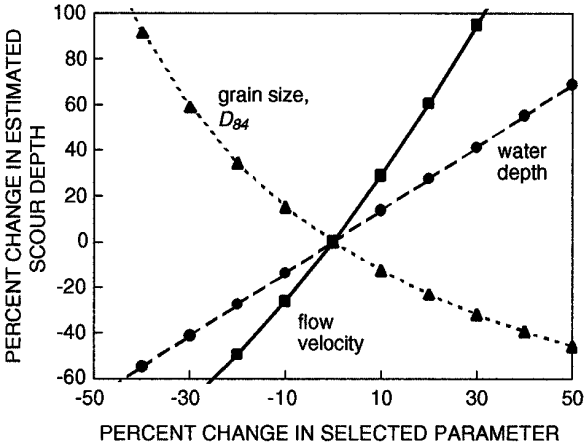

Figure 2. Change in estimated scour depth as a function of change in water depth, flow velocity, and grain size.

COMPARISON OF EQUATION RESULTS

The New York scour equation and three other scour equations were applied to the total New York database through 1943-96 for comparison. These were the FHWA equation, the Mueller-modified FHWA equation, and the Froehlich equation. The total New York database was selected, rather than the discrete database from which the New York equation was derived, because the other equations are intended to estimate maximum scour. Using the total New York database also would test the New York equation when applied to other data, which include scour depths possibly resulting from multiple high flows, ice, or debris.

The FHWA equation, used by many State Departments of Transportation (Richardson and Davis 1995) is:

$$y_s = 2.0 \cdot a \cdot K_1 \cdot K_2 \cdot K_3 \cdot K_4 \left[\frac{y_1}{a} \right]^{0.35} \cdot Fr_1^{0.43} , \quad (6)$$

where y_s = scour depth;
a = pier width (m);
y_1 = water depth directly upstream from pier (m);
Fr_1 = Froude number directly upstream from pier;
K_1 = correction factor for pier-nose shape;

K_2 = correction factor based on ratio of pier length to pier width and the alignment of flow to pier;
K_3 = correction factor for streambed condition; and
K_4 = correction factor for armoring by bed-material size.

The K_4 coefficient was added in 1995 to reduce scour estimates for streambeds containing large bed material. The K_4 coefficient is applied when the median grain size, D_{50}, of the armor layer is ≥ 60 mm. The K_4 coefficient ranges from 0.7 to 1.0 and is calculated from equations from HEC-18 (Richardson and Davis 1995). The D_{50} of the armor layer at the bridge sites evaluated in this study ranges from 22 mm to 68 mm; only one site (4 measurements) had a $D_{50} \geq 60$ mm. Results of the FHWA equation as applied to the total New York database are given in Table 2. Two sets of values are listed in Table 2 for this equation: (1) K_4 for sites where $D_{50} \geq 60$ mm (4 measurements, mean K_4 = 0.997), and (2) K_4 applied to all 116 measurements (no grain-size restriction, mean K_4 = 0.898). The resulting FHWA scour values (K_4 based on $D_{50} \geq 60$ mm) are plotted as a function of measured scour (mean error 2.8 m) in figure 3A. Calculating K_4 for all measurements (no grain-size restriction) reduced the mean error to 2.6 m (figure 3B).

Table 2. Statistics for scour equations applied to total New York database (116 measurements). [All values in meters. FHWA, Federal Highway Admin.]

Statistic	Equation				
	FHWA[1]	FHWA[2]	Mueller	Froehlich	New York
Error (estimated value minus measured value)					
Max.	6.0	6.0	2.9	2.3	0.5
Min.	0.9	0.6	0.1	-0.2	-0.8
Median	2.6	2.4	1.1	0.7	-0.1
Mean	2.8	2.6	1.2	0.8	-0.1
Std. dev.	1.0	1.1	0.6	0.4	0.3
Scour estimate					
Max.	7.0	7.0	3.5	2.7	1.5
Min.	0.9	0.6	0.8	0.4	-0.1
Median	3.0	2.7	1.4	1.1	0.2
Mean	3.1	2.9	1.5	1.1	0.2
Std. dev.	1.1	1.2	0.6	0.4	0.3

[1] K_4 calculated for measurements where $D_{50} \geq 60$ mm (4 measurements)
[2] K_4 calculated for all measurements

Mueller (1996) proposed an alternative K_4 coefficient for the FHWA equation. If $D_{50} < 2$ mm, or if $D_{95} < 20$ mm, then K_4=1; if $D_{50} \geq 2$ mm and if $D_{95} \geq 20$ mm and if:

$$\frac{V_0 - V'_{cD_{50}}}{V_{cD_{50}} - V'_{cD_{95}}} > 0 \ , \tag{7}$$

then

$$K_4 = 0.4\left(\frac{V_0 - V'_{cD_{50}}}{V_{cD_{50}} - V'_{cD_{95}}}\right)^{0.15} \ , \tag{8}$$

otherwise $K_4 = 1$;

where D_{50} = median grain size of the armor layer;
D_{95} = grain size exceeding that of 95 percent of the armor layer;
V_0 = approach-flow velocity just upstream from pier;
$V'_{cD_{50}}$ = approach velocity corresponding to critical velocity and incipient scour in accelerated flow region at pier for grain size D_{50};

$V'_{cD_{95}}$ = approach velocity corresponding to critical velocity and incipient scour for grain size D_{95}; and

$V_{cD_{50}}$ = critical velocity for incipient motion for grain size D_{50}.

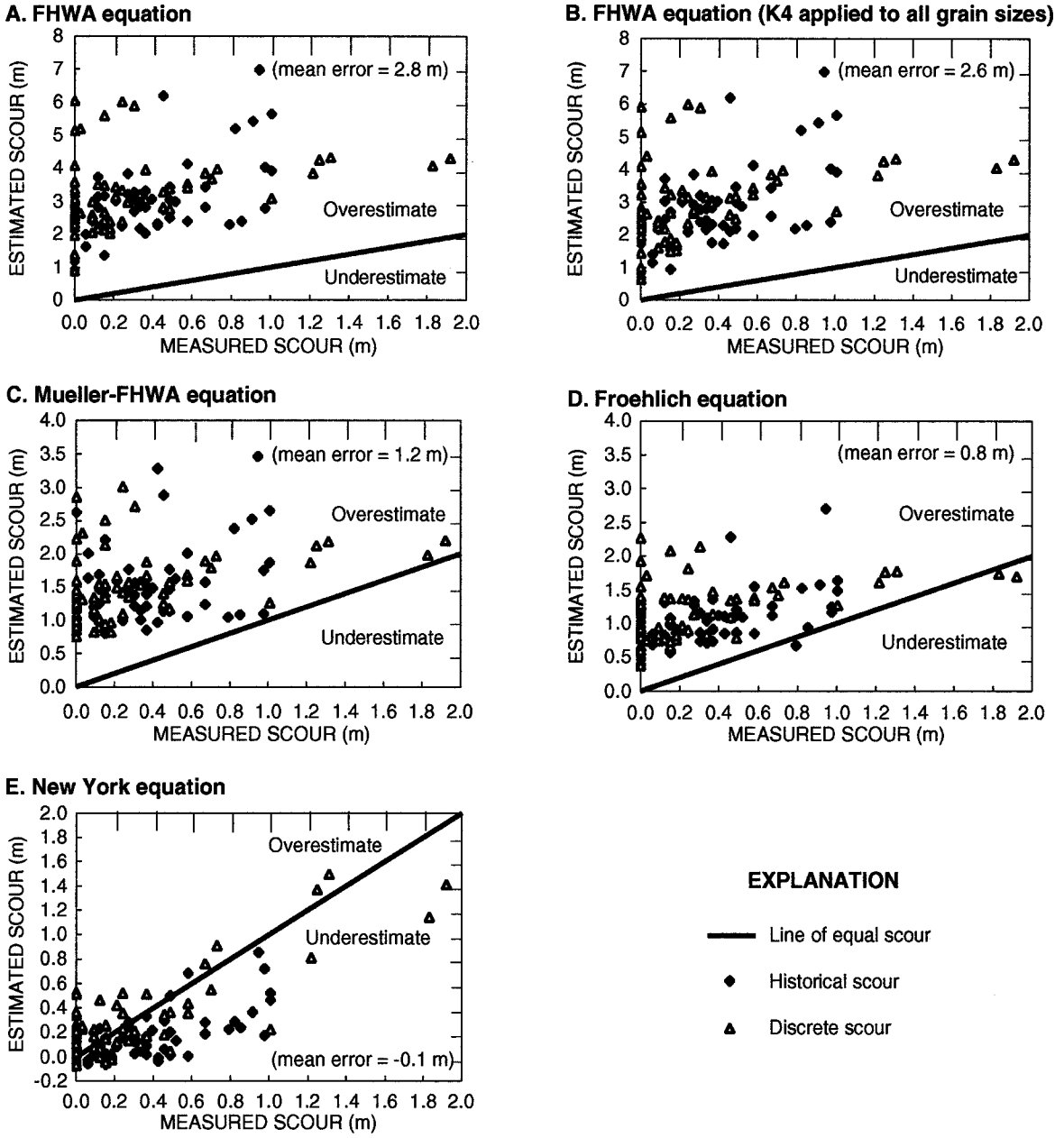

Figure 3. Scour estimated from the following equations in relation to 116 measurements: A. FHWA (Federal Highway Administration) equation. B. FHWA equation (K4 applied to all grain sizes). C. Mueller-modified FHWA equation. D. Froehlich equation. E. New York equation.

The Mueller-K_4 coefficient ranged from 0.27 to 1.0 in the total New York database, and had a mean value of 0.508. The estimated values from the Mueller-modified FHWA equation are plotted as a function of the measured scour values (1943-96) in figure 3C. As indicated in Table 2, the Mueller equation overestimated the measured scour (mean error 1.2 m) but gave lower values than the FHWA equation. The Mueller equation also did not underestimate scour for any measurement in the total New York database.

The Froehlich scour equation is a linear regression equation developed from field measurements (Froehlich 1988). For piers aligned with the flow, the Froehlich equation is:

$$y_s = 0.32\ f\, g^{-0.1} V_0^{0.2} y_0^{0.36} b^{0.62} D_{50}^{-0.08}, \qquad (9)$$

where f = coefficient for pier-nose shape (0.7 for sharp nose, 1.0 for round nose, and 1.3 for square nose);
g = gravitational constant;
V_0 = approach velocity just upstream from pier;
y_0 = water depth just upstream from pier;
b = pier width; and
D_{50} = median grain size of bed material.

As a regression equation, the Froehlich equation would be expected to overestimate scour for half of the database from which it was developed and to have a mean error of 0.0 m. When applied to the total New York database, the equation gave a mean error of 0.8 m and overestimated 113 of the 116 New York scour measurements. A plot of the Froehlich scour estimates as a function of measured scour is given in figure 3D.

The New York scour equation underestimated 74 (64 percent) of the 116 scour measurements and gave a mean error of -0.1 m (Table 2). The negative error is a result of the historical data in the total database (the mean error for historical data only was -0.2 m). The New York equation would not be reliable for streams whose variables exceed the range of values from which the equation was derived. A plot of the New York equation scour estimates in relation to the measured values is given in figure 3E, and statistics on the New York equation's results are included in Table 2. The slightly negative scour estimates shown in Figure 3E are a result of the equation's negative intercept (eq. 5).

The range and distribution of values resulting from the four scour equations are depicted as box plots in Figure 4. Scour estimates from each equation and measured scour are plotted in figure 4A, and the error for each equation (estimated value minus measured scour) is plotted in figure 4B.

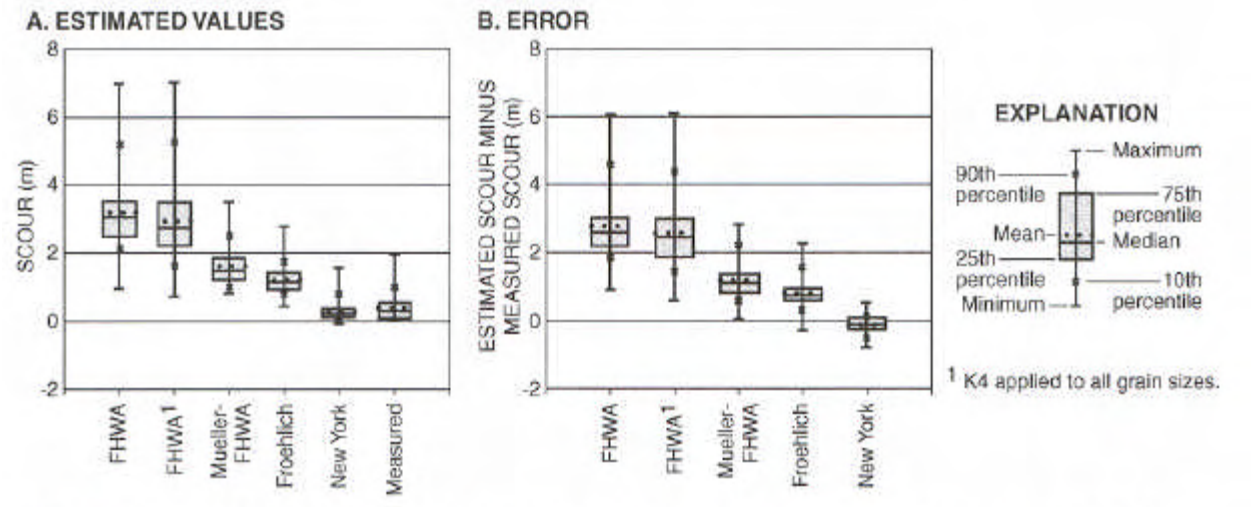

Figure 4. Range and distribution of scour-depth values obtained from selected equations applied to total New York database (1943-96, 116 measurements): A. Estimated and measured values. B. Equation error.

SUMMARY AND CONCLUSIONS

The New York scour equation is a linear regression equation based on 61 field measurements made at selected bridge piers in New York streams during 1972-96. The equation was developed from measurements associated with specific peak discharges in coarse streambeds. The scour-depth estimate is proportional to the magnitude of stream force near a pier and inversely proportional to grain size.

The New York equation and three others — the FHWA equation, the Mueller-modified FHWA equation, and the Froehlich equation — were applied to the 116 measurements in the total New York database (1943-96). The total database consisted of 61 field measurements that are associated with specific peak discharges and 55 historical scour measurements that could be affected by multiple flows, ice, or debris. Results from the New York scour equation ranged from an underestimate of -0.8 m to an overestimate of 0.5 m (mean error -0.1 m).

The FHWA equation's K_4 coefficient, as modified by Mueller, reduced most FHWA scour estimates; whereas the unmodified K_4 coefficient reduced only 4 of the 116 scour estimates (where $D_{50} \geq 60$ mm). The FHWA and the Mueller equations did not underestimate scour for any measurement in the database. The FHWA equation overestimated scour by 0.9 to 6.0 m (mean error 2.8 m). Removing the grain-size restriction from the K_4 coefficient in the FHWA equation reduced the mean error to 2.6 m. The Mueller-modified FHWA equation overestimated scour by 0.1 to 2.9 m (mean error 1.2 m). The Froehlich equation results ranged from an underestimate of -0.2 m, to an overestimate of 2.3 m (mean error 0.8 m).

REFERENCES

Butch, G.K. (1991). "Measurement of bridge scour at selected sites in New York, excluding Long Island." Water Resources Investigations Report 91-4083, U.S. Geological Survey, 17 p.

Butch, G.K. (1993a). "Estimating bridge scour in New York from historical U.S. Geological Survey streamflow measurements." ASCE Hydraulic Engineering '93, Proceedings of 1993 Conference, v.2, 1866-1871.

Butch, G.K. (1993b). "Relation of local scour to hydraulic properties at selected bridges in New York." ASCE Hydraulic Engineering '93, Proceedings of 1993 Conference, v.2, 1872-1875.

Butch, G.K., and Lumia, R., (1994). "Effects of flow duration on local scour at bridge piers in New York." ASCE Hydraulic Engineering '94, Proceedings of 1994 Conference, v.1, 46-50.

Butch, G.K. (1996). "Scour-hole dimensions at selected bridge piers in New York." ASCE Hydraulic Engineering '96, Proceedings of 1996 Conference, (cdrom).

Helsel, D.R., and Hirsch, R.M., (1992). "Statistical methods in water resources." Amsterdam, [The Netherlands], Elsevier Science B.V. Publishers, 522 p.

Froehlich, D.C. (1988). "Analysis of onsite measurements of scour at piers." ASCE Hydraulic Engineering, Proceedings of 1988 Conference, 534-539.

Mueller, D.S. (1996). "Local scour at bridge piers in nonuniform sediment under dynamic conditions." Ph.D. dissertation, Colorado State University, 212 p.

Richardson, E.V., and Davis, S.R. (1995). "Evaluating scour at bridges." Federal Highway Administration Hydraulic Engineering Circular 18, Publication No. FHWA-IP-90-017, 204 p.

SYMBOLS

D_{50} = median grain size of bed material;
D_{84} = grain size exceeding that of 84 percent of the armor layer;
D_{90} = grain size exceeding that of 90 percent of the armor layer;
D_{95} = grain size exceeding that of 95 percent of the armor layer;
Fr_1 = Froude number directly upstream from pier;
K_1 = correction factor for pier-nose shape;
K_2 = correction factor based on ratio of pier length to pier width and the alignment of flow to pier;
K_3 = correction factor for bed condition;
K_4 = correction factor for armoring by bed-material size;
R^2 = coefficient of determination;
Sf = stream force;
a = pier width (FHWA equation);
b = pier width (Froehlich equation);
g = gravitational constant;
w = unit width of flow;
V_0 = approach-flow velocity just upstream from pier;
$V_{cD_{50}}$ = critical velocity for incipient motion for grain size D_{50};
$V'_{cD_{50}}$ = approach velocity corresponding to critical velocity and incipient scour in accelerated flow region at pier for grain size D_{50};
$V'_{cD_{95}}$ = approach velocity corresponding to critical velocity and incipient scour in accelerated flow region at pier for grain size D_{95};
y_0 = water depth just upstream from pier (Froehlich equation);
y_1 = water depth directly upstream from the pier (FHWA and New York equation);
y_s = scour depth;
f = Froehlich coefficient for pier-nose shape;
r = density of water.

BRIDGE ABUTMENT EROSION PROBLEM SOLVED WITH A SMALL SCALE PHYSICAL SEDIMENT TRANSPORT MODELING APPROACH

**By David C. Gordon, Hydraulic Engineer & Robert D. Davinroy, District Potamologist,
Applied River Engineering Center, U.S. Army Corps of Engineers,
St. Louis District, St. Louis, Missouri**

U.S. Army Corps of Engineers – St. Louis District
Applied River Engineering Center
Foot of Arsenal Street
St. Louis, Missouri 63118
Phone: 314-263-4230
Fax: 314-263-4166
Email: david.gordon@mvs02.usace.army.mil

Abstract: Big Creek is a gravel bottom stream located in rural Lincoln County, Missouri, approximately 50 miles northwest of St. Louis. Shortly after a new bridge was constructed over the stream, an upstream lateral erosion problem developed that threatened the structure's abutments. Local reports indicated that the stream's bank erosion rate increased severely after the new bridge was built. The misalignment of the bridge opening in respect to the stream planform, and the constriction of the stream caused by the width of the bridge opening, had led to severe bank erosion problems both upstream and downstream of the bridge crossing. County officials worried that further high water events and additional erosion on the bridge abutments could cause a catastrophic failure to the structure.

In 1995, county officials sought the expertise of the U.S Army Corps of Engineers to solve the problem and preserve the structure. To address the problem and design a solution, the Corps of Engineers decided to use a newly developed, small-scale, physical hydraulic, sediment transport modeling approach. This approach, called micro modeling, enabled engineers to study the problem and design a small-scale, economically and environmentally sensible solution. The physical modeling technique also allowed county officials and local farmers whose land was being affected by the erosion, to view the model and discuss possible remedial actions. The final design was the result of a cooperative engineering effort between the Corps of Engineers, Lincoln County Officials, and local landowners.

Through a cost share program in 1997, the Corps of Engineers and Lincoln County constructed a small rock structure in the stream to reduce the severe abutment erosion and realign the stream's thalweg. Since the construction of the small 30-foot rock dike, strategically located 600 feet upstream of the bridge, the river training structure has caused the thalweg of the stream to adjust and realign. The area of scour along the bridge abutment has been converted to a naturally depositional area. The vertically eroding bankline located upstream of the bridge has experienced a new growth of natural vegetation and begun to revert back to a more natural slope. The stream thalweg now makes a smoother, more natural transition through the bridge opening. Photos taken before and after construction show the dramatic changes in the river regimen.

INTRODUCTION

Background: Big Creek is a typical meandering gravel bed stream found in the central Missouri. The bed material consists of mainly gravels, sands, and silts. Courser gravels and cobbles exist, although their quantity and occurrence is significantly less. The approximate physical stream parameters of Big Creek are as follows:

- Average Slope ≅ 6.4 ft/mile or 0.12 %
- Average Channel Depth at Bankfull Flow ≅ 10 feet
- Average Channel Width at Bankfull Flow ≅ 150 feet
- Average Width to Depth Ratio ≅ 15
- Deepest Channel Depth Encountered ≅ 19 feet

The Problem: In 1995, Lincoln County highway commissioners presented to the U.S. Army Corps of Engineers a very common problem that faces many local governments. Big Creek was rapidly eroding a bridge abutment and the nearby banklines at a bridge crossing for rural County Highway 729. The abutment was in danger of completely failing and threatening the structural integrity of the bridge

Historically, Big Creek had been a somewhat stable stream. However, with increased runoff from land use changes that have occurred in the basin and channel constriction of the stream at the bridge crossing, the tendency for lateral bank erosion had dramatically increased both upstream and downstream of the bridge. The aerial photo in Figure 1 shows the degree of bankline erosion that has occurred. The lateral movement of the stream was more significant where adequate vegetation buffers were not maintained between the crop fields and the stream.

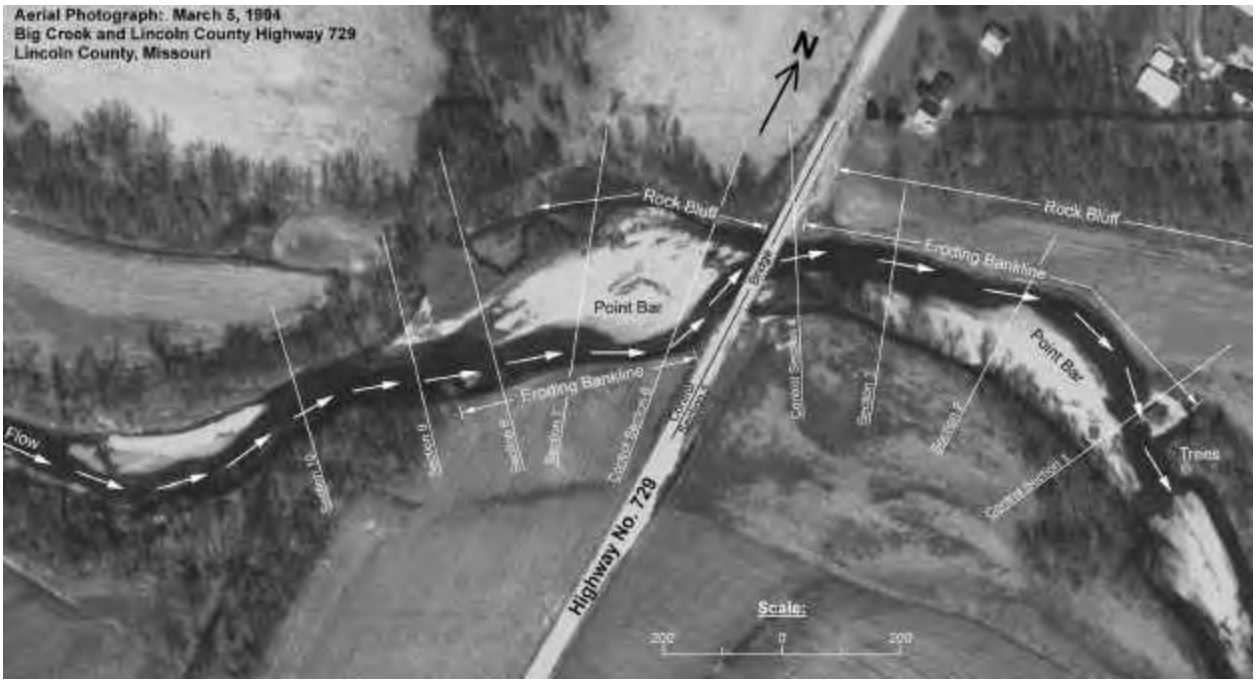

Figure 1: 1994 Aerial Photograph of Big Creek at Lincoln County Highway 729.

In the early 1990's, a new bridge crossing was constructed across Big Creek on Lincoln County Highway No. 729. The support for the 25 feet wide by 220 feet long concrete bridge consists of three sets of bridge piers and two earthen abutments. Since the new bridge was built, the stream channel upstream of the bridge had moved laterally in a southward direction approximately 100 feet. The lateral movement of the thalweg had caused a majority of the flow to be directed at the right descending bridge abutment. The scour experienced along this abutment had threatened the integrity of both the road and the bridge. Therefore, county road crews had to continuously repair this abutment for the temporary protection of the road and bridge.

The flow patterns through the bridge opening were orientated in a nearly parallel direction to the bridge crossing (Figure 1). Immediately downstream of the bridge opening, flow patterns were directed against the left descending bankline, threatening the left descending bridge abutment as well. Therefore, possible abutment failure existed on both the left and right descending sides of the bridge opening.

Figure 1 shows a complete overview of the study conditions. Conditions of the stream in the vicinity of the bridge crossing were described as follows:

- The right descending bankline was actively eroding and did not contain any sustained vegetation. This bankline feature extended from the bridge abutment to a point 500 feet upstream of the bridge.
- Both banklines at least 500 feet upstream of this bridge were heavily wooded and stable.
- A large point bar was located along the left descending bankline upstream of the bridge crossing. The size and rapid growth of the point bar was directly related to the migration of the right descending bankline. This depositional area indicated that the majority of flow was concentrated along the right descending bankline.
- The left descending bankline immediately upstream of the bridge was a wooded, natural rock bluff. This condition was evident to a point approximately 400 feet upstream of the bridge.
- The bridge crossing was severely misaligned with the thalweg of the stream channel.
- Downstream of the bridge, the right descending bankline was heavily vegetated. A small point bar was located along this bankline. The majority of flow was concentrated along the left descending bankline.
- The left descending bankline downstream of the bridge was vertical and devoid of any vegetation. This condition was evident from the bridge to approximately 700 feet downstream to a small outcropping of trees. Approximately 100 feet beyond this bankline was the continuation of the rock bluff described upstream of the bridge.

The study was performed by the Corps of Engineers to address the existing sediment transport response occurring in the vicinity of the bridge crossing. This included investigating the bridge abutment erosion, the detrimental flow alignment through the bridge opening, and the excessive bankline erosion. The goal of the study was to develop improved flow conditions through the bridge opening and protect the bridge abutments through the use of channel regulation structures.

MICRO MODELING

Engineers with the St. Louis District decided to approach the problem using the assistance of a newly developed, innovative modeling technique called micro modeling. Micro Modeling is extremely small-scale physical sediment transport modeling of a river or stream. River engineers use these models to replicate the mechanics of flowing water and sediment in a river on an area the size of a normal tabletop. It is a cost effective hydraulic river engineering technology used by engineers for the purpose of resolving some of the major sedimentation problems that surround rivers and streams. The models are relatively inexpensive to build and operate because of the very small-scale at which they are studied. Results from these models can be obtained in just a few short months.

The theory behind sediment transport modeling on a micro scale is that small streams behave very similar to large rivers. A river or stream, no matter how large or small, is a body of flowing water and sediment. The mechanics of moving water and sediment remain similar on both large rivers and small streams. Therefore, a small stream can actually be described as a model of a larger river.

Micro Models are composed of four innovative design components: the model insert, the table top sized hydraulic flume, the automated operating system which controls the flow of water and sediment, and the data collection system. The model inserts, which define the river, stream, or lake under study, are constructed from plastic composites including acrylic, polystyrene, urea, and laminate. The inserts are built to extremely high tolerances of scales so that accurate and reproducible measurements during model testing can be made. The inserts are placed within the tabletop-sized hydraulic flume and filled with plastic, sand-like sediment particles.

The hydraulic flume is made of waterproof marine grade plywood to withstand the weight of water and sediment, as well as people leaning on the model while participating in hands-on experiments. The flume houses a water and sediment reservoir, a pump, a magnetic flow meter and an industrial process control valve. The slope of the flume is adjusted by the use of rotational jacks located within the cavity of the flume.

The operating system consists of custom designed computer hardware and software. The system automatically controls the flow of water and sediment through the model, which keeps the model in equilibrium. An equilibrium condition means that the rise and fall of the water level and the sediment load is the same at both the entrance and exit of the model reach at all times, which is similar to the mechanics of an actual river or stream. To control these flows, the operating system employs software that electronically controls a process control valve and monitors a magnetic flow meter.

The data collection system employs a three-dimensional laser scanner that is used to collect the contours of the changing bed sediment in the model. The laser is an extremely accurate measuring device, which collects hundreds of thousands of data points over the length of the model. The data points are then used to create computer generated bathymetric survey maps. Engineers compare the bathymetry of the model to the bathymetry of the actual river to determine if the model is calibrated.

One of the greatest advantages provided by a Micro Model is the ability to convey highly complex hydraulic concepts to non-technical, non-engineering clients and partners. Engineers use the dynamic hydraulics of the model to demonstrate these concepts and allow the engineer, biologist, farmer, towboat pilot, landowner, etc., to communicate with each other in an effective and efficient manner. Because of this benefit, partners from all agencies and groups can remain intimately involved from the beginning of a project to its conclusion. Everyone has the opportunity to test their ideas in the model with the ability to touch and observe the effects they create. Ideas that produce positive effects are further tested scientifically by experienced river engineers. The model results are presented to all the partners with a formulated group solution as the ultimate goal.

Big Creek Micro Model: The model used for this study was constructed according to the high resolution 1994 aerial photograph shown in Figure 1. The model employed a horizontal scale of 1 inch = 50 feet, or 1:600, and a vertical scale of 1 inch = 10 feet, or 1:120, for a 5 to 1 distortion ratio. This distortion supplied the necessary forces required for the simulation of sediment transport conditions similar to those of the prototype (Davinroy).

The micro model insert was constructed of water-resistant polystyrene and measured 6 feet long by 29 inches wide by 3 inches deep. The bed material used was granular plastic urea with a specific gravity of 1.4. The banks of the stream were formed with sheet metal inserts which were designed for easy removal for the possibility of examining the effects of future meandering within certain highly erodible areas of the study reach. Bridge abutments, dikes, and weirs were modeled with oil based clay.

In all model tests, the effective discharge or hydrograph was used. Each hydrograph was a repeatable triangular response representing low to high flows within the channel, with peak flow in the model representing top of bank flows in the prototype. The recurrence interval of bankfull flow in the prototype is approximately 1.5 years (Leopold). Stages in the model were recorded by both a staff gage and a digital electronic micrometer.

The calibration of the model involved the adjustment of water discharge, sediment volume, hydrograph time scale, model slope, and entrance conditions of the model. Several different physical combinations of these variables were tested to develop sediment transport conditions considered to be representative of those experienced in the prototype. Data available from the prototype used for the calibration process included surveyed cross sections, contours surrounding the bridge crossing, aerial photographs, and on-site field inspections. Once the favorable comparison of several surveys of model tests to field survey data was made, the model was considered calibrated. The calibrated bed configuration, or Base Test, served as the comparison for all future tests. This represented the average expected sediment response of the prototype over an extended period of time. Observations and data collected from the base test indicated that the flow lines and sediment transport trends of the model and the prototype were very similar.

Solution: Several alternative design plans were tested in the model. The procedure for analyzing each alternative involved implementing the desired plan, running 5 consecutive design hydrographs, observing the sediment transport through the channel, and surveying the bed of the

model. The micro model tests determined that the most cost-effective design solution to the bridge scour problem was the implementation of a level crested 25 foot long dike at elevation top of bank, strategically placed 600 feet upstream of the bridge on the right descending bankline. The model indicated that the structure redirected a majority of flow toward the left descending rock bank and eliminated the scour against the right descending bridge abutment. The design also developed flow lines nearly perpendicular to the bridge crossing.

It was determined that a 30-foot long dike should be constructed in the river at the location specified by the model design alternative. The additional length was added to account for any stone launching off the end of the structure. The launched material would naturally armor the creek bed near the dike to reduce localized scour. The design also called for revetment to be placed on the right descending bankline upstream and downstream of the dike as well as on the left descending bankline adjacent to the dike. This measure would ensure bankline stability throughout the area of constriction caused by the structure. The left descending vertical bankline just downstream of the bridge would also be stabilized with revetment to protect the north bridge abutment from any back eddies that would develop from the new flow patterns.

The scope of the study focused primarily on reducing scour at the right descending abutment of the bridge crossing. Therefore, the lateral bank erosion problem downstream of the bridge along the left descending bankline was not addressed. Tests were conducted in the model to determine if future bankline migration would negatively effect positive changes realized from structural alternatives implemented upstream of the bridge.

RESULTS

The recommended design was constructed in the summer of 1997. After the first high water event, the stream bed demonstrated an immediate positive reaction. With the passing of each event, the bed configuration gradually developed as indicated by the micro model. Figure 2 shows a photograph taken from the top of the bridge facing upstream before the construction of the dike. Figure 3 was taken from the same location 1 ½ years after construction. The photos show a dramatic shift of the thalweg from the right descending bank towards the left descending bank. The thalweg has cut a new location through the depositional area, which has isolated the remnants of the old point bar along the right descending bankline. The right descending bankline downstream of the dike has begun to naturally repair itself with vegetation. The area near the southern bridge abutment has begun to fill with sediment indicating that it is now a depositional area. Additional maintenance to the banklines and bridge abutments after construction has not been required and only periodic monitoring of the streambed has been needed.

This project would not have been possible without the support of the farmers who own the land adjacent to the creek. Because they had already lost land due to the lateral bank erosion caused by the new bridge, the landowners were extremely skeptical of any structure designed to remedy the problem. In fact, they were going to deny access to the stream from their land for construction purposes. Only after engineers enabled the farmers to observe the micro model in action did they accept the design and allow access to the construction site.

Figure 2: Looking Upstream from the Bridge Before Dike Construction

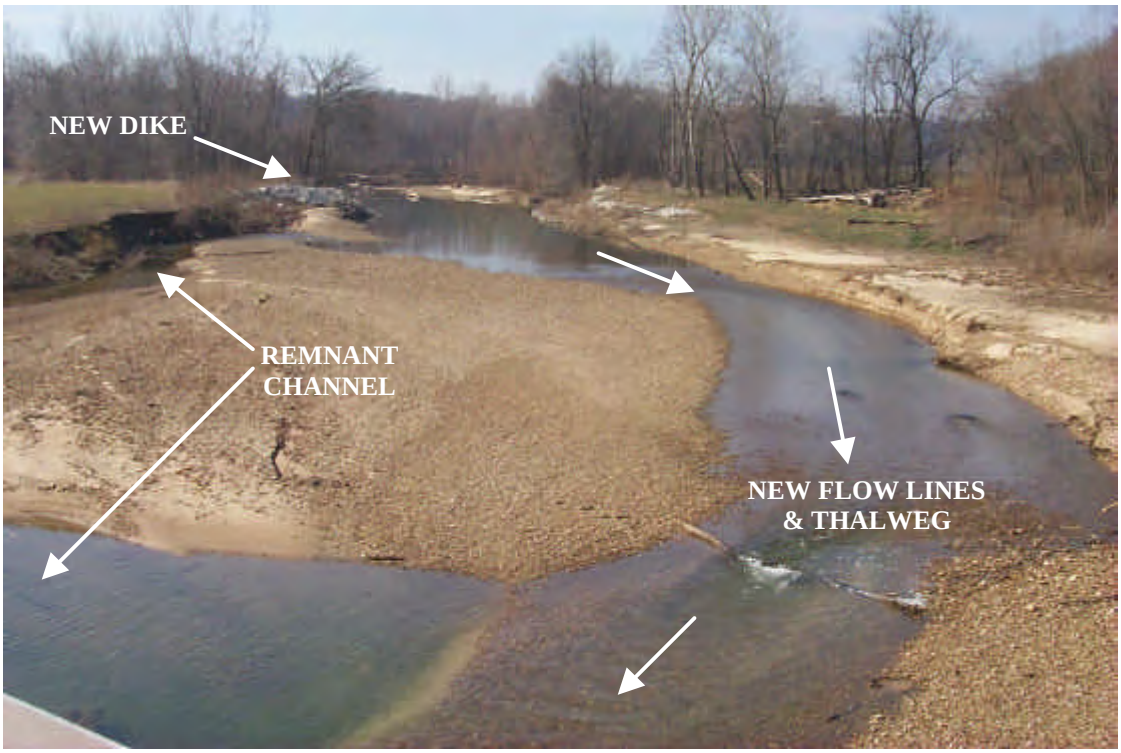

Figure 3: Looking Upstream from the Bridge 1.5 Years After Dike Construction

REFERENCES

Davinroy, Robert D., 1994, Physical Sediment Modeling of the Mississippi River on a Micro Scale, University of Missouri-Rolla Thesis.

Leopold, Luna B., 1995, A View of the River

SUSPENDED-SEDIMENT BUDGET AND YIELDS FOR THE LAGRANGE POOL OF THE ILLINOIS RIVER, OCTOBER 1994-SEPTEMBER 1997

By: Gary P. Johnson[1]

During October 1994 to September 1997, the U.S. Geological Survey (USGS) monitored suspended-sediment loads for the main-stem inflow, main-stem outflow, and four major tributaries of the LaGrange Pool of the Illinois River. On the basis of these data, a suspended-sediment budget and yields for the LaGrange Pool were calculated.

The main-stem inflow site, Illinois River at Pekin, drained 14,585 square miles (mi^2), which is 55% of the 26,743 mi^2 total drainage area of the main-stem outflow site, Illinois River at Valley City. During the study period, the Illinois River at Pekin transported an annual average suspended-sediment load of 1,510,000 tons, which computes to an annual average yield of 103 tons/mi^2 (figure 1). The Illinois River at Valley City transported an annual average suspended-sediment load of 5,010,000 tons, which computes to an annual average yield of 188 tons/mi^2. The increase in average yield between the two main-stem sites was attributed to the four major tributaries: the Mackinaw River near Green Valley (1,073 mi^2 drainage area, annual average suspended-sediment load of 355,000 tons, and annual average yield of 332 tons/mi^2), the Spoon River at Seville (1,636 mi^2 drainage area, annual average suspended-sediment load of 1,040,000 tons, and annual average yield of 638 tons/mi^2), Sangamon River at Oakford (5,093 mi^2 drainage area, annual average suspended-sediment load of 932,000 tons, and annual average yield of 183 tons/mi^2), and the LaMoine River at Ripley (1,293 mi^2 drainage area, annual average suspended-sediment load of 623,000 tons, and annual average yield of 482 tons/mi^2).

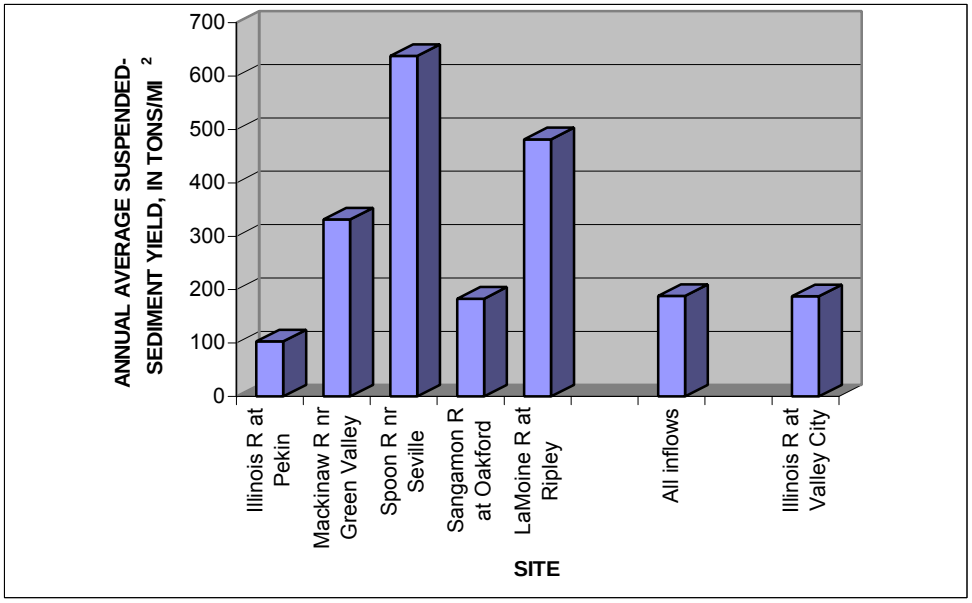

Figure 1. Annual average suspended-sediment yield of the Illinois River and major tributaries in the LaGrange Pool, Illinois River.

The main-stem inflow and four tributaries collectively drained 23,680 mi^2 (89% of the drainage area at the main-stem outflow), with an annual average suspended-sediment load of 4,460,000 tons, and annual average yield of 188 tons/mi^2. This load is equal to the outflow yield of 188 tons/mi^2 at Valley City, indicating that during the study period, sediment entered and exited LaGrange Pool at the same rates.

1- Hydrologist/Engineer, U.S. Geological Survey, Urbana, Ill.

EVOLUTION AND TIMING OF SUSPENDED-SEDIMENT TRANSPORT FOLLOWING THE 1980 MOUNT ST. HELENS ERUPTION

Jon J. Major, Hydrologist, U.S. Geological Survey, Vancouver, Washington

Abstract: Continuous monitoring of streamflow and suspended-sediment discharges from disturbed basins following the catastrophic 1980 eruption of Mount St. Helens reveals when, and under what conditions, sediment redistribution occurs following a major landscape disturbance. The redistributed sediment includes material deposited by the eruption as well as centuries-old sediment that has been remobilized from storage. Suspended-sediment yields, as much as 10^4 Mg/km^2/yr shortly after the eruption, declined nonlinearly in all basins for more than a decade. Yet, after 20 years, suspended-sediment yields from some basins remain 10-100 times greater than typical background values. Suspended sediment is transported dominantly by stormflows; more than 50% of the suspended–sediment load is transported in 1 to 4 weeks each year. Very large floods ($p<0.01$) have transported as much as 50% of the annual suspended-sediment load in a single day from some basins. Although large stormflows can transport quantitatively significant volumes of sediment, the majority of the annual suspended-sediment load is transported by common stormflows. On average, about half of the annual suspended-sediment load is transported by stormflows that have return intervals of less than 1.5 years. Discharges smaller than mean annual flow transport #10% of the annual suspended-sediment load. Two decades of monitoring suspended-sediment discharges and channel geometry changes in the aftermath of the catastrophic Mount St. Helens eruption demonstrate the long-term instability of eruption-generated detritus and show that geomorphically significant evolution of disturbed watersheds generally proceeds under commonplace hydrologic conditions.

INTRODUCTION

Explosive volcanic eruptions can severely disrupt water and sediment fluxes in watersheds. Geomorphic and hydrologic responses to disturbances caused by explosive volcanic eruptions commonly are rapid and dramatic, and as a result posteruption sediment yields can greatly exceed preeruption yields (Major et al., 2000). Disruptions of watershed hydrology and geomorphology by volcanic eruptions are particularly significant because subsequent prolonged sediment transport can cause environmental, social, and economic damages that equal or exceed those caused directly by an eruption (e.g., Mercado et al., 1996). Despite the significance of sediment redistribution following explosive eruptions (or other substantial landscape disturbances) there is a dearth of global long-term data to adequately address such fundamental questions as: (1) How does sediment yield evolve following major landscape disturbance? (2) How long does excess sediment yield persist above background level? (3) Does sediment yield evolve monotonically with time, or is there significant temporal variation? (4) Does volcanogenic disturbance process greatly influence consequent sediment yield? (5) What is the influence of hydrology on geomorphic evolution of a disturbed landscape? (6) When, and under what conditions, is sediment typically redistributed? In this paper, I present a summary perspective of nearly 20 years of suspended-sediment yield in the aftermath of the 1980 Mount St. Helens eruption, and examine the timing and hydrologic conditions of sediment transport. I focus on suspended sediment because bedload data are limited and suspended sediment averaged ≥ 80% of the total sediment discharge (Lehre et al., 1983; Simon, 1999).

VOLCANOGENIC LANDSCAPE DISTURBANCE

The catastrophic 1980 eruption of Mount St. Helens affected some watersheds severely, others mildly (Lipman and Mullineaux, 1981). Watersheds proximally north of the volcano underwent the most severe disturbance (Fig. 1). A large debris avalanche deposited 2.5 km^3 of debris in the upper North Fork Toutle River valley (Glicken, 1998), and a consequent directed blast ravaged 600 km^2 of rugged terrain and blanketed the landscape with up to 1 m of gravelly to silty sand tephra (Hoblitt et al., 1981; Waitt, 1981). The avalanche deposit buried 60 km^2 of valley to a mean depth of 45 m and severed surface drainage between the upper and lower North Fork Toutle River watershed (Lehre et al., 1983; Janda et al., 1984). Local liquefaction of that deposit spawned the North Fork Toutle River lahar (Janda et al., 1981; Fairchild, 1987). Fallout from the eruption column blanketed proximal areas east-northeast of the volcano with silty-sand and gravel tephra to tens of centimeters (Waitt and Dzurisin, 1981). On the volcano=s western, southern, and eastern flanks, pyroclastic currents triggered lahars that flowed many tens of kilometers, but deposited only tens of centimeters to a few meters of coarse, gravelly sand on valley floors and floodplains (Janda et al., 1981; Pierson, 1985; Major and Voight, 1986; Fairchild, 1987; Scott, 1988). The eruption and its aftermath are particularly well suited for an analysis

of the issues outlined above because: (1) the eruption was a single event composed of a mosaic of volcanogenic processes; (2) sediment was distributed broadly and abruptly across the landscape; (3) water and sediment fluxes have been systematically monitored for nearly two decades, and (4) there has been an increase in precipitation and runoff in the past several years in response to a possible climatic shift (e.g., Mantua et al., 1997).

SEDIMENT YIELD

After the eruption, streamgaging stations were established to monitor discharges of water and suspended sediment from basins affected by the blast current, debris avalanche, and lahars (Dinehart, 1998). Annual suspended-sediment yields, monitored at five stations along the larger rivers draining Mount St. Helens (Fig. 1), were as much as 500 times greater than probable background level, and generally declined nonlinearly for more than a decade (Fig. 2; Major et al., 2000). Long-term monitoring of suspended sediment demonstrates that magnitudes of erosion and sediment release are greatly influenced by volcanogenic disturbance process and streamflows, and that yields do not decline smoothly with time but are punctuated by excursions (Fig. 2).

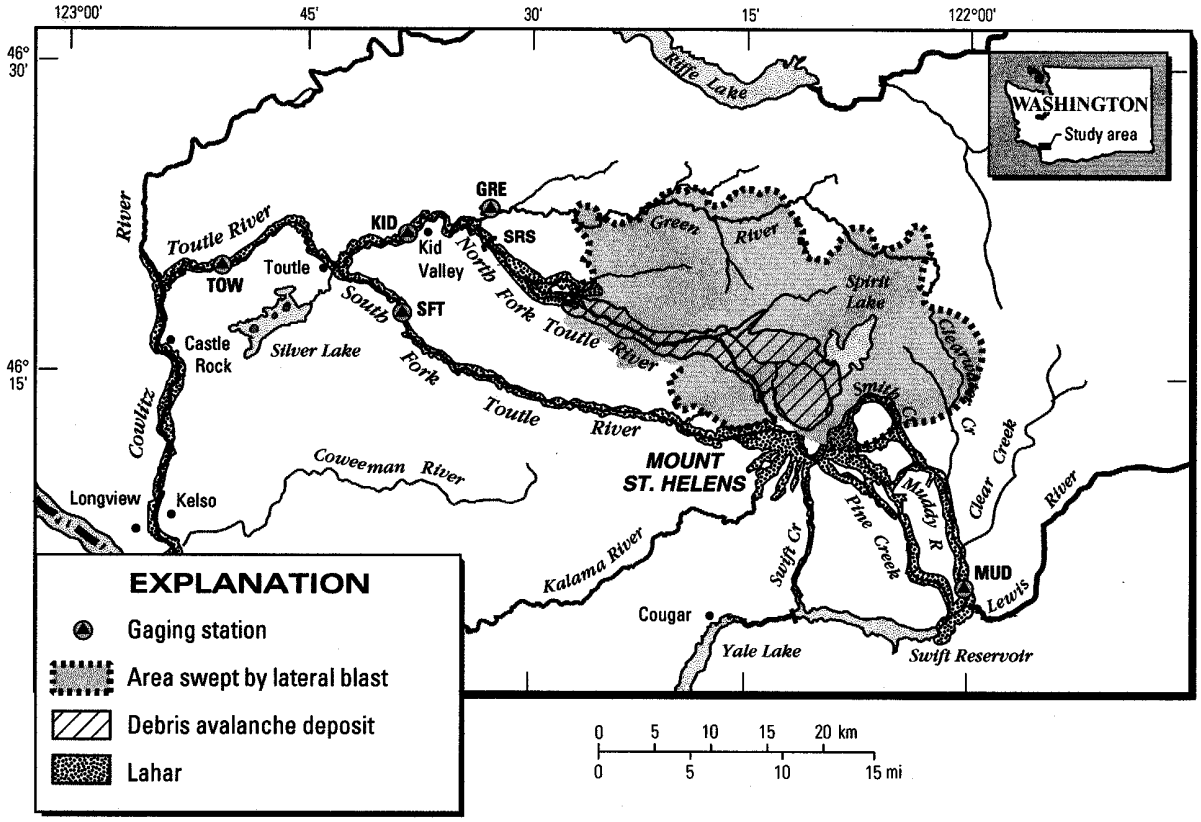

Figure 1. Effects of Mount St. Helens 1980 eruption and location of streamgaging stations. TOW, KID, SFT, MUD, GRE are gaging stations. SRS, sediment retention structure. (After Major et al., 2000).

Basin-Specific Transport: From 1980 to 1999, the Toutle River transported more than 300 x 10^6 Mg (1 Mg = 1 metric ton) of suspended sediment past TOW gage (Fig. 1). Nearly half of that sediment was transported by syneruptive lahars (Dinehart, 1998; Major et al., 2000). Erosion associated with drainage development across the avalanche deposit (Lehre et al., 1983; Janda et al., 1984) as well as bank erosion along the North Fork Toutle River downstream of the avalanche deposit (Meyer and Janda, 1986) contributed to the enormous sediment discharges measured along the lower North Fork Toutle River at KID and along the lower Toutle River at TOW (Figs. 1 and 2).

A sediment retention structure (SRS) constructed upstream from KID (Fig. 1) impounds most of the sediment eroded from the avalanche deposit (US Army Corps of Engineers, 1984). The dam began trapping sediment in November 1987 (WY 1988), and by 1999 had trapped ~100 x 10^6 Mg of sediment (US Army Corps of Engineers, 2000). Downstream of the dam, subsequent sediment discharges measured at KID and TOW plummeted, and as a result the KID gage was decommissioned in 1994. Monitoring of annual sediment accumulation behind the dam, combined with assumptions about the percentage of sediment transported as bedload (Major et al., 2000), indicate that sediment was released from the debris-avalanche deposit more slowly than estimated from projection of the sediment-yield trend through 1987 (Fig. 3; Major et al., 2000). Twenty years after emplacement, the average annual suspended-sediment yield from the debris-avalanche deposit remains about 10^4 Mg/km^2, 100 times greater than the background levels typical of many western Cascades rivers.

Suspended-sediment yields from two lahar-affected basins (South Fork Toutle and Muddy; Fig. 1) are substantially less than from the avalanche deposit (Fig. 2). From 1982 to 1999, stormflows transported about 15 x 10^6 and 20 x 10^6 Mg of suspended sediment from the South Fork Toutle and Muddy River basins, respectively. From 1982 to 1985, yields from these basins dropped rapidly (Fig. 2), but the average yield then reached a plateau at about 10^3 Mg/km^2, 10 times greater than typical background level.

The Green River (Fig. 1), affected solely by the blast current, transported the least suspended sediment. From 1982 to 1994, stormflow transported 1.4 x 10^6 Mg of suspended sediment from the basin. With minor fluctuations, the annual suspended-sediment yield from Green River basin declined persistently; within five years it had returned to levels typical of western Cascades rivers, and by 1994 was as little as 15 Mg/km^2 (Fig. 2), at which time the station was shut down.

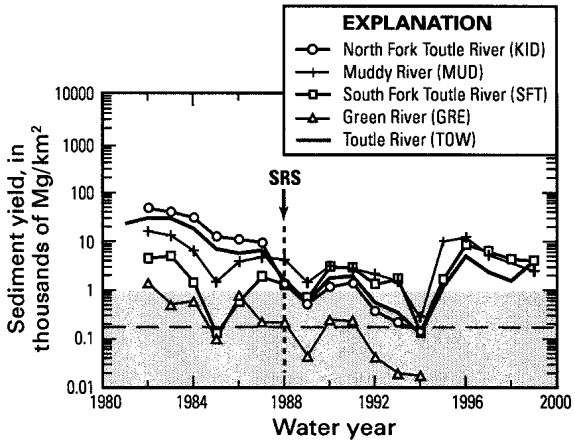

Figure 2. Annual suspended-sediment yields at Mount St. Helens. See Figure 1 for basin disturbances and station locations. Shaded region depicts range of, and dashed line depicts mean value of, mean annual yields of several western Cascade Range rivers (US Geological Survey , 2000). (After Major et al., 2000).

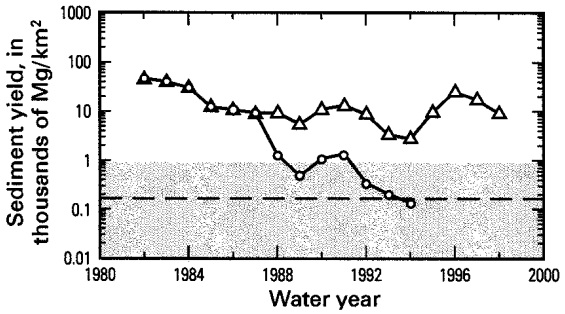

Figure 3. Annual suspended-sediment yield at KID projected (triangles) in absence of sediment dam. Measured yield (circles) shown for comparison. See Figure 2 for additional information. (After Major et al., 2000).

Effects of streamflow: A 20-year perspective on suspended-sediment yield at Mount St. Helens shows that broad hydrologic trends can significantly perturb sediment discharge and substantially lengthen extrapolated recovery times (Figs. 2 and 3; Major et al., 2000). Sediment discharges in consecutive wet years (1995-1999) demonstrate that dormant sediment at Mount St. Helens remains mobile, and that suspended-sediment yields in several basins remain far from equilibrium. From 1995 to 1999, mean annual discharges in most basins were about 40%-50% greater than those during 1981 to 1994 (Major et al., 2000). As a result, suspended-sediment yields from the North Fork Toutle, South Fork Toutle, and Muddy River basins increased as much as 10-50 times and approached or exceeded average values measured within a few years after the eruption (Figs. 2 and 3; Major et al., 2000).

TIMING AND DISCHARGE CONDITIONS OF SEDIMENT TRANSPORT

Transit Times of Suspended Sediment: Analysis of transit times of suspended sediment from basins at Mount St. Helens shows that the majority of annual suspended-sediment transport occurs during limited periods of a few weeks or less. More than 50% of the annual suspended sediment in the North Fork Toutle and Toutle Rivers has been transported in 10-27 days during the period of study, whereas 50% of the suspended-sediment transport occurs in less than one week in the South Fork Toutle, Green, and Muddy River basins (Table 1). Comparable transit times are observed in regional basins unaffected by the eruption (e.g., Chehalis River; Table 1), but in those basins, sediment loads pale in comparison to those from basins affected by the Mount St. Helens eruption.

Suspended-sediment is transported dominantly by seasonal stormflows. Individual large floods can be particularly significant. For example, the 1996 suspended-sediment yield from Muddy River basin was about 75% of the maximum annual yield recorded in 1982, and 50% of the 1996 annual yield was transported in a single day. The impact of an individual flood is further highlighted by comparing suspended-sediment yields and annual runoff in 1996 and 1997. In the Muddy, Toutle, and South Fork Toutle basins, the 1997 annual runoff equaled or exceeded that of 1996 (Major et al., 2000), yet the 1996 sediment yields were 40%-140% greater as the result of a single large flood.

Table 1. Summary of mean transit times (days ∀ 1s) for percentages of annual suspended-sediment discharges.

River (gage)	Period	50%	60%	75%	90%
Toutle (TOW)	1981-1998	16 ∀ 13	27 ∀ 21	55 ∀ 37	119 ∀ 59
	1981-1987	25 ∀ 17	40 ∀ 26	77 ∀ 45	149 ∀ 67
	1988-1998	11 ∀ 6	18 ∀ 10	41 ∀ 23	101 ∀ 48
NFk Toutle (KID)	1982-1994	25 ∀ 15	40 ∀ 22	77 ∀ 35	150 ∀ 45
	1982-1987	24 ∀ 12	39 ∀ 19	79 ∀ 32	156 ∀ 43
	1988-1994	27 ∀ 18	41 ∀ 26	75 ∀ 39	145 ∀ 49
SFk Toutle (SFT)	1982-1998	5 ∀ 2	7 ∀ 2	12 ∀ 4	28 ∀ 10
Green (GRE)	1982-1994	5 ∀ 3	8 ∀ 5	18 ∀ 12	50 ∀ 33
Muddy (MUD)	1982-1996	7 ∀ 4	11 ∀ 6	24 ∀ 12	66 ∀ 25
Chehalis	1962-1971	18 ∀ 4	24 ∀ 5	41 ∀ 8	79 ∀ 11

Transport Discharge Conditions: While individual stormflows can transport quantitatively significant amounts of sediment, they may not be the most geomorphically effective flows over the long term (Wolman and Miller, 1960). To assess a long term perspective of water discharge and its relation to suspended-sediment transport in the aftermath of the Mount St. Helens eruption, I have examined suspended-sediment transport with respect to mean annual flow, mean annual flood (average maximum discharge), and bankfull discharge. Despite considerable noise, the cumulative percentage of transported suspended sediment increases with increasing water discharge (Fig. 4). Table 2 summarizes the water discharge (Q_{50}), culled from Figure 4, below which 50% of the cumulative suspended-sediment load is transported. For example, on average, half of the suspended sediment transported from the South Fork Toutle basin is moved by water discharges less than or equal to 5000 cfs. Table 2 also summarizes the approximate return interval of discharges of magnitude Q_{50}, and compares this discharge to the magnitude of the mean annual flow and the mean annual flood. In all cases, Q_{50} is several times greater than the mean annual flow, a fraction of the mean annual flood, and has a return

Table 2. Water discharges for 50% cumulative suspended-sediment transport.

River	Q_{50} (cfs)	~return interval (years)	Q_{mean} (cfs)	$Q_{mean\ flood}$ (cfs)	$Q_{bankfull}$ (cfs)	times mean flow	times mean flood
Toutle							
overall	8600	< 1.1	2060	19760	13850	4.2	.44
pre-SRS	7115	< 1.1	--	--	--	3.5	.36
post-SRS	10185	< 1.25	--	--	--	4.9	.52
NFk Toutle							
overall	3700		1070	13180	--	3.5	.28
pre-SRS	4090		--	--	--	3.8	.31
post-SRS	3220		--	--	--	3.0	.24
SFk Toutle	4990	< 1.4	610	8100	5240	8.2	.62
Green	2905	< 1.25	502	6090	3765	5.8	.48
Muddy	4845	< 1.4	863	8080	5350	5.6	.60

Table 3. Approximate percentages of suspended-sediment load transported by various water discharges.

River	$Q < Q_{mean}$	$Q < Q_{mean\ flood}$	$Q < Q_{bankfull}$
Toutle			
overall	11	100	80
pre-SRS	13	100	99
post-SRS	9	99	70
NFk Toutle			
overall	12	100	--
pre-SRS	11	100	--
post-SRS	14	100	--
SFk Toutle	3	83	53
Green	5.5	100	66
Muddy	6.5	85	56

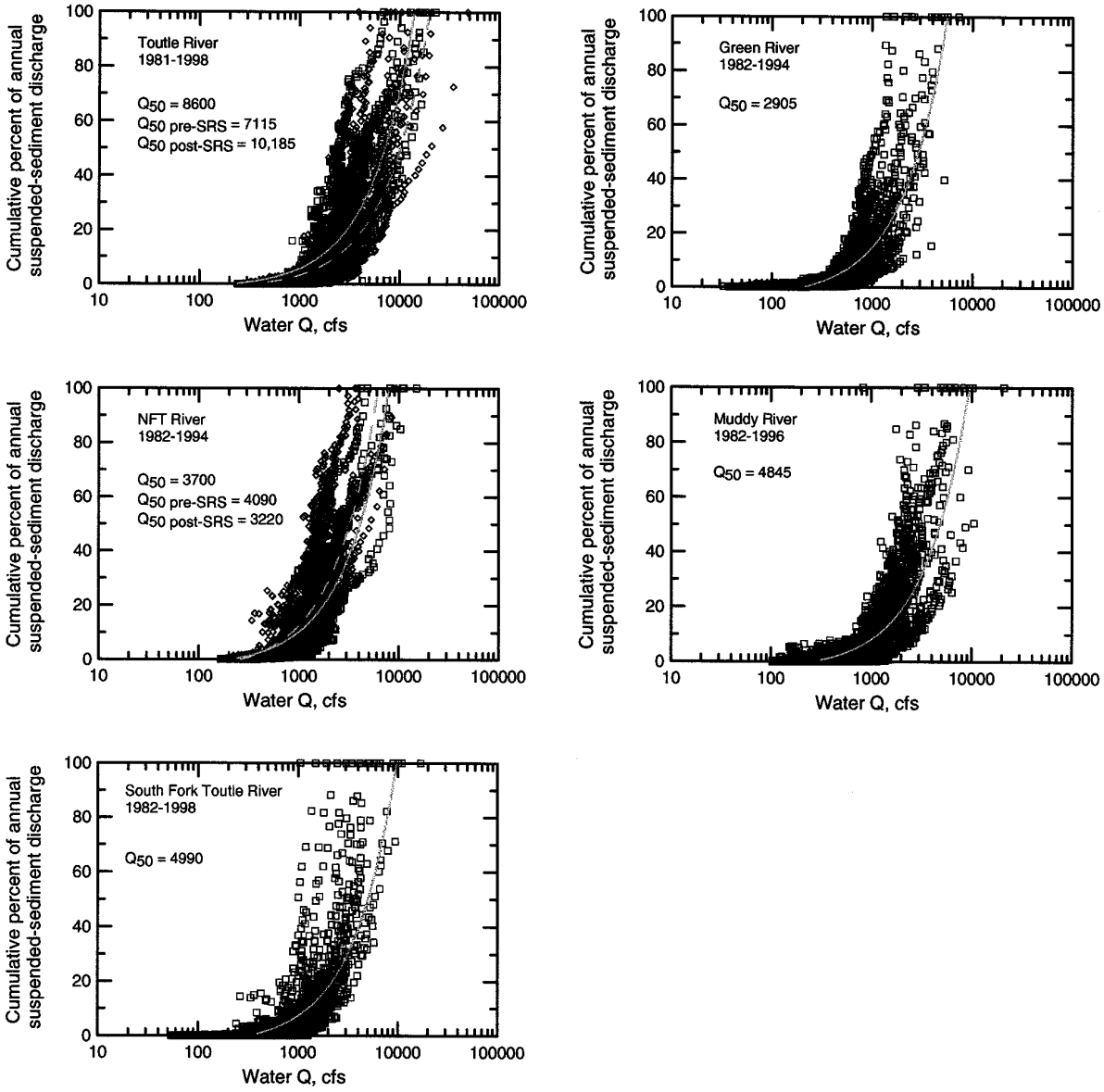

Figure 4. Cumulative percentage of annual suspended-sediment transport versus water discharge. Scatterplot represents a 5-point moving average of water discharge. Solid lines represent linear regression model. Q_{50} is the discharge (in cfs) below which 50% of cumulative annual suspended sediment is transported. Plots for the Toutle and North Fork Toutle Rivers show linear regressions for pre- and post-sediment-retention-dam periods.

interval of less than 1.5 years. These data highlight the importance of stormflows on suspended-sediment transport; discharges smaller than the mean annual flow transport #10% of the annual suspended-sediment load (Table 3).

A calculation of the approximate percentage of suspended sediment transported annually at bankfull discharge provides an assessment of the relative importance of stormflow magnitudes on sediment redistribution. For this analysis, bankfull discharge is approximated as the discharge having a return interval of about 1.5 years (Dunne and Leopold, 1978). Adopting this definition for bankfull discharge shows that discharges less than or equal to bankfull are responsible for transporting more than 50 percent of the annual suspended-sediment load for the period of study (Table 3), and thus are the discharges that are most effective over time.

CONCLUSIONS

Sediment yields in the aftermath of explosive volcanic eruptions typically decline nonlinearly as physical and vegetative controls diminish sediment supply (e.g., Pierson et al., 1992; Janda et al., 1996; Major et al., 2000). At Mount St. Helens, suspended-sediment yields dropped rapidly over the first few years, but then slowed over the next decade. However, spatial and temporal perturbations resulting from hydrologic fluctuations are likely to punctuate, or even temporarily reverse, long-term trends, which complicates projection of time to equilibrium. Suspended sediment at Mount St. Helens is transported mainly by episodic stormflows having return intervals # 1.5 years. However, infrequent large ($p<0.01$) stormflows have transported significantly large amounts of sediment.

Twenty years after the eruption of Mount St. Helens, suspended-sediment yields remain 1 to 2 orders of magnitude above typical background levels in basins where mass-flow sediments were deposited in channels. In basins where the geomorphic impact was dominantly hillslope disturbance, suspended-sediment yields returned to background level within five years. The perspective of suspended-sediment transport in the aftermath of significant landscape disturbance at Mount St. Helens demonstrates the long-term instability of eruption-generated detritus, and shows that measures designed to mitigate sediment transport in the aftermath of severe explosive eruptions must remain functional for decades.

REFERENCES

Dunne, T., and Leopold, L.B., 1978, Water in Environmental Planning. W.H. Freeman and Company, New York, 818 p.

Dinehart, R.L., 1998, Sediment transport at gaging stations near Mount St. Helens, Washington, 1980-1990. Data collection and analysis: U.S. Geological Survey Professional Paper 1573, 105 p.

Fairchild, L.H., 1987, The importance of lahar initiation processes, in Costa, J.E., and Wieczorek, G.F., eds., Debris flows/avalanches: Process, recognition, and mitigation: Geological Society of America Reviews in Engineering Geology, v. 7, p. 51-62.

Glicken, H., 1998, Rockslide-debris avalanche of May 18, 1980, Mount St. Helens volcano, Washington: Geological Survey of Japan Bulletin, v. 49, p. 55-106.

Hoblitt, R.P., Miller, C.D., and Vallance, J.W., 1981, Origin and stratigraphy of the deposit produced by the May 18 directed blast, in Lipman, P.W., and Mullineaux, D.R., The 1980 eruptions of Mount St. Helens, Washington: U.S. Geological Survey Professional Paper 1250, p. 401-420.

Janda, R.J., Meyer, D.F., and Childers, D., 1984, Sedimentation and geomorphic changes during and following the 1980-1983 eruptions of Mount St. Helens, Washington: Shin Sabo, v. 37, no. 2, p. 10-21, and no. 3, p. 5-19.

Janda, R.J., Scott, K.M., Nolan, K.M., and Martinson, H.A., 1981, Lahar movement, effects, and deposits, in The 1980 eruptions of Mount St. Helens, Washington, in Lipman, P.W., and Mullineaux, D.R., The 1980 eruptions of Mount St. Helens, Washington: U.S. Geological Survey Professional Paper 1250, p. 461-478.

Janda, R.J., Daag, A.S., Delos Reyes, P.J., Newhall, C.G., Pierson, T.C., Punongbayan, R.S., Rodolfo, K.S., Solidum, R.U., and Umbal, J.V., 1996, Assessment and response to lahar hazard around Mount Pinatubo, 1991-1993, in Newhall, C.G., and Punongbayan, R.S., eds., Fire and mud: Eruptions and lahars of Mount Pinatubo, Philippines: Quezon City, Philippine Institute of Volcanology and Seismology, and Seattle, University of Washington Press, p. 107-140.

Lehre, A.K., Collins, B.D., and Dunne, T., 1983, Post-eruption sediment budget for the North Fork Toutle River drainage, June 1980-June 1981: Zeitschrift für Geomorphologie, Supplement Band 46, p. 143-165.

Lipman, P.W., and Mullineaux, D.R., eds., 1981, The 1980 eruptions of Mount St. Helens, Washington: U.S. Geological Survey Professional Paper 1250.

Major, J.J., and Voight, B., 1986, Sedimentology and clast orientations of the 18 May 1980 southwest flank lahars, Mount St. Helens, Washington: Journal of Sedimentary Petrology, v. 56, p. 691-705.

Major, J.J., Pierson, T.C., Dinehart, R.L., and Costa, J.E., 2000, Sediment yield following severe volcanic disturbance--a two decade perspective from Mount St. Helens: Geology, v. 28, p. 819-822.

Mantua, N.J., Hare, S.R., Zhang, Y., Wallace, J.M., and Francis, R.C., 1997, A Pacific interdecadal climate oscillation with impacts on salmon production: Bulletin of the American Meteorological Society, v. 78, p. 1069-1079.

Mercado, R.A., Bertram, J., Lacsamana, T., and Pineda, G.L., 1996, Socioeconomic impacts of the Mount Pinatubo eruption, in Newhall, C.G., and Punonbayan, R.S., eds., Fire and mud: Eruptions and lahars of Mount Pinatubo, Philippines: Quezon City, Philippine Institute of Volcanology and Seismology, and Seattle, University of Washington Press, p. 1063-1070.

Meyer, D.F., and Janda, R.J., 1986, Sedimentation downstream from the 18 May 1980 North Fork Toutle River debris avalanche deposit, Mount St. Helens, Washington, in Keller, S.A.C., ed., Mount St. Helens: Five years later: Cheney, Eastern Washington University Press, p. 68-86.

Pierson, T.C., 1985, Initiation and flow behavior of the 1980 Pine Creek and Muddy River lahars, Mount St. Helens, Washington: Geological Society of America Bulletin, v. 96, p. 1056-1069.

Pierson, T.C., Janda, R.J., Umbal, J.V., and Daag, A.S., 1992, Immediate and long-term hazards from lahars and excess sedimentation in rivers draining Mount Pinatubo, Philippines: U.S. Geological Survey Water-Resources Investigation Report 92-4039, 35 p.

Scott, K.M., 1988, Origins, behavior, and sedimentology of lahars and lahar-runout flows in the Toutle-Cowlitz River system: U.S. Geological Survey Professional Paper 1447-A, 74 p..

Simon, A., 1999, Channel and drainage-basin response of the Toutle River system in the aftermath of the 1980 eruption of Mount St. Helens, Washington: U.S. Geological Survey Open-File Report 96-633, 130 p.

U.S. Army Corps of Engineers, 1984, Mount St. Helens, Washington, Feasibility Report and Environmental Impact Statement, v. 1, 104 p.

U.S. Army Corps of Engineers, 2000, Cowlitz River Basin Water Year 1998 Hydrologic Summary: Mount St. Helens, Washington, Toutle River and North Fork Toutle River, 94 p.

U.S. Geological Survey, 2000, Suspended-sediment database: http://water.usgs.gov/osw/techniques/sediment.html; accessed June 2000.

Waitt, R.B., 1981, Devastating pyroclastic density flow and attendant air fall of May 18--stratigraphy and sedimentology of deposits, in Lipman, P.W., and Mullineaux, D.R., eds., The 1980 eruptions of Mount St. Helens, Washington: U.S. Geological Survey Professional Paper 1250, p. 439-460.

Waitt, R.B., and Dzurisin, D., 1981, Proximal airfall deposits from the May 18 eruption--stratigraphy and field sedimentology, in Lipman, P.W., and Mullineaux, D.R., eds., The 1980 eruptions of Mount St. Helens, Washington: U.S. Geological Survey Professional Paper 1250, p. 601-616.

Wolman, M.G., and Miller, J.P., 1960, Magnitude and frequency of forces in geomorphic processes: J. Geology, v. 68, p. 54-74.

MIXED-SIZE SEDIMENT TRANSPORT MODEL FOR NETWORKS OF ONE-DIMENSIONAL OPEN CHANNELS

By James P. Bennett, Hydrologist, U. S. Geological Survey, Lakewood, Colorado

INTRODUCTION

Described here is a general model for predicting the transport of mixed sizes of sediment by flow in simple networks of open channels. The simulation package is intended for sediment routing, prediction of erosion and deposition following dam removal, and to compute scour in channels at road crossings or other artificial structures. Channels appropriate for simulation are characterized as one-dimensional, that is as having negligible lateral variability in the processes of flow, sediment transport, and any resulting bed elevation adjustment. The location and shape of channel banks are user specified and all bed elevation changes take place between these banks and above a user-specified bedrock elevation. Because the time scale of the processes of channel bed sorting and elevation adjustment are long compared to those typically treated with unsteady flow algorithms and the simulated reaches are typically short, the model treats input hydrographs as step-wise steady-state. Computation of sediment transport emphasizes the sand-size range (.0625-2.0 mm) but the user may select any desired range of particle diameters including silt and finer (<0.0625 mm). A computation time step for sediment transport may be specified by the user, but the true time step is often determined by a minimum bed elevation change that is also user specified. The model computes the time evolution of total transport and the size composition of bed- and suspended-load sediment through any cross-section of interest. It also tracks bed surface elevation and size composition. The objective of this report is to outline the theoretical basis and assumptions, and limitations of the flow and transport algorithms and to describe how the concepts are incorporated into the algorithms. Example predictions of bed level and size composition adjustment are included for a period after the removal of a small dam.

The model is written in the FORTRAN programming language for implementation on personal computers using the Windows ™ operating system and, along with certain graphical output capability, is accessed from a graphical user interface (GUI). The GUI provides a framework for selecting input files and parameters for a number of components of the sediment transport process. The user may specify up to 20 sediment sizes to be used in all aspects of the simulation. Otherwise there is no limitation as to numbers of channels, channel junctions, cross-sections, or points defining the cross-sections. As part of data input, the user may set the original bed sediment composition in any number of layers of known thickness at each cross-section. Following simulation, for individual channel segments and selected times during the simulation period, the GUI accommodates display of longitudinal plots of either bed elevation and size composition or of transport rate and size composition of the various transported components. For individual cross-sections, the GUI also allows display of time series of transport rate and size composition of the various components and of bed elevation and bed-surface size composition. With the exception of sediment particle sizes (in mm) and time (in days) the model employs only MKS units.

THEORETICAL DEVELOPMENT

Flow Simulation: The flow computation algorithm of the model accepts time-varying hydrographs but the computation procedure for individual channels solves the steady-state problem for the instantaneous discharge at the beginning of the time step in question and uses the resulting hydraulic variables to compute transport-related characteristics for the entire time increment. This is appropriate because the time scale of the transport-related processes is much longer than that of the unsteady flow processes and it is convenient because solution of the steady-state flow equation is much less cumbersome and more stable than for the transient state. The latter is especially important in the present situation because the flows must sometimes be computed numerous times each simulation step due to the iterative procedure required for certain networks. For the steady-state situation, the Navier-Stokes equations for free-surface flow in a channel reduce to

$$\frac{d}{dx}\left(\frac{v^2}{2g}+z\right)+S_f=0. \qquad (1)$$

where, as shown in figure 1, v is mean flow velocity, z is water surface elevation, g is the gravitational constant, and S_f is the friction slope obtained from solving the Manning formulation for S.

$$v=\frac{1}{n}D^{2/3}S^{1/2} \qquad (2)$$

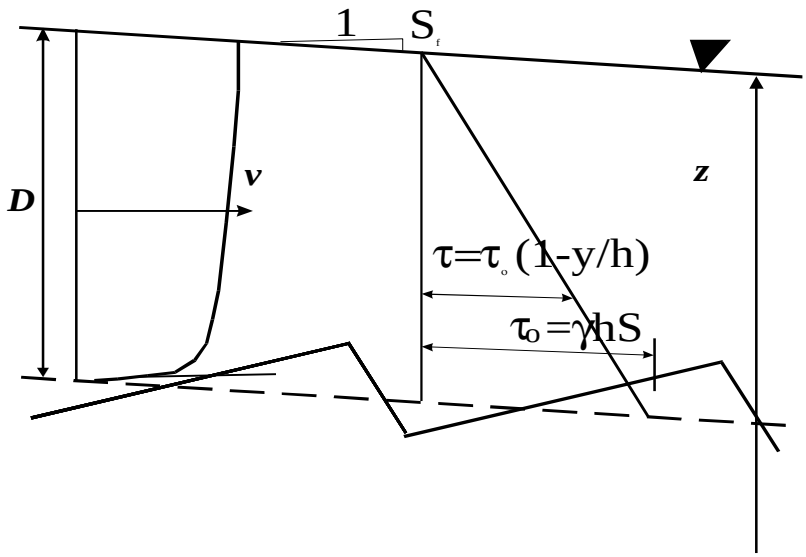

Figure 1. Definition sketch for flow-related variables.

Typically, the flow in streams and canals is subcritical which requires specification of the (boundary condition) water surface elevation at the downstream-most cross-section and a

solution procedure that marches downstream-to-upstream. As described by Chaudhry (1993) this can be accomplished using Newton iteration to solve for z_1 in the discrete version of (1)

$$f(z_1) = z_1 + \frac{Q^2}{2g}\left(A_1^{-2} - A_2^{-2}\right) - dx\bar{S}_f - z_2 = 0 \qquad (3)$$

where Q is the flow rate in the channel, A is cross-section area, and subscripts 1 and 2 refer respectively to the upstream and downstream sections. The Manning n resistance coefficients of (2) are cross-section averages obtained by integration at the same time as the cross-section area A is computed. For the bank and bedrock segments of each cross-section, user-specified values are employed. The user also specifies a resistance coefficient for the alluvial section of the channel bed but has the option of using values computed specifically for the modeled situation using the techniques and procedures described by Bennett (1995).

Using (3), it is convenient to confirm that subcritical flow exists upstream of a particular cross-section, 2, by using the critical flow elevation at section 1 to determine the appropriate variables in the expression. If a negative value is obtained for $f(z_1)$, subcritical flow exists at 1 and solution may proceed. If not, a hydraulic jump exists between the two sections. The jump is ignored in the model but a search is conducted in the upstream direction until another subcritical flow section is reached. Following this, supercritical flow is routed downstream to the previously determined subcritical section.

For individual channels within the network, the upstream boundary condition is always a specified discharge. The discharge may come from a time series, or from conservation of mass at a channel junction within the network. External flow boundary condition specification includes water temperature. There are 5 possible downstream boundary conditions. These include specified water-surface elevation time series, hydraulic depth vs discharge rating curve, normal flow depth for a downstream channel with specified slope, water surface elevation at a specified internal channel junction, and sharp crested weir elevation and crest width. The rating curve and weir boundary conditions may be specified at internal channel junctions, as well as at locations where water leaves the simulation network. For weirs at junctions, a check is made for submergence and the discharge relationship adjusted accordingly. This is not done in the case of an internally applied rating curve. If a channel discharges to a junction that has water surface elevation lower than the critical elevation for that channel, the critical elevation is used as the downstream boundary condition for the channel.

Channel Networks: The simulation network may consist of several channel segments interconnected at one or more internal junctions. This allows the user to conveniently deal with tributary or delta networks, with flow around islands, or flow through multiple openings in embankments. The junctions are assumed to have no plan area, so no storage of water or sediment within them is permitted. Mass is conserved in that all flow entering a junction leaves it and, with the exemptions mentioned above, all channels entering or leaving have the same water-surface elevation. The network is termed simple in that the user must be able to specify the direction of flow in each of the channels. At each time step, the flow simulation algorithm iterates through the entire network until neither the downstream water-surface elevation nor the input discharge varies significantly for any channel. For each iteration at each junction, water-surface elevation is determined by adjusting it until the sum of discharges leaving the junction

differs from that entering by less than a factor of 1 in 1000. (For each individual channel, discharge is the variable to be solved for and the boundary conditions are stage-stage.) Once the flow rates in all channels have been determined, sediment is distributed to channels leaving junctions in proportion to the flow rates to those channels.

Sediment Transport Simulation: All sediment transport calculations are made on an individual size class basis. The user may select (with a limit of 20) the number and magnitudes of the particle size-class boundaries. Because particles finer than the smallest and coarser than the largest selected boundaries are treated as being of those sizes, the simulation considers one more size range than selected. The transport characteristics for the size ranges are determined for the geometric mean of the size boundaries and the water temperature of the channel flow. Bed load and suspended transport are assumed to occur in separate layers as described by Bennett (1995).

Assuming transport in equilibrium with bed sediment of known size distribution f_i $(\sum f_i = 1.)$ the model follows Wiberg (1987) in incorporating a Meyer-Peter-type formulation

$$f_i = f_i f_o (t_*' - (t_{*i})_{cr})^{1.5} \tag{4}$$

for predicting bedload transport rate. In (4), $t_*' =$ the nondimensional bottom shear stress corrected for the form drag of bedforms, $(t_{*i})_{cr}$ = the nondimensional critical Shields stress for incipient motion of particles of diameter d_i , and the nondimensional bed load transport

$$f_i = \frac{b_i}{\left[(s-1) g d_i^3\right]^{0.5}}, \tag{5}$$

where s= ratio of specific gravity of particles to that of water, b_i =the unit volumetric bed load transport rate of the size fraction. In the Meyer-Peter and Müller (1949) version of (4), $f_o = 8$, and this is the default value taken for this user-adjustable parameter in the model. If the size distribution of the channel falls into the sand range, the procedures of Bennett (1995) are incorporated to determine a form drag correction for bottom shear stress, whether or not the modeler uses the alluvial channel resistance formulation in flow simulation.

Assuming steady, uniform flow and equilibrium transport in the longitudinal direction, the vertical conservation of mass equation for suspended sediment can be solved analytically to yield

$$C_{zi} = C_{ai} \left(\frac{h-a}{a} \frac{z}{h-z} \right)^{v_{si} / k u_*} \tag{6}$$

where C_{zi}= the concentration at elevation z above the bed and v_{si}=the fall velocity of the sediment. In (6), a =a height above the bed at which the reference concentration C_{ai} is specified; following McLean (1992), the elevation adopted here is a=δ, the saltation or bedload layer thickness. Equation (6) is known as the Rouse equation and the ratio $v_s / k u_*$ as the Rouse number. Even in the simplest situation, computation of the suspended load by integration of the velocity-concentration product over the flow depth must be accomplished numerically. The model uses numerical integration schemes described by Nakato (1984). In (6) $u_* = \sqrt{t_o / r}$,

the shear velocity, wherein t_o = bottom shear stress and r =unit weight of the fluid. Zyserman and Fredsoe (1994) conclude that when bedforms are present the suspended load can best be determined when C_a is evaluated using form-drag corrected or grain shear stress and the Rouse number is computed using total shear stress. For computing reference-level concentration, the model uses a formulation from Smith and McLean (1977),

$$C_{ai} = f_i \frac{C_b g_o S_*^{'}}{1 + g_o S_*^{'}}. \qquad (7)$$

In (7) C_b is the volume concentration of sediment in the bed and is on the order of 0.65, and $S_*^{'} = \frac{t_o^{'}}{t_{cr}} - 1$, called transport strength or normalized excess shear stress. Following McLean (1992), t_{cr} is based on d_{50}, the median bed sediment size. Parameter γ_o is dimensionless with default value=0.004 and is user-adjustable during simulation.

The development in the previous two paragraphs is based on the assumption of a uniform reach of constant bed sediment composition of length sufficient to achieve equilibrium between the bed sizes and the transport. Such situations do not always exist, for example, a sand-transporting flow in a cobble-bedded reach or sand and silt depositing flow entering a reservoir or an over-bank expansion. The transport algorithms account for such dis-equilibrium, on a size-by-size basis by computing f_i and C_{ai} for the input size distribution to an increment of channel segment, as well as from its bed size distribution. Considering channel hydraulics, the largest feasible transport rate is selected. In situations where there may be deposition from an entering flow, fall-velocity, depth, and average flow velocity are considered in computing the applicable downstream value of C_{ai} . Equations (4)-(7) embody the only transport relationships incorporated in the sediment model and although they will reasonably well represent transport processes into the silt-size range (d<0.0625mm), they will not adequately simulate erosion of deposits of cohesive materials.

Bottom Size Composition and Elevation Accounting: An active layer concept is used to track bed surface size composition changes. Its use is based on the physically reasonable assumption that only the near-surface fraction of the bed can be sorted through by the flow during a realistic simulation time step. As long as there is sediment in an increment of a channel segment, the active layer is present, its thickness is set at some fraction of flow depth. The default fraction is 0.15 and the parameter is user-adjustable. For sand bed channels, a reasonable value is 0.3, which is a commonly observed ratio of bedform height to flow depth. Active layer composition is used to set the size fractions, f_i, at the start of a transport time step. During the step, only sizes present in the active layer may be eroded from it. To satisfy mass conservation, sediment is added to the active layer during a time step in the amount that the upstream supply rate exceeds the downstream export rate. Similarly, up to the amount present therein, sediment is taken from the active layer to supply the required excess of export over import rate for that size. If not enough sediment is available in the active layer to satisfy the excess capacity, the export rate is adjusted downward accordingly. At the completion of the time step, active layer composition is re-adjusted based on the new hydraulic conditions and considering the changes in sediment volume during the step. If layer volume remains constant and net deposition has occurred, the

excess sediment from the active layer is added to a second layer called the inactive layer. If the active layer is deficient in volume, an appropriate amount is added from the next underlying layer, if available. For stable hydraulic conditions, if net erosion has occurred over a particular channel increment, the second layer may not be present. The user can specify as many layers of different sediment size composition as desirable in a simulation scenario. Once sediment has been incorporated from one of these layers into the active layer, the original layer's surface elevation is adjusted downward to conserve mass; no sediment may ever be added to an original layer.

The active layer concept also permits simulation of armoring, the development of a coarse protective layer that does not allow erosion, on the surface of otherwise transportable underlying deposits. If a size fraction, present in appreciable proportion (arbitrarily set at 5 percent) in the active layer, can not be transported by prevailing hydraulic conditions, then new rules are established for adjusting the active layer composition. The volume of the active layer is set so that it contains just enough of the limiting size and coarser particles to form a one-diameter layer on the surface of the channel bed if all finer sediment were eroded from the layer. The amount of material in the active layer is then fixed until hydraulic conditions again suffice to transport the sediment size that established the original restriction. If this happens, the previous rules of active layer adjustment are applied.

Channel bed elevation accounting is accomplished by keeping strict track of sediment solids volume on a size-by-size basis in each of the layers between each pair of cross-sections in a channel segment. Because the section shapes and distance between them is known, the elevation can be determined by numerical integration until the encompassed volume equals the amount stored in the increment. The bed porosity is assumed to be 0.3.

EXAMPLE APPLICATION: DAM REMNANT REMOVAL, MUSKEGON RIVER

A 6 m hydroelectric dam constructed during 1916 on the Muskegon River in Big Rapids MI was partially removed in 1966. Aggradation of sediment from upstream had resulted in partial filling of the dam pool and the removal of 4.3 m of the dam resulted in transport of an unknown volume of sediment from the impoundment area. Transport and deposition of these sediments significantly changed the characteristics of the downstream channel. In support of a proposal by the city of Big Rapids to remove the remaining 1.7 m of the dam, USGS was retained to predict and then to monitor the behavior of present-day channel deposits subsequent to the remnant's removal. Using stratigraphy and cross-sections from Westjohn (1997), it was determined that the present-day deposit is about 1 m deep at the dam and tails out to the original bed material cobbles approximately 1.8 km upstream. The mean size of the deposited sediment averages 0.97 mm and that of the original bed averages 64 mm. The study reach was modeled as a network of two channels with the upstream segment ending at the dam site. Figure 2 shows a screen plot of model results after 10 days of average July flow for the Muskegon River and figure 3 shows a more detailed longitudinal profile for the reach upstream of the dam after one year of average monthly flows. The simulation indicates that the channel should have returned nearly to its original profile during that time span.

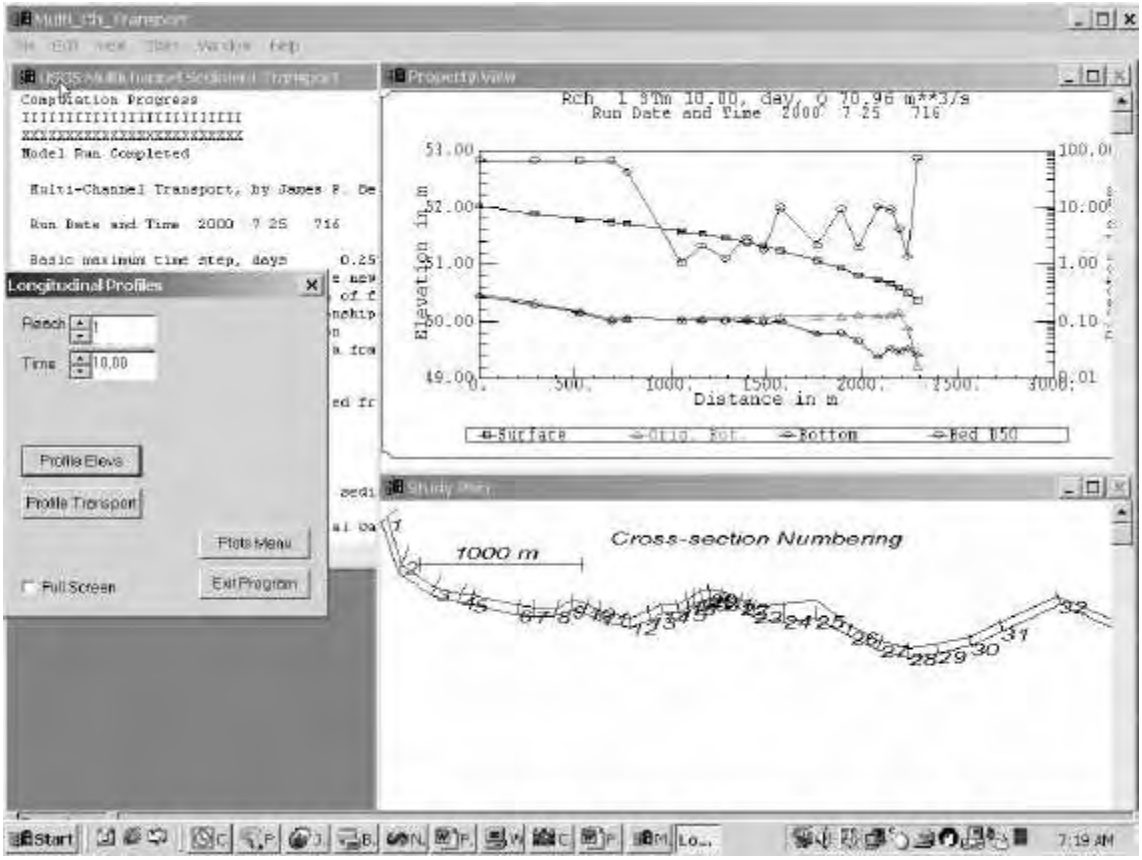

Figure 2. Screen plot of model results after 10 days of simulation following removal of the Muskegon River dam remnant. Property View shows longitudinal profiles of original and 10-day bed elevation and the corresponding bed surface median particle diameters for the channel reach upstream of the dam.

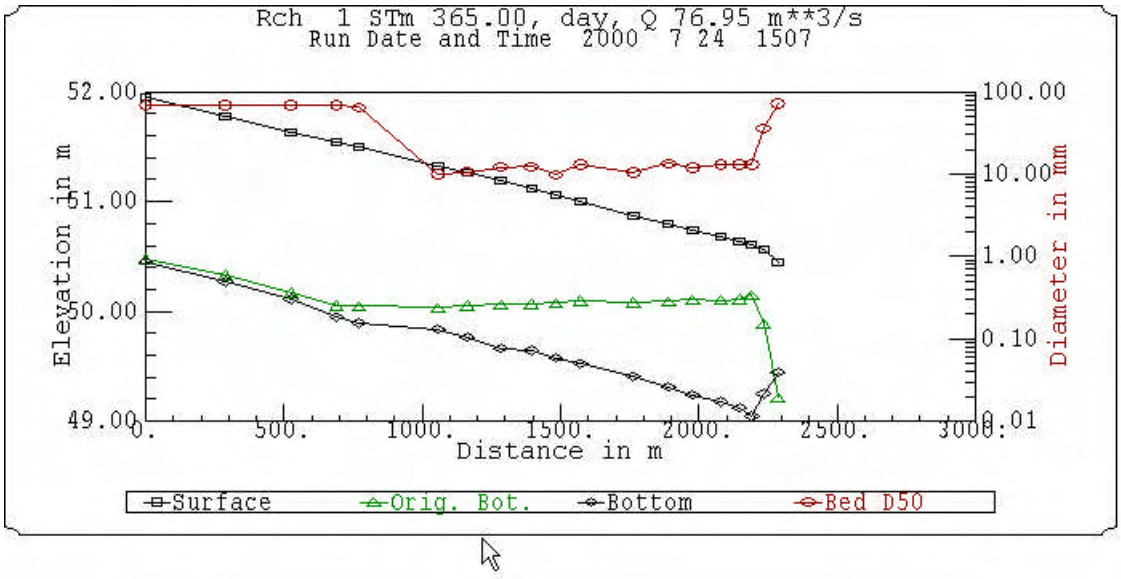

Figure 3. Original and one-year simulation longitudinal bed elevation and surface particle size profiles for the reach upstream of the removed Muskegon River dam remnant.

REFERENCES

Bennett, J. P., 1995, Algorithm for resistance to flow and transport in sand-bed channels, Jour. of Hydraulic Engineering, Am. Soc. of Civil Engineers, 121(8), 578-590.

Chaudhry, M. H., 1993, *Open-channel flow*, Prentice Hall, Englewood Cliffs, NJ 08763, 483 pp.

Cunge, J. A., Holly, F. M., Jr., and Verwey, A., 1983, *Practical aspects of computational river hydraulics*, Pitman Publishing Ltd., London, UK, 420pp.

Henderson, F. M., 1966, *Open channel flow*, The MacMillan Company, Toronto, Ontario, Canada, 522 pp.

McLean, S. R., 1992, On the calculation of suspended load for noncohesive sediments, *J. Geophys. Res.*, 97(C4), 5759-5770.

Meyer-Peter, E., and Müller, R., 1948, Formulas for bed-load transport, Proc. 2nd Congress IAHR, Stockholm, Sweden, 39-64.

Nakato, T., 1984, Numerical integration of Einstein's integrals, *J. Hydr. Engrg*., ASCE, 110(12), 1863-1868. Smith, J. D., and McLean, S. R., 1977, Spatially averaged flow over a wavy surface, *J. Geophys. Res.*, 84(12), 1735-1746.

Westjohn, D. B., 1997, Stratigraphy, sedimentology, and volume of sediments behind a dam relic on the Muskegon River, Big Rapids, Michigan, USGS, WRIR, 97-4069, 14pp.

Wiberg, P. L., 1987, Mechanics of bedload transport, Ph. D. Dissertation, U. Washington, Seattle, 133 pp.

Zyserman, J. A., and Fredsoe, J., 1994, Data analysis of bed concentration of suspended sediment, *J. Hydr. Engrg*., ASCE, 120(9), 1021-1042.

SPACING OF STEP-POOL SYSTEMS IN GRAVEL-BED RIVERS

By A.R. Maxwell, Graduate Researcher, Washington State University, Pullman, Washington; A.N. Papanicolaou, Assistant Professor, Washington State University, Pullman, Washington

Abstract: The spacing of step-pools in high-gradient streams is examined experimentally. Results from a laboratory study are compared with existing field data, and found to agree well with previously established trends. An equation is presented which describes the spacing of pools within a step-pool system, within certain limits of applicability. This equation accurately predicted the spacing in a field case study, as well.

INTRODUCTION

Step-pools defined: High-gradient gravel bed rivers are common in many parts of the world, typically in mountainous areas such as the Cascade Range in the United States. Such rivers are important in conveying spring runoff, particularly in view of the late spring rain-on-snow events common in the Pacific Northwest, which tend to cause flooding in the lowlands. This behavior has been observed by the first author over a number of years, and of further importance is the high likelihood of roadway failure due to the erosive power of the seasonal high flows. With the decrease in funding for National Forest Service road maintenance (US Dept. of Agriculture, 2000) for example, the importance of proper construction of culverts and bridges at roadway crossings is even more critical, as washed-out structures may take years to replace. Creating a pseudo-natural streambed can prevent excessive erosion due to a discontinuity in the stream, created by construction of a bridge, culvert, or other structures which affect the riparian environment. Natural streambed morphology in such cases varies from pool-riffle sequences at slopes $S < 0.02$, coarse riffles or cascades at slopes of 0.03 — 0.07, and step-pools at slopes of 0.04 — 0.20 (Grant et al., 1990). This separation of morphological categories by slope has been corroborated by the work of Billi et al. (1998), and is also consistent with the pioneering study of step-pool formation by Whittaker and Jaeggi (1982). The present study focuses on the step-pool, as the formation of this morphology is still controversial in the existing literature (e.g. Abrahams et al., 1995; Billi et al., 1998). The step-pool is characterized by a staircase-like channel profile (Figure 1), formed by large stones arranged in a transverse manner across the channel; the backwater effect produced by this step creates a local pool and acts to dissipate a significant amount of energy (Duckson and Duckson, 1995; Abrahams et al., 1995).

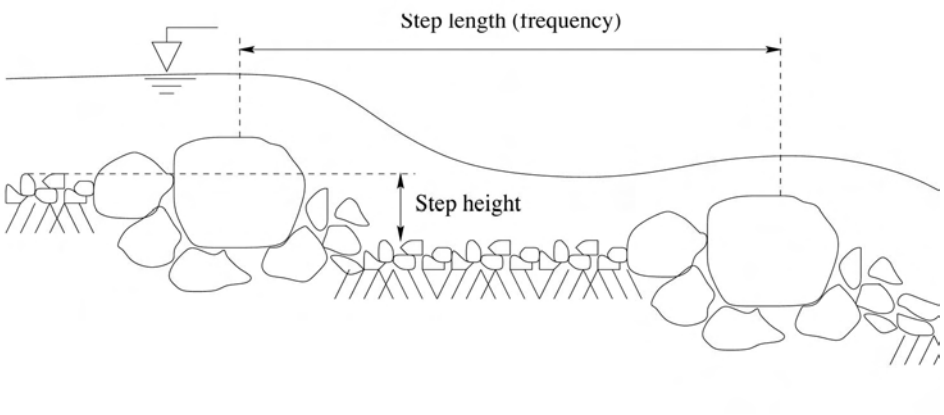

Figure 1. Idealized sketch of a typical step-pool

Previous studies: The existing literature focuses primarily on the qualitative description of step-pools, and formative conditions for this morphology. A combination of laboratory (e.g. Whittaker and Jaeggi, 1982; Whittaker, 1987; Abrahams et al., 1995) and field studies (e.g. Grant et al., 1990; Duckson and Duckson, 1995; Billi et al., 1998) have contributed significantly to the state of knowledge regarding step-pool morphology. Grant et al. (1990), combining results with those of Whittaker (1987), expressed step-pool spacing as a function of channel slope (1)

$$L = \frac{0.3113}{S^{1.188}} \qquad (1)$$

where S is slope in percent and L is step spacing in meters. However, Billi et al. (1998) were unable to reconcile this with their field data. Billi et al. proposed addition of the step height as an additional parameter, and found that a logarithmic formula of the following type (2) was a good fit:

$$L = K_1 + K_2 \ln\left(\frac{d_{step}}{S}\right) \qquad (2)$$

where K_1 and K_2 are constants, and d_{step} is step height; it should be noted that this formula is dimensional in nature. The qualitative aspects of step-pool systems (i.e. spacing and height of steps and pools) are as yet unpredictable, and the present laboratory study seeks to unify existing results, while contributing to engineering design of step-pools in its own right. A laboratory study was deemed most appropriate to study step-pool formation, as this allows control of sediment size, flow conditions, and slope of the channel, as well as enabling more accurate measurements to be made.

EXPERIMENTAL SETUP

The testing for the present study was performed in the R.L. Albrook Hydraulics Laboratory of Washington State University. The primary test apparatus was a tilting, water-recirculating flume (Figure 2) which is 21 m (70 ft) long, 0.91 m (3 ft) wide, and 0.61 m (2 ft) deep. One side of the flume was transparent acrylic, which permits side viewing of the flow, and the slope of the flume is variable from —0.5-14%. Water flow was provided by pumping from a large, semi-enclosed

sump, located under the flume, and volumetric flowrate was measured with a magnetic flowmeter. A total station instrument was used to measure bed changes, and straightedges were used to measure flow depths.

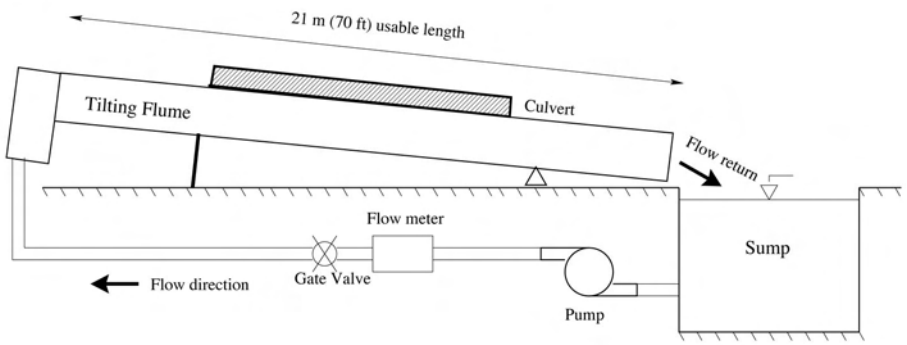

Figure 2. Schematic of flume (not to scale).

Gravel was placed in the culvert and flume to provide a countersunk depth of approximately 35% of the culvert diameter. Particle size ranged from 6 mm (1/4 in) to 200 mm (8 in) overall, and three sediment size distributions were tested. A well-graded mixture was necessary to enhance bed stability by particle interlock, as well as minimize groundwater flow (thereby providing greater flow depths and improving fish passage conditions).

Methodology: Various authors (e.g., Bettess, 1984; Suszka, 1991) have shown that sediment motion at high slopes is dependent on the relative submergence of the particle, H/D_{84}, where H is flow depth and D_{84} is the 84^{th} percentile median axis particle diameter. Consequently, the depth and sediment size are significant parameters of interest in the present study.

Each test series with a particular sediment size distribution and bed slope was begun by thoroughly mixing the sediment in the bed to minimize stratification; following this, the centerline of the bed was surveyed with the total station. Water flow was then increased gradually, to prevent the bed from being eroded immediately by an initial wave of water, and flow was then fixed at a given relative submergence, with flow depth determined by averaging a series of measurements taken along the bed with a straightedge. The test was terminated when stable bedforms had developed, or if massive erosion (failure) was evident. Some degree of subjectivity is inherent in these determinations, but the initial tests were repeated until a consistent methodology was established and repeatability was observed. Following termination of a test, the bed was again surveyed and the next flow scenario was run. When failure was observed, the next slope/sediment combination was tested, repeating the established procedure.

RESULTS

Step-pool formation was observed at all slopes tested (3%, 5%, and 7%), and the bedforms in the culvert were quite obvious, particularly at low flows. The step-pool configuration will form naturally, over a time period which varies depending on flow and slope conditions. It is a

stable bedform, i.e., the larger clasts tend to cluster together and shelter the smaller, more mobile particles (Figure 3).

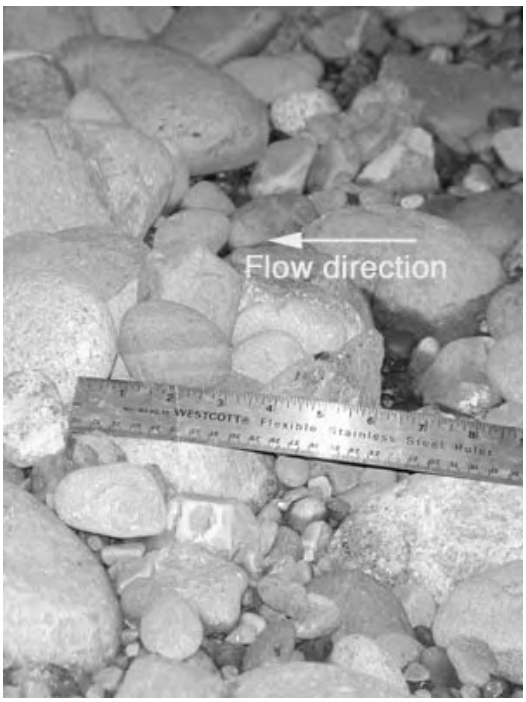

Figure 3. Step formation, smaller particles piled against upstream side (pool).

The average step length from each run was measured, and plotted with the data obtained by Billi et al. (1998) from the Rio Cordon river (Figure 4). As previously noted, various authors (e.g. Whittaker, 1987; Grant et al., 1990) have established correlations between step spacing and channel slope, most of which appear to be site-specific. In addition, the findings by Billi et al. (1998) indicate that step spacing is dependent on step height as well as channel slope. This partially explains the disagreement that exists between the Billi et al. (1998) method and the Grant et al. (1990) and Whittaker (1987) studies. The relationship proposed by Billi et al. (1998) is rewritten here in US customary units as

$$L = 20.4 \ln\left(\frac{d_{step}}{S}\right) - 47.57 \qquad (3)$$

where d_{step} is the step height, S denotes the slope, and L is the step spacing both expressed in feet. To provide a direct comparison between the Billi et al. (1998) study with the experimental data of the present study, the scaling technique discussed by Maxwell and Papanicolaou (1999), is used to scale the flume data to represent a prototype stream identical to that investigated by Billi et al., using stream width as the horizontal scale parameter. The curve-fit to the present data results in the following equation:

$$L = 22.69 \ln\left(\frac{d_{step}}{S}\right) - 39.59 \qquad (4)$$

where d_{step} and L are in feet. Figure 4 provides a comparison between the Billi et al. field measurements and the flume data collected in this study.

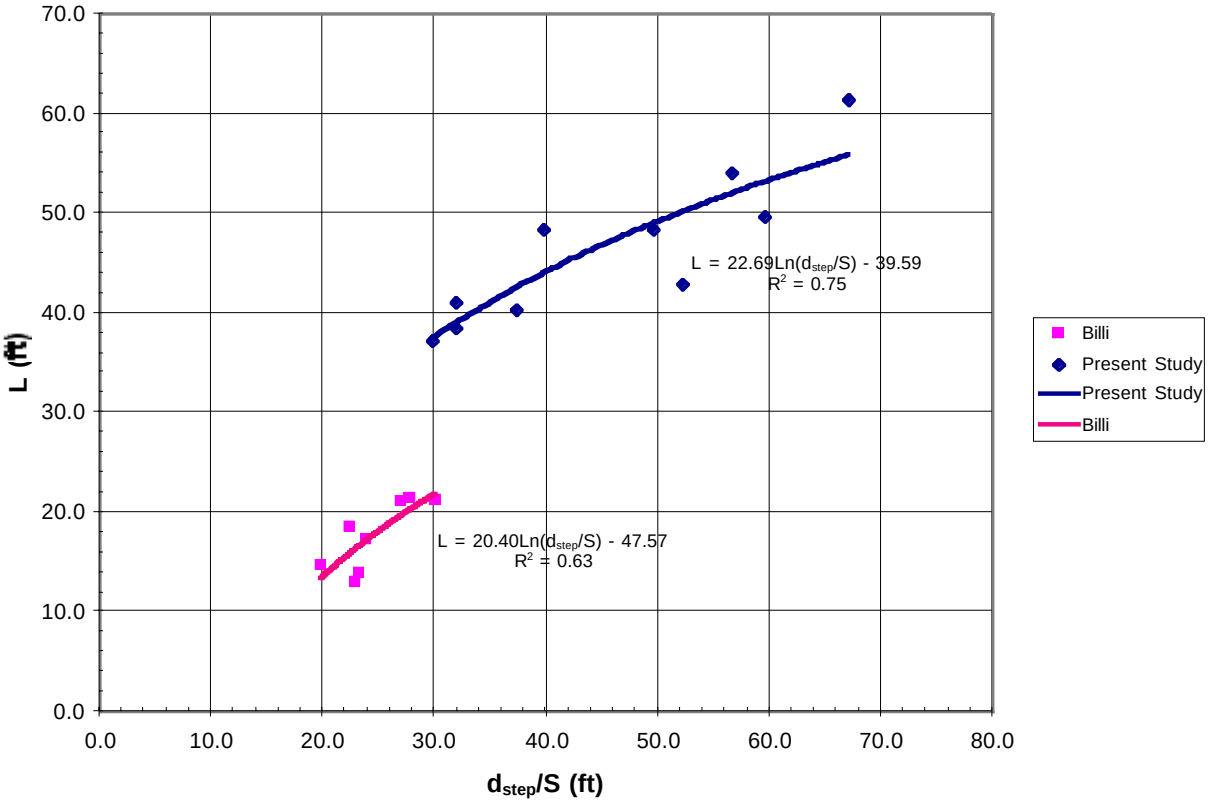

Figure 4. Data from present study and Billi et al. study

The plot of the best-fit equations (3) and (4) in Figure 4 suggests that the Billi et al. (1998) study predicts higher step frequencies than the present study. This is probably justifiable considering that the slope in the Billi et al. (1998) study varies within the 7-19% range while the slope in the current investigation varies within the 3-7% range. However, further comparison of the best-fit lines in Figure 4, represented by equations (3) and (4), reveals that both data sets present similar trends. Equations (3) and (4) have approximately the same slope, with the only difference in the magnitude of the intercept. Although this is partially attributable to the different slope ranges that the two data sets represent, it also implies that there is a potential discrepancy in the determination of the d_{step} during the field measurements of Billi et al. This is a reasonable assertion to make, considering the degree of difficulty involved in measuring step heights of high gradient streams. By contrast, laboratory measurements are generally performed under well-controlled conditions, minimizing any errors measuring d_{step}. To substantiate this assertion the Billi et al. original field measurements for step height are adjusted here by using (5), developed by Maxwell (2000).

$$\frac{d_{step}}{H}\sigma^{0.5} = 2.0\left[\frac{Q}{\sqrt{gH^5}}\left(\frac{D_{50}}{H}\right)^{1.5}\right]^{0.31} \qquad (5)$$

Equation 5 presents step height as a function of volumetric flow rate, Q; gravitational acceleration, g; median particle diameter, D_{50}; and the geometric standard deviation of the sediment mixture, σ. As Billi et al. did not record flow depth data for all cases, one specific (high-flow) case was used to extend the data from the present study to the range of values reported by Billi et al. The adjusted data set is plotted in Figure 5 with the data from the present study. In order to provide a single expression that describes the variation of step spacing L as a function of the ratio d_{step}/S for a slope varying within the range of 3-19%, the adjusted Billi et al. data and the flume data are plotted on the same axes in Figure 5.

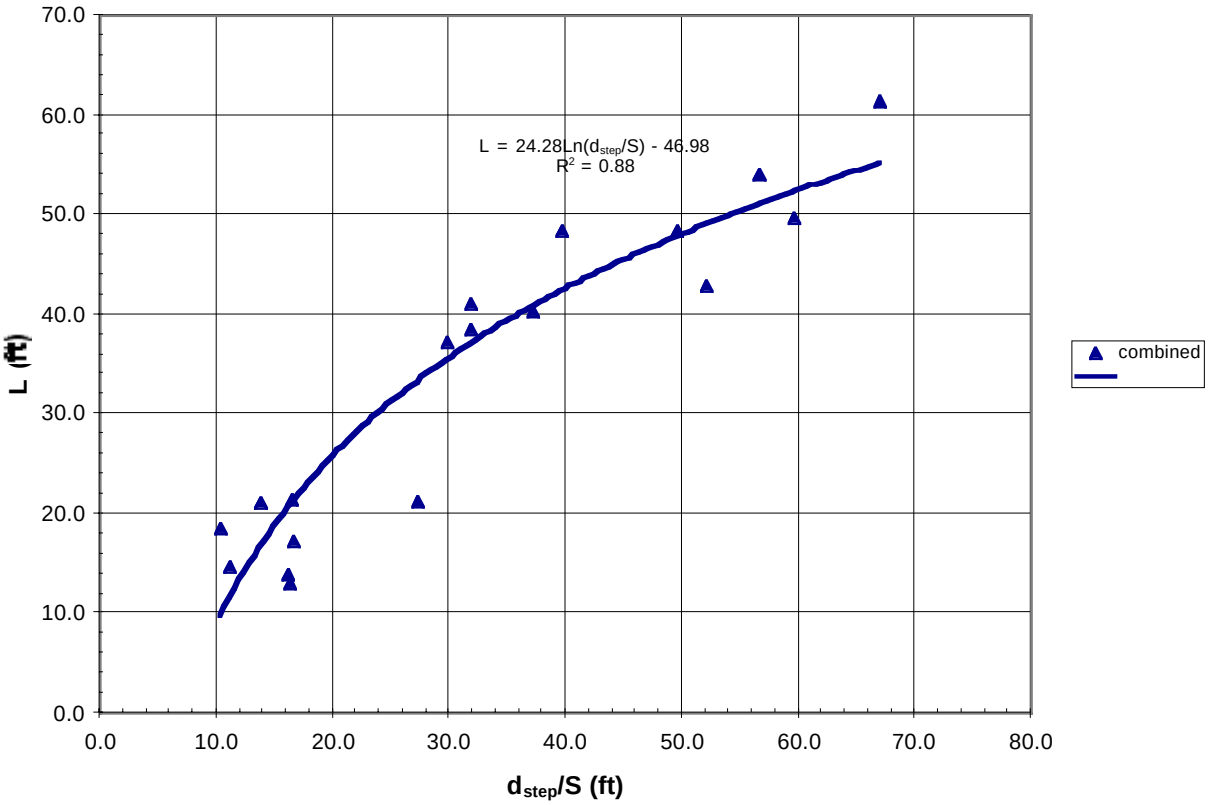

Figure 5. Combined curve fit from present study and Billi et al. study

The combined data clearly show the logarithmic trend reported by Billi et al., resulting in (6):

$$L = 24.28\ln\left(\frac{d_{step}}{S}\right) - 46.98 \qquad (6)$$

The logarithmic fit appears to describe the data very well. Equation (6) is directly applicable to streams of similar width to the Rio Cordon field study, and may be scaled to apply in other cases.

This equation has been applied successfully to a section of the Big Quilcene River in Washington State, which has a width of approximately 22 feet at the measured section and a slope of 4.4%. Step height and length was determined using a total station, and for the measured step height of 1 foot, the step spacing was calculated to be 29 feet. The measured value of the spacing was approximately 28 feet, which is well within reason.

CONCLUSIONS

An equation was developed which successfully predicts spacing of steps in step-pool streams. A combination of laboratory and field work was employed in the process, and the resulting equation is applicable to streams of similar width. It is hoped that this study will further interest in step-pool morphology, as well as contribute to design of step-pool channel configurations in high-gradient stream restoration projects.

ACKNOWLEDGEMENT

Funding for the project was provided by the Washington State Department of Transportation, under contract T9902-27. The assistance of James Schafer, WSDOT Project Manager, is gratefully acknowledged, as is the oversight of the Salmon Research Advisory Committee, whose members include Ken Bates, Pat Powers, and Bob Bernard. Pat Syms and Robert Hilldale were instrumental in experimental setup and testing of the model.

REFERENCES

Abrahams, A.D., Li, G., Atkinson, J.F., 1995, Step-pool streams: Adjustment to maximum flow resistance. *Water Resources Research*, AGU, 31(10), 2593-2602

Bettess, R., 1984, Initiation of sediment transport in gravel streams. *Proc. Instn. Civ. Engrs*, Part 2,Technical Note 407, 77, 79-88.

Billi, P., D Agostino, V., Lenzi, M.A., Marchi, L., 1998, Bedload, Slope and Channel Processes in a High-Altitude Alpine Torrent. *Gravel-Bed Rivers in the Environment*, ed. P.C. Klingeman et al., Water Resources Publications, LLC, Highlands Ranch, CO

Duckson, D.W., Duckson, L.J., 1995, Morphology of Bedrock Step Pool Systems. *Water Resources Bulletin*, AWRA, (31)1, 43-51

Grant, G.E., Swanson, F.J., Wolman, M.G., 1990, Pattern and Origin of Stepped Bed Morphology in High-Gradient Streams, Western Cascades, Oregon. *Geol. Soc. Am. Bull.*, 102, 340-352

Maxwell, A.R., 2000, Geomorphologic Characteristics of High Gradient Gravel Bed Streams. MS Thesis, Washington State University, Pullman, WA

Maxwell, A.R., Papanicolaou, A.N., 1999, Physical Modeling of Sediment In High Gradient Streams, *Proc. 1999 ASCE International Water Resource Engineering Conference*, Aug. 8-12, Seattle, WA

Suszka, L., 1991, Modification of transport rate formula for steep channels. Lecture Notes in Earth Sciences, ed. A. Armanini and G. DiSilvio, Springer-Verlag, Berlin, 59-70

US Dept. of Agriculture, 2000, USDA Forest Service FY 2000 and FY 2001 Annual Performance Plan. March, 2000, Washington D.C.

Whittaker, J.G., 1987, Sediment Transport in Step-pool Streams. *Sediment Transport in Gravel-bed Rivers*, eds. C.R. Thorne, J.C. Bathurst and R.D. Hey, John Wiley & Sons, Ltd.

Whittaker, J.G., Jaeggi, M.N.R., 1982, Origin of Step-Pool Systems in Mountain Streams, *J. Hyd. Div.*, Proc. ASCE, ASCE, 108(HY6)

THE USGS MULTI-DIMENSIONAL SURFACE WATER MODELING SYSTEM

R. R. McDonald, J. P. Bennett and J. M. Nelson;
U.S. Geological Survey, Denver, Colorado, 80225, USA

Abstract: The U.S. Geological Survey (USGS) Multi-Dimensional Surface Water Modeling System is a generic Graphical User Interface (GUI) for computational models of flow and transport in channels. The modeling system is intended to provide the operations program of the USGS the tools necessary to study and evaluate surface water issues including: TMDLs, water rights, channel restoration and habitat assessment. The GUI is a standard graphical modeling interface that provides the user with interactive graphical tools for grid generation, managing model-specific attributes and boundary conditions and visualization of modeling results. The GUI is generic in the sense that it prescribes a fixed input and output data structure that is sufficiently general to be used by any model of flow or transport from 1-dimensional to multi-dimensional. The generic data structure allows easy incorporation of a number of models into the framework. We present progress on the modeling system to date and discuss future directions and goals.

INTRODUCTION

The modeling system described here is being developed to provide user-friendly tools to study and evaluate both flow and constituent transport in channels. Multi-dimensional models are appropriate where quantitative spatial information is required, such as flow velocity, constituent concentration, or channel evolution. Contemporary surface water issues including TMDLs, channel restoration, habitat assessment, and water rights often require this kind of specific spatial information and may benefit from the predictive and heuristic results of careful modeling.

The purpose of this paper is to give an overview of the multi-dimensional surface water modeling system. We will give examples of the capabilities of the modeling system at present as well as discuss future additions. The interface is in a preliminary design and testing stage. Therefore, the arrangement and layout of the graphic tools and controls may change slightly from what is presented here; however, the general capabilities and goals of the modeling system will remain the same.

GENERIC MODELING SYSTEM

SYSTEM ARCHITECTURE: The modeling system is a standard graphical modeling interface for Windows based systems. The interface is built with Visual C++. We use 3D MasterSuite, a sophisticated commercial scientific visualization library developed by Template Graphics Software (2000) based on Silicon Graphics Open-Inventor 3D graphics library. This allows us to rapidly develop professional quality graphics and focus our development efforts on the modeling tools.

The modeling system is generic in the sense that it uses an input and output (I/O) data structure that is sufficiently general for any model of flow or transport from 1-dimensional to multi-dimensional. The generic data structure allows existing models to be incorporated into the framework with relatively simple changes to the model I/O structure. Model specific information

is exchanged between the numerical models and the modeling system through an I/O file. At present, the I/O files use NetCDF, which is a self-describing data format with both Fortran and C libraries for reading and writing data. The NetCDF data format allows model data and attributes to be located by key-names, eliminating the need for formatted data.

System Interface: The basic modeling interface is shown in Figure 1. The interface display consists of a standard menu to access interface commands. Toolbars contain tools used to create or edit graphic objects such as raw topographic data or the numerical grid location and geometry (Figure 1- top and bottom toolbars respectively). The graphics control manages the visualization classes (Scatter, Image, Scalar etc.), their attributes, and the graphic module displayed in the graphics view. The graphics view has two options: a 2D viewer as seen in Figure 1 or a 3D viewer as seen in Figure 2. The view controls have, among other features, the ability to pan, translate, rotate, and zoom the images.

At present there are two graphic modules: a raw data module shown in Figure 1 and a grid module shown in Figure 2. The visualization classes available to the user depend on the graphic module in use. There are two basic visualization classes, Scatter and Image, common to both graphic modules. The Scatter class is used to represent the raw topographic data. There is a suite of editing tools that allow the user to add, modify, or delete the raw data. The Image class controls the viewing of geo-referenced images (Bitmap, JPEG, or TIFF images) that may be imported into the graphic scene and used for onscreen digitizing of topographic features or as a textural backdrop.

Raw Data Module: The raw data module is used as a utility module for viewing and editing raw data and creating the numerical grid. The principal data component of this module is a triangulated mesh of the raw topographic data. The mesh provides both a view of the topographic data on which the numerical finite difference grid will be built and an option for mapping the raw topography onto the numerical grid.

Many coordinate systems and corresponding numerical grid structures are used in flow and transport models. The orthogonal curvilinear system has been widely used in modeling river flows (Nelson et al, 2000). Our initial development efforts have focused on tools for building orthogonal curvilinear grids. The orthogonal curvilinear system has several advantages when used in river channels. For example, the number of grid nodes can be minimized, reducing the computation time, and the system naturally divides local velocity vectors into streamwise and cross-stream components, which are commonly used in analyzing velocity data.

The technique for constructing the numerical grid in the modeling system is outlined in Figure 3. The location of the grid is defined by a number of control points that represent the centerline of the grid. The user places the locations of the control points interactively on the screen. Two control points define a rectilinear grid and three or more points define a curvilinear orthogonal grid. The number of streamwise and cross-stream grid nodes and the width of the grid are defined in a dialog box. A selection of tools allows the location and curvature of the grid to be fine tuned.

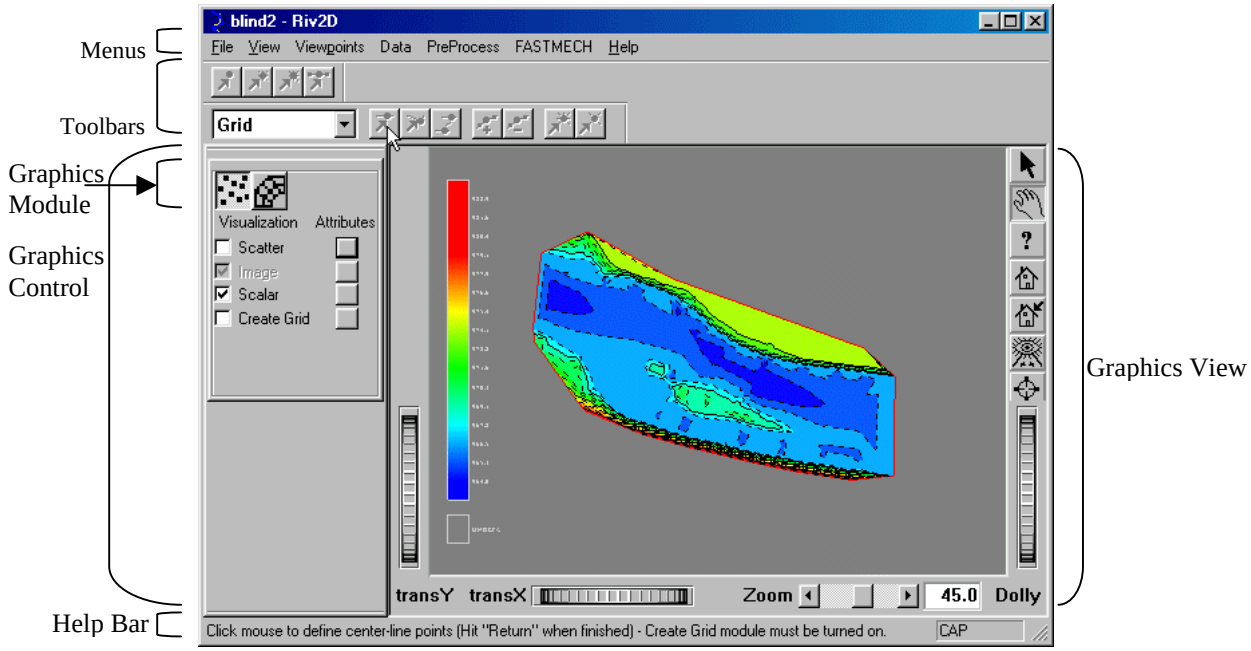

Figure 1: The modeling interface with the raw data module and 2-D viewer activated. The interface is composed of a menu bar, and 4 basic views – toolbars, graphics control, graphics view and help bar. Shown here is an example of raw topographic data (scalar data) expressed in a triangulated filled mesh. The data are from a reach of the Snake River in Idaho.

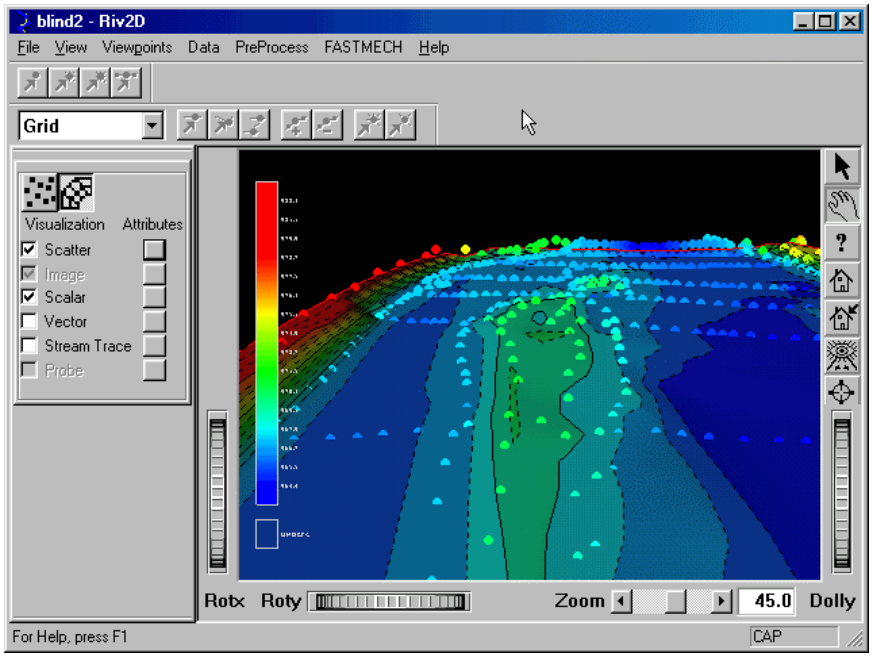

Figure 2: The modeling interface with the grid module and 3-D viewer activated. The numerical grid with the raw data expressed as scatter points are rotated and zoomed in and shown in 3-D. Note the different data objects available for viewing compared with those in Figure 1.

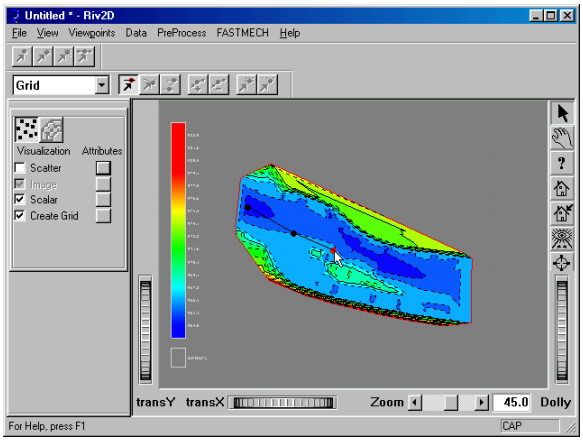

(A)

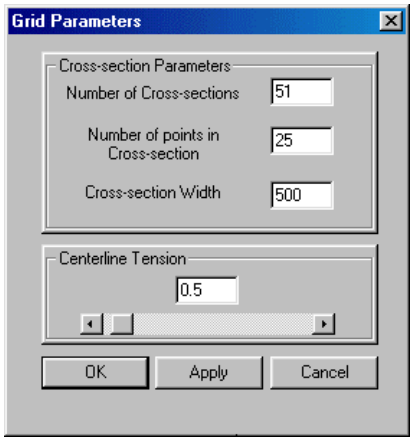

(B)

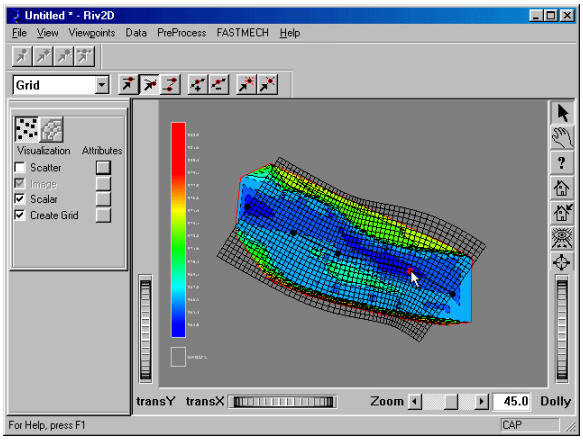

(C)

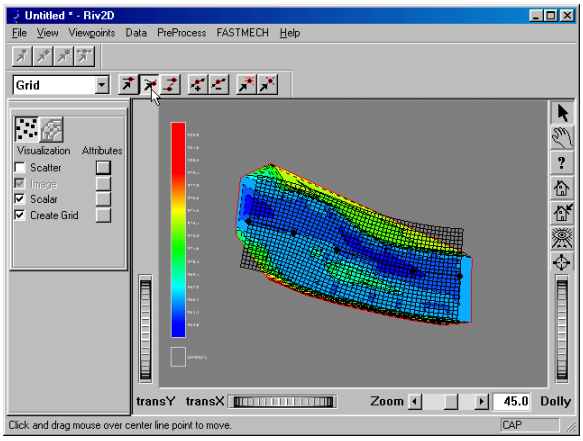

(D)

Figure 3: Creating Numerical Grid. A) The grid location is described by a centerline of control points that are defined by the user. B) The number of nodes in the streamwise and cross-stream directions, and the width of the grid are chosen in a dialog. C) The user can interactively fine tune the location of the grid by dragging individual control points or by moving the entire grid. D) The resulting orthogonal curvilinear grid. A rectilinear grid can be built by defining two control points.

There are numerous possibilities for mapping the raw data elevations onto the numerical grid. Standard approaches such as nearest neighbor and interpolation using the triangulated grid of the raw data are available. An approach that we have found particularly effective where the data are sparse or collected in cross sections is a slight modification of the nearest neighbor approach. The nearest neighbor points are searched in a curved bin with a specified streamwise length and cross-stream width. The curvature of the bin is defined by the local curvature of the grid node being searched. If no points are found, the bin is expanded, preserving its initial aspect ratio, until one or more raw data points are found. The resulting elevation of the grid node is the distance-weighted average of the elevation of the raw data points found. When one considers

that channel topography, following the channel, commonly has much more variation in the cross-stream direction than the streamwise direction, choosing a long and narrow bin that reflects this observation generally produces a good mapping of the raw data onto the numerical grid.

2D Grid Module: Presently, the 2D Grid Module is used primarily to visualize results. The principal data component of the grid module is the 2D numerical grid defined in the raw data module. Any number of scalar or vector data sets may be assigned to the grid and visualized in standard ways. In addition there is a visualization class for streamlines and particle tracking animations on vector fields. Ultimately, the 2D Grid Module will have visualization classes and tools for viewing and editing node properties and both boundary and initial conditions.

Visualization Class Attributes: Data type attributes can be set by choosing the option button associated with the visualization class in the graphic control. For example Figure 4 shows some of the attributes associated with vector and scalar visualization classes. In general, there is broad control of the attributes. Similar control is available for all visualization classes.

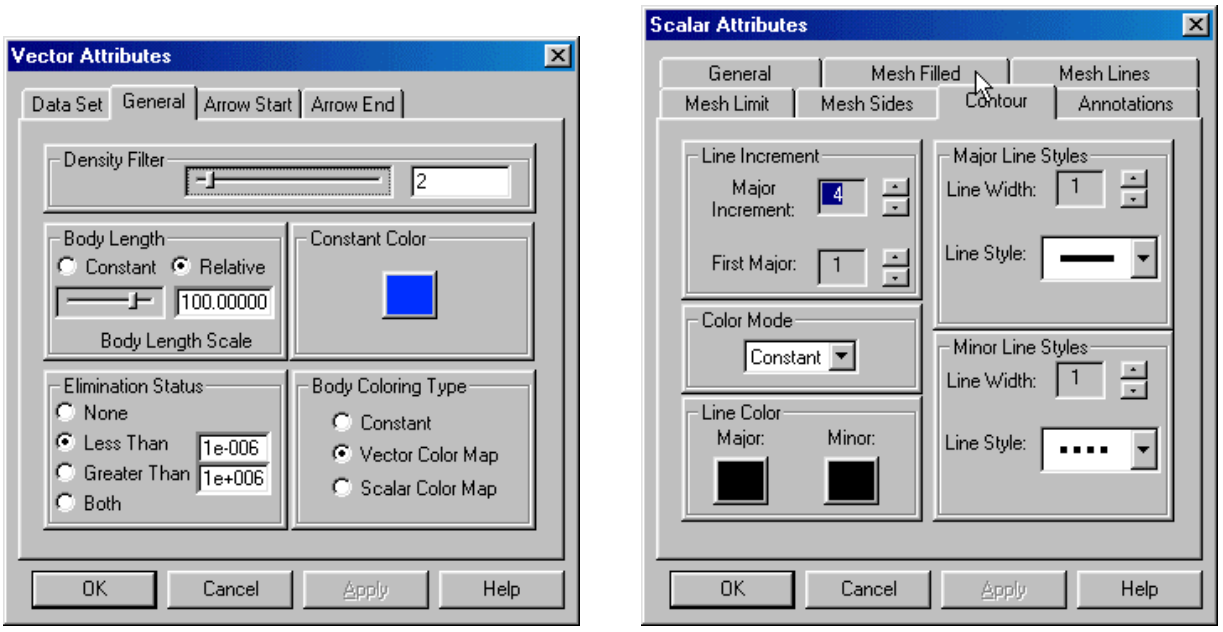

(A) **(B)**

Figure 4: (A) Vector attributes dialog. The General tab selected here shows general vector attributes and their options. The other tabs not shown allow for selection of the data set and attributes associated with the arrows or symbols used for the start and end of the vectors. (B) Scalar attributes dialog. The Contour tab allows selection of the contour color and line style.

MODELING SYSTEM CAPABILITIES AND GOALS

The end product we are working towards is a system capable of modeling flow and transport in a network of channels. The system would be able to model the channel network in one dimension and specific reaches of interest in two or more dimensions. The modeling system at present represents a tangible beginning towards this goal.

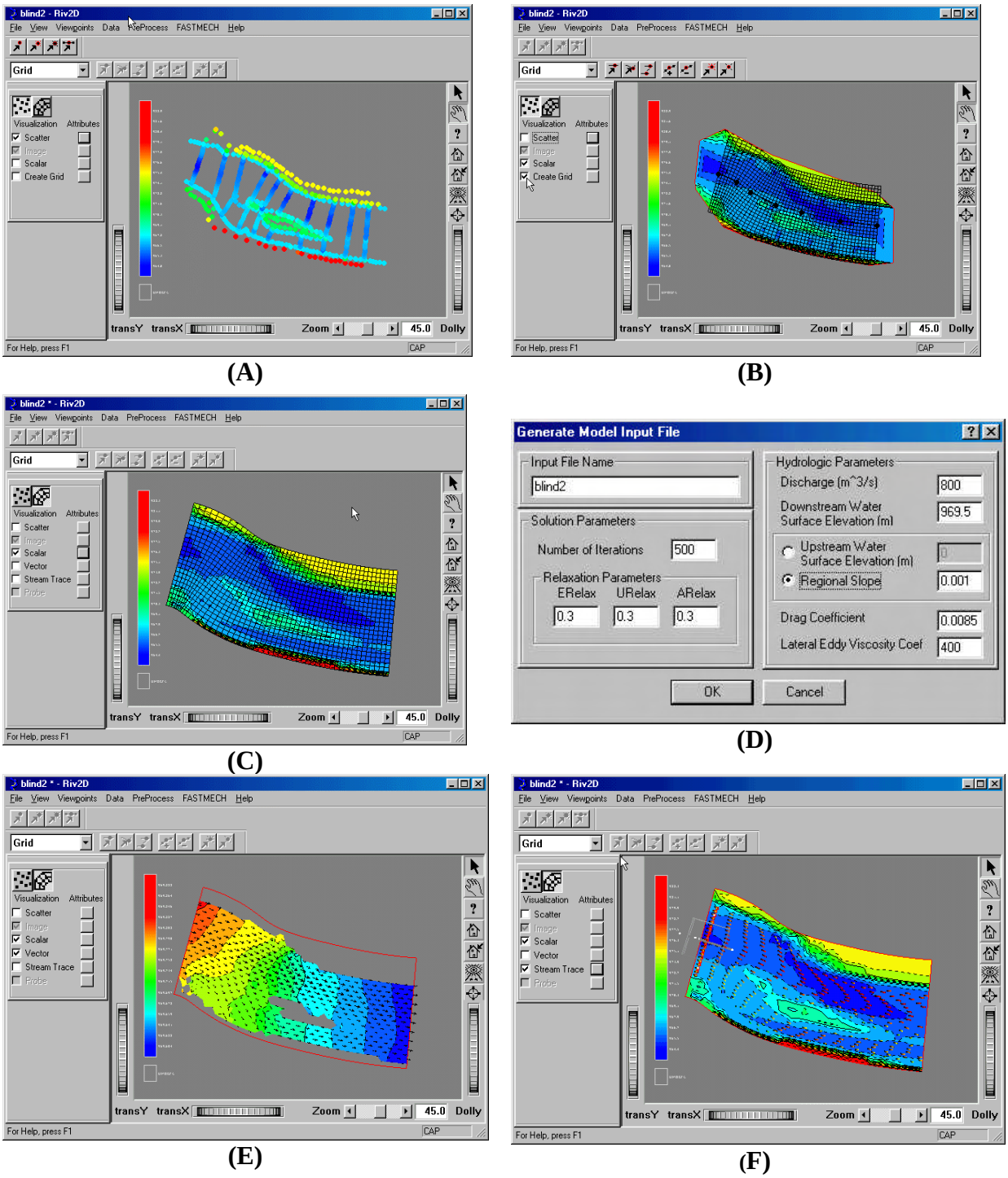

Figure 5: A graphical view of the basic steps to generate a model of flow. A) Import raw topographic data. B) Define grid geometry and location. C) Map raw topographic elevations onto grid. D) Define boundary conditions and model parameters. The results shown here are E) flow velocity vectors and contours of the surface water elevation and F) particle tracks of flow velocity and topography contours.

At the time of this writing, we have a nearly complete 2D flow modeling system that is capable of building, running, and visualizing results of steady-state 2D flow models as outlined graphically in Figure 5. Raw topographic data can be imported into the system and viewed as a scatter data set or as a triangulated mesh. There are tools available for interactively editing the raw data. Geo-referenced images can be imported into the background of the scene. These images are often helpful in editing the raw data or as an enhancement to the view of the data and modeling results. The numerical grid is built and edited graphically. Model parameters are entered easily with dialogs. Finally, there is flexibility in viewing the results with both 2D and 3D views.

Several limitations towards our goal of a truly generic system remain. We are currently developing a suite of tools and data structures for defining both boundary conditions and material properties more specifically. These are also necessary for a complete definition of the generic data structure. With these tools in place, we will extend development with pre- and post-processing tools for 3D grids and flow models. Once the flow-modeling component is in place, we will develop the transport component of the system. Our initial efforts will be aimed at sediment transport while keeping our sights on general constituent transport.

REFERENCES

Nelson, J. M., Bennett, J. P. Wiele, S. M., 2000, Modeling Flow, Sediment Transport, and Bed Evolution. In, Tools in Fluvial Geomorphology, In Press.

Template Graphics Software, Inc., 2000, 3D MasterSuite, 5330 Carroll Canyon Road, Suite 201 San Diego, CA 92121-3758

The use of firm, trade, and brand names in this report is for identification purposes only and does not constitute endorsement by the U. S. Government.

ECO-HYDRAULIC MODEL APPLICATION IN A STEEP RANGELAND WATERSHED

Shawkat Ali, Research Associate, Eco-Hydraulics Research Group, University of Idaho, Boise, Idaho; Peter Goodwin, Associate Professor, Eco-Hydraulics Research Group, University of Idaho, Boise, Idaho; Charles W. Slaughter, Professor, Eco-Hydraulics Research Group, University of Idaho, Boise, Idaho

Abstract

While river basin management has commonly focused on downstream high-order reaches, natural resource managers are increasingly concerned with small, low-order stream systems and riparian environments in the headwaters of river basins. Water, sediment and many water quality constituents for rivers are typically derived from upland contributing watersheds as well as from lower-elevation streamside zones and banks. This is particularly evident for the topographically complex landscapes of the interior Pacific Northwest and Great Basin regions, where meltwater from high-elevation snowpacks is the primary water source for rivers traversing extensive semiarid lowlands. Application of an eco-hydraulic model to a high-gradient stream reach is demonstrated for a rangeland watershed system, in which hydrologic regime of headwaters and mid-elevation sectors is intimately linked to streamflow and channel processes in low-elevation, higher-order stream reaches.

INTRODUCTION

Societal concern for preserving and restoring streams, and increasing developmental pressures to satisfy multiple, often conflicting objectives, are coinciding in major river systems and in small headwater streams. Natural resource managers are increasingly concerned with relatively small, low-order stream systems and riparian environments located in the headwaters of river basins (e.g., Beschta and Platts, 1986; Leonard et al., 1997). Management actions in flood control and structural flow regulation have commonly focused on downstream river sectors. Consequently, fluvial geomorphology management/stream restoration projects are typically undertaken for selected stream segments or river reaches, such as the Middle Reach of the Russian River (Florsheim and Coats, 1997) or the lower Willamette River (Philip Williams and Associates Ltd., 1996). There is increasing recognition that solving problems in reservoirs, estuaries and coastal receiving waters may rely heavily on management of the headwaters and upper reaches of watersheds. Pressures are increasing on all segments of river systems, from headwater snowfields to tidal estuaries, to satisfy multiple objectives, e.g., flood control, power generation, recreation, navigation, fisheries, domestic and industrial water supplies, wildlife habitat, and irrigation. One consequence is a reexamination of traditional hydrologic and hydraulic approaches in river management (Dunne and Leopold 1978; Havno and Goodwin 1995; Beschta et al., 1995; McCully, 1996).

IN-STREAM HYDRAULIC CHARACTERISTICS

The model used to assess flood risk and mass transport may have a significant influence on the comparison of different management approaches. Many physical processes simulated by models are well understood, such as the attenuation of a floodwave in a one-dimensional system (for example, Cunge et al. 1980) and the variation of roughness coefficients with stage (van Rijn 1993). However, most research and model development has focused on one-dimensional models in which floodplains are treated as either offstream storage or are incorporated into the conveyance of the main channel. The conveyance of the entire channel can be estimated as a single section with weighted hydraulic characteristics or by the

"method of slices." Alternatively, the flow on the floodplain can be considered as a stored volume. In the method of offstream storage, there is no dynamic connection between the floodplain and river, and only the conservation of mass component of the St. Venant equations is considered (Cunge et al. 1980). In the method of slices, the channel cross-section is divided into regions of similar roughness, velocity and depth. The total channel flow is estimated by summing the regions or slices (Ackers 1993). Recent findings from the Science and Engineering Research Council Flood Control Facility at HR Wallingford, U.K. (Ackers 1993; Greenhill and Sellin 1993; Willetts and Hardwick 1993) show that errors using these methods can be significant. For example, predictions of discharge can be in error by as much as the bankfull discharge in the main channel (or up to 35% of total discharge) under some circumstances.

Most research on the importance of floodplain function has concentrated on the lower reaches of large river systems. Questions being addressed in our current study include the role of floodplains in low-order tributaries, and the influences of channel/floodplain interactions on sediment transport. The research is being conducted in a high-relief rangeland experimental watershed.

RESEARCH SITE

This research was conducted in the Reynolds Creek Experimental Watershed (RCEW) in the Owyhee Mountains of southwestern Idaho. RCEW (Figure 1) was established in 1960 for hydrologic research in semiarid rangelands of the interior Pacific Northwest, emphasizing climate, snow and frozen soils, hydrologic processes, streamflow and erosion (Slaughter and Hanson 1998). Reynolds Creek is a third-order perennial tributary to the Snake River, developed in basalts and sandstones overlying Cretaceous granitics. Vegetation is primarily sagebrush/bunchgrass/bitterbrush communities with limited aspen and coniferous forest stands in moist, high-elevation sites. RCEW is 77 % public lands. The primary land use is livestock grazing, with irrigated fields along the creek at lower elevations. Unlike most watersheds, RCEW is carefully inventoried and its hydrologic regime is monitored in detail, including precipitation (16 sites), detailed climate (3 sites representing low, middle and high elevations) and streamflow (7 sites). RCEW thus offers a field laboratory for process research and application of management concepts.

The RCEW landscape (like many western upland watersheds) has high relief, rapid change of topography over short distances, and concomitant steep gradients of climatic parameters, which result in highly diverse vegetation and land use patterns. Elevation within the 234 km^2 RCEW varies from 1098 m to 2195 m. Measured annual precipitation has varied from 163 mm to 1588 mm, with from 20% (lowest, warmest sites) to over 75% (high elevations) received as snow (Hanson and Johnson, 1993). Seasonal precipitation varies strongly with elevation (Figure 2).
Availability of water in lower stream reaches is dependent on rain and snow at upper elevations.

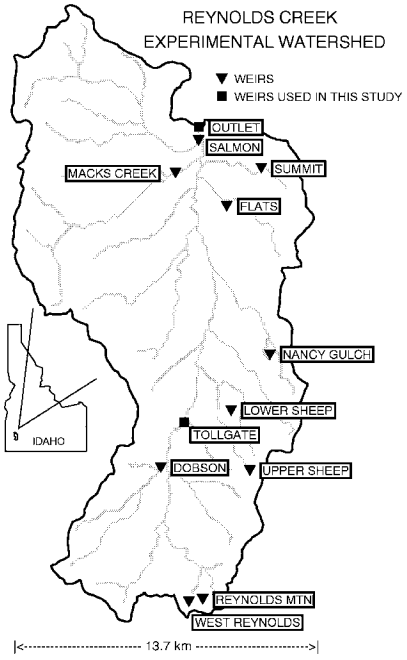

Figure 1. Reynolds Creek Experimental Watershed, Idaho, USA and annually

Runoff is highly variable at all scales (Pierson et al. 1994) and streamflow is highly variable seasonally (Figure 3). Unit-area sediment yield from RCEW increases downstream (with increasing drainage area), in part due to strong influence of mid-elevation rain-on-snow and rain-on-frozen-soil events in winter and early spring prior to melt of upper-elevation snow (Seyfried et al., 1990; Slaughter et al., 1996).

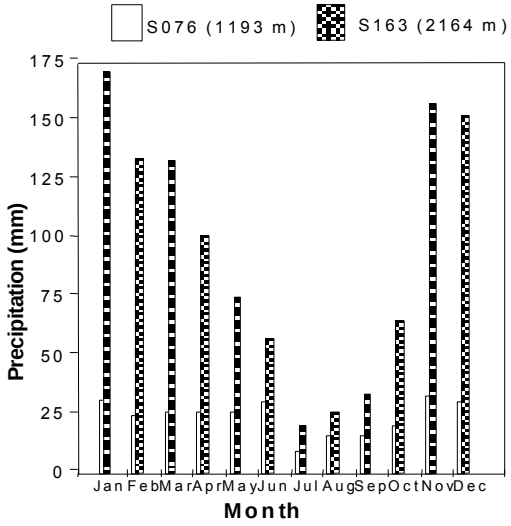

Figure 2. Mean monthly precipitation at two Elevation in RCEW

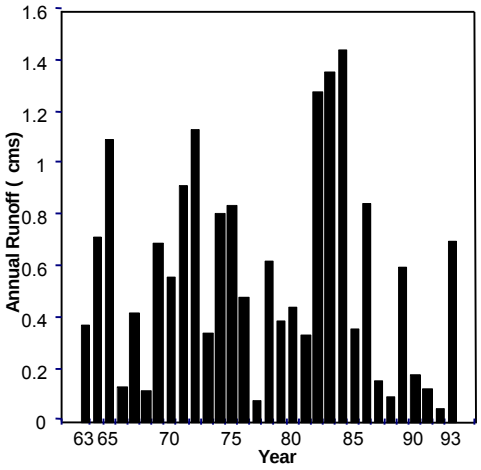

Figure 3. Variation in annual runoff at outlet Weir, RCEW

HYDRAULIC FACTORS

The main channel of Reynolds Creek between Tollgate Weir (elevation 1412 m, contributing drainage area 5444 ha) and Outlet Weir (elevation 1108 m, contributing drainage area 23,400 ha) was chosen to test application of selected hydraulic and hydrologic model concepts to steep-gradient rangeland streams (Slaughter and Goodwin 1998; Slaughter et al 1998). This stream sector (see Figure 1) includes both confined reaches with bedrock control (e.g., immediately downstream from Tollgate Weir) and broad alluvial reaches in the lower, northern valley. Streamside land use is predominantly grazing or irrigated agriculture. A detailed survey, including establishment of a permanently monumented control network, was performed for this stream sector in 1987. Twenty-four channel/floodplain cross-sections were initially surveyed between the two weirs.

Table 1. Stream length between Tollgate and Outlet weirs.

Method	Stream length, m
Map – straight line between weirs	13,203
Map – stream course between weirs	14,082
Survey – straight line segments between channel cross-sections	14,021
Detailed survey of thalweg	17,073

Stream length was determined by direct map straight-line measurement between the two weirs, by tracing the stream course on maps, by straight-line interpolation between cross-sections, and by direct survey of the low-water thalweg through the entire reach between Outlet and Tollgate weirs. Results are shown in Table 1. While the map stream course length and straight-line-between-cross-sections lengths correspond closely (at ~14,000 m), the actual stream length directly surveyed in the channel along the thalweg is >17,000 m, or 22% greater. The selection of appropriate stream length depends upon the problem under consideration. For example, at high flows the cross-section-linked distances are appropriate for flow and sediment modeling, but for modeling in the dry, low-flow season the additional

3 km of channel measured along the thalweg could be important to flow travel time and to measured and simulated water temperatures.

The generalized stream thalweg profile (Figure 4) is smoothly concave. Initial attempts to simulate routing of measured streamflow though the surveyed channel incorporating the 24 channel cross-sections between Tollgate and Outlet weirs, utilizing a conventional 1-D hydraulic model originally designed for large alluvial rivers, were unsuccessful. The model indicated that flow was super-critical throughout the entire stream sector; this result was attributed to use of an estimated value of Manning's *n* of 0.05 for the entire segment, and the steep generalized channel gradient, >0.04 in the upper sectors of the stream (Figure 4). Continuous super-critical flow over 17 km of stream is a physical impossibility; many researchers (e.g. Grant 1997; Chang 1994) have shown that supercritical flows rarely exist in natural rivers except in local reaches.

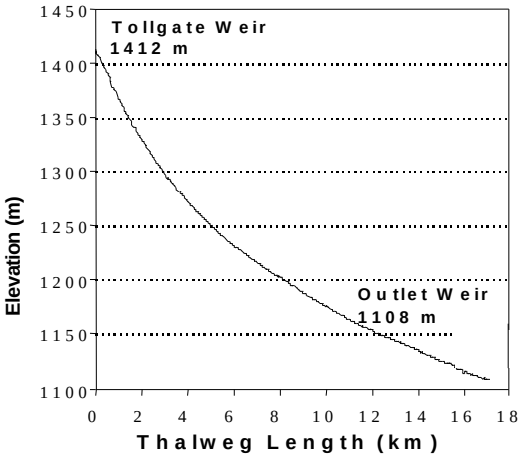

Figure 4. Reynolds Creek thalweg profile

A more detailed look at the stream channel was obtained through survey of additional channel cross-sections (64 total). At more detailed scale, considerable irregularity in stream structure is seen, with bedrock controls and alluvial valley reaches providing localized sectors of steeper and shallower gradient (Figure 5), and the roughness coefficient varies between 0.034 and 0.06. Flow will be super-critical at local channel controls, but sub-critical flow predominates in the intervening shallower-gradient reaches. This result confirms the important role of channel form roughness and local geologic controls in the channel. When a global roughness coefficient was used in the model to force the flow to subcritical conditions, there was poor correspondence with observed flow depths. Under actual conditions of varying flow in high-gradient streams, the roughness varies dramatically with stage and use of a single generalized value of Manning's *n* is inappropriate.

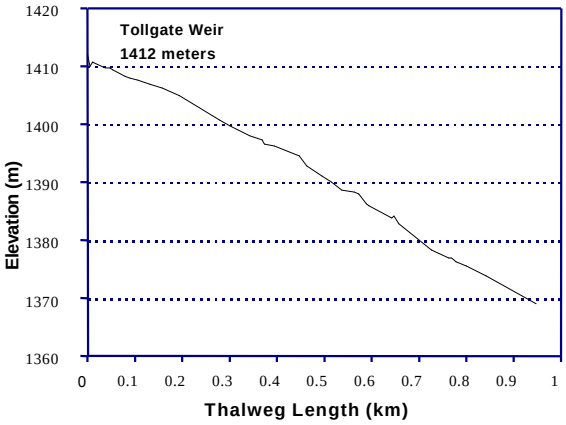

Figure 5. Detailed thalweg profile, upper Kilometer of Reynolds Creek

A question being addressed in our current research is the role of floodplains in low-order tributaries. The bed slope in RCEW is steep and the ratio of bankfull channel width to floodplain width is much lower than in the higher-order reaches further downstream. The variation of travel time with peak flow rate for selected flood events in RCEW is given in Figure 6. It can be inferred that over-bank (floodplain) flows can have strong influence on travel times in low-order headwater streams, similar to the influence demonstrated for mainstem rivers (Slaughter and Goodwin 1998). Most sediment prediction equations vary with the mean velocity of the channel by a power of 2 to 4, so small errors in the velocity may quickly compound to large errors in sediment discharge.

The concept of dominant (channel forming) discharge is widely embraced in fluvial geomorphology, and may be defined as the stream discharge which transports the maximum quantity of sediment over the long term. It is assumed that this flow rate exerts the most amount of work within the channel over a long period of time. Application of this concept in upland, headwater streams is inadequately understood for channels whose slope and form are primarily governed by geologic controls, and it is unclear whether the dominant discharge has physical meaning in such stream reaches. The recurrence interval of the dominant discharge typically increases in more arid and steeper catchments. For example, typical recurrence intervals of 3-12 years were estimated for many streams in southern California (Philip Williams and Associates, San Francisco, Personal Communication 1997). We calculated the dominant discharge for Reynolds Creek by several different methods, with widely varying results (Goodwin et al 1998). Current research at RCEW is investigating the relationship between channel form, bed material composition, geomorphic controls, streamflow and dominant discharge.

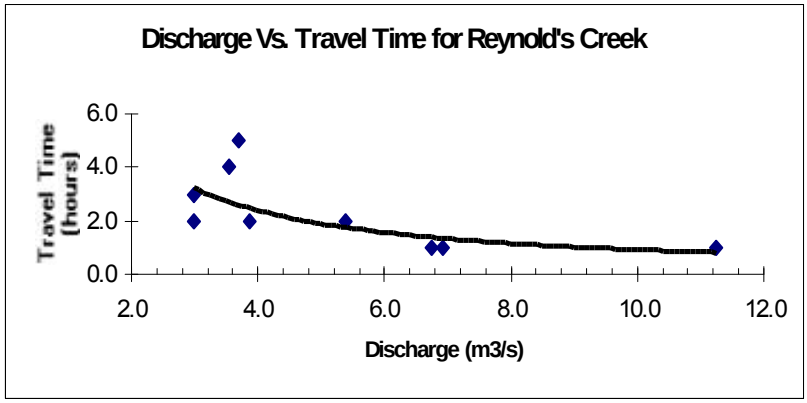

Figure 6. Varying travel times for high flow-events, RCEW

Sediment transport is influenced by the detailed stream channel geometry. The use in models of generalized slope and roughness coefficients can lead to significant errors in estimation of sediment transport at discharges different than the calibrated values. Sediment cannot be mobilized until the

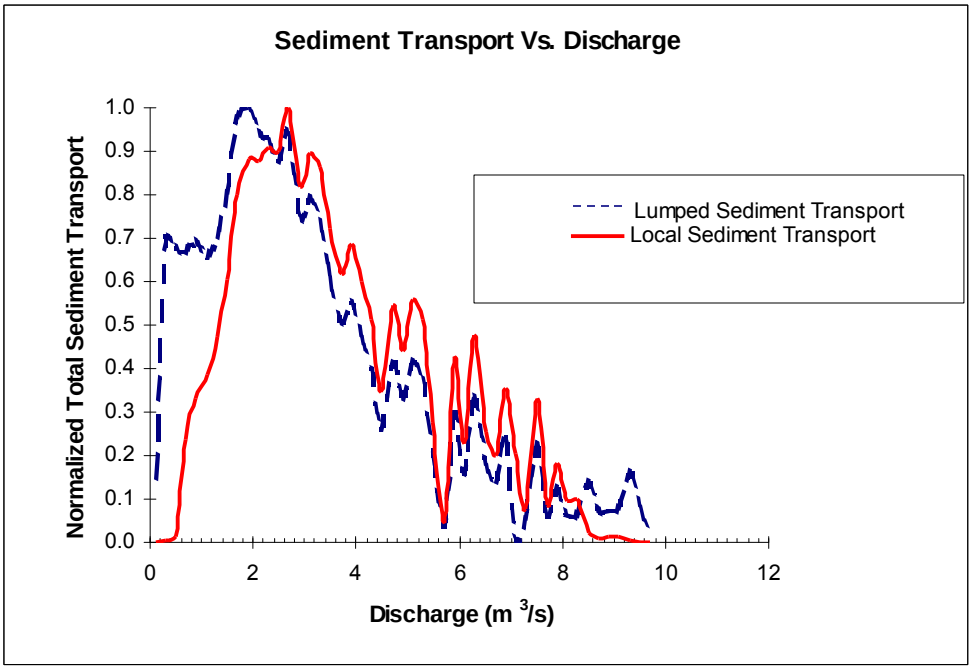

Figure 7. Sediment transport modeled with lumped and detailed (local) data

discharge exceeds a certain stream competence threshold (unique to each reach). We modeled sediment transport in lower Reynolds Creek using both generalized coefficients from a low-resolution survey, and detailed survey information (Figure 7). Normalized sediment transport calculated with coarse "lumped" channel survey data would have incorrectly shown considerable sediment transport at low flows.

CONTINUING RESEARCH

We currently are applying a hydrodynamic simulation model and associated sediment transport model (Danish Hydraulics Institute 2000) to data from the Reynolds Creek stream reach between Tollgate Weir and Outlet Weir. Measured streamflow, channel geometry and bed material data will be utilized in investigation of bedload transport through specific stream reaches under scenarios of high- and low-recurrence interval flows, using standard bedload transport equations, to explore application to high-gradient semi-arid stream systems.

CONCLUSIONS

Low-order, steep-gradient headwaters catchments in western range and forest lands are exceedingly complex. Simplified, generalized descriptive data commonly available to resource managers and simulation modelers may lack adequate site-specific detail for many model applications. While computer models are increasingly used in making decisions and setting priorities for river and watershed management, uncertainty about appropriate input data for such models should be recognized. Emerging river management strategies incorporate ecological, geomorphological, water quality, social and planning considerations. These approaches may require different, more detailed information than the traditional "clearwater" hydraulic analysis traditional in flood planning studies. This study has demonstrated the need for very detailed physical data to support hydrologic, hydraulic and sediment transport model application in a low-order, steep-gradient rangeland watershed setting.

Spatial variability in watershed characteristics, high spatial and temporal variability in climate, precipitation and streamflow, and high-resolution local channel detail must be incorporated into hydraulic models used in analysis and project design. Long-term hydrologic records allow exploration of other questions such as determination of dominant discharge for specific stream sectors (Goodwin et al., 1998). These types of information developed for Reynolds Creek Experimental Watershed will be utilized in further testing selected hydrologic/hydraulic models, previously utilized in higher-order rivers, in this rangeland stream system.

ACKNOWLEDGMENTS

This paper is largely based on material submitted for journal publication (Slaughter, Goodwin and Marbury, accepted). Research was supported by the Eco-Hydraulics Research Group, University of Idaho, Boise, Idaho, and the Northwest Watershed Research Center, USDA-Agricultural Research Service, Boise, Idaho.

REFERENCES

Ackers, P., White, W.R. 1973, Sediment transport: new approach and analysis. Journal of the Hydraulics Division, ASCE, 99(11), 2041-2060.

Beschta, R.L., Platts, W.S., Kauffman, J.B., Hill, M.T., 1995, Artificial stream restoration: money well spent or an expensive failure? Streamnotes October 1995, Stream Systems Technology Center, USDA Forest Service, Ft. Collins, CO, 7 p. (http://www.stream.fs.fed.us/streamnt).

Danish Hydraulic Institute, 2000, MIKE 11 Web Site - River Modeling Software, http://www.dhisoftware.com/mike11/

Beschta, R.L., Platts, W.S., 1986, Morphological features of small streams: significance and function. Water Resources Bulletin 22(2), 369-379.

Chang, H.H., 1998, Fluvial processes in river engineering. Krieger, 432p.

Cunge, J.A., Holley, F.M., Verwey, A., 1980, Practical aspects of computational river hydraulics. Monographs and Surveys in Water Resources Engineering, Vol. 3. Pitman, London, 240 p.

Dunne, T., Leopold, L.B., 1978, Water in Environmental Planning. W.H. Freeman, San Francisco, CA, 818 p.

Florsheim, J., Coats, R.N. Coats, 1997, Dynamic equilibrium as a model for restoration in rivers and wetlands. pp. 69-82 IN Sommarstrom, S. (ed). Proceedings Sixth Biennial Watershed Management Conference. Water Resources Center Report 92, University of California, Davis, CA.

Goodwin, P., Slaughter, C.W., Marbury, R., 1998, Dominant discharge as a design criteria in river restoration. Proceedings Wetlands Engineering & River Restoration Conference 1998, American Society of Civil Engineers, 23-27 March 1998, Denver, CO. CD-ROM.

Grant, G.E., 1997, Critical flow constraints on flow hydraulics in mobile-bed streams: a new hypothesis. Water Resources Research 33(2), 349-358.

Greenhill, R.K., Sellin, R.H.J., 1993, Development of a simple method to predict discharges in compound meandering channels. Proceedings Institution of Civil Engineers: Water, Maritime & Energy 101, 37-44.

Hanson, C.L., Johnson, G.L., 1993, Spatial and temporal precipitation characteristics in southwest Idaho. pp. 394-401 IN Management of irrigation and drainage systems: integrated perspectives. Proceedings 1993 National Conference on Irrigation and Drainage Engineering, July 21-23, Park City, Utah. American Society of Civil Engineers, New York NY.

Havno, K., Goodwin, P., 1995, Towards an integrated approach for hydrologic, geomorphic and ecologic understanding of river corridors. Discussion Paper in Seminar 2: Hydraulic Modeling of Ecological Criteria. XXVI IAHR Congress, London, 6 p.

Leonard, S., Kinch, G., Elsbernd, V., Borman, M., Swanson, S., 1997, Riparian area management. TR 1737-14, National Applied Resource Sciences Center, USDI Bureau of Land Management, Denver, CO, 63 p.

McCully, P., 1996, Silenced rivers. Zed Books, Highlands, NJ, 350 p.

Philip Williams and Associates, Ltd., 1996, An evaluation of flood management benefits through floodplain restoration on the Willamette River, Oregon. Report #1082, Philip Williams and Associates, San Francisco. Report prepared for River Network, 60 pp.

Pierson, F.B., Blackburn, W.H., Van Vactor, S.S., Wood, J.C., 1994, Partitioning small scale spatial variability of runoff and erosion on sagebrush rangeland. Water Resources Bulletin 30, 1081-1089.

Seyfried, M.S., Wilcox, B.P., Cooley, K.R., 1990, Environmental conditions and processes associated with runoff from frozen soil at Reynolds Creek Watershed. pp. 125-134 in Cooley, K.R. (ed.) Frozen soil impacts on Agricultural, Range, and Forest Lands. CRREL Spec. Rep. 90-1. U.S. Army Cold Regions Research and Engineering Laboratory, Hanover NH.

Slaughter, C.W., Cooley, K.R., Hanson, C.L., Pierson, F.B., Hartzmann, R.L., Huber, A.L., Awang, J.B., 1996, Baseline sediment yield from dissimilar headwaters research watersheds. pp. X30-X37 In: Sedimentation Technologies for Management of Natural Resources in the 21st Century, Proceedings of the Sixth Federal Interagency Sedimentation Conference, Las Vegas NV.

Slaughter, C.W., Goodwin, P., 1998, Hydrologic modeling approaches for integrated management of stream systems. pp. I-119 - I-125 IN Proceedings First Federal Interagency Hydrologic Modeling Conference. Subcommittee on Hydrology, Interagency Advisory Committee on Water Data, Vol 1. Water Information Coordination Program, U.S. Geological Survey, Reston VA.

Slaughter, C.W., Goodwin, P., Huber, L., 1998, Upland watershed considerations for comprehensive river restoration. Proceedings Wetlands Engineering & River Restoration Conference 1998, American Society of Civil Engineers, 23-27 March 1998, Denver CO. CD-ROM.

Slaughter, C.W., Goodwin, P., Marbury, R. (Accepted) Watershed considerations for integrated stream modeling. International Journal of Sedimentation Research.

Slaughter, C.W., Hanson, C.L., 1998, Sustained research into hydrology of rangeland headwaters: Reynolds Creek Experimental Watershed, Idaho, USA. Chapter 23, pp. 257-261 IN Haigh, J.J. et al (eds). Headwaters: Water Resources and Soil Conservation. World Association of Soil and Water Conservation. A.A. Balkema/Rotterdam/Brookfield VT.

van Rijn, L.C., 1993, Principles of sediment transport in rivers, estuaries and coastal seas. Aqua Publications, Amsterdam.

Willetts, B.B., Hardwick, R.I., 1993, Stage dependency for over-bank flow in meandering channels. Proceedings Institution of Civil Engineers: Water, Maritime & Energy 101, 45-54.

Figures:

1. Reynolds Creek Experimental Watershed.
2. Annual precipitation at two elevations, RCEW.
3. Cumulative annual streamflow from RCEW, 19 - 19 .
4. Stream profile between Tollgate and Outlet weirs, RCEW.
5. Stream profile, 1000 m reach immediately downstream from Tollgate Weir.
6. Variable travel times with high flows, RCEW.
7. Normalized sediment transport calculated with lumped and detailed channel survey data, RCEW.

CHARACTERISTICS OF FLOW AND EROSION IN A NATURAL STREAM WITH LOESS-TYPE BANKS

By: Rob Hilldale, Grad. Res. Assistant, Dept. of Civil Engineering, Washington State University, Pullman, WA; Athanasios Papanicolaou, Asst. Prof., Dept. of Civil Engineering, Washington State University, Pullman WA

Contact Points: rhilldale@wsu.edu and apapanic@wsu.edu

Abstract A field study is being conducted to determine the effects of turbulence on the undercutting of loess-type banks. Specifically, field measurements of flow and sediment characteristics are being collected at two cross sections within the reach to record any possible changes encountered in turbulent flow patterns and to account for the effects of channel morphology on bank undercutting. Current analytical methods determine bank failure via fluvial entrainment by comparing the shear strength value for the bank material, against a critical bed shear stress induced by the flow (calculated using uniform bed shear stress, e.g. Millar and Quick, 1998). These methods do not account for the role of turbulence in sediment entrainment, thus underpredicting the conditions for which erosion occurs. Recent developments in geophysical flows support the opinion that near-bed turbulence is responsible for channel erosion and bank failure. These studies have shown that in many cases the instantaneous stresses can be up to 60 times greater than the mean shear stress (Jain 1992). The present study accounts for the effects of turbulence and provides a comparison between magnitudes of the turbulent instantaneous stress tensor and that of the soil strength at the basal portion of the bank.

INTRODUCTION

Site Description The area of study is located in the Palouse region of southeast Washington very near the Idaho border. The Palouse region is known for its fertile soil (Steward et al., 1975) and was created by aeolian dust dunes forming rolling hills over the basalt surface. The loess soil is as deep as 200 ft in some places and the basalt is exposed in the lower portions of the valleys. (Alt and Hyndman 1998, p. 205).

Specifically, the reach of interest within Union Flat Creek is located approximately five miles south of Pullman, WA. Flow conditions vary greatly throughout the year. Flow rates are in the range of less than 10 to greater than 100 cfs. Water depths range from four to six feet in the spring to one to two feet in late summer. Channel width averages 60 to 75 ft although the width of the water surface does not exceed approximately 50 ft in winter and 12 ft during the summer. The channel averages 9 ft deep however water depths only reach this level during extreme events. The stream is flanked on both sides by wheat fields. Reed Canary Grass is the dominant plant species found within the channel. Its root systems act to strengthen the cohesive soil present along the banks (Millar & Quick, 1993). While the vertical or near vertical portions of the lower bank are cohesive soils with a d_{50} of 0.10 mm, the bed texture of Union Flat Creek is primarily comprised of cobble sized sediments with a d_{50} of 180 mm. Figures 1 and 2 provide a sketch of a typical cross section and sampling locations in the area of study and Table 1 summarizes the material properties.

Prior to the 1950's, the stream was naturally braided. During that period the creek was forced into one channel to maximize the farmable area in the flat. Since the reconstruction of the channel, it has incised to a depth of approximately nine feet (top of bank to lowest point of bed). During the incision process, fine sediments were carried away and the stream eroded down to the existing layer of cobble and basalt. This boulder/cobble layer is, on average, 13 cm deep and serves as a pavement layer. Below the cobble is a layer of fine gravel and coarse sand, on average 23 cm deep. Below the fine gravel and sand is a basalt layer that extends across the entire Palouse region (Figure 1).

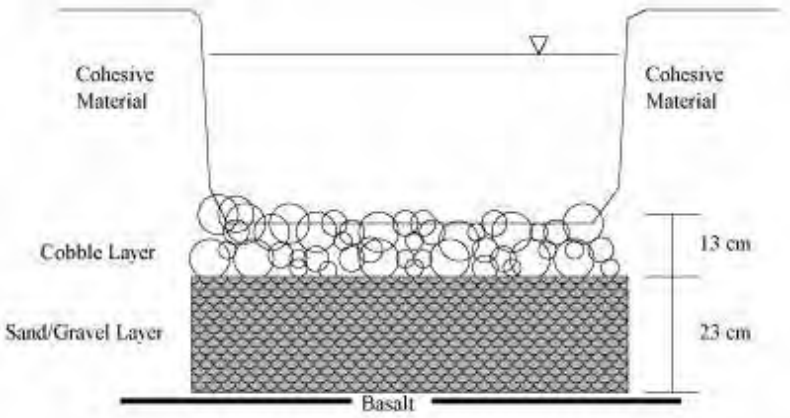

Figure 1: Sketch of the bed, lower bank and substrate material composition.

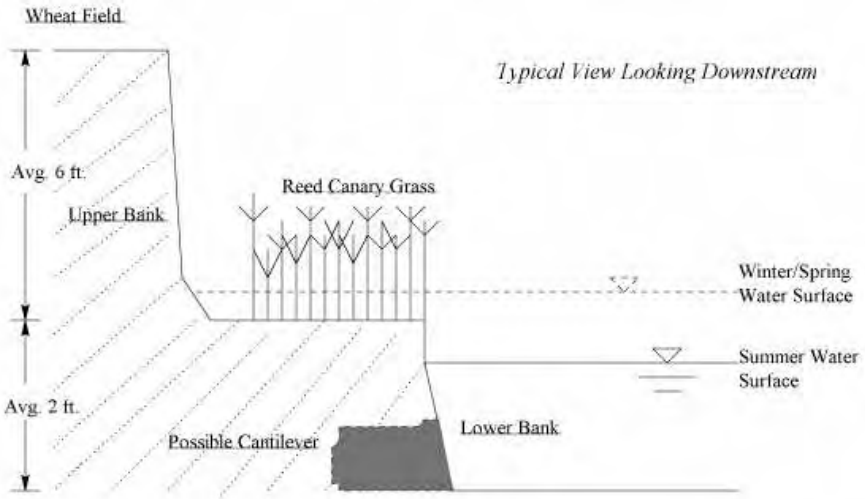

Figure 2: Typical cross section showing sample locations and seasonal water surfaces.

	Field	**High Bank**	**Low Bank**	**Bed**
Liquid Limit	37.5	36.5	41.9	-----
Plastic Limit	30.7	27.7	33.0	-----
Plasticity Index	6.8	9.43	9.0	-----
%Boulders	0	0	0	32
%Cobbles	0	0	0	30
%Gravel	0	14	0	37
%Sand	12	70	60	1
%Silt	78	11	27	0
%Clay	10	5	13	0
$\mathbf{d_{50}}$	0.11mm	0.55mm	0.08mm	180mm
$\mathbf{G_s}$	2.68	2.68	2.68	2.65
c_u	-----	35 kPa (at toe)	15 - 30 kPa	-----
c	-----	-----	2 kPa	-----
f	-----	-----	38.7^0	-----

Table 1: Properties and characteristics of bed material and soil at specified locations given in Figure 2.

The field site was surveyed using an Electronic Distance Measuring device (EDM). Horizontal and vertical information was obtained to define the channel geometry. Three cross sections were surveyed (cross sections #1, #2 and #3) and soil and velocity data are being taken at cross sections #1 (xs-1) and #3 (xs-3) (Figure 3).

Cross section #3 occurs in a slight bend in the channel where the local bed slope is greater than the rest of the reach (2.2% over a distance of 40 ft compared to an average of 0.38% for the rest of the reach). At this location the stream is braided, with three smaller channels developed within the main channel. Flow measurements were taken in the deepest of the three channels. Here flow expansion and separation occurs, creating turbulence characteristics unique to this location.

Cross section #1 is positioned within a straight stretch having no constrictions or braiding. The local slope at cross section #1 is 0.26% and the flow here is fully developed and typical of the study reach. Velocity and turbulence data will be taken at this location in the fall when flows increase from low summer conditions.

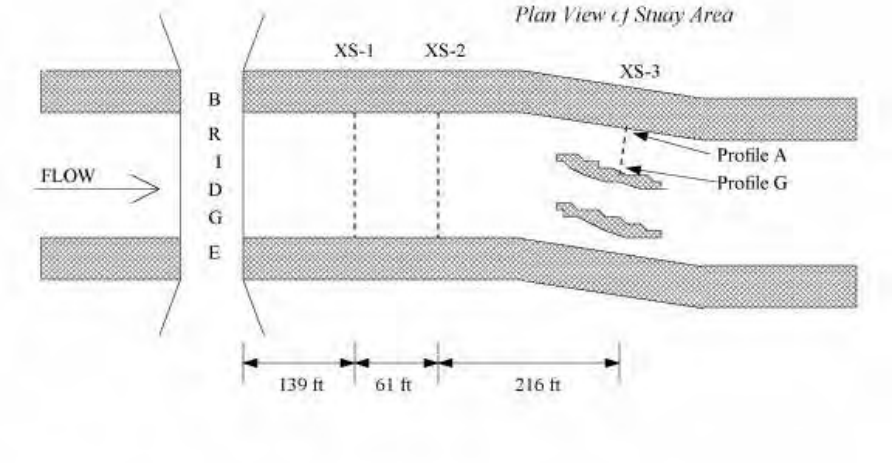

Figure 3: Plan view of study site showing locations of cross sections #1, #2 and #3 (xs-1, xs-2 and xs-3 respectively). Shaded regions are areas of weed growth. Islands are shown in the bend where braiding occurs. Seven profiles of velocity data were taken at cross section #3, the location of profiles A and G are shown.

Critical Review Bank material typically erodes in two manners, as fluvial entrainment and as mass failure (fluvial entrainment is discussed in the Methodology portion). Mass erosion refers to slumping or collapse of the banks when a critical bank height is reached (Millar and Quick, 1998). Critical bank heights for cohesive and partly cohesive banks have been investigated by several authors (e.g. Casagli et al., 1999, Simon and Rinaldi, 2000 and Lohnes and Handy, 1968). These evaluations use a form of the Mohr-Coulomb equation

$$t = c + s\left(\tan f\right) \tag{1}$$

to evaluate the strength of the soil as it relates to planar or rotational failure of the banks (where τ is the shear strength, s is the normal stress, c is cohesion and f is the angle of internal friction). This type of mass failure occurs as a result of either an increase in pore pressures when saturated (Simon and Rinaldi, 2000) or an undercutting of the basal portion of the bank by fluvial erosion (Darby et al., 2000). Mass failure can be evaluated using either effective stress (s') or total stress (s) values. Effective stress is defined as $s' = s - m$ (where m denotes pore pressure). 'Total stress' analyses are used for undrained conditions because this represents the worst case condition (Millar & Quick, 1998). During undrained conditions, s' remains constant even when s increases due to a take up in m. As a result, $f = 0$. This is not to say that the soil is frictionless, rather that undrained soil strength is independent of s. This gives a total stress value equal to undrained cohesion (c_u) (Spangler and Handy 1982, page 433; Atkinson 1993, page 108).

Millar and Quick (1998) evaluated fluvial erosion using their model to obtain total soil shear stress values (τ_{crit}) and compared them to fluid shear stress (τ_{bank}) obtained by $\tau_{bank} = \gamma YS$, where γ = specific weight of the fluid, Y = depth of flow and S = slope. A "total stress" analysis will be used in this paper to evaluate soil strength in terms of fluvial erosion, i.e. $\tau_{crit} = c_u$. These values are obtained in-situ using a Torvane shear stress tester.

Flow stress will be obtained by evaluating turbulence to arrive at a value of instantaneous stress given by

$$t_0 = -\rho u_{\max}^2 = -\rho\left(\bar{u} + u'\right)^2 \quad (2)$$

where $\bar{u}$ is the time averaged velocity and *u'* is the fluctuating velocity in the streamwise direction (evaluated near the basal portion of the lower bank) and ρ is the fluid density. This method accounts for the temporal and spatial effects of the flow, as opposed to an average value (γRS) obtained by Millar & Quick (1998) which assumes uniform flow.

OBJECTIVE

The overarching goal of this investigation is to determine the effects of turbulent flow on the undercutting of loess-type banks. Specifically, a comparison between magnitudes of the turbulent instantaneous stress tensor and that of the soil strength at the basal portion of the bank is made. A secondary goal will be to determine erosive capabilities due to turbulent stresses over a spatial and temporal variation. This will include a comparison of the turbulence characteristics at cross sections #1 and #3.

MEASUREMENTS

A SonTek Acoustic Doppler Velocimeter (ADV) has been employed to acquire velocity data at cross section #1 and will be employed at cross section #3. Evaluation of the data is performed with WinADV software to obtain instantaneous and time averaged values of velocity in a 3D Cartesian coordinate system (x = streamwise direction, y = lateral direction & z = vertical direction; u,v & w are instantaneous velocities in each of the above three directions, respectively). Profiles of velocity and turbulence intensity have been obtained at seven vertical profiles in cross section #3 (Figure 3). Because point G in cross section #3 is the point where flow increases due to the presence of the braid, that point is considered in this analysis.

The evaluation of soil properties required many tests, performed in the lab and at the field site. In the laboratory, a sieve analysis was performed on the bed and bank material to determine size distributions. It was necessary to supplement the sieve analysis of the bank material with a hydrometer analysis due to a significant portion of the sample having diameters less than 0.075 mm (#200 sieve). The results of the hydrometer analysis were combined with the results of the sieve analysis to obtain a complete distribution. According to the USCS the soil is classified as ML based on the plastic and liquid limits. To obtain values of f (angle of internal friction) and c (cohesion), a series of direct shear tests were performed on the lower bank soil. The normal loads applied during the tests ranged from 5 kPa to 30 kPa. A residual shear value for each normal load was obtained and a plot of normal load values (abscissa) vs. residual shear values (ordinate) was made. The resulting slope of the line is f and the y-intercept is c. All lab tests followed the procedures outlined in Soil Mechanics Lab Manual (Das, 1997) and were performed in accordance with proper ASTM standards. The undrained strength (c_u) was determined in-situ with a Torvane shear stress tester. These are the values that will be compared to values of t_0 to determine the critical bank erosion conditions. The Torvane tester is a vane-type shear tester with a diameter of 2.5 cm and vanes having a depth of 0.5cm. The tester is placed on a flat surface of the soil with the vanes embedded and turned slowly with constant pressure until the soil is sheared. The value in kg/cm^2 is read directly from the dial. This is converted to Pascals to obtain a value of stress in kPa.

METHODOLOGY

The backbone of the proposed methodology is based on the consideration that near bed turbulent structures (i.e. sweeps, ejections, inward, and outward interactions) are the primary events causing bank toe erosion (known also as fluvial erosion or bank undercutting). Fluvial erosion refers to the removal of sediment by flow either as aggregates or as individual grains (Millar & Quick, 1998). Therefore, a comparison between the magnitudes of the different turbulent stress components (normal and shear) and the undrained strength of the soil is suggested. The justification here is that current approaches underestimate bank toe erosion since they provide a comparison between a uniform shear stress and the critical strength of the soil. Moreover, most of the present approaches treat the bank toe erosion process as a "black box" phenomenon by ignoring any localized processes that may occur such as, the effects of channel bank shape or channel bank morphology. Specifically, El Shewey et al. (1996) and Clifford (1996) have shown that channel expansion or channel restriction due to the presence of channel braiding or a bend significantly

affects the nature of the flow. In the case of channel expansion (the case studied here, xs-3), separation occurs at the bank toe resulting in flow with higher turbulence production near the water surface. The log-wake law is not applicable in this case and the turbulence intensity profiles do not satisfy the exponential relationship proposed by Nezu and Nakagawa (1993) (Figure 4).

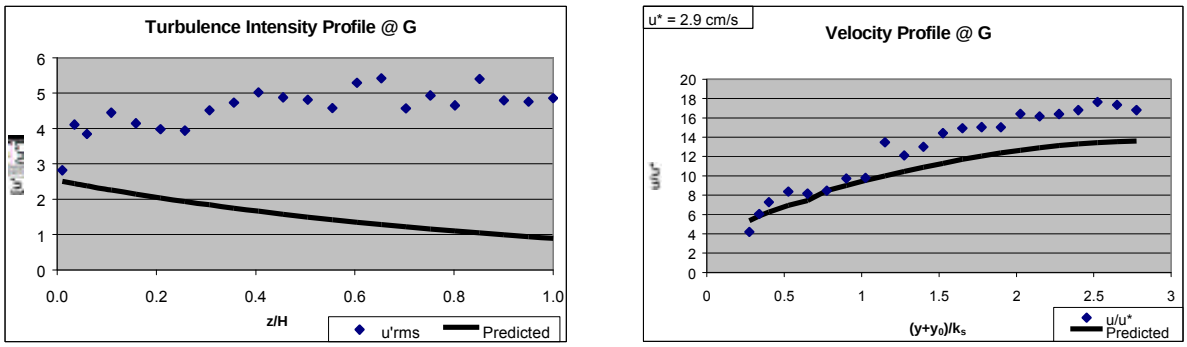

Figure 4: Turbulence intensity and velocity at xs-3, location G. Turbulence intensity is predicted by Nezu and Nakagawa (1993) and the velocity profile is predicted by the log-wake law (Song et al. 1994).

While the undertaken investigation seeks to provide a comparison for the bank toe erosion processes for a straight stretch (no irregular channel morphology is present) and a bend (channel effects are pronounced in the latter case) only the results obtained for the bend are presented. The methodology that is involved here consists of the following steps: 1) Analyze detailed flow measurements along seven vertical locations. This includes 3,000 measurements per point with an average of 26 points per vertical locations for cross section # 3. The measurements are obtained via an ADV. 2) Use the WinADV program to get the time averaged velocities, the Reynolds stress, the velocity standard deviation and skewness, and the PDF (probability density function) of the velocities. 3) Obtain the time series of the velocities. 4) Use the quadrant analysis of Lu and Wilmarth (1972) to determine the nature of coherent structures. 5) Generate velocity profiles and turbulent intensity profiles and compare them to the log law and exponential relationship of Nezu and Nakagawa (1993) respectively. 6) Find the temporal and spatial characteristics of turbulence by using autocorrelation and crosscorrelation functions.

In the present study, the comparison is made between the normal turbulent stress, defined in equation (2), and the undrained strength. Although other comparisons will be reported in a following publication, it was considered here that the normal instantaneous stress is responsible for the bank toe erosion. This is justified here by the findings of Nelson et al. (1995) and Papanicolaou et al. (2000) who have have shown that normal stress expressed as function of the streamwise velocity squared plays a more significant role in sediment entrainment than Reynolds stress $\left(-\rho\overline{u'w'}\right)$. The authors emphasize the importance of both streamwise as well as vertical velocity causing sediment entrainment, however, measurements obtained at Union Flat Creek show that streamwise velocities are three times greater than vertical velocity for the same volume of measurements.

The fluvial erosion in Union Flat Creek occurs at the basal portions of the bank below the root layer that is formed by the Reed Canary Grass. As fluvial erosion continues to undercut the bank, a cantilever is formed. Cantilevers as long as 60 cm have been measured in the reach (Figure 2).

The added strength of the soil provided by the root systems will be accounted here . It has been recorded in the literature (Millar and Quick, 1998) that grass roots provide 3 to 4 times higher soil resistance to fluid forces than soils without roots. This will be accounted here by comparing various soil samples enriched with roots which are obtained from the bank with a reconstructed soil sample having no roots present. Torvane measurements show c_u values as low as 15 kPa at basal portions of the bank where root diameters are smaller and concentrations are lower. Conversely, c_u values in regions of higher root concentration and larger root diameters show values up to 35 kPa. This leaves the basal portions of the banks more vulnerable to fluvial erosion due to their weaker strengths.

Figure 5 provides the time series of the velocities recorded at profile G of cross section #3 (Figure 2). The time series are employed here to determine the maximum value of the instantaneous velocity in the longitudinal direction.

.The u_{max} values obtained at cross section #3 were 171.1 cm/s , measured June 1st, 2000 and 64.28 cm/s, measured July 3rd, 2000. Both of these values were taken from profile G at the right bank (Figure 3). The resulting τ_0 values are 2.93 kPa and 0.395 kPa respectively. Both of these values are significantly less than measured values of soil strength (15 kPa at the weakest locations measured). The condition of no erosion has been verified by close examination of suspended material with a microscope. The material in suspension is biological and exists at a concentration of 11 mg/l. This concentration was obtained by taking grab samples from the stream and passing a known volume through filter paper. The sample was then weighed after drying for 24 hours.

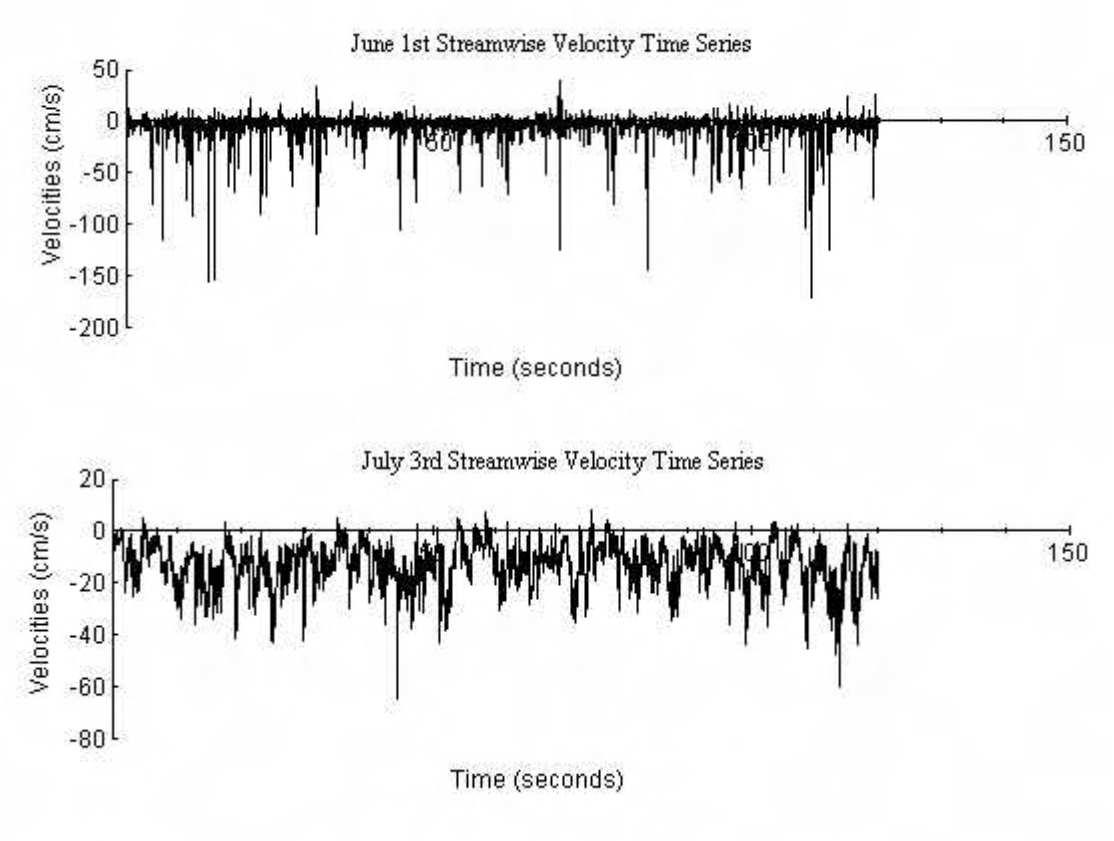

Figure 5: Time series velocities for the streamwise direction (u) for June 1 and July 3.

It is expected that measurements during increased flows will yield shear stresses exceeding the measured undrained strength of the soil in the banks. Turbidity visibly increases during winter and spring months, which strongly indicates that erosive conditions exist in the creek. Measurements during high flows will be taken at both cross sections #1 and #3. This will provide the ability to compare turbulence in a spatial manner within the reach of Union Flat Creek as well as verifying the procedures outlined in this paper.

The root systems from the Reed Canary Grass act to increase the "cohesion" of the soil on the lower bank. Preliminary investigations indicate at least a doubling of soil strength when grass roots of the type mentioned are present.

ACKNOWLEDGEMENTS

The authors would like to thank Dr.'s Dave Yonge, Balasingam Muhunthan and Steve Juul for their technical assistance and Jenny Filipy for her assistance in acquiring data during the project. This project has been funded by the USGS.

REFERENCES

Alt, D.D., Hyndman, D.W., 1998, Roadside Geology of Washington, Mountain Press Publishing Company, Missoula, MT.

Atkinson, J. 1993, An Introduction to the Mechanics of Soils and Foundations Through Critical State Soil Mechanics. McGraw-Hill Book Co., Inc. London.

Casagli, N., Rinaldi, M., Gardini, A., Curini, A., 1999, Pore Water Pressure and Stability: Results from a Monitoring Site on the Sieve River, Italy. Earth Surface Processes and Landforms, vol. 24, p. 1095 - 1114.

Clifford, N.J., 1996, Morphology and Stage-Dependent Flow Structure in a Gravel-bed River. Coherent Flow Structures in Open Channels, Edited by P.J. Ashworth, S.J. Bennett, J.L. Best and S.J. McLellend, John Wiley & Sons Ltd.

Das, B.M., 1997, Soil Mechanics Lab Manual, Engineering Press, Austin TX.

Darby, S.E., Gessler, D., Thorne, C.R., 2000, Technical Communication: Computer Program for Stability Analysis of Steep, Cohesive Riverbanks. Earth Surface Processes and Landforms, vol. 25, p. 175 - 190.

El-shewey, M.I.A., Joshi, S.G., Sharma, S.D., 1996, A Study of Turbulent Flows Through Sudden Open Channel Transitions Using Laser Doppler Velocimetry. FED-Vol. 237 Fluids Engineering Division Conference, vol. 2, ASME.

Jain, S., 1992, Note on Lag in Bedload Discharge. Journal of Hydraulic Engineering, vol. 118, no. 6, p. 481 – 511.

Lohnes, R.A., Handy, R.L., 1968, Slope Angles in Friable Loess. Journal of Geology, vol. 76, no. 3, p. 247 – 258.

Lu, S.S, Wilmarth, W.W., 1973, Measurements of the Structure of the Reynolds Stress in a Turbulent Boundary Layer. Journal of Fluid Mechanics, vol. 60, part III, p. 481 – 511.

Millar, R. G., Quick, M.C., 1993, Effect of Bank Stability on Geometry of Gravel Rivers. Journal of Hydraulic Engineering, vol. 119, no. 12, p. 1343 – 1363.

Millar, R. G., Quick, M.C., 1998, Stable Width and Depth of Gravel Bed Rivers with Cohesive Banks. Journal of Hydraulic Engineering, vol. 124, no. 10, p. 1005 – 1013.

Nelson, J.M., Shreve, R.L., McLean, S.R., Drake, T.G., 1995, Role of Near-Bed Turbulence Structure in Bed Load Transport and Bed Form Mechanics. Water Resources Research, vol. 31, no. 8, p. 2071 – 2086.

Nezu, I., Nakagawa, H., 1993, Turbulence in Open Channel Flows, A.A. Balkema, Rotterdam/Brookfield.

Papanicolaou, A.N., Diplas, P., Dancey, C.L., Balakrishnan, M, 2000, Surface Roughness Effects in Near Bed Turbulence: Implications to Sediment Entrainment. Journal of Engineering Mechanics, ASCE, in press.

Simon, A., Rinaldi, M., 2000, Channel Instability in the Loess Area of the Midwestern United States. Journal of the American Water Resources Association, vol. 36, no. 1, p. 133 – 150.

Song, T., Graf, W.H., Lemmin, U, 1994, Uniform Flow in Open Channels With Movable Gravel Bed. Journal of Hydraulic Research, vol. 32, no. 6, p. 861-876.

Spangler, M.G., Handy, R.L., 1982, Soil Engineering, 4th Edition, Harper & Row Publishers, Inc., New York.

Stewart, et al., Control of Pollution From Cropland. U.S. E.P.A., Report No. 600/2-75-026.

APPLICATION OF MODIFIED EINSTEIN METHOD USING INCREMENTAL CHANNEL GEOMETRY

[1]Patrick S. O'Brien, USACE, New Orleans [2]Alex McCorquodale, P.E., University of New Orleans

[1]Hydraulic Engineer, Hydraulic Design Section, U.S. Army Corps of Engineers, CEMVN-ED-HD, New Orleans, Louisiana 70160-0267, 504-862-1860;
Patrick.S.O'brien@mvn02.usace.army.mil
[2]FMI Professor for Environmental Modeling, Department of Civil and Environmental Engineering, University of New Orleans, New Orleans, LA 70148; jamce@uno.edu

Abstract: Sediment samples are taken at Tarbert Landing, MS throughout the year to estimate the total sediment load at this section of the Mississippi River. Suspended sediment is sampled at 5 depths along 4 verticals. Bed material samples are also taken at each vertical and a composite gradation is computed. Velocities are measured at each vertical and a velocity distribution is developed. The nominal sediment load is the product of the sediment concentration at each sample point times the discharge associated with the area of influence of that point, which is summed over the entire cross section. This procedure assumes that the load in the unsampled zone is a simple extrapolation of the sampled zone. The Modified Einstein method is an established procedure to improve the extrapolation from the sampled to the unsampled zone. The usual procedure is to lump the river section into a single equivalent section. In this study, the river segment is divided into panels corresponding to the areas associated with the four vertical locations. The results from each panel are then summed to obtain the representative load for the river at that cross section. A mathematical software package (MATHCAD™) was employed to complete the Modified Einstein procedure on each panel and subsequently for the entire river section. The load estimates by the Modified Einstein using panel procedure and the composite section procedure are almost identical. However, the Modified Einstein extrapolation gave total loads that were about 20% higher than the nominal loads.

INTRODUCTION

The Louisiana Gulf Coast is experiencing alarming land loss of over 20 mi^2/yr. There are many factors responsible for this loss, including reduced fresh water input, reduced sediment input, reduced nutrient input, increased saltwater intrusion, subsidence and sea level rise. Sediment load in the Mississippi River is emerging as a valuable resource for South Louisiana. If this sediment can be transported to the areas of coastal land loss the rate of land loss can be significantly reduced.

In sediment resource management it is important to quantify the resource. This paper looks at procedures for estimating the unsampled sediment in the Mississippi River. The unsampled load refers to the sediment that is transported in the zone below the lowest sediment sampling point. The thickness of this zone at 90% of channel depth may be as much as 6 feet or more. The nominal load for a measurement station is estimated as the discharge weighted load for each area represented by a vertical. These loads are then summed to get the total load. While this is a

reasonable way to extrapolate the fine sediment component it can lead to large errors of the course sediment load.

Because of its excellent flow and sediment measurement records, Tarbert Landing was selected for a case study of the proposed procedures. The paper provides estimates of the differences between the nominal fine and coarse loads and the respective revised loads calculated by the Modified Einstein (1955) (ME) method. The loads determined by the ME method are calculated by a panel procedure based on the vertical sampling distribution and the standard method using a composite sample for the entire cross section.

SITE DESCRIPTION

Tarbert Landing is located at lower Mississippi River Mile 306.3 as shown in Figure 1. This site is important because it is used to monitor the sediment load of the Mississippi main stem that is available for transport to the Gulf of Mexico (WES 1990). Figure 2 shows a typical cross-section at the measurement section. The bed material is predominantly sand with a median size of 0.35mm (Catalyst, et al 1999). The bed material moves in partly in suspension, partly in the bed layer via large dunes, and also by saltation. The mean water surface slope at the site is $3x10^{-5}$. The Manning's n for the site is approximately 0.025. The flow ranges from 100,000 to 1,200,000 cfs.

Figure 1 - Mississippi River at Tarbert Landing, MS RM 306.3

SAMPLING

Suspended sediment and bed material samples are taken at 4 vertical locations across the cross section. The station numbers corresponding to each vertical are 1400, 2200, 2800, and 3400 feet. Five samples per vertical are taken at depths of 15 %, 30%, 50%, 70%, and 90% of the maximum depth for a total of 20 samples. Figure 2 shows a typical cross-section at the measurement section with the sample points. Point-integrating samplers are used for the suspended sediment samples, the P-61 weighing 105 lb is used at lower flows and the P-63

suspended sediment samples, the P-61 weighing 105 lb is used at lower flows and the P-63 weighing 200 lbs is used at higher flows. Conventional velocity measurements are made at each sample location. Grain size analysis is performed for each suspended sample and tabulated. Bed material samples are taken at each vertical and combined for grain size analysis. A combined suspended grain size analysis representative of the entire cross section is computed and tabulated. A fathometer records the cross section from waters edge to waters edge.

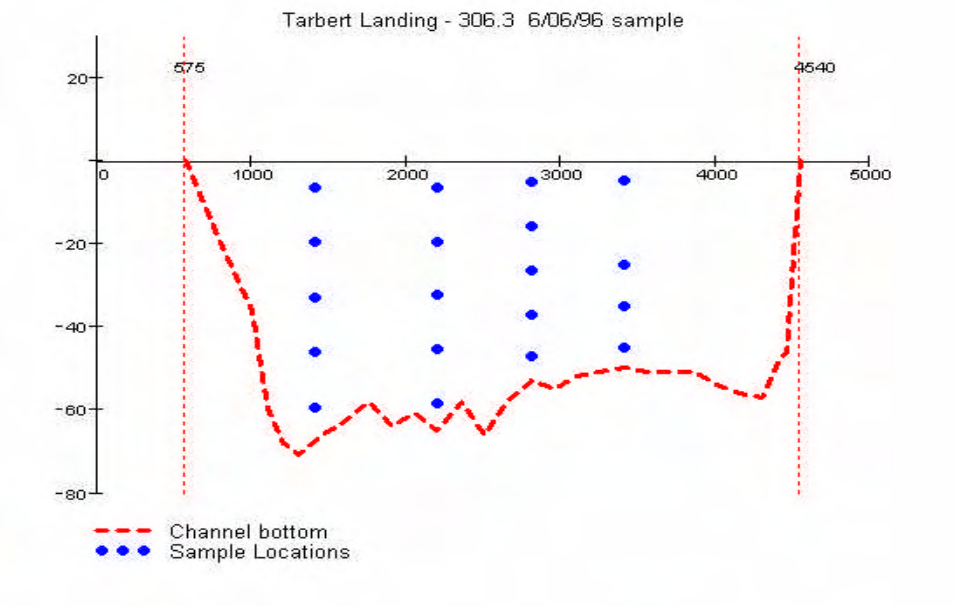

Figure 2 - Cross Section at Tarbert Landing RM 306.3 Looking Upstream (from fathometer reading, all values in feet.)

DATA ORGANIZATION

A total of 16 datasets were selected from available Tarbert Landing sediment samples contained in the New Orleans District sediment database for this study (Table 1). These data were collected over a period of 12 months in 1996 by the US Army Corps of Engineers, New Orleans District (NOD 1996a). Data from these files, stage hydrographs, and the fathometer readings taken with the sample were combined into EXCEL files corresponding to sample dates. Hydraulic parameters obtained from HEC RAS were added and these files were used as model input. In addition the River stages (NOD 1996b) at Red River Landing, LA [Mile 302.4] and Knox Landing [Mile 313.4], were obtained for the period of sediment sampling. An estimated water surface slope at Tarbert Landing was obtained using these stage hydrographs with corresponding sample dates are shown in Table 1. The data consisted of discharge, velocity, suspended sediment concentrations and grain size distributions at 4 verticals and at 5 points in each vertical, bed sediment grain size distribution. The file also contains a calculation of measured load for each of the 20 sample points, along with the discharge, velocity and area associated with each of the 20 samples.

Table 1. Tabulation of Data for the Model.

Date	Stage ft	Discharge Cfs	Temperature deg C	Velocity fps	Concentration ppm	WS Slope ft/ft
02-01-96	38.8	660,592	4	4.35	535.41	3.64E-05
02-15-96	38.1	622,650	4	4.14	205.26	3.02E-05
03-14-96	34.6	553,634	7	3.9	274.48	3.74E-05
03-28-96	35.0	563,209	10	3.97	271.61	3.82E-05
04-11-96	38.0	604,258	11	4.06	225.87	3.49E-05
04-25-96	32.1	488,382	17	3.82	420.17	3.67E-05
05-22-96	49.2	925,534	20	4.77	260.98	3.67E-05
06-06-96	52.7	1,023,226	24	4.91	155.44	3.34E-05
06-19-96	51.6	934,527	24	4.61	210.62	2.2E-05
7-18-96	30.0	388,299	29	3.33	163.11	3.27E-05
08-01-96	31.9	461,794	28	3.68	202.91	4.16E-05
10-10-96	30.0	413,664	21	3.41	199.68	3.68E-05
11-21-96	38.3	610,045	12	4.01	286.87	3.74E-05
12-05-96	43.6	810,846	8	4.61	392.61	3.65E-05
12-19-96	46.9	932,756	8	4.89	227.55	3.5E-05
12-30-96	45.4	829,000	7.5	4.46	217.28	3.94E-05

MODELING SOFTWARE

The sediment transport methods selected for use in this analysis are mathematically complex and challenging to apply without the use of computer programs. Most of the charts developed for use with the ME method are plotted on logarithmic scales, where a slight error may translate into a significant difference in the final answer using hand calculations. Existing computer applications of these procedures do provide increased accuracy and consistency in the calculation. MATHCAD™ made by MathSoft, Inc. was the software chosen to design a computer application because of its ability to evaluate complex mathematics, its ability to interface with Microsoft Office products, and its ability to perform computations with explicit units and do automatic unit conversion. All of the standard functions used in the Modified Einstein procedure are built into the MATHCAD worksheet.

ANALYSIS

In order to apply the ME method, hydraulic properties of the channel cross section are needed, as well as measured data such as velocity, sediment concentration, and bed material. Using fathometer points taken during the sampling, a simple HEC RAS model was created. The model consists of two identical cross sections based on the fathometer readings spaced 30 feet apart. Measured discharge is used as the upstream boundary condition with the downstream boundary condition being the water surface recorded at the time of the sample. The Manning's n value used is varied until the energy grade slope output given by HEC RAS matches the estimated water surface slope. The hydraulic properties needed to perform the ME calculation were obtained from the HEC RAS output.

The ME method was applied in two ways: a) the traditional approach of constructing a composite of the measured verticals [Version "C"] and b) the revised approach of applying the ME method to the individual panels and then summing the resulting loads to obtain the total load in each class [Version "I"]. In order to apply the revised approach, hydraulic properties corresponding to each sediment sample's vertical must be determined. The sediment data sheet contains a tabulation of the suspended sediment concentration, gradation, area, discharge and velocity associated with each of the 20 suspended samples taken. To apply the panel procedure, this information was segregated into groups corresponding to the sample verticals. This information was further subdivided into 3 zones, left middle, and right by combining the 2 middle verticals. The suspended sediment measurements and gradations were discharge weighted and composite values were then assigned to each zone. The necessary hydraulic properties needed to complete the ME calculation were obtained from the HEC RAS model. In order to derive these properties in this channel configuration, the flow distribution option in HEC RAS was used. This option allows the user to specify the locations in which they would like the program to calculate flow distribution output (HEC 1998). During the normal profile computations, at each location where the distribution is requested, the program will calculate the flow, area, wetted perimeter, percentage of conveyance, and average velocity for each slice defined by the user. For this study, the slices were defined at the stations corresponding to the vertical samples. The middle zone was defined by assigning the bounding stations as overbank points, LOB (left overbank) and ROB (right overbank).

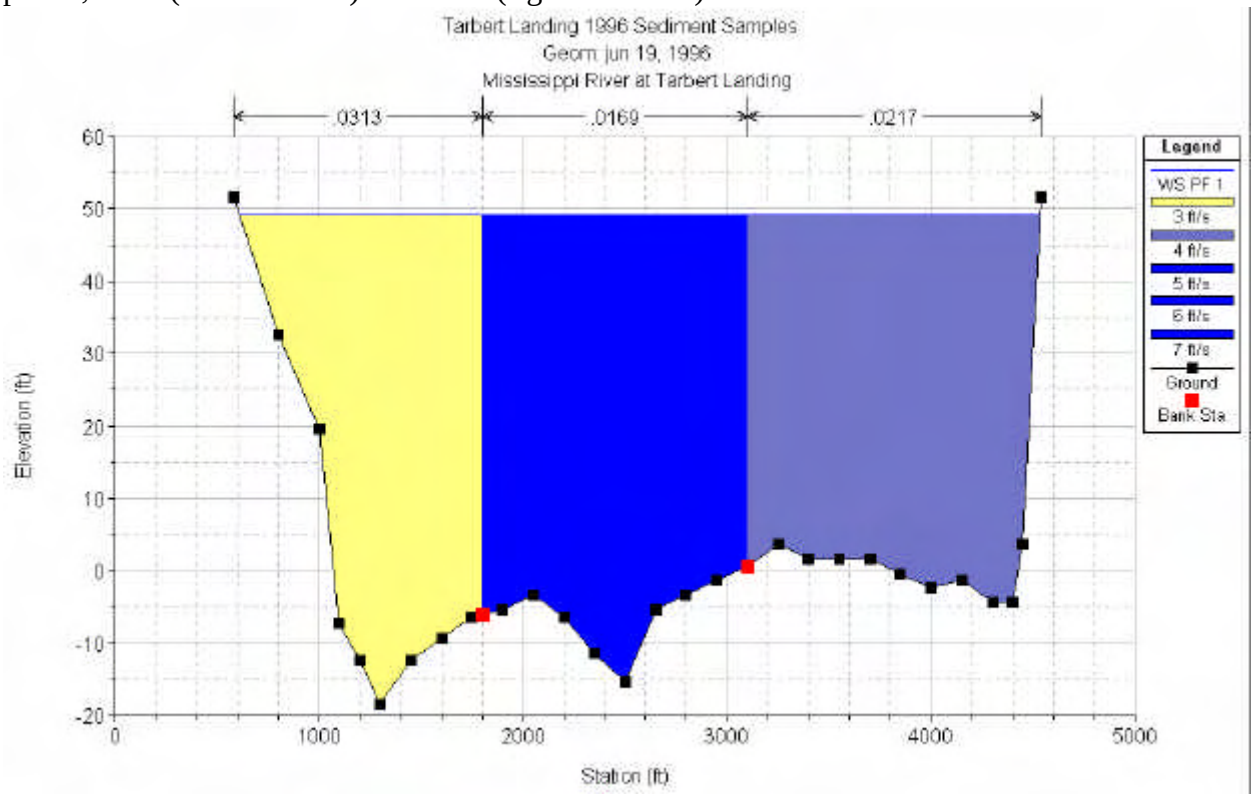

Figure 3 - Cross Section Plot from HEC RAS showing flow distribution panels

This designation provided the additional opportunity of more discretely defining the Manning's n value of the channel in each of the 3 zones. HEC RAS runs were made to determine the hydraulic properties corresponding to each zone needed for the ME calculation. The discharge in

each flow distribution panel corresponded closely with the discharge associated with the panels created from the consolidated sample data. HEC RAS runs were made varying the Manning's n value in each panel until the energy grade slope matched the estimated water surface slope. This procedure was necessary to balance the discharge produced in the HEC RAS flow distribution slices with the panels created with the sample data. This also ensured that the correct average velocity for each slice was used in the ME calculation. For the individual panel approach HEC RAS was used to obtain the panel geometry and "n" values. All loads were compared with the nominal loads.

RESULTS OF LOAD ESTIMATION PROCEDURES

Table 2 summarizes the total load estimates by the nominal method and Versions "C" and "I" of the Modified Einstein Method. Table 3 compares the two versions of ME for the wash load and the sand load.

DISCUSSION OF RESULTS

Table 2 shows that there is no significant difference between the two versions (C and I) of the ME method; however, there is a significant difference of approximately (+20%) between the total ME loads and the total nominal loads. Table 3, indicates that this difference is even greater for the coarse fraction where the ME method gives 36% higher sand loads than the nominal method. There are relatively small differences (approximately 10%) between the nominal fine load and the Modified Einstein loads due to the strong dependence of both methods on the measured concentrations of fine sediment.

Table 2. Comparison off Total Sediment Load Estimates by Different Methods

Date	Discharge cfs	Sampled Load tons/day	Modified Einstein Load tons/day "C"	Modified Einstein Load tons/day "I"	Difference "I"-"C" tons/day
02-01-96	660,592	954,962	1,063,154	1,061,542	-1,612
02-15-96	622,650	345,072	419,537	419,535	-2
03-14-96	553,634	410,297	485,362	484,859	-503
03-28-96	563,209	413,034	493,307	492,796	-511
04-11-96	604,258	368,510	442,771	438,876	-3,895
04-25-96	488,382	554,049	618,223	615,379	-2,844
05-22-96	925,534	652,170	805,915	798,311	-7,604
06-06-96	1,023,226	429,437	525,503	521,246	-4,257
06-19-96	934,527	531,437	598,078	592,457	-5,621
7-18-96	388,299	171,009	211,507	211,633	126
08-01-96	461,794	253,002	321,583	320,735	-848
10-10-96	413,664	223,025	284,136	283,847	-289
11-21-96	610,045	472,512	594,830	586,780	-8,050
12-05-96	810,846	859,537	1,019,032	1,011,046	-7,986
12-19-96	932,756	573,084	662,709	659,986	-2,723
12-30-96	829,000	486,339	629,660	631,824	2,164

Table 3. Fine, Coarse Sediment Load Estimates by Different Methods

Date	Discharge cfs	Nominal Coarse tons/day	ME "I" Coarse tons/day	Nominal Fine tons/day	ME "I" Fine tons/day
02-01-96	660,592	262,443	245,633	692,519	815,909
02-15-96	622,650	109,243	135,120	235,829	284,415
03-14-96	553,634	107,705	152,361	302,592	332,498
03-28-96	563,209	103,120	143,930	309,914	348,866
04-11-96	604,258	123,231	151,271	245,279	287,605
04-25-96	488,382	37,892	82,885	516,156	532,494
05-22-96	925,534	232,111	295,004	420,059	503,307
06-06-96	1,023,226	160,251	198,640	269,186	322,606
06-19-96	934,527	164,702	167,995	366,736	424,462
7-18-96	388,299	8,734	40,462	162,276	171,171
08-01-96	461,794	34,865	80,228	218,137	240,507
10-10-96	413,664	19,194	63,073	203,831	220,774
11-21-96	610,045	93,962	157,694	378,550	429,086
12-05-96	810,846	165,135	229,036	694,402	782,010
12-19-96	932,756	151,046	169,135	422,037	490,851
12-30-96	829,000	159,894	238,867	326,445	392,957

Although differences between the incremental method and composite calculation are small, difference between loads by grain size class may be larger as a result of variation of the suspended gradation by panel; this is not picked up in these results because the differences cancel each other out. In general the fine material load may be slightly overstated by the composite method and the coarser fractions may be slightly understated. The incremental method would also a better result if bed material gradations were done at each sample vertical instead of using a gradation based on a composite sample.

Einstein (1950) divided the flow resistance into two components or hydraulic radii, i.e. R' and R" representing respectively the resistance due to grain roughness and bed form drag. For wide alluvial channels, the resistance to form drag must be added to resistance due to grain roughness. The divided resistance approach can be expressed in terms of the hydraulic radius and is given by the following relation: R = R' + R". R' and R" were calculated for the composite channel and the individual panels. The relative effect of roughness due to bedforms, particularly dunes at Tarbert Landing is illustrated by plotting the ratio of R" (form roughness) calculated from the middle zone against the estimated energy slope at Tarbert Landing as shown in Figure 4. This shows a definite increasing R" with the energy slope due to dunes in the middle of the channel at high energy slopes. The R" calculated from the composite channel is shown for comparison.

CONCLUSIONS

This study confirms that the current practice of using a composite of all the panels is justified. However, this may not be the case for other river sections with greater variation in depth. This approach may also be used to check the adequacy of a sampling compositing procedure or

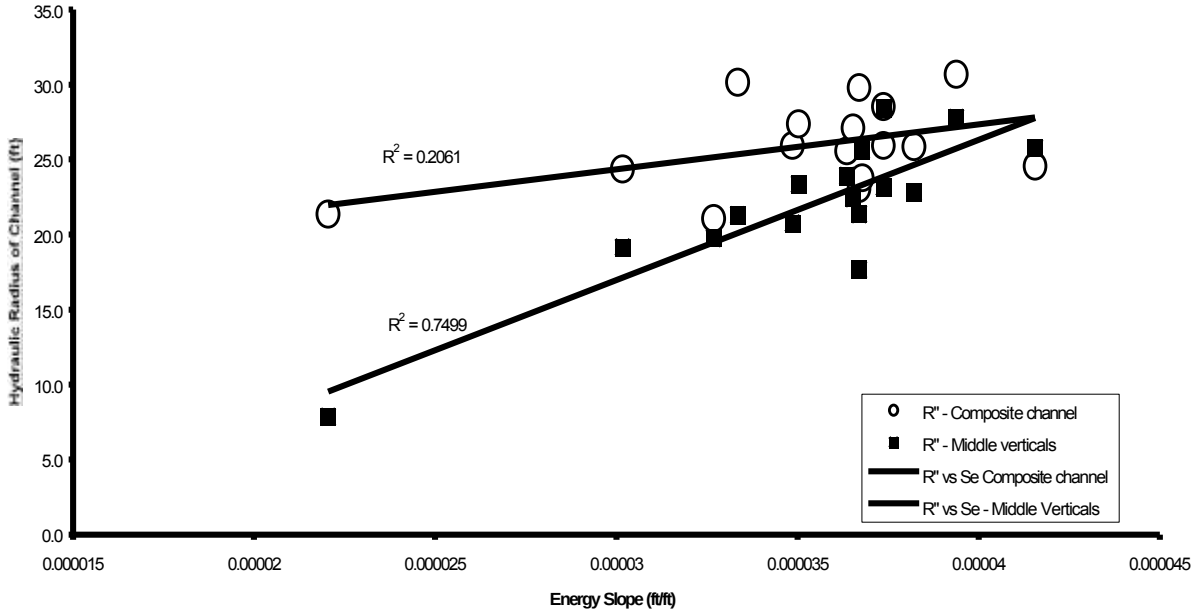

Figure 4. R" versus Estimated Energy Slope at Tarbert Landing, MS

interpolation when sample data are missing. The ME method provides an estimate of the possible error in the nominal load. ME uses a hydrodynamically based extrapolation from the sampled zone to the unsampled zone. Since the unsampled zones in the lower Mississippi River are quite large (approximately 5 ft) a considerable error is possible in the extrapolation by the nominal procedure. At Tarbert Landing a gross estimate of the under-estimation of the total loads is 21% and the sand load is 36%. Sampling done using ADCP (Acoustic Doppler Current Profiler) technology may also produce a more accurate result, especially at lower flows where the unsampled sand loads may be greater.

REFERENCES

Einstein, H.A. 1950, "The Bed Load Function for Sediment Transportation in Open Channels, " Technical Bulletin 1026, US Department of Agriculture, SCS, Washington, DC.

Catalyst-Old River Hydroelectric Limited Partnership, 1999. "Lower Mississippi River Sediment Study", Volumes 1-5, Vidalia, LA, May.

U.S. Army Corps of Engineers, New Orleans District, 1996a. " NOD Sediment Database", New Orleans, LA.

U.S. Army Corps of Engineers, New Orleans District, 1996b. "NOD Water Control Database", New Orleans, LA.

U.S. Army Corps of Engineers, Waterways Experiment Station, 1990. "Downward Trend in Mississippi River Suspended Loads". Vicksburg, MS.

U.S. Army Corps of Engineers, Hydrologic Engineering Center, September 1998. "HEC-RAS River Analysis System, Users Manual", Davis, CA.

EVALUATION OF SELECTED BEDLOAD EQUATIONS UNDER TRANSPORT- AND SUPPLY-LIMITED CONDITIONS

By Vicente L. Lopes, School of Renewable Natural Resources, University of Arizona, Tucson, AZ; W. R. Osterkamp, U.S. Geological Survey, Tucson, AZ; Miguel Bravo-Espinosa, Centro Nacional de Investigacion para Produccion Sostenible, Morelia, Mexico

Abstract: Hydraulic and sediment data from 22 alluvial channels in the United States were used to evaluate the performance of selected bedload equations. The applicability of the equations improved by the explicit recognition of a stream-reach condition of bedload transport as one of three transport categories: non-supply-limited 1 (NSL-1), non-supply-limited 2 (NSL-2), and supply-limited (SL). The equations by Parker et al. (1982) and Meyer-Peter and Muller (1948) adequately predicted sediment transport in channels with NSL-1 condition, whereas the Bagnold (1980) and Schoklisch (1962) equations performed well in channels with NSL-2 and SL conditions. Overall the best equations were those of Schoklitsch, which had the ability to predict the trend of measured bedload data for eight of 22 streams, and the Bagnold equation, which duplicated the trend of measured data in seven streams.

INTRODUCTION

Several comparisons of bedload equations have been made since DuBoys and Straub (Straub 1935) proposed their equation. Few studies, however, document an evaluation of the equations' basic assumptions. A major assumption behind the development of bedload equations is that the channel has an unlimited supply of sediment Clearly, there is a need for an improved identification of sediment-supply conditions before a bedload equation is applied. Bathurst et al. (1987a) agreed that further research on sediment prediction is required, notably under conditions of limited sediment availability where effects of external supply and particle-size distributions are important.

Bathurst et al. (1987b) assessed the applicability of six bedload equations for steep mountain streams affected by limited sediment availability and bed armoring. They used flume data to evaluate the equations under non-supply-limited conditions and field data to assess them under conditions of limited sediment availability. They concluded that where sediment availability is unlimited, bedload discharge is best predicted by the Schoklitsch (1962) equation. Where sediment availability is limited, however, the Schoklitsch equation should be applied separately for each size fraction and external sediment additions should be considered.

Hoey and Sutherland (1991) attempted to evaluate the Bagnold (1980) equation with a small-scale braided-river model. They found that the equation over-predicted measured bedload-transport rates when applied to channels in equilibrium or aggrading and under-predicted when the equation was applied to degrading channels. Gomez and Church (1989) used a set of 410 bedload events from field and flume measurements to test 12 bedload equations for gravel-bed channels. They concluded that none of the tested equations performed consistently because of limitations of the data used and the complexity of the transport phenomena. They noted that the prediction of bedload transport under limited hydraulic information is best accomplished by using equations based on the stream-power concept, whereas the Einstein (1950) and Parker et al. (1982) equations should be used when local hydraulic information is available.

Questions remaining to be answered include: If sediment-transport conditions are explicitly taken into account, does the bedload-transport prediction improve? Do bedload-transport equations show a consistent relation to sediment-transport conditions? If so, what are the equations that give the most accurate predictions of bedload discharge for different conditions? The purpose of this paper is to evaluate the performance of selected bedload equations under different conditions of bedload transport in alluvial channels.

METHODS

Selection of bedload equations Data from 22 alluvial channels in the United States and a classification for bedload-transport condition proposed by Bravo-Espinosa (1999) were used in this study to evaluate the performance of selected bedload equations. Table 1 shows the 22 alluvial channels with their respective drainage areas, dominant geology, and land-use history. Seven bedload equations were selected based on extent of use, theoretical content, and recentness: Kalinske (1947), Meyer-Peter and Muller (1948), Einstein-Brown (Brown, 1950), Schoklitsch (1962), Yalin (1963), Bagnold (1980), and Parker et al. (1982).

Although based on different approaches, these equations rely primarily on the same general assumptions: (1) the fluid and sediment properties are steady and uniform; (2) there is an infinite and continuous supply of sediment particle sizes represented for some component of the bed material, (3) there is a specific relation between hydraulic and sedimentological parameters and the rate at which the bedload is transported, and (4) the sediment stored in a reach can be neglected (Graf 1971; Gomez and Church 1989; Reid and Dunne 1996). These conditions are not well met in many natural streams; therefore, it would appear pertinent to classify streams in a way that conforms to the above assumptions.

Bedload-transport condition Alluvial channels have self-adjusting boundaries. Their beds, banks, and flood plains are composed of material that has been or can be transported by streamflow (Schumm 1977; Richards 1982). Over short periods (1-10 years), an alluvial channel can adjust its morphology to a broad range of sediment-supply and transport conditions (Nordin 1985; Montgomery and Buffington 1997).

Bravo-Espinosa (1999) used a relation proposed by Lane (1955) to classify bedload transport in a stream reach into, non-supply-limited 1 (NSL-1) condition, non-supply-limited 2 (NSL-2) condition, and supply limited (SL) condition. A sediment-transport condition was defined as a reach-level characteristic determined over short periods by the availability or supply of sediment of a given particle-size range and the ability of the stream to transport that supply.

A stream reach with a NSL-1 condition was defined as a reach where bedload transport is not limited by its availability for all particle size classes. A stream reach with a NSL-2 condition was defined as a reach where bedload transport is limited by its availability for some particle size classes. The NSL-2 condition differs from the NSL-1 condition by not having a sediment supply that is continuously available in and outside the channel reach. That is, the supply of transportable material may vary markedly along the channel, and, therefore, the location of a sampling site affects the measured transport rate. A stream reach with a SL condition was defined as a reach where bedload transport is limited by its availability for all particle size classes.

Comparison of bedload equations The inequality coefficient (U) was used to evaluate how well a bedload equation predicted bedload discharge in a stream reach of similar bedload-transport conditions. The inequality coefficient (U) is defined as:

$$U = \frac{rmse}{\left[\frac{1}{n}\sum_{i=1}^{n}\left(Q_{bo}\right)_i^2\right]^{1/2} + \left[\frac{1}{n}\sum_{i=1}^{n}\left(Q_{bp}\right)_i^2\right]^{1/2}} \qquad (1)$$

where rmse is the root-mean-square error, defined as:

$$rmse = \left[\sum_{i=1}^{n} \frac{\left(Q_{bo} - Q_{bp}\right)_i^2}{n} \right]^{1/2} \quad (2)$$

where Q_{bo} is the measured bedload discharge, Q_{bp} is the predicted bedload discharge, i denotes a given flow, and n is the total number of flows. The scaling of the denominator is such that U always falls between 0 and 1. If U = 0, then $Q_{bp} = Q_{bo}$ and there is a perfect fit. If U =1, then $Q_{bp} \neq Q_{bo}$ and the equation lacks predictive value. For the purpose of this paper, an equation was assumed to have the ability to represent the measured data when $U \leq 0.5$.

RESULTS AND DISCUSSION

Results of comparisons of bedload-transport predictions and measurements according to bedload-transport condition are summarized in Table 2. As an example, Fig. 1 provides a comparison of measured and predicted bedload-transport rates for all selected equations for site 14, the Chippewa River at Durand, Wisconsin, which has a non-supply-limited 1 (NSL-1) condition. Presumably because the riverbed at Durand is braided, contains sand bars, and is unarmored, the Bagnold, Meyer-Peter and Muller, and Schoklitsch equations succeeded in approximating the measured data (Fig. 1; Table 2). Predictions by the Einstein-Brown, Kalinske, Parker and others, and Yalin equations, however, did not conform well to the measured data at Durand.

Inspection of Table 2 reveals that for stream reaches with non-supply-limited 1 (NSL-1) condition, the equation by Parker and others predicted the trend of measured values in five of 10 gravel-bed streams (U varied from 0.36 to 0.46), but it did poorly for the other five streams (U varied from 0.83 to 1.0). Although the Oak Creek data were used in the development of the equation by Parker and others, these data were considered in this analysis because our purpose was to evaluate bedload equations by grouping stream reaches according to bedload-transport condition. That is, if one equation performed well for a particular channel, it was expected that the equation would perform well for channels with similar bedload-transport condition. Equations by Schoklitsch and Meyer-Peter and Muller predicted trends well in four of 11 streams (Table 2; sites 11, 12, 14, 22), whereas the equation by Bagnold performed well in three streams. The other equations were successful in one of 11 streams.

For stream reaches with a non-supply-limited 2 (NSL-2) condition, the Bagnold and Schoklitsch equations reflected well the path of measured values in two of seven streams (Table 2; sites 15, 20). For stream reaches with a supply-limited (SL) condition, the Bagnold and Schoklitsch equations yielded values that fitted the trend of measured values in two of four streams (Table 2; sites 13, 16). These results are consistent with those of Bathurst et al. (1987b), who showed that bedload discharge was best predicted by the Schoklitsch (1962) equation where supply-limited conditions occurred. Regarding the performance of the Bagnold (1980) equation, Hoey and Sutherland (1991) showed that this equation provides predictions best when applied to degrading channels, or in other words, SL channels.

SUMMARY AND CONCLUSIONS

In this study the problem of improving the applicability of bedload equations by the explicit recognition of a channel's condition of bedload transport and sediment availability was explored. The results of this study are based on records of 22 alluvial channels of the United States classed according to three bedload-transport conditions. The main conclusions are:

(1) The equations by Parker et al. (1982) and Meyer-Peter and Muller (1948) adequately predicted sediment transport in channels with non-supply-limited 1 (NSL-1) condition, whereas the Bagnold

(1980) and Schoklisch (1962) equations are performed well in channels with non-supply-limited 2 (NSL-2) and supply-limited (SL) conditions.

(2) On the basis of the number of streams for which an equation performed well, the best equations were those of Schoklitsch, which predicted the trend of measured bedload data (U values less than 0.5) for eight of 22 streams, and the Bagnold equation, which predicted the trend of measured data in seven streams.

REFERENCES

Bagnold, R. A. 1980. 'An empirical correlation of bedload transport rates in flumes and natural rivers.' Proc. Roy. Soc., London, A, 372, 453-473.

Bathurst, J. C., Graf, W. H., and Cao, H. H. 1987a. 'Bedload discharge equations for steep mountain rivers.' In: C. R. Thorne, J. C. Bathurst, and R. D. Hey (eds.), Sediment transport in gravel-bed rivers, John Wiley & Sons, Inc., Chichester, UK, 453-477.

Bathurst, J. C., Leeks, G. J. L., and Newson, M. D. 1987b. 'Discussion of bed load transport measurements by the vortex-tube trap on Virgilio Creek, Italy.' In: C. R. Thorne, J. C. Bathurst, and R. D. Hey (eds.), Sediment transport in gravel-bed rivers, John Wiley & Sons, Inc., Chichester, UK, p. 610.

Bravo-Espinosa, M. 1999. Prediction of bedload discharge for alluvial channels, PhD dissertation, University of Arizona, Tucson, AZ, 276 pp.

Brown, C. B. 1950. 'Sediment transportation.' In: Rouse, H (ed.), Engineering hydraulics, John Wiley & Sons, Inc., New York, NY., 769-857.

Einstein, H. A. 1950. 'The bed-load function for sediment transportation in open channel flows.' Tech. Bull. No. 1026, U.S.D.A, Soil Conservation Service, Washington, DC.

Gomez, B., and Church, M. 1989. 'An assessment of bed load sediment transport formulae for gravel bed rivers.' Water Resour. Res., 25(6), 1161-1186.

Graf, W. H. 1971. 'Hydraulics of sediment transport.' McGraw-Hill, Inc., New York, NY.

Hoey, T. B., and Sutherland, A. J. 1991. "Channel morphology and bedload pulses in braided rivers: A laboratory study", Earth Surface Processes and Landforms, 16,

Kalinske, A. A. 1947. 'Movement of sediment as bed load in rivers.' Am. Geophys. Union, 28(4), 615-620.

Lane, E. W. 1955. "The importance of fluvial morphology in hydraulic engineering", in Proceedings, American Society of Civil Engineers, 81, 1-17.

Meyer-Peter, E., and Muller, R. 1948. 'Formulas for bed-load transport.' Rep. 2nd Meeting, Int. Association for Hydraulic Structures Res., Stockholm, 39-64.

Montgomery, D. R., and Buffington, J. M. 1997. "Channel-reach morphology in mountain drainage basins", Geological Society of America Bulletin, 109(5), 596-611.

Nordin, C. F. Jr. 1985. "The sediment loads of rivers", in Rodda, J. C. (Ed.), Facets of hydrology, John Wiley & Sons, New York, NY., 183-204.

Parker, G., Klingeman, P. C., and McLean, D. G. 1982. 'Bedload and size distribution in paved gravel-bed streams.' J. Hydr. Div., ASCE, 108(HY4), 544-571.

Reid, L. M., and Dunne, T. 1996. Rapid Evaluation of Sediment Budgets. Catena Verlag, Germany, 164 pp.

Richards, K. 1982. Rivers: Form and Process in Alluvial Channels. Meuthuen, New York, 358 pp.

Schoklitsch, A. 1962. 'Handbuch des wasserbaues.' Springer-Verlag, Vienna, 1, 173-177.

Schumm, S. A. 1977. The Fluvial System. John Wiley & Sons, Inc., New York, NY, 338 pp.

Straub, L. G. 1935. 'Missouri River report.' In-House Document 238, 73rd Congress, 2nd Session, U.S. Government Printing Office, Washington, DC.

Yalin, M. S. 1963. 'An expression for bed bed-load transportation.' J. Hydr. Div., ASCE, 89(HY3), 221-250.

TABLE 1. Geology and Land-use Information for Study Basins.

Site	River Basin	USGS Station Number*	Drainage Area km^2	Dominant Geology	Land-Use History
1.	SF Payette R., ID	13235000	1181	Granite	Upper basin: grazing, mining, timbering
2.	Boise R., ID	13185000	2150	Granite	97% forestland; 0.081km/km^2 road density
3.	SF Salmon R., ID	13310700	855	Granite	1950-66:15% logged, road construction
4.	Valley Ck., ID	13295000	381	Granite and alluvial deposits	Grazing since 1972; in 1994 grazed 64%
5.	Johnson Ck., ID	13313000	552	Granite	Moderately roaded; 15% fire impacted
6.	Selway R., ID	13336500	4950	Granite and metamorphic	Fire occurrence 13% basin, minimally roaded
7.	Lochsa R., ID	13337000	3056	Granite and gneiss	38% basin roaded, high fire threat
8.	NF Clearwater R., ID	13340600	3522	Granite and schists	Lower basin: highly roaded and logged
9.	Clearwater R., ID	13342500	24790	Basalt, metamorphic, and granite	Not available
10.	Snake R., WA	13334300	240766	Basalt, granite, and sedimentary	Not available
11.	NF Toutle R., WA	14241100	736	Andesite, basalt, and rhyolite	1980: 61% area within blast, Mt. St. Helens
12.	Toutle R., WA	14242580	1285	Andesite, basalt, and rhyolite	1980: 36% area within blast, Mt. St. Helens
13.	Chip. R, Pepin., WI	ns	24371	Silt-sand deposits and dolomite	Not available
14.	Chip. R, Durand, WI	5369500	23335	Silt-sand deposits, and sandstone	Not available
15.	Wisconsin R., WI	5407000	26940	Outwash, silt-sand, and sedimentary	Southern part of basin: farmland 90%, forestry 10%
16.	Yampa R., CO	9260050	19840	Sedimentary	89% basin timber harvesting and grazing [1978]
17.	Williams Fork R., CO	9036000	232	Metasedimentary and igneous	Not available
18.	La Garita Ck., CO	8231000	158	Igneous and alluvial deposits	Not available
19.	NF S. Platte R., CO	ns	985	Metasedimentary and granite	Not available
20.	Horse Ck., CO	ns	28	Granite	Not available
21.	Oak Ck., OR	ns	7	Basalt	Not available
22.	East Fork R., WY	ns	500	Granite, sedimentary, and moraines	Not available

*ns: no station number

TABLE 2. Inequality Coefficients (U) for the Prediction of Bedload Discharge by Selected Bedload Equations

Site	Meyer	Yalin	Einstein-B	Kalinske	Schoklitsch	Parker et al.	Bagnold
						Inequality Coefficients	
Non-Supply Limited 1							
2. Boise	0.8796	0.9946	0.9941	0.9266	0.9298	0.3759	0.9639
3. SF Salmon	0.5361	0.9974	0.9975	0.9636	0.9453	0.9898	0.9550
5. Johnson	0.9932	0.9998	0.9998	0.9974	0.9980	0.9994	0.9988
6. Selway	0.9883	0.9994	0.9993	0.9926	0.9905	0.4128	0.9946
7. Lochsa	0.9894	0.9998	0.9998	0.9976	0.9961	0.3621	0.9974
8. NF Clearwater	0.9853	0.9999	0.9999	0.9991	0.9988	0.9996	0.9992
11. NF Toutle	0.3176	0.3141	0.3970	0.2523	0.4975	0.4401	0.6045
12. Toutle	0.3808	0.7920	0.8933	0.6278	0.4263	0.8297	0.4439
14. Chippewa-Durand	0.4397	0.8827	0.8688	0.5150	0.1275	0.8356	0.2432
21. Oak	0.9239	0.9867	0.9910	0.9678	0.9238	0.4633	0.9178
22. East Fork	0.4761	0.8195	0.8300	0.6252	0.3649	0.7837	0.3610
Non-Supply Limited 2							
1. SF Payette	0.9639	0.9963	0.9963	0.9774	0.9589	0.9683	0.9795
4. Valley	0.9034	0.9970	0.9978	0.9855	0.9623	0.9878	0.9674
9. Clearwater	0.9495	0.9761	0.9686	0.7440	0.6724	0.5588	0.8289
15. Wisconsin	0.6058	0.9279	0.8952	0.4842	0.3172	0.9161	0.2222
18. Garita	0.8975	0.9995	0.9995	0.9930	0.9934	0.9979	0.9957
19. NF South Platte	0.6589	0.9966	0.9968	0.9488	0.9530	0.7154	0.9686
20. Horse	0.4114	0.7736	0.8436	0.6898	0.4426		0.4180
Supply Limited							
10. Snake	0.8520	0.9907	0.9875	0.8847	0.8325	0.8982	0.9321
13. Chippewa-Pepin	0.5615	0.8853	0.8691	0.5736	0.4634	0.8254	0.3311
16. Yampa	0.5141	0.9477	0.9345	0.4493	0.4032	0.9389	0.4338
17. Williams Fork	0.9848	0.9977	0.9981	0.9861	0.9809	0.9301	0.9880

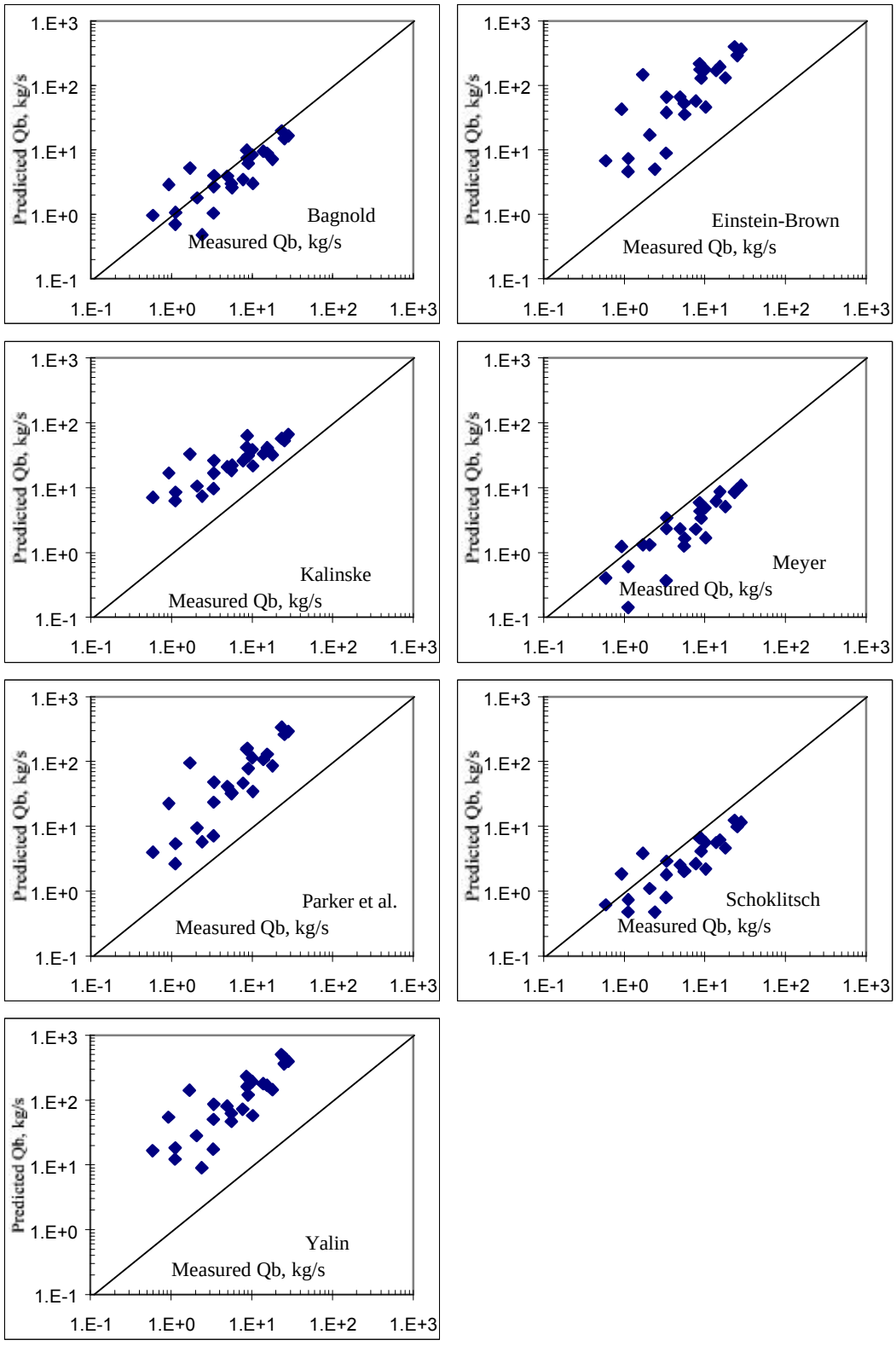

FIG. 1. Comparisons of predicted and measured bedload rates for Chippewa River at Durand, WI

WHAT REGULATES SUSPENDED-SEDIMENT TRANSPORT IN A GIVEN SETTING? GRAIN SIZE OF BED SEDIMENT OR FLOW?

D. M. Rubin, Geologist, U.S. Geological Survey, Santa Cruz, California, and
D. J. Topping, Hydrologist, U.S. Geological Survey, Reston, Virginia

INTRODUCTION

Background and purpose It might be argued that the key question to ask when beginning an investigation of a natural sediment-transporting flow is whether transport is limited mainly by flow strength or sediment supply. The answer to this question determines whether research should focus on the relation between flow strength and sediment transport, the rate at which sediment of different grain sizes is supplied to the flow, or both. For a given setting, this is the key question that must be answered prior to either designing a sediment-transport measurement program or constructing a sediment-transport model or budget. This is also the key question to answer when calculating total maximum daily loads (TMDLs) for sediment.

Rubin and Topping (in press) developed a technique to evaluate the importance of changes in flow strength relative to changes in sediment supply in regulating the rate of sediment transport. If that technique determines that changes in suspended-sediment transport in a river (or on a continental shelf) are regulated mainly by flow, then a measure of the flow strength (e.g., the boundary shear stress, shear velocity, or discharge of water) may be an adequate predictor of sediment transport. In contrast, if changes in sediment transport are regulated mainly by changes in bed-sediment grain size, then measurements of sediment input will be a more accurate predictor of sediment transport than any measure of flow strength.

Definitions

Flow-regulated transport and bed-sediment-regulated transport In a system where flow-induced changes in transport are large relative to bed-sediment grain-size-induced changes in transport, transport is defined to be flow-regulated. At the other extreme, where changes in bed-sediment grain size are the dominant factor regulating sediment transport, transport is defined to be grain-size-regulated.

Suspended sediment, suspended bed material, and wash load Suspended sediment includes two kinds of load: suspended bed material and wash load. In this paper, the term suspended sediment is applied to suspended bed material (thus excluding wash load). Suspended bed material includes those grain sizes that occur in substantial amounts in the bed, whereas wash load is finer than the bed sediment (Einstein and Chien, 1953). Another approach—compatible with (Einstein and Chien, 1953)—might be to base definitions on the concentration gradient; wash load would include those sizes having a concentration that remains constant with height above the bed.

APPROACH

Flow-regulated transport Laboratory flumes that recirculate both sediment and water are ideal for studying flow-regulated transport, because grain size on the bed (D_b) remains nearly constant. Under such conditions, increases in shear velocity (u_*) from one experiment to another cause increases in concentration (C), grain size of suspended sediment (D_s), and sediment transport (q). D_s and C increase because stronger flows are able to suspend coarser sediment and more sediment, and q increases for two reasons: concentrations are higher and more water is discharged. Because C and D_s increase with shear velocity, they are positively correlated (Fig. 1a).

Bed-sediment grain-size-regulated transport Grain-size-regulated transport can be studied by comparing data collected with differing bed-sediment grain sizes for a narrow range of u_*. Under such conditions, coarsening of the bed sediment causes concentration to decrease, while causing the median diameter of the suspended sediment to increase. As a result of these opposite responses to changes in D_b, C is inversely related to D_s where transport is grain-size regulated (Fig. 1b).

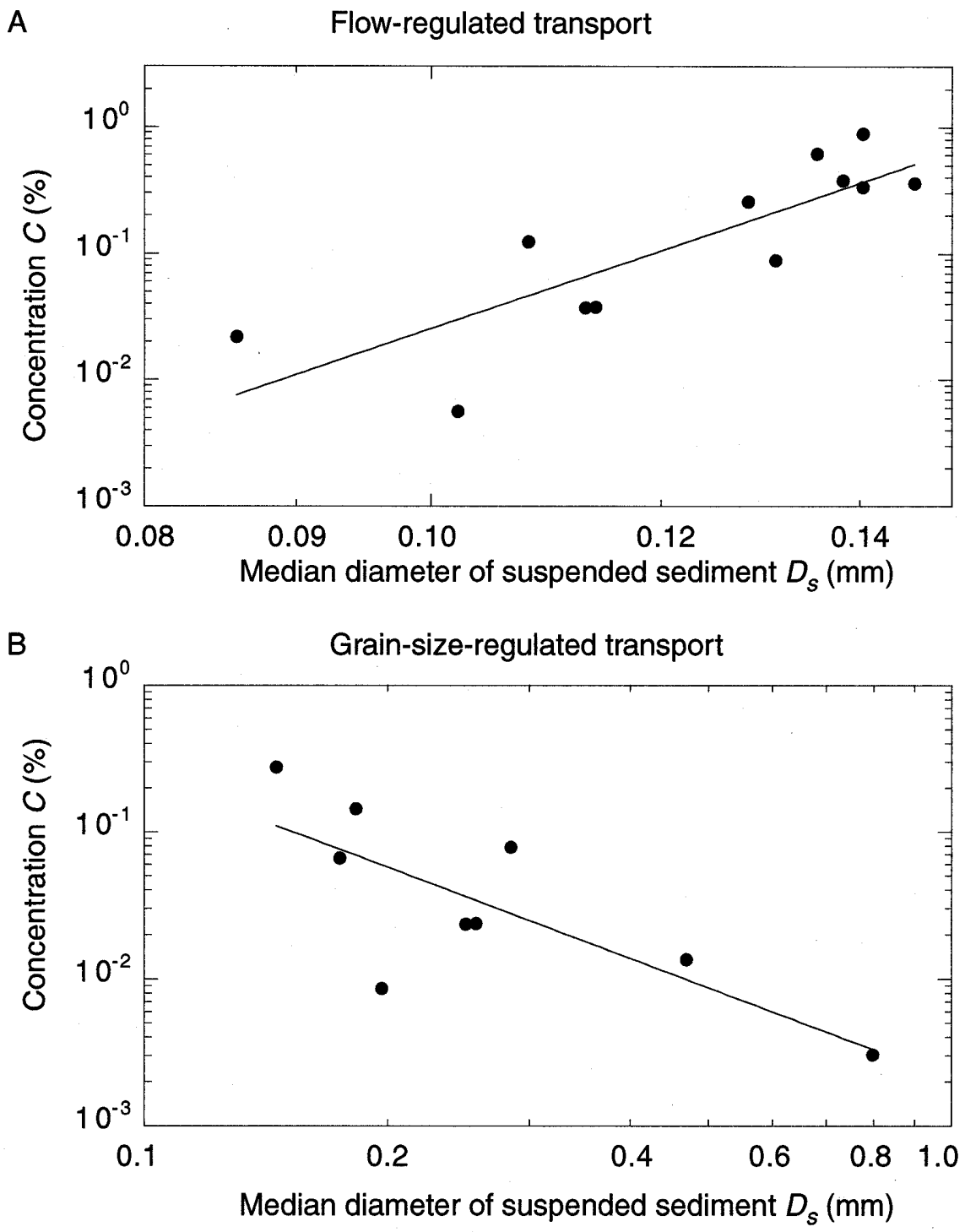

Figure 1. Relations between concentration and grain size for flow-regulated transport (**A**) and grain-size-regulated transport (B). **A**. Flow-regulated transport. Data are from laboratory experiments of Guy et al. (1966, Table 9); for all runs depth was 15-16 cm; sand in flume had a median diameter of 0.33 mm and sigma phi of 1.04. Concentration is weight percent of suspended sediment. C and D_s are positively correlated, because both increase with u_*. **B.** Grain-size-regulated transport in flume experiments. Plotted points represent all runs with u_* between 7.0 and 8.0 cm/s in data of Guy et al. (1966, Tables 2-8). Increasing the grain size of sediment on the bed caused the concentration of suspended sand to decrease and the median diameter of suspended sediment to increase.

Quantifying the relative importance of grain-size regulation and flow regulation of suspended-sediment transport If transport in all flows were regulated purely by changes in flow or by changes in bed sediment, then the sign of $\Delta C/\Delta D_s$ would be a definitive distinguishing characteristic (positive for flow-regulated transport and negative for grain-size-regulated transport). Because all intermediate conditions are possible, however, definitive evaluation is more complicated. Rubin and Topping (in press) followed the approach discussed below.

Most models of suspended-sediment transport express transport as a function of some combination of flow properties (such as u_*, water slope, and water depth) and bed-sediment grain-size properties (such as median diameter D_b and standard deviation). The simplest approach to quantifying the relative importance of a single change in both flow and a change in bed-sediment texture is to evaluate their individual impacts on the transport rate. For such a change, this measure α can be defined as

$$a = \frac{\log\left[q(flow_1, grain\text{-}size_1) / q(flow_1, grain\text{-}size_2)\right]}{\log\left[q(flow_1, grain\text{-}size_1) / q(flow_2, grain\text{-}size_1)\right]} \qquad (1)$$

where q gives the sediment-transport rate as a function of both flow and bed-sediment grain size; subscripts refer to conditions at two times. The numerator quantifies the extent to which a change in transport rate is influenced by the change in bed-sediment grain size (holding flow constant), while the denominator quantifies the effect of the change in flow alone. α is a dimensionless number that describes how much of a change in transport is caused by a change in bed sediment relative to a change in flow. Where sediment transport is regulated primarily by changes in bed-sediment grain size, $|\alpha| >> 1$; where transport is regulated primarily _by changes in flow, $|\alpha| << 1$; and where transport is regulated equally by changes in flow and bed sediment, $|\alpha| = 1$.

To evaluate the functional relations expressed in eq (1), Rubin and Topping (in press) used the following approach:
(1) A numerical model based on McLean (1992) was used to calculate concentration of suspended sediment at 500 logarithmically spaced elevations above the bed, for 129 size classes of bed sediment binned in 1/16 ϕ increments. The algorithm was used to predict mean concentration and median grain diameter for more than 1000 combinations of flow variables, including 11 median grain diameters (0.03 to 1.2 mm), 20 values of u_* (from below threshold of transport to upper plane-bed regime), 3 depths (10, 100, and 1000 cm), and both narrow and wide log-normal bed-sediment grain-size distributions. The computations were repeated for a more complex algorithm that included development of dunes.
(2) Concentration and grain size of suspended sediment were averaged through the water column.
(3) The computed results were then approximated by equations expressing the dependent variables (C and Ds) as power functions of the independent variables (u_* and D_b).
(4) The equations derived in step (3) were rearranged, so that the independent variables u_* and D_b were expressed in terms of the more easily observed dependent variables C and D_s. This sequence of steps led to

$$a = \left(\frac{K}{J+1}\right)^{\frac{-L\left(\frac{\log\Delta C}{\log\Delta D_s}\right)+J}{M\left(\frac{\log\Delta C}{\log\Delta D_s}\right)-K}} \qquad (2)$$

where the values of J and K for various models listed in step (1) are given in Table 1.

Table. 1 Values of J, K, L, and M in equations (2 and 5), determined by fitting power laws to computational results.

Model	J	K	L	M
Without dunes; sigma phi=0.55	3.5	-2.5	0.15	1.0
Without dunes; sigma phi=1.4	3.5	-1.5	0.4	0.5
With dunes; sigma phi=0.55	5.0	-3.0	0.2	0.7
With dunes; sigma phi=1.4	3.5	-1.5	0.3	0.5

The symbol ? in eq (2) applies to a single change in conditions; for results to be representative of a more extensive set of time-series measurements, it is necessary to replace the ? with a statistical measure. The approach taken here is to replace ? with the standard deviation of a variable, so that $\log\Delta C/\log\Delta D_s$ is replaced by

$$\left|\frac{\log\Delta C}{\log\Delta D_s}\right| \approx \frac{s(\log C)}{s(\log D_s)} \tag{3}$$

where $s(\log C)$ and $s(\log D_s)$ represent the standard deviations of $\log C$ and $\log D_s$, respectively. This approach of substituting the standard deviation of a variable for a single change (?) in that variable is equivalent to the reduced major axis technique for fitting a line to a scatter plot of x-y data (p. 200-204 in Davis, 1986). Eq (3) predicts the absolute value of $\log\Delta C/\log\Delta D_s$, but not the sign of this quantity. In some cases, the sign can be determined by inspection; in other cases it may be necessary to determine whether the positive or negative sign gives a better fit to the data (Davis, 1986).

Tracking grain size of bed sediment that is accessible to the flow Once it has been established that grain-size regulation of sediment transport is important in a particular sediment–transport system ($|\alpha|$ approaches or exceeds 1), it may be desirable to monitor changes in grain size of sediment on the bed. This is useful for at least three goals: (1) quantifying changes through time in the degree of winnowing or armoring downstream from a dam, (2) measuring the extent to which tributaries have contributed fine sediment to the bed of a channel (as is important in determining the timing of artificial floods in the Colorado River in Grand Canyon), and (3) measuring the spatial (depth-related) variation of grain size of sediment on the bed in pools, bars, and floodplains.

A dimensionless measure of grain size of sediment on the bed, β, can be defined as

$$b = \frac{D_b}{D_{bm}} \tag{4}$$

where D_b is the median grain diameter of bed sediment at an instant in time, and D_{bm} is the average of a sequence of median diameters at the same location. Thus, β is a measure of the relative coarseness of sediment at one point on the bed. As Rubin and Topping (in press) showed, β can also be expressed as a function of the dependent variables C and D_s relative to their mean or median values

$$b = \left(\frac{C}{C_m}\right)^{\frac{-L}{JM-KL}} \left(\frac{D_s}{D_{sm}}\right)^{\frac{J}{JM-KL}} \tag{5}$$

The exponent of the concentration ratio is negative, whereas the exponent of the grain-size ratio is positive (Table 1). As a result, the relative bed coarseness, β, increases as concentration decreases and as grain size increases (as intuition would suggest). Bed-sediment grain size is proportional to β and can be calculated by multiplying β by the time-averaged bed-sediment grain size for a particular reach.

The relation between bed sediment and suspended sediment expressed in eq (5) reflects at least three kinds of changes. First, grain size of sediment at a point on the bed (or within a reach) can change through time as a result of deposition of sediment from upstream or tributaries, winnowing of the bed, or erosion and excavation of underlying substrate. Second, the depth to which sediment in the substrate interacts with the flow may vary with flow strength (Wiberg, et al., 1994). For example, a weak flow that generates ripples on the bed will exchange sediment with the uppermost few centimeters of the sediment substrate. In contrast, a stronger flow that generates large dunes will exchange sediment with a greater depth within the substrate. Third, as stage increases, a river may gain access to finer sediment that occurs on high-elevation channel-margin bars and floodplains. Of these three changes, only the first reflects actual changes on the bed; the latter two changes in grain size reflect lateral or vertical changes in the region of the channel interacting with the flow. Measured changes in β reflect all of these factors.

EXAMPLES

Calculation of α An example of grain-size regulation of sediment transport occurred during an experimental flood on the Colorado River in Grand Canyon in 1996 (Rubin et al., 1998; Topping et al., 1999). For the seven days of the flood experiment, clear water was released from Glen Canyon Dam at the rate of 1270 m^3/s. In response to this erosive flow, the bed at the Grand Canyon gage coarsened, which caused suspended sediment to both coarsen and decrease in concentration. The resulting negative correlation between suspended-sediment concentration and grain size (Fig. 2a) demonstrates that grain-size regulation was important during this event. Calculated values of α for data collected at 3 reaches during the flood were -1.5, -3.3, and -6.3, indicating that changes in sediment transport were regulated primarily by changes in bed-sediment grain size ($|\alpha| > 1$).

Calculation of β The same observations of suspended-sediment concentration used to calculate α can be used to calculate changes in the relative coarseness of sediment on the bed during the flood (Fig. 2b). Comparison with sampled bed sediment not only shows good agreement, but the smoother trend of the calculated values suggests that the calculations may be more representative of the system than measurements at a single cross-section. In this case, where river discharge was constant, changes in β reflect actual changes in grain size of sediment on the bed. In other situations, where discharge is free to vary, calculated changes in β can reflect changes in grain size on the bed, as well as changes in the region of the bed that is accessible to the flow. The predicted values of bed-sediment diameter are in close agreement with observed values. The predicted values have less scatter than the values observed at a single cross-section and may be more representative of the river.

APPLICATIONS

The technique developed by Rubin and Topping (in press) and summarized in this paper has important applications with respect to: (1) designing sediment-transport measurement programs, (2) constructing sediment-transport models, (3) providing a starting point for the accurate determination of TMDLs for sediment, and (4) determining whether changes in upstream sediment budgets are positive or negative. First, this technique allows one to best design a sediment-transport measurement program. If, in a given situation, the dominant regulator of sediment transport is the flow, then an approximately stable relationship exists between the discharge of water and sediment transport (i.e., a stable sediment rating curve exists). In this case, measurements can be collected so that they best define a sediment rating curve (i.e., they are uniformly distributed across the entire range of flows). In contrast, if the dominant regulator of sediment transport is the grain size of the bed sediment, then sediment transport is controlled by changes in the upstream sediment supply and no stable sediment rating curve exists; measurements need to be closely spaced in time. In a similar manner, this technique provides a guide to knowing the pertinent physical processes to include in a sediment transport model. If the dominant regulator of sediment transport is the flow, then a model can be constructed that predicts a stable sediment rating curve by assuming that the channel geometry and bed sediment are in equilibrium with the flow. However, if the dominant regulator of sediment transport is the grain size of the bed sediment, then a totally different type of model needs to be constructed, one that routes sediment downstream from its source. A third application of this technique involves the calculation of TMDLs for sediment. In the case where the flow is the dominant regulator of sediment transport, TMDLs can be easily calculated using stable sediment rating curves (either measured or modeled). However, in the case where bed sediment grain size is the dominant regulator of sediment transport, TMDLs can only be calculated by determining the maximum naturally occurring daily supply of sediment. Finally, this technique allows upstream sediment budgets to be interpreted based on data from only one site. By determining whether β is increasing or decreasing over long time scales, one can determine whether the upstream supply of fine sediment is decreasing or increasing over long time scales.

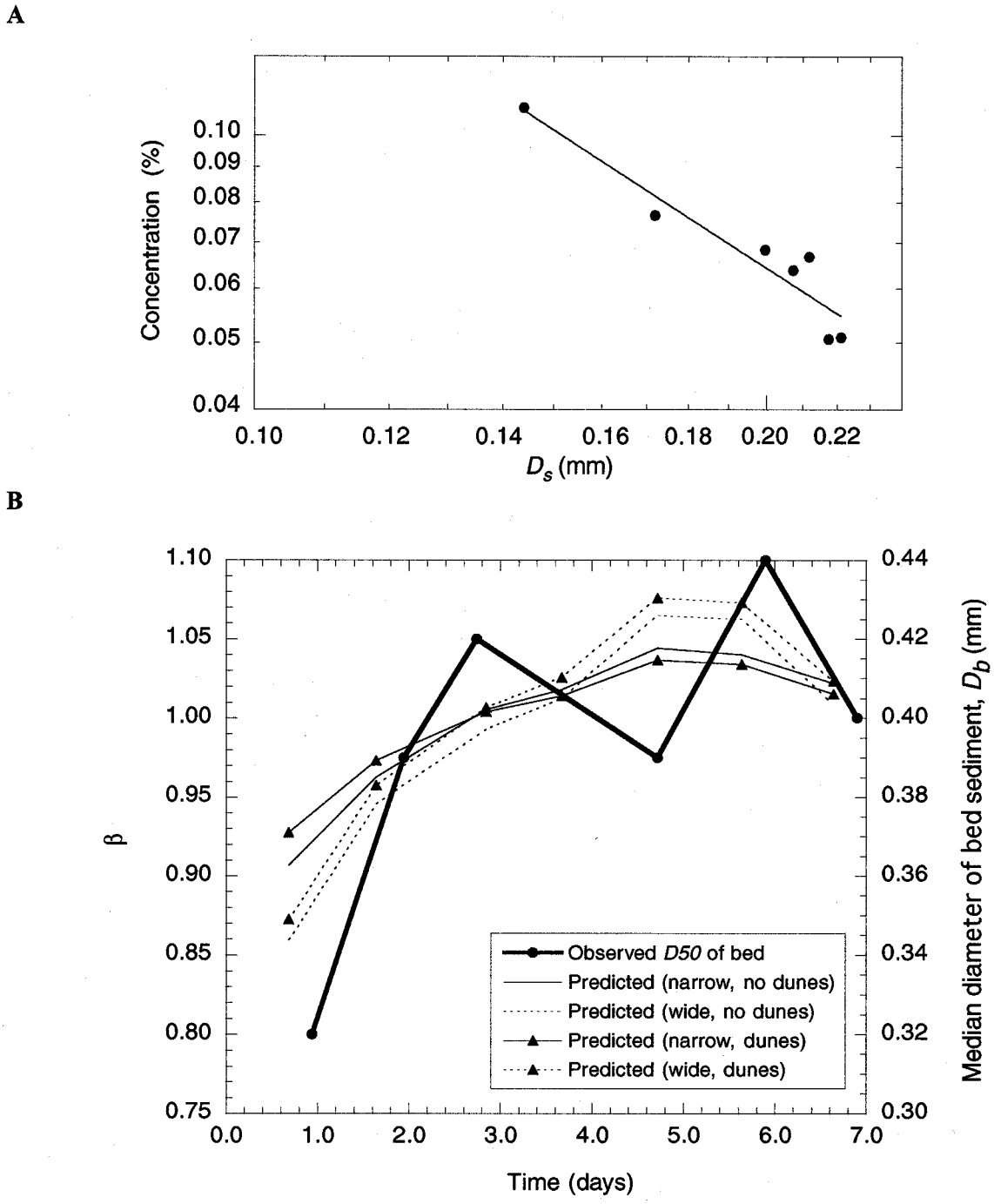

Figure 2. α and β during the 1996 flood experiment in Grand Canyon. **A.** Concentration and grain size for grain-size-regulated transport at Grand Canyon gage during the 1996 flood experiment. As sediment on the bed was winnowed, suspended sediment decreased in concentration and increased in grain size; concentration and grain size are negatively correlated (α = -1.5). **B.** Plot of β and predicted and observed bed-sediment median diameter. Observed bed-sediment median diameter was determined from samples collected at 3-5 locations at the Grand Canyon gage cableway (Rubin et al., 1998; Topping et al., 1999); β was calculated using eq (5) and suspended-sediment measurements; predicted values of bed-sediment median diameter were calculated by expressing β relative to the median diameter of all bed samples.

REFERENCES

Davis, J. C., 1986, *Statistics and Data Analysis in Geology,* New York, John Wiley & Sons, Inc., 646 p.

Einstein, H. A., and Chien, N., 1953, Transport of sediment mixtures with large ranges of grain size. Missouri River Division U.S. Army Corps of Engineers, No. 2, 72 p.

Guy, H. P., Simons, D. B., and Richardson, E. V., 1966, Summary of alluvial channel data from flume experiments, 1956-61. USGS Professional Paper 462-I, 96 p.

McLean, S. R., 1992, On the calculation of suspended load for noncohesive sediments. Journal of Geophysical Research 97, 5759-5770.

Rubin, D. M., Nelson, J. M., and Topping, D. J., 1998, Relation of inversely graded deposits to suspended-sediment grain-size evolution during the 1996 flood experiment in Grand Canyon. Geology 26, 99-102.

Rubin, D. M. and Topping, D. J., Quantifying the relative importance of flow regulation and grain-size regulation of suspended-sediment transport (α) and tracking changes in grains size of fine sediment on the bed (β). In press, Water Resources Research.

Topping, D. J., Rubin, D. M., Nelson, J. M., Kinzel, P. J., III, and Bennett, J. P., 1999, Linkage between grain-size evolution and sediment depletion during Colorado River floods. *in* Webb, R. H., Schmidt, J. C., Marzolf, G. R., and Valdez, R. A., eds., *The 1996 Controlled Flood in Grand Canyon,* Washington, D.C., American Geophysical Union, Geophysical Monograph 110, 71-98.

Wiberg, P. L., Drake, D. E., and Cacchione, D. A., 1994, Sediment resuspension and bed armoring during high bottom stress events on the northern California inner continental shelf: measurements and predictions, Continental Shelf Research 14, 10/11, 1191-1219.

Contact:
David M. Rubin
Coastal and Marine Geology
USGS Pacific Science Center
University of California at Santa Cruz
1156 High Street
Santa Cruz, CA 95064
831-459-3156
drubin@usgs.gov
http://walrus.wr.usgs.gov/seds/

David J. Topping
USGS WRD
12201 Sunrise Valley Drive, MS 430
Reston, VA 20192
703-648-5895
dtopping@usgs.gov